SUPPORTING INFORMATION

Parent 1,4-dihydro-[1,2,3]triazolo[4,5-*d*][1,2,3]triazole and its derivatives as precursors for the design of promising high energy density materials†

Agata N. Kuznetsova,[a,b] Nikita E. Leonov,[a] Oleg V. Anikin,[a] Michael S. Klenov,*[a] Aleksandr M. Churakov,*[a] Yurii A. Strelenko,[a] Roman A. Novikov,[a] Ivan V. Fedyanin,[c] Alla N. Pivkina,[d] Tatiana S. Kon'kova,[d] Valery P. Sinditskii,[e] Anastasia D. Smirnova[e] and Vladimir A. Tartakovsky[a]

[a]N. D. Zelinsky Institute of Organic Chemistry Russian Academy of Sciences, 47 Leninsky prospect, Moscow, 119991, Russian Federation. E-mail: klenov@ioc.ac.ru, churakov@ioc.ac.ru.

[b]Department of Chemistry, Lomonosov Moscow State University, 1 Leninskie Gory, Moscow, 119991, Russian Federation.

[c]A. N. Nesmeyanov Institute of Organoelement Compounds Russian Academy of Sciences, 28 Vavilova st., Moscow, 119991, Russian Federation.

[d]N. N. Semenov Federal Research Center for Chemical Physics Russian Academy of Sciences, 4 Kosygin st., Moscow, 119991, Russian Federation.

[e]Mendeleev University of Chemical Technology, 9 Miusskaya Square, Moscow, 125047, Russian Federation.

Table of contents

1. General methods

1.1. Safety precautions

Although we have encountered no difficulties during preparation and handling of compounds described in this paper, they are potentially explosive energetic materials which are sensitive to impact and friction. Mechanical actions of these energetic materials, involving scratching or scraping, must be avoided. Any manipulations must be carried out by using appropriate standard safety precautions.

1.2. General information

^{1}H, ^{13}C, ^{14}N and ^{15}N NMR spectra were recorded with Bruker DRX-500 (500.1, 125.8, 36.1, 50.7 MHz, respectively) and Bruker AV600 (600.1, 150.9, 43.4, 60.8 MHz, respectively) spectrometers. *Chemical shifts* are reported in delta (δ) *units*, parts per million (ppm) downfield from internal TMS (^{1}H, ^{13}C) or external CH_3NO_2 (^{14}N, ^{15}N negative values of δ_N correspond to upfield shifts). Solid-state NMR experiments were recorded on a Bruker AVANCE III WB 400 MHz spectrometer equipped with 4.0 mm DVT MAS BB/HF probe (15 kHz) and 2.5 mm DVT MAS BB/HF probe (35 kHz) (^{1}H – 400.1 MHz, ^{13}C – 100.6 MHz, ^{15}N – 40.6 MHz, ^{81}Br – 100.25 MHz). Samples were spun at 9.5–14 kHz (4.0 mm probe) at the magic angle (MAS) using ZrO_2 rotors. ^{1}H MAS spectra were recorded using single-pulse sequence with 45° pulse at 14 kHz MAS with a recycle delay of 15 sec. ^{13}C-CP/MAS spectra were recorded with a recycle delay of 12 sec and contact times of 6 msec at 10.5 kHz MAS. ^{15}N-CP/MAS spectra were recorded with a recycle delay of 30–38 sec and with a smooth change in the CP transfer duration from 2 msec to 18 msec at 9.5 kHz MAS. 2D ^{15}N–^{1}H CP-FSLG-HETCOR spectra were recorded at 13 kHz MAS in a rotor-synchronized mode with RF field 98 kHz for FSLG and using a smooth change in the CP transfer duration from 300 msec to 6000 msec. The ^{13}C, ^{15}N, and 2D ^{15}N–^{1}H HETCOR spectra were recorded under high-power proton decoupling conditions using "spinal64". Chemical shifts for ^{1}H and ^{13}C are relative to external adamantane sample; ^{15}N chemical shifts were calculated to this scale and were checked using ^{15}N-labelled-glycine sample. Magic angle was calibrated precisely to the spinning side bands

in ^{81}Br spectra of the KBr sample. The IR spectra were recorded with a Bruker ALPHA-T spectrometer in the range 400–4000 cm^{-1} (resolution 2 cm^{-1}) as pellets with KBr or as a thin layer. High-resolution ESI mass spectra (HRMS) were recorded with a Bruker micrOTOF II instrument. Thermal behavior was studied using Netzsch DSC 204 HP under 0.1 or 2 MPa of nitrogen. Few drops of sample (0.6–3 mg) or sample near 0.5 mg were placed in closed aluminum crucibles with pierced lids and then heated linearly with 5 °C·min^{-1} rate up to 400 °C. The impact and friction sensitivities were determined using a STANAG[1,2] protocol and BAM-type impact and friction machines (further details can be found elsewhere[3]). Density was measured with a Micromeritics AccuPyc II 1340 gas pycnometer. Silica gel 60 Merck (15–40 μm) was used for flash and column chromatography. Analytical thin-layer chromatography (TLC) was carried out on Merck silica gel 60 F254 aluminum sheets. All reagents were purchased from Acros and Sigma-Aldrich. *Solvents were purified* before use, according to standard procedures. All other reagents were used without further purification. *N*-(5-Amino-2*H*-1,2,3-triazol-4-yl)formamide (**2**) was prepared according to the reported procedure.[4]

2. Experimental procedures and characterization

2.1. Synthesis of *N*-(4-diazo-4*H*-1,2,3-triazol-5-yl)formamide (3)

N-(5-Amino-2*H*-1,2,3-triazol-4-yl)formamide (**2**) (6.35 g, 50.0 mmol) was dissolved in CF_3CO_2H (40 mL) at 25 °C. The resulting solution was cooled to 10 °C, then $NaNO_2$ (4.15 g, 60.1 mmol) was added in several portions over 1 h at a temperature of 5–10 °C. After stirring for 1 h, EtOH (50 mL) was added and the reaction mixture was stirred for 30 min. The precipitate was then filtered off, washed with EtOH (3 × 15 mL) and dried under reduced pressure to give diazotriazole **3** (5.89 g, 85% yield) as a white solid.

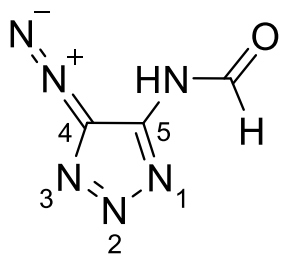

DSC (5 °C·min^{-1}): T_m = 178 °C, T_{onset} = 183 °C (dec.). ^{1}H NMR (600.13 MHz, [D$_6$]DMSO): δ = 8.45 (s, 1 H, C(O)H), 12.28 (br. s, 1 H, NH) ppm. ^{13}C NMR (150.9 MHz, [D$_6$]DMSO): δ = 101.9 (C-4), 145.5 (C-5), 161.3 (C=O) ppm. ^{14}N NMR (43.4 MHz, [D$_6$]DMSO): δ = –145 (C=N^+=N^-, $\Delta\nu_{½}$ = 300 Hz) ppm. ^{15}N NMR ([INVGATED], 60.8 MHz, [D$_6$]DMSO): δ = 32.9, –20.6, –24.5, –50.4, –144.5 (C=N^+=N^-), –249.5 (NH) ppm. IR (KBr): ν = 3140 (w), 2971 (w), 2221 (s), 1703 (s), 1691 (s), 1540 (s), 1382 (m), 1354 (m), 1275 (w), 1237 (m), 1200 (w) cm^{-1}. HRMS (ESI): m/z calcd for $C_3H_2N_6O$ $[M + H]^+$ 138.0876; found 138.0873. Elemental analysis calcd (%) for $C_3H_2N_6O$: C 26.09, H 1.46, N 60.86; found: C 25.98, H 1.23, N 60.32.

2.2. Synthesis of 5-amino-1*H*-1,2,3-triazol-4-diazonium chloride (4)

N-(4-Diazo-4*H*-1,2,3-triazol-5-yl)formamide (**3**) (0.6 g, 4.38 mmol) was added portionwise to the concentrated hydrochloric acid (36 wt-%, 5 mL) and the resulting solution was vigorously stirred at 25 °C for 1 h. Then the reaction mixture was concentrated under reduced pressure at 35 °C. The resulting product was recrystallized from methanol (5 mL) at –20 °C to give diazonium salt **4** (0.51 g, 89%) as yellow crystals.

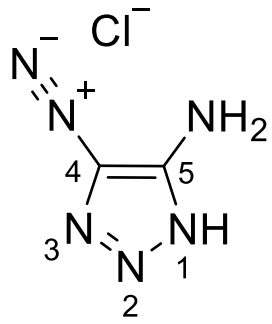

DSC (5 °C·min^{-1}): T_{onset} = 140 °C (dec.). ^{1}H NMR (500.16 MHz, [D$_6$]DMSO): δ = 7.55 (br. s, 2 H, NH$_2$), 9.38 (br. s, 1 H, NH) ppm. ^{13}C NMR (125.8 MHz, [D$_6$]DMSO): δ = 99.3 (C-4), 151.6 (C-5) ppm. ^{14}N NMR (36.1 MHz, [D$_6$]DMSO): δ = –142 (C–*N*$^+$≡N, $\Delta\nu_{½}$ = 700 Hz) ppm. ^{15}N NMR ([INVGATED], 50.7 MHz, [D$_6$]DMSO): δ = –12.2, –32.3, –145.3 (C–*N*$^+$≡N), –216.0, –232.6, –360.4 (NH$_2$) ppm. IR (KBr): ν = 3450 (w), 3232 (w), 3051 (m), 2782 (w), 2684 (m), 2627 (m), 2182 (s), 1669 (s), 1451 (m), 1325 (w), 1277 (m), 1219 (m) cm^{-1}. HRMS (ESI): m/z calcd for $C_2H_3N_6^+$ $[M]^+$ 111.0414; found 111.0417. Elemental analysis calcd (%) for $C_2H_3ClN_6$: C 35.56, H 5.47, N 41.47; found: C 35.60, H 5.51, N 41.37.

2.3. Synthesis of 5-amino-4-diazo-1*H*-1,2,3-triazole (5)

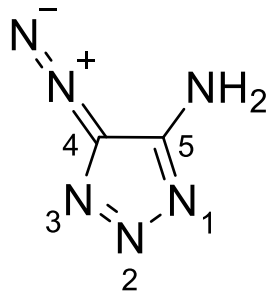

Method A. The solution of NaOH (40 mg, 1.0 mmol) in H$_2$O (1.0 mL) was added dropwise to the solution of 5-amino-1*H*-1,2,3-triazol-4-diazonium chloride (**4**) (146 mg, 1.0 mmol) in H$_2$O (1.0 mL) at 0 °C. The reaction is accompanied by the color changes from yellowish to dark-red. The reaction mixture was stirred at 0 °C for 5 min. The red precipitate was then filtered off and 30 mg of this precipitate was dissolved in D$_2$O (0.5 mL) at 10 °C. The resulting solution was placed into NMR tube. The ^{13}C and ^{14} N NMR spectra for compound **5** were recorded at 10 °C.

Method B. *N*-(4-Diazo-4*H*-1,2,3-triazol-5-yl)formamide (**3**) (274 mg, 2.0 mmol) was added portionwise to the solution of NaOH (80 mg, 2.0 mmol) in H$_2$O (4 mL) at 0 °C. The reaction is accompanied by the color changes from yellowish to dark-red. The reaction mixture was stirred at 0 °C for 5 min. The red precipitate was then filtered off and 30 mg of this precipitate was dissolved in D$_2$O (0.5 mL) at 10 °C. The resulting solution was placed into NMR tube. The ^{13}C and ^{14} N NMR spectra for compound **5** were recorded at 10 °C.

^{13}C NMR (150.9 MHz, D$_2$O): δ = 95.1 (C-4), 159.4 (C-5) ppm. ^{14}N NMR (43.4 MHz, D$_2$O): δ = –140 (C=*N*$^+$=N$^-$, $\Delta\nu_{½}$ = 400 Hz), –325 (NH$_2$, $\Delta\nu_{½}$ = 2000 Hz) ppm.

2.4. Synthesis of 1,4-dihydro[1,2,3]triazolo[4,5-*d*][1,2,3]triazole (TT 1) from 5-amino-1*H*-1,2,3-triazol-4-diazonium chloride (4)

The solution of 5-amino-1*H*-1,2,3-triazol-4-diazonium chloride (**4**) (0.73 g, 5.0 mmol) in H_2O (5 mL) was added dropwise to the solution of NaOH (0.60 g, 15.0 mmol) in H_2O (5 mL). The resulting red solution was refluxed for 15 min. A color change of the reaction mixture from dark-red to colorless was observed. Then the mixture was cooled to 25 °C, concentrated hydrochloric acid (36 wt-%, 1.3 ml, 15.0 mmol) was added dropwise to the solution. The precipitate was filtered off and dried in air to give 1,4-dihydro[1,2,3]triazolo[4,5-*d*][1,2,3]triazole (TT **1**) (0.33 g, 60%) as a white solid. An analytical sample of TT **1** for combustion calorimetry was obtained according the next manner. Suspension of TT **1** (2.5 g) in H2O (250 mL) was vigorously stirred at 25 °C. Then the precipitate was filtered off, washed with H_2O (3 × 20 mL), dried in air for 3 days, then dried under reduced pressure for 24 h. TT **1** (2.04 g, 82%) was obtained as a white solid.

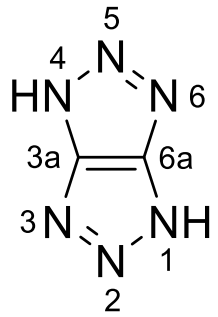

DSC (5 °C·min^{-1}): T_{onset} = 193 °C (dec.). ^{1}H NMR (600.13 MHz, [D$_6$]DMSO): δ = 15.38 (br. s, 2 H, NH) ppm. ^{13}C NMR (150.9 MHz, [D$_6$]DMSO): δ = 153.3 (C-3a and C-6a) ppm. ^{15}N NMR ([INVGATED], 60.8 MHz, [D$_6$]DMSO): δ = –36.0 (N-2 and N-5), –105.9 (N-1, N-3, N-4, N-6) ppm. Solid-state ^{1}H NMR (400.16 MHz): δ = 14.18 (br. s, 2 H, NH) ppm. Solid-state ^{13}C NMR (100.6 MHz): δ = 147.3 (C-3a and C-6a) ppm. Solid-state ^{15}N NMR (40.6 MHz): δ = –7.8 (N-2 and N-5), –77.8 (N-3 and N-6), –168.3 (N-1 and N-4) ppm. IR (KBr): ν = 3175 (s), 1572 (w), 1464 (w), 1433 (w), 1352 (s), 1267 (s), 1195 (w), 1129 (s), 1041 (s) cm^{-1}. HRMS (ESI): m/z calcd for $C_2H_2N_6$ $[M + H]^+$ 110.0775; found 110.0770. Elemental analysis calcd (%) for $C_2H_2N_6$: C 21.82, H 1.83, N 76.35; found: C 21.86, H 1.84, N 76.21.

2.5. Synthesis of 1,4-dihydro[1,2,3]triazolo[4,5-*d*][1,2,3]triazole (TT 1) from *N*-(4-diazo-4*H*-1,2,3-triazol-5-yl)formamide (3)

N-(4-Diazo-4*H*-1,2,3-triazol-5-yl)formamide (**3**) (4.14 g, 30.0 mmol) was added to the solution of NaOH (3.60 g, 90.0 mmol) in H_2O (45 mL) at 25 °C in several portions over

10 min. The resulting red solution was refluxed for 15 min. A color change of the reaction mixture from dark-red to colorless was observed. Then the mixture was cooled to 25 °C, concentrated hydrochloric acid (36 wt-%, 8 mL, 90.0 mmol) was added dropwise to the solution. The precipitate was filtered off, washed with H_2O (3 × 20 mL) and dried in air. TT **1** (3.04 g, 92%) was obtained as a white solid, identical (TLC, ^{1}H, ^{13}C NMR) to the product prepared according to the procedure above.

2.6 Synthesis of 5-amino-1*H*-1,2,3-triazol-4-diazonium chloride (4) from 1,4-dihydro[1,2,3]-triazolo[4,5-*d*][1,2,3]triazole (TT 1)

1,4-Dihydro[1,2,3]triazolo[4,5-*d*][1,2,3]triazole (TT **1**) (0.55 g, 5 mmol) was added in one portion to the concentrated hydrochloric acid (36 wt-%, 1.3 mL, 15 mmol) and the resulting suspension was refluxed for 30 min. Then the reaction mixture was concentrated under reduced pressure at 35 °C. The resulting product was recrystallized from methanol (5 mL) at –20 °C. Salt **4** (0.68 g, 93%) was obtained as yellow crystals, identical (^{1}H, ^{13}C, ^{14}N NMR) to the product prepared according to the procedure above.

2.7. Synthesis of disodium salt of [1,2,3]triazolo[4,5-*d*][1,2,3]triazole dihydrate (6a·2H₂O)

1,4-Dihydro[1,2,3]triazolo[4,5-*d*][1,2,3]triazole (TT **1**) (1.10 g, 10.0 mmol) was added to the solution of NaOH (0.80 g, 20.0 mmol) in MeOH (30 ml) and the reaction mixture was stirred at 25 °C for 30 min. The reaction mixture was concentrated under reduced pressure at 35 °C to give disodium salt of [1,2,3]triazolo[4,5-*d*][1,2,3]triazole dihydrate (**6a**·2H_2O) (1.54 g, 99%) as a beige solid.

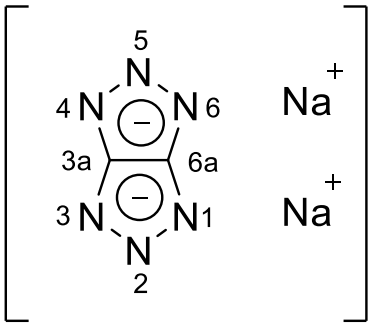

× 2H_2O

DSC (5 °C·min^{-1}): T_{onset} = 207 °C. ^{13}C NMR (150.9 MHz, D_2O): δ = 162.2 (C-3a and C-6a) ppm. ^{15}N NMR (60.8 MHz, D_2O): δ = 1.7 (N-2 and N-5), –88.5 (N-1, N-3, N-4, N-6) ppm. IR (KBr): ν = 3443 (s), 1688 (m), 1611 (m), 1385 (s), 1195 (w) cm^{-1}. Elemental analysis calcd (%) for $C_2N_6Na_2 \cdot 2H_2O$: C 12.64, H 2.12, N 44.21; found: C 12.67, H 2.07, N 44.15.

2.8. Synthesis of dipotassium salt of [1,2,3]triazolo[4,5-*d*][1,2,3]triazole (6b)

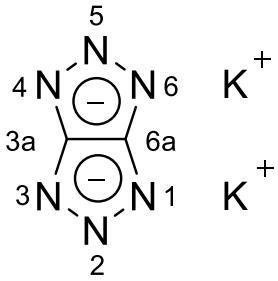

1,4-Dihydro[1,2,3]triazolo[4,5-*d*][1,2,3]triazole (TT **1**) (1.10 g, 10.0 mmol) was added to the solution of KOH (1.12 g, 20.0 mmol) in MeOH (50 ml) and the reaction mixture was stirred at 25 °C for 30 min. The reaction mixture was concentrated under reduced pressure at 35 °C to give dipotassium salt of [1,2,3]triazolo[4,5-*d*][1,2,3]triazole (**6b**) (1.85 g, 99%) as a beige solid (decomp. without melting > 250 °C).

^{13}C NMR (150.9 MHz, D_2O): δ = 162.5 (C-3a and C-6a) ppm. ^{15}N NMR (60.8 MHz, D_2O): δ = 4.7 (N-2 and N-5), –86.8 (N-1, N-3, N-4, N-6) ppm. IR (KBr): ν = 3434 (s), 1638 (w), 1395 (s), 1142 (m) cm^{-1}. Elemental analysis calcd (%) for $C_2N_6K_2$: C 12.90, N 45.12; found: C 12.93, N 45.09.

2.9. Synthesis of bistetraethylammonium salt of [1,2,3]triazolo[4,5-*d*][1,2,3]triazole heptahydrate (6c·7H$_2$O)

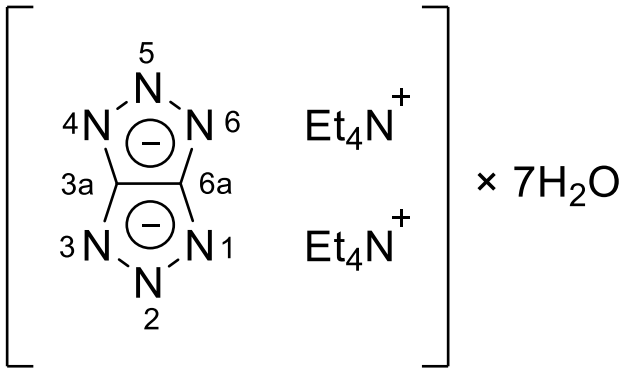

1,4-Dihydro[1,2,3]triazolo[4,5-*d*][1,2,3]-triazole (TT **1**) (2.20 g, 20.0 mmol) was added to the 25% aqueous solution of Et_4NOH (23 ml) and the reaction mixture was stirred at 25 °C for 3 days. The reaction mixture was concentrated under reduced pressure at 45 °C to give bistetraethylammonium salt of [1,2,3]triazolo[4,5-*d*][1,2,3]triazole (**6c**·7H_2O) (7.34 g, 99%) as a beige solid.

DSC (5 °C·min^{-1}): T_m = 56 °C, T_{onset} = 109 °C (dec.). ^{1}H NMR (600.13 MHz, D_2O): δ = 0.96 (t, $^3J_{H,H}$ = 7.3 Hz, 24 H, CH_3), 2.84 (q, $^3J_{H,H}$ = 7.3 Hz, 16 H, CH_2) ppm. ^{13}C NMR (150.9 MHz, D_2O): δ = 6.0 (CH_3), 51.2 (CH_2), 162.1 (C-3a and C-6a) ppm. ^{14}N NMR (43.4 MHz, D_2O): δ = –318 (Et_4N^+, $\Delta\nu_{½}$ = 20 Hz) ppm. ^{15}N NMR (60.8 MHz, D_2O): δ = –11.3 (N-2 and N-5), –88.9 (N-1, N-3, N-4 and N-6), –318.1 (Et_4N^+) ppm. IR (KBr): ν = 3421 (s),

2964 (s), 2876 (s), 2784 (w), 2735 (w), 1915 (s), 1681 (w), 1566 (w), 1489 (s), 1416 (w), 1382 (m), 1276 (w), 1183 (m), 1152 (m), 1130 (w), 1109 (w) cm^{-1}. Elemental analysis calcd (%) for $C_{18}H_{40}N_8 \cdot 7H_2O$: C 43.70, H 11.00, N 22.65; found: C 43.73, H 11.05, N 22.60.

2.10. Methylation of TT-salts 6a–c. Synthesis of 1,5-dimethyl[1,2,3]triazolo[4,5-*d*]-[1,2,3]triazole (7a), 2,5-dimethyl[1,2,3]triazolo[4,5-*d*][1,2,3]triazole (7b), 1,6-dimethyl[1,2,3]triazolo[4,5-*d*][1,2,3]-triazole (7c) and 1,4-dimethyl[1,2,3]triazolo-[4,5-*d*][1,2,3]triazole (7d)

Table TS1. Methylation[a] of TT-salts **6a–c**.

Entry	Starting compound	Methylation reagent	Reaction conditions	Time, h	Temperature, °C	Yield[b] (%)			
						7a	**7b**	**7c**	**7d**
1	**6a**·$2H_2O$	MeI	DMF	48	25	24	19	3	1
2	**6a**·$2H_2O$	Me_2SO_4	MeOH	48	25	11	14	3	1
3	**6b**	MeI	DMF	48	25	32	25	6	5
4	**6b**	MeI	18-crown-6[c], H_2O/CH_2Cl_2[d]	72	25	11	21	5	1
5	**6b**	Me_2SO_4	MeOH	48	25	9	15	7	3
6	**6c**·$7H_2O$	MeI	MeCN	72	25	**57**	**25**	**9**	**5**
7	TT **1**	MeI	DBU (2 equiv,), MeCN	48	25	23	19	0	0

[a]Reactions were run with 5 mmol of starting compound, 10 mmol of MeI in minimum amount of solvent. [b]Isolated yields. [c]10% mol.% of 18-crown-6 was used. [d]1/1 = v/v.

General procedure: Methylation reagent (Entries 1, 2, 4, 6, 7 – MeI, entries 2, 5 – Me_2SO_4; 2 mmol) was added dropwise to a stirred solution of corresponding TT-salt (5 mmol) in corresponding solvent (see Table TS 1). The reaction mixture was vigorously stirred at 25 °C until the starting compound disappeared (TLC control). In the case of entries 1–5 the reaction mixture was poured into H_2O (50 mL) and extracted with EtOAc (5 × 20 mL). The combined organic extracts were washed with water (25 mL), brine (25 mL), dried with anhydrous Na_2SO_4 and concentrated under reduced pressure. In the case of entries 6 and 7 the reaction mixture was concentrated under reduced pressure. The residue was purified by preparative column chromatography on silica gel (petroleum ether/ EtOAc, 1:1) to give triazolotriazoles **7a** (R_f = 0.73) as a beige solid, **7b** (R_f = 0.89) as white crystals, **7c** (R_f = 0.17) as a yellow solid and **7d** (R_f = 0.63) as white crystals.

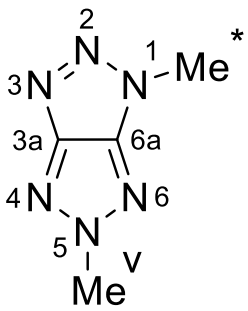

Data for triazolotriazole 7a: DSC (5 °C·min^{-1}): T_m = 90 °C, T_{onset} = 201 °C (dec.). ^{1}H NMR (600.13 MHz, [D$_6$]DMSO): δ = 4.27 (s, 3 H, Me*), 4.43 (s, 3 H, Me^v) ppm. ^{13}C NMR (150.9 MHz, [D$_6$]DMSO): δ = 35.2 (Me*), 43.9 (Me^v), 146.5 (C-6a), 160.8 (C-3a) ppm. ^{14}N NMR (43.4 MHz, [D$_6$]DMSO): δ = –71 (N-6, $\Delta\nu_{½}$ = 2100 Hz), –117 (N-5, $\Delta\nu_{½}$ = 600 Hz), –179 (N-1, $\Delta\nu_{½}$ = 870 Hz) ppm. ^{15}N NMR ([INVGATED], 60.8 MHz, [D$_6$]DMSO): δ = 14.2 (N-2), –57.7 (N-3), –74.1 (N-6), –91.3 (N-4), –116.4 (N-5), –178.1 (N-1) ppm. ^{15}N NMR ([INEPT, with decoupling], 60.8 MHz, D$_6$]DMSO): δ = 14.4 (N-2), –73.9 (N-4 or N-5 or N-6), –91.2 (N-4 or N-5 or N-6), –116.4 (N-4 or N-5 or N-6), –178.2 (N-1) ppm. ^{15}N NMR ([INEPT], without decoupling, 60.8 MHz, [D$_6$]DMSO): δ = 14.2 (q, ^3J = 1.82 Hz, N-2), –57.7 (t, ^4J = 0.30 Hz, N-3), –74.1 (q, ^3J = 2.43 Hz, N-4 or N-5 or N-6), –91.2 (q, ^3J = 2.43 Hz, N-4 or N-5 or N-6), –116.4 (q, ^2J = 2.43 Hz, N-4 or N-5 or N-6), –178.1 (q, ^2J = 1.82 Hz, N-1) ppm. IR (KBr): ν = 3451 (s), 1599 (s), 1502 (w), 1470 (s), 1459 (s), 1355 (s), 1321 (m), 1271 (w), 1239 (m), 1185 (s) cm^{-1}. HRMS (ESI): m/z calcd for $C_4H_6N_6$ [M + H]$^+$ 139.0727; found 139.0723. Elemental analysis calcd (%) for $C_4H_6N_6$: C 34.78, H 4.38, N 60.84; found: C 34.81, H 4.44, N 60.68.

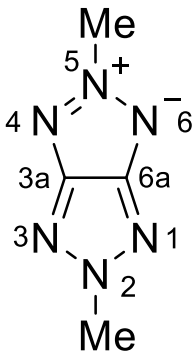

Data for triazolotriazole 7b: DSC (5 °C·min^{-1}): T_m = 224 °C. T_{onset} > 278 °C. ^{1}H NMR (600.13 MHz, [D$_6$]DMSO): δ = 4.50 (s, 6 H, Me) ppm. ^{13}C NMR (150.9 MHz, [D$_6$]DMSO): δ = 44.4 (Me), 157.5 (C-3a and C-6a) ppm. ^{14}N NMR (43.4 MHz, [D$_6$]DMSO): δ = –80 (N-1, N-3, N-4, N-6, $\Delta\nu_{½}$ = 1200 Hz), –109 (N-2 and N-5, $\Delta\nu_{½}$ = 250 Hz) ppm. ^{15}N NMR ([INVGATED], 60.8 MHz, [D$_6$]DMSO): δ = –79.9 (N-1, N-3, N-4, N-6), –107.8 (N-2 and N-5) ppm. ^{15}N NMR ([INEPT], 60.8 MHz, [D$_6$]DMSO): δ = –79.9 (t, ^3J = 3.29 Hz, N-1, N-3, N-4, N-6), –107.8 (t, ^2J = 3.56 Hz, N-2 and N-5) ppm. IR (KBr): ν = 3472 (s), 3039 (m), 1500 (s), 1452 (m), 1329 (s), 1291 (m), 1270 (w), 1233 (s), 1039 (s) cm^{-1}. HRMS (ESI): m/z calcd for $C_4H_6N_6$ [M + H]$^+$ 139.0727; found 139.0723. Elemental analysis calcd (%) for $C_4H_6N_6$: C 34.78, H 4.38, N 60.84; found: C 34.80, H 4.45, N 60.69.

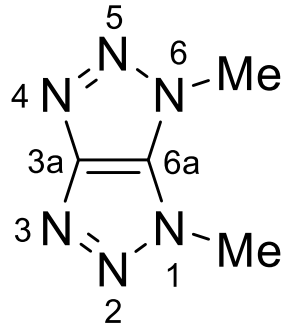

Data for triazolotriazole 7c: DSC (5 °C·min^{-1}): T_m = 167 °C, T_{onset} = 167 °C (dec.). ^{1}H NMR (600.13 MHz, [D$_6$]DMSO): δ = 4.23 (s, 6 H, Me) ppm. ^{13}C NMR (150.9 MHz, [D$_6$]DMSO): δ = 35.2 (Me), 136.4 (C-3a or C-6a), 167.0 (C-3a or C-6a) ppm. ^{14}N NMR (43.4 MHz, [D$_6$]DMSO): δ = 4 (N-2 and N-5, $\Delta\nu_{½}$ = 2000 Hz), –57 (N-3 and N-4, $\Delta\nu_{½}$ = 1000 Hz), –186 (N-1 and N-6, $\Delta\nu_{½}$ = 1500 Hz) ppm. ^{15}N NMR ([INVGATED], 60.8 MHz, [D$_6$]DMSO): δ = 3.3 (N-2 and N-5), –54.6 (N-3 and N-4), –179.0 (N-1 and N-6) ppm. ^{15}N NMR ([INEPT], 60.8 MHz, [D$_6$]DMSO): δ = 3.3 (q, ^3J = 1.82 Hz, N-2 and N-5), –54.6 (t, ^3J = 0.61 Hz, N-3 and N-4), –179.0 (q, ^2J = 1.82 Hz, N-1 and N-6) ppm. IR (KBr): ν = 3436 (s), 2954 (w), 1650 (s), 1524 (w), 1431 (w), 1388 (m), 1267 (w), 1232 (s), 1197 (s) cm^{-1}. HRMS (ESI): m/z calcd for $C_4H_6N_6$ $[M + H]^+$ 139.0727; found 139.0723. Elemental analysis calcd (%) for $C_4H_6N_6$: C 34.78, H 4.38, N 60.84; found: C 34.79, H 4.41, N 60.71.

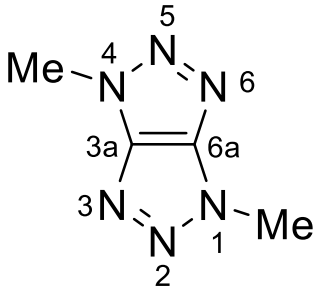

Data for triazolotriazole 7d: DSC (5 °C·min^{-1}): T_m = 188 °C, T_{onset} = 188 °C (dec.). ^{1}H NMR (600.13 MHz, [D$_6$]DMSO): δ = 4.26 (s, 6 H, Me) ppm. ^{13}C NMR (150.9 MHz, [D$_6$]DMSO): δ = 35.1 (Me), 150.6 (C-3a and C-6a) ppm. ^{14}N NMR (43.4 MHz, [D$_6$]DMSO): δ = 4 (N-2 and N-5, $\Delta\nu_{½}$ = 2000 Hz), –57 (N-3 and N-6, $\Delta\nu_{½}$ = 1000 Hz), –186 (N-1 and N-4, $\Delta\nu_{½}$ = 1500 Hz) ppm. ^{15}N NMR ([INVGATED], 60.8 MHz, [D$_6$]DMSO): δ = 7.5 (N-2 and N-5), –71.9 (N-3 and N-6), –172.2 (N-1 and N-4) ppm. ^{15}N NMR ([INEPT], 60.8 MHz, DMSO-d$_6$): δ = 7.5 (q, ^3J = 1.82 Hz, N-2 and N-5), –71.9 (t, ^4J = 0.61 Hz, N-3 and N-6), –172.2 (q, ^2J = 1.82 Hz, N-1 and N-4) ppm. IR (KBr): ν = 3429 (s), 3025 (w), 1495 (m), 1469 (m), 1451 (m), 1355 (s), 1321 (m), 1237 (m), 1155 (s), 1140 (s) cm^{-1}. HRMS (ESI): m/z calcd for $C_4H_6N_6$ $[M + H]^+$ 139.0727; found 139.0725. Elemental analysis calcd (%) for $C_4H_6N_6$: C 34.78, H 4.38, N 60.84; found: C 34.82, H 4.39, N 60.59.

2.11. Synthesis of 1,5-di-*tert*-butyl[1,2,3]triazolo[4,5-*d*][1,2,3]triazole (8) and 1,3,5-tri-*tert*-butyl[1,2,3]triazolo[4,5-*d*][1,2,3]triazol-1-ium perchlorate (9)

*t*BuOH (5.0 mL, 3.875 g, 52.4 mmol) was added dropwise to a solution of 1,4-dihydro[1,2,3]triazolo[4,5-*d*][1,2,3]triazole (TT **1**) (0.55 g, 5.0 mmol) in 70% aqueous $HClO_4$ (5 mL) and the reaction mixture was stirred for 3 h. Then the resulting mixture was poured into mixture of H_2O (50 mL) and EtOAc (50 mL). The precipitate formed was then filtered off, washed with H_2O (2 × 10 mL) and dried under reduced pressure to give perchlorate **9** (0.49 g, 26%) as a white solid. The combined filtrates were extracted with EtOAc (5 × 10 mL), washed with H_2O (3 × 15 mL) and brine (2 × 10 mL), dried with Na_2SO_4, and concentrated under reduced pressure at 35 °C. The residue was purified by preparative thin-layer chromatography on silica gel (petroleum ether/EtOAc, 5:1, R_f = 0.55) to give triazolotriazole **8** (0.59 g, 53%) as white crystals, m.p. 97–98 °C.

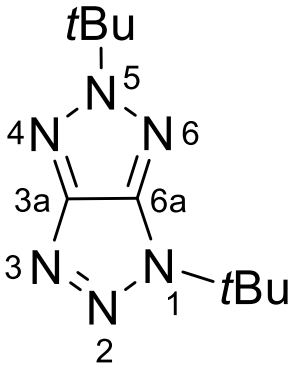

Data for triazolotriazole 8: DSC (5 °C·min^{-1}): T_m = 96 °C, T_{onset} = 236 °C (dec.). ^{1}H NMR (500.13 MHz, $CDCl_3$): δ = 1.78 (s, 9 H, *t*Bu), 1.81 (s, 9 H, *t*Bu) ppm. ^{13}C NMR (125.8 MHz, $CDCl_3$): δ = 28.6 (C*Me*$_3$), 29.3 (C*Me*$_3$), 59.5 (*C*Me$_3$), 65.4 (*C*Me$_3$), 144.7 (C-6a), 160.5 (C-3a) ppm. IR (KBr): ν = 2986 (s), 2940 (m), 2878 (w), 1568 (m), 1464 (s) 1373 (s), 1330 (m), 1226 (s), 1192 (s), 1167 (s), 1110 (s), 1072 (s), 1006 (s) cm^{-1}. HRMS (ESI): m/z calcd for $C_{10}H_{18}N_6$ $[M + H]^+$ 223.1666; found 223.1660. Elemental analysis calcd (%) for $C_{14}H_{26}N_6$: C 60.40, H 9.41, N 30.19; found: C 60.45, H 9.45, N 30.15.

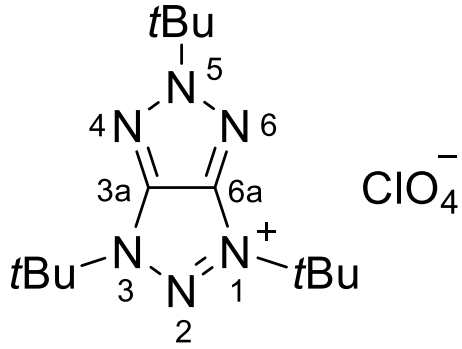

Data for salt 9: DSC (5 °C·min^{-1}): T_{onset} = 210 °C (dec.). ^{1}H NMR (500.16 MHz, [D_4]methanol): δ = 1.88 (s, 9 H, *t*Bu), 1.93 (s, 18 H, *t*Bu) ppm. ^{13}C NMR (125.8 MHz, [D_4]methanol): δ = 29.2 (C*Me*$_3$), 29.3 (C*Me*$_3$), 67.3 (*C*Me$_3$), 69.5 (*C*Me$_3$), 147.6 (C-3a and C-6a) ppm. IR (KBr): ν = 2991 (m), 1464 (w), 1378 (m), 1345 (m), 1243 (w),

1197 (m), 1170 (s), 1096 (s) cm^{-1}. Elemental analysis calcd (%) for $C_{14}H_{27}N_6O_4Cl$: C 44.38, H 7.18, N 22.18; found: C 44.43, H 7.22, N 22.15.

2.12. Synthesis of 1,3,5-tri-tert-butyl[1,2,3]triazolo[4,5-d][1,2,3]triazol-1-ium perchlorate (9) from 1,4-dihydro-[1,2,3]triazolo[4,5-d][1,2,3]triazole (TT 1).

*t*BuOH (5.0 mL, 3.875 g, 52.4 mmol) was added dropwise to a solution of 1,4-dihydro[1,2,3]triazolo[4,5-*d*][1,2,3]triazole (TT **1**) (1.00 g, 9.1 mmol) in 70% aqueous $HClO_4$ (5 mL) at 25 °C. The reaction mixture was vigorously stirred at this temperature for 24 h. Then the resulting mixture was poured into mixture of H_2O (100 mL) and EtOAc (100 mL). The precipitate formed was then filtered off, washed with H_2O (2 × 10 mL) and dried under reduced pressure. Salt **9** (2.03 g, 60%) was obtained as a white solid, identical (^1H, ^{13}C NMR) to the product prepared according to the procedure above.

2.13. Synthesis of 4-amino-5-(morpholinodiazenyl)-2*H*-1,2,3-triazole (11)

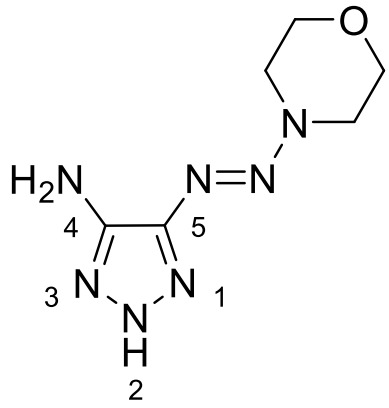

The solution of morpholine (1.9 mL, 16.4 mmol) in MeCN (5 mL) was added dropwise to the suspension of 5-amino-1*H*-1,2,3-triazol-4-diazonium chloride (**4**) (1.60 g, 10.9 mmol) in MeCN (10 mL) at 25 °C. The reaction mixture was vigorously stirred at this temperature for 2 days. Then the resulting mixture was poured into H_2O (50 mL) and extracted with EtOAc (5 × 20 mL). The combined organic extracts were washed with water (25 mL), brine (25 mL), dried with anhydrous Na_2SO_4 and concentrated under reduced pressure to give triazene **11** (1.14 g, 53%) as a beige solid, m.p. 119–120 °C (dec.).

^1H NMR (600.13 MHz, [D_6]DMSO): δ = 3.61 (t, $^3J_{H,H}$ = 5.0 Hz, 4 H, NCH_2), 3.74 (t, $^3J_{H,H}$ = 5.0 Hz, 4 H, OCH_2), 5.26 (br. s, 2 H, NH_2) ppm. ^{13}C NMR (150.9 MHz, [D_6]DMSO): δ = 47.5 (NCH_2), 65.5 (OCH_2), 139.9 (C-4), 141.3 (C-5) ppm. IR (KBr): ν = 3461 (m), 3324 (s), 2964 (w), 1638 (m), 1608 (s), 1439 (s), 1353 (m), 1173 (m), 1114 (s), 1017 (m) cm^{-1}. HRMS (ESI): m/z calcd for $C_6H_{11}N_7O$ $[M + H]^+$ 198.1098; found 198.1104. Elemental

analysis calcd (%) for $C_6H_{11}N_7O$: C 36.54, H 5.62, N 49.72; found: C 36.58, H 5.67, N 49.62.

2.14. Synthesis of 4-amino-2-methyl-5-(morpholinodiazenyl)-2*H*-1,2,3-triazole (12)

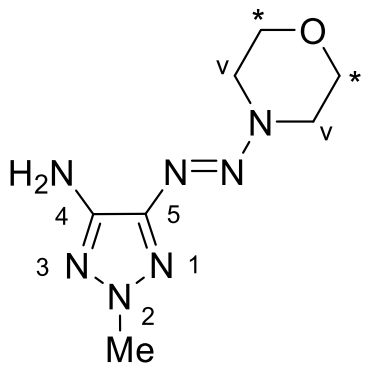

Diazomethane solution in Et_2O (50 mL), obtained from *N*-methyl-*N*-nitrosourea (3.12 g, 30.3 mmole) according to the literature method,[5] was added dropwise (for 30 min) to a suspension of triazene **11** (1.14 g, 5.79 mmol) in EtOAc (50 mL) at 0 °C. The reaction mixture was vigorously stirred at this temperature for 5 h. Then the resulting mixture was concentrated under reduced pressure at 30 °C. The residue was purified by preparative thin-layer chromatography on silica gel (EtOAc, R_f (**12**) = 0.5) to give triazene **12** (0.77 g, 63%) as a yellow solid, m.p. 112–113 °C (dec.).

^{1}H NMR (600.13 MHz, [D$_6$]acetone) δ = 3.66 (t, $^3J_{H,H}$ = 5.0 Hz, 4 H, NCH_2), 3.80 (t, $^3J_{H,H}$ = 5.0 Hz, 4 H, OCH_2), 3.89 (s, 3 H, Me), 4.98 (br. s, 2 H, NH_2) ppm. ^{13}C NMR (150.9 MHz, acetone-d$_6$) δ = 41.6 (Me), 48.6 (NCH_2), 66.9 (OCH_2), 141.7 (C-4 or C-5), 144.0 (C-5 and C-4) ppm. IR (KBr): ν = 3448 (s), 3298 (s), 3199 (w), 2961 (w), 2924 (w), 2868 (w), 1614 (s), 1541 (m), 1433 (s), 1368 (w), 1345 (s), 1200 (w), 1175 (s), 1116 (s) cm^{-1}. HRMS (ESI): m/z calcd for $C_7H_{13}N_7O$ $[M + H]^+$ 212.1254; found 212.1262. Elemental analysis calcd (%) for $C_7H_{13}N_7O$: C 39.80, H 6.20, N 46.42; found: C 39.83, H 6.24, N 46.33.

2.15. Synthesis of 4-azido-2-methyl-5-(morpholinodiazenyl)-2*H*-1,2,3-triazole (13)

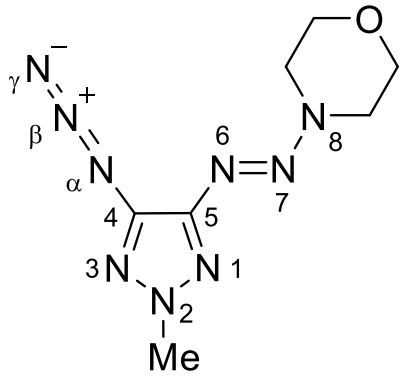

$NOBF_4$ (386 mg, 3.3 mmol) was added in one portion to the solution of triazole **11** (633 g, 3.0 mmol) in dry MeCN (20 mL) at 0 °C under an argon atmosphere. The reaction mixture was stirred at this temperature for 1 h and then was added dropwise (for 10 min) to the solution of NaN_3 (0.975 g, 15.0 mmol) in H_2O (10 mL) at 0 °C. The resulting mixture was extracted with CH_2Cl_2 (3

× 25 mL). The combined organic extracts were washed with water (25 mL), brine (25 mL), dried with anhydrous Na_2SO_4 and concentrated under reduced pressure. The residue was purified by preparative thin-layer chromatography on silica gel (petroleum ether/EtOAc, 5:1, R_f = 0.09) to give azidotriazole **13** (554 mg, 78%) as a pale-yellow solid.

DSC (5 °C·min^{-1}): T_m = 69 °C, T_{onset} = 110 °C (dec.). ^{1}H NMR (600.13 MHz, [D$_6$]acetone): δ = 3.71–3.92 (m, 8 H, NCH_2 and OCH_2), 4.07 (s, 3 H, Me) ppm. ^{13}C NMR (150.9 MHz, [D$_6$]acetone): δ = 41.6 (Me), 43.9 (CH_2), 51.7 (CH_2), 65.2 (CH_2), 66.6 (CH_2), 134.8 (C-4 or C-5), 146.0 (C-5 or C-4) ppm. ^{14}N NMR (43.4 MHz, [D$_6$]acetone): δ = 77 (N-7, $\Delta\nu_{½}$ = 1000 Hz), –45 (N-1, N-3, N-6, $\Delta\nu_{½}$ = 2400 Hz), –138 (N-β, $\Delta\nu_{½}$ = 150 Hz), –149 (N-γ, $\Delta\nu_{½}$ = 500 Hz), –210 (N-8, $\Delta\nu_{½}$ = 900 Hz), –302 (N-α, $\Delta\nu_{½}$ = 1800 Hz) ppm. ^{15}N NMR (60.8 MHz, [D$_6$]acetone): δ = 76.6 (N-7), –41.1 (N-6), –60.1 (N-1 or N-3), –64.7 (N-3 or N-1), –137.8 (N-β), –148.3 (N-γ), –151.0 (N-2), –209.2 (N-8), –302.8 (N-α) ppm. IR (KBr): ν = 2962 (w), 2935 (w), 2874 (w), 2129 (s), 1504 (m), 1435 (s), 1370 (m), 1294 (s), 1263 (w), 1203 (m), 1185 (s), 1118 (s) cm^{-1}. HRMS (ESI): m/z calcd for $C_7H_{11}N_9O$ [M + H]$^+$ 238.1159; found 238.1162. Elemental analysis calcd (%) for $C_7H_{11}N_9O$: C 35.44, H 4.67, N 53.14; found: C 35.48, H 4.71, N 53.10.

2.16. Synthesis of 2-methyl-5-morpholino-2*H*-[1,2,3]triazolo[4,5-*d*][1,2,3]triazol-5-ium-4-ide (10)

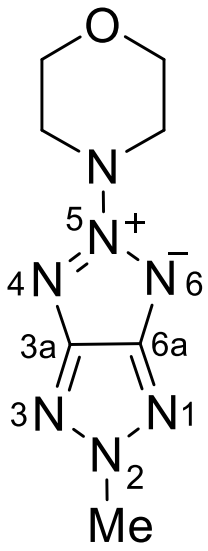

The solution of azidotriazole **13** (555 mg, 2.34 mmol) in toluene (20 mL) was refluxed for 5 h. Then the reaction mixture was concentrated under reduced pressure at 35 °C and the residue was purified by preparative thin-layer chromatography on silica gel (petroleum ether/EtOAc, 5:1, R_f = 0.22) to give triazolo-triazole **10** (240 mg, 49%) as a white solid.

DSC (5 °C·min^{-1}): T_m = 164 °C, T_{onset} = 245 °C (dec.). ^{1}H NMR (600.13 MHz, $CDCl_3$) δ = 3.59 (t, $^3J_{H,H}$ = 6.0 Hz, 4 H, NCH_2), 3.96 (t, $^3J_{H,H}$ = 6.0 Hz, 4 H, OCH_2), 4.47 (s, 3 H, Me) ppm. ^{13}C NMR (150.9 MHz, $CDCl_3$) δ = 44.2 (Me), 55.5 (NCH_2), 66.1 (OCH_2), 154.9 (C-3a and C-6a) ppm. ^{14}N NMR (43.4 MHz, $CDCl_3$): δ = –78 (N-1, N-3, N-4, N-6, $\Delta\nu_{½}$ = 1300 Hz), –

110 (N-2 and N-5, $\Delta\nu_{½}$ = 400 Hz) ppm. ^{15}N NMR (60.8 MHz, $CDCl_3$): δ = –77.5 (N-1, N-3, N-4, N-6), –77.8 (N-1, N-3, N-4, N-6), –89.6 (N-5), –110.5 (N-2), –257.4 (morpholine) ppm. IR (KBr): ν = 2989 (w), 2976 (w), 2929 (w), 2873 (w), 2360 (w), 2340 (w), 1338 (m), 1322 (m), 1246 (m), 1207 (w), 1141 (w), 1113 (s) cm^{-1}. HRMS (ESI): m/z calcd for $C_7H_{11}N_7O$ $[M + H]^+$ 210.1098; found 210.1107. Elemental analysis calcd (%) for $C_7H_{11}N_7O$: C 40.19, H 5.30, N 46.87; found: C 40.22, H 5.34, N 46.80.

3. NMR Data

3.1.1. ^{1}H NMR spectrum of TT 1

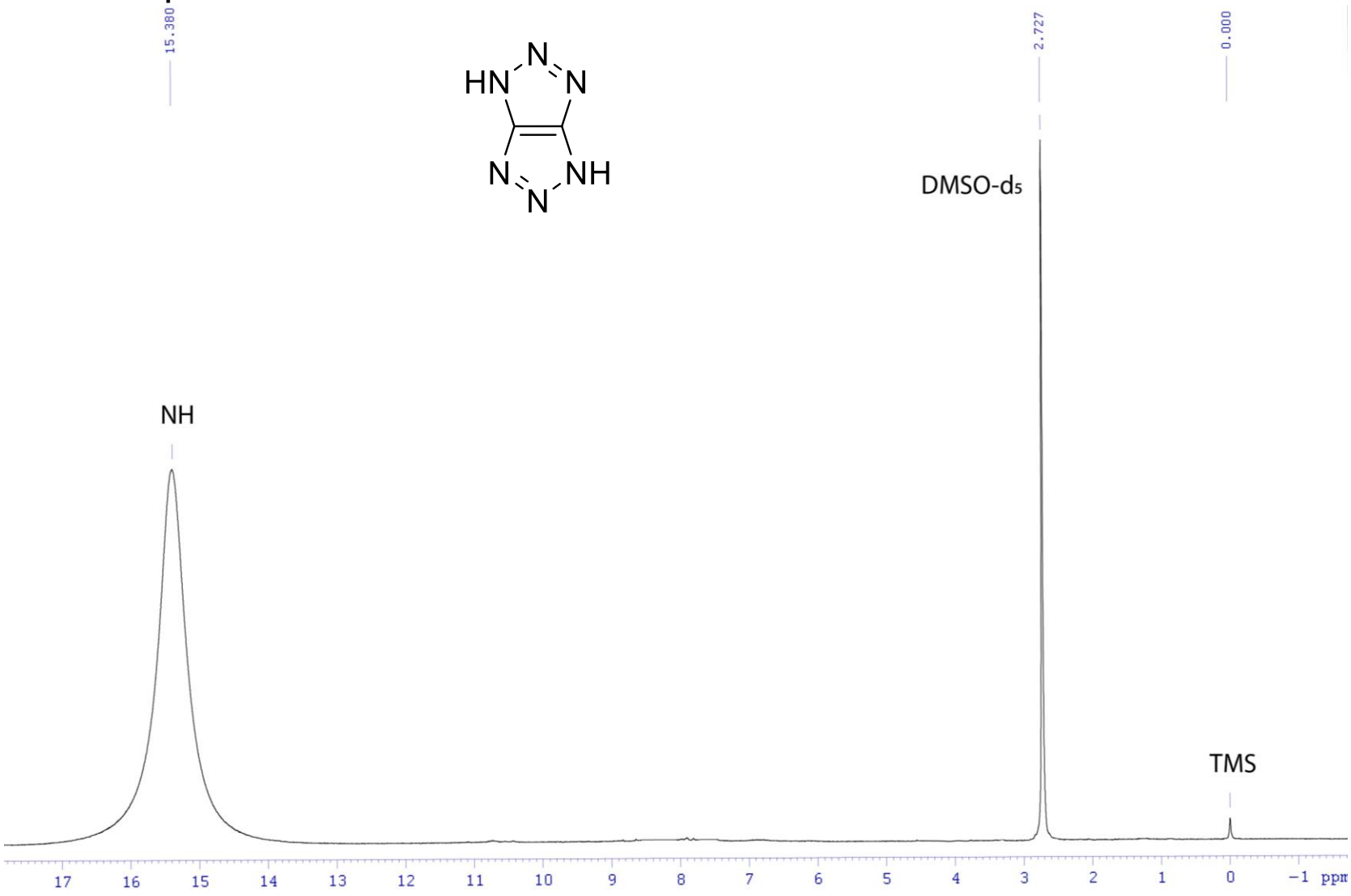

3.1.2. ^{13}C NMR spectrum of TT 1

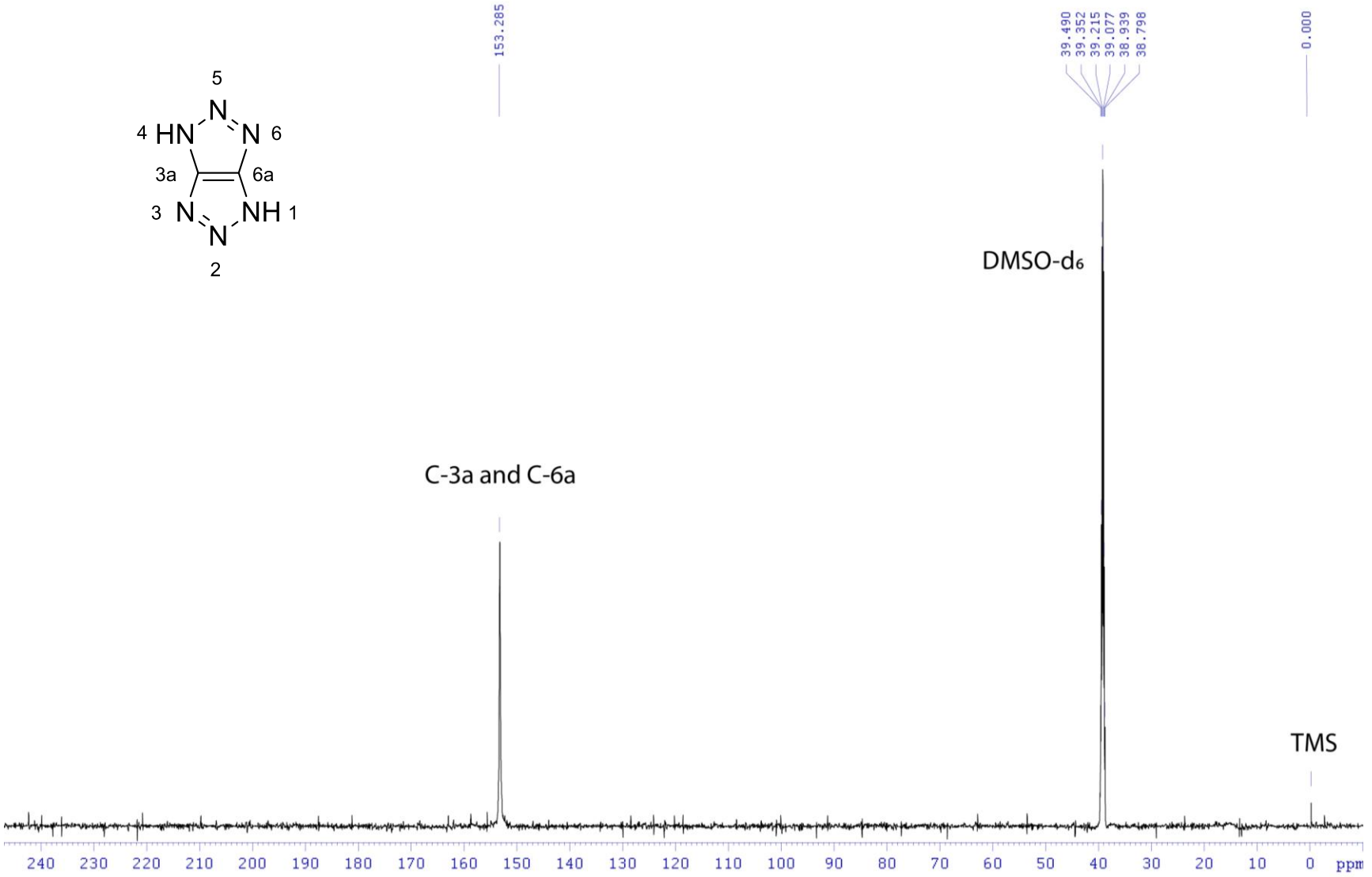

3.1.3. ^{15}N NMR [INVGATED] spectrum of TT 1

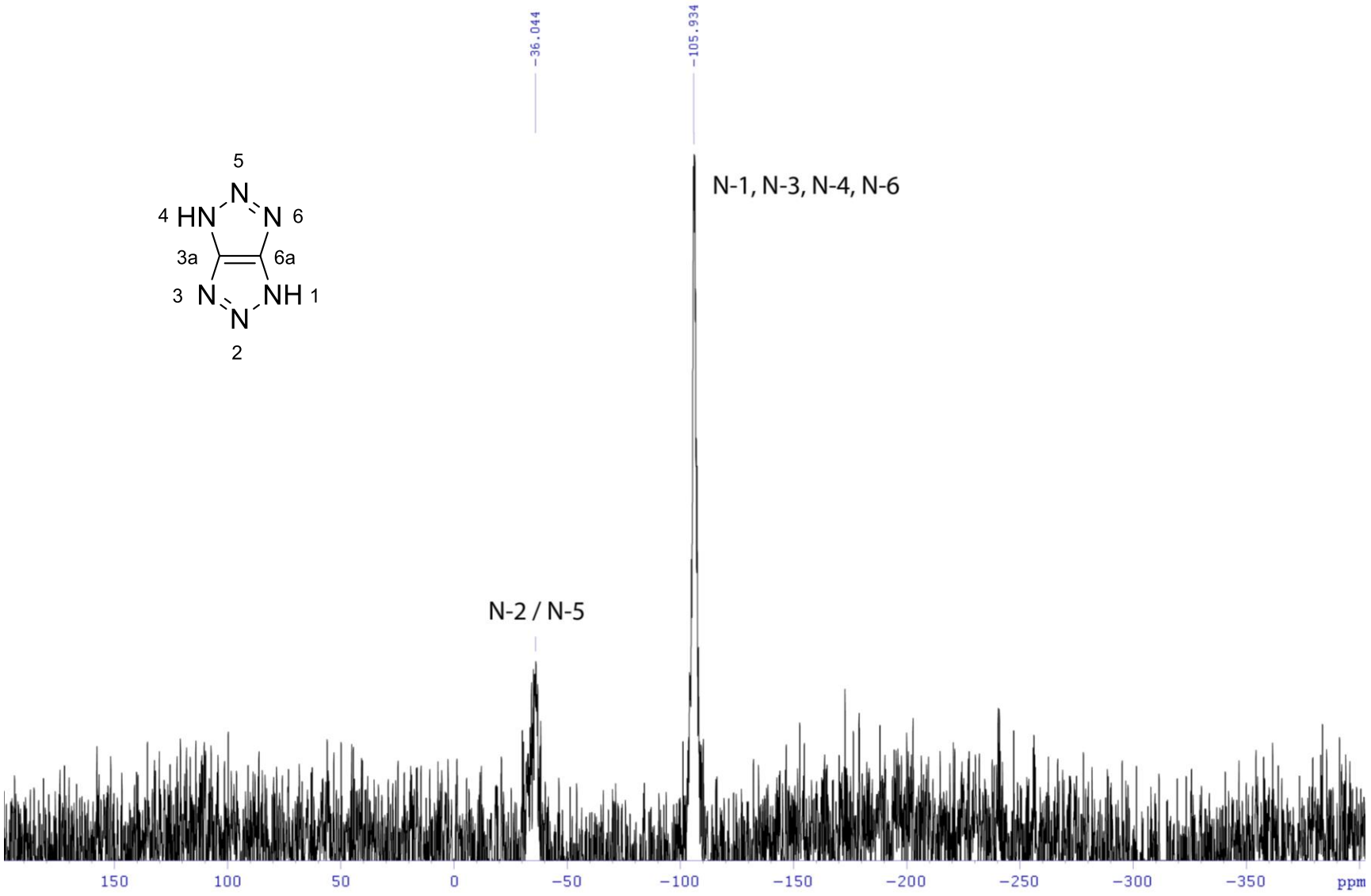

3.1.4. Solid-state ^{1}H NMR spectrum of TT 1

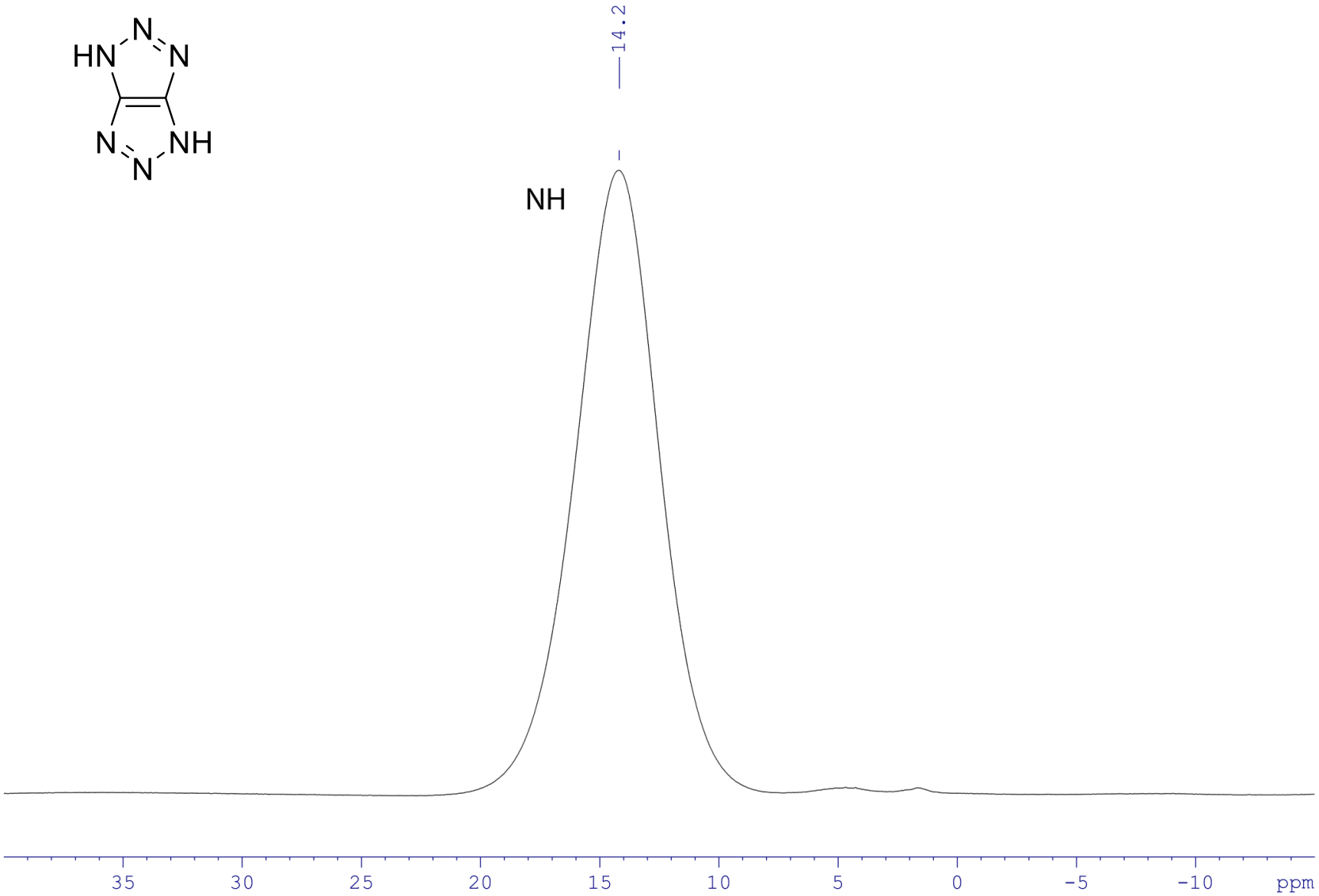

3.1.5. Solid-state ^{13}C NMR spectrum of TT 1

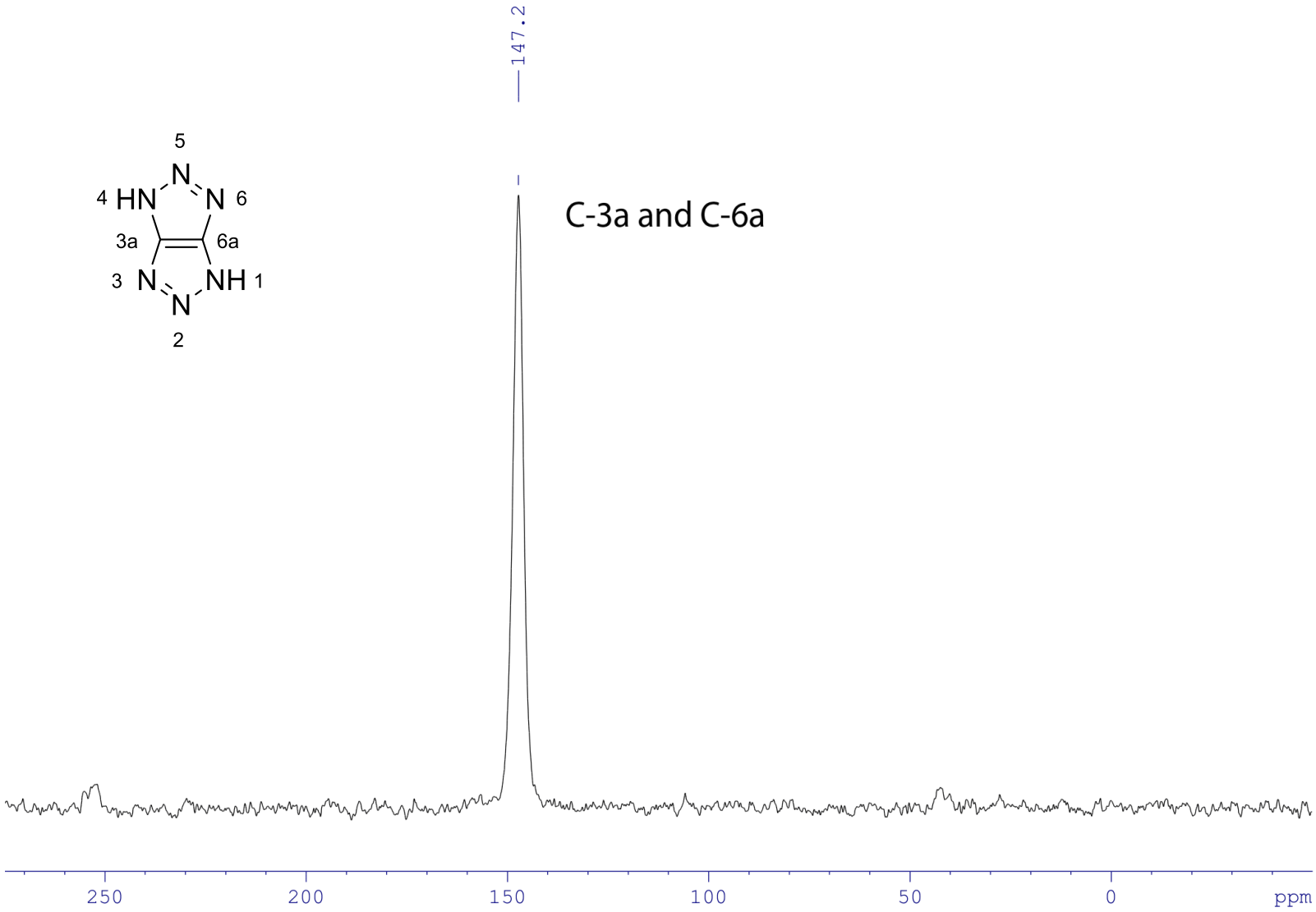

3.1.6. Solid-state ^{15}N NMR spectrum of TT 1 (9.5 kHz MAS, 3 msec CP)

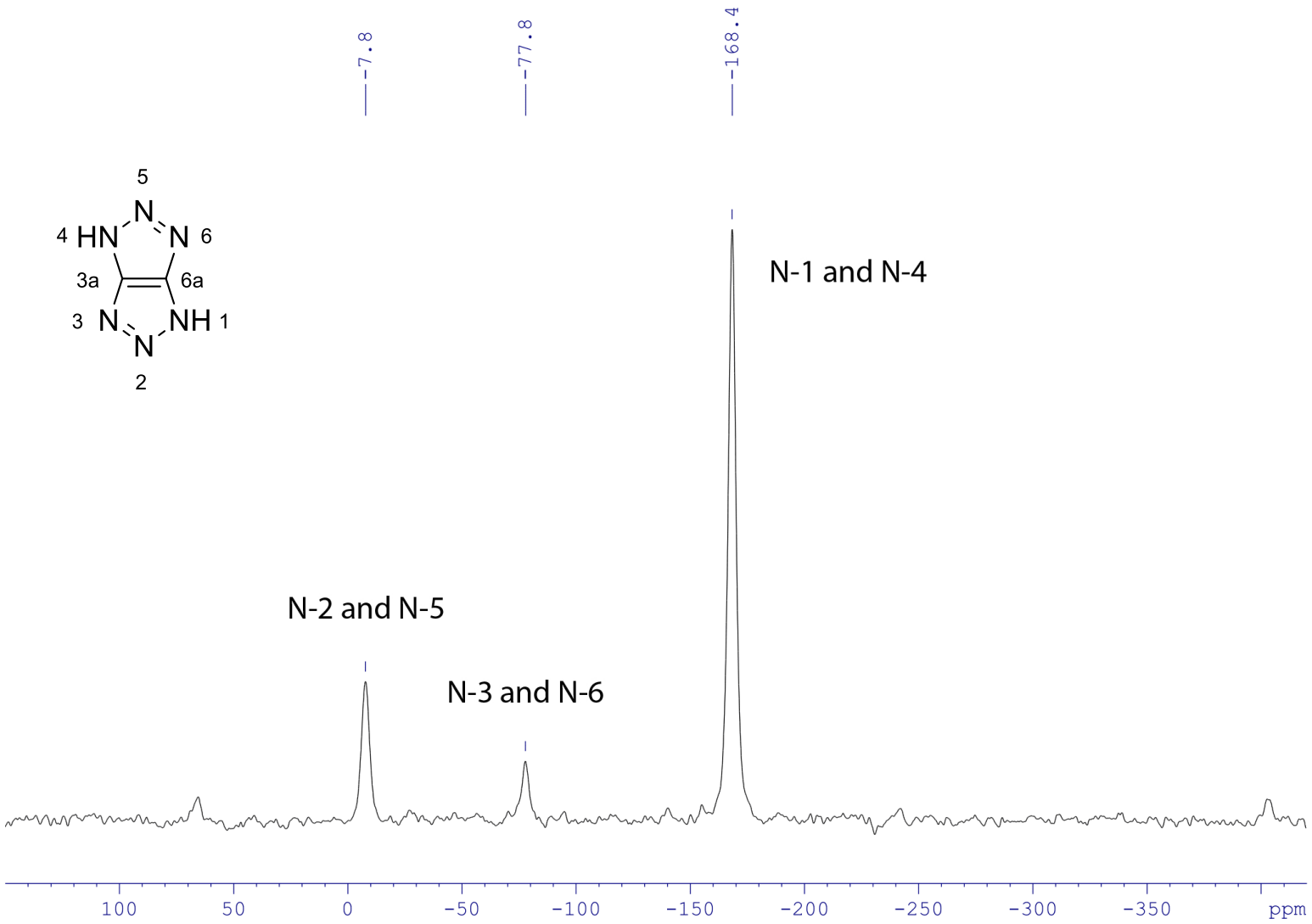

3.1.7. Solid-state ^{15}N NMR spectrum of TT 1 (9.5 kHz MAS, 18 msec CP)

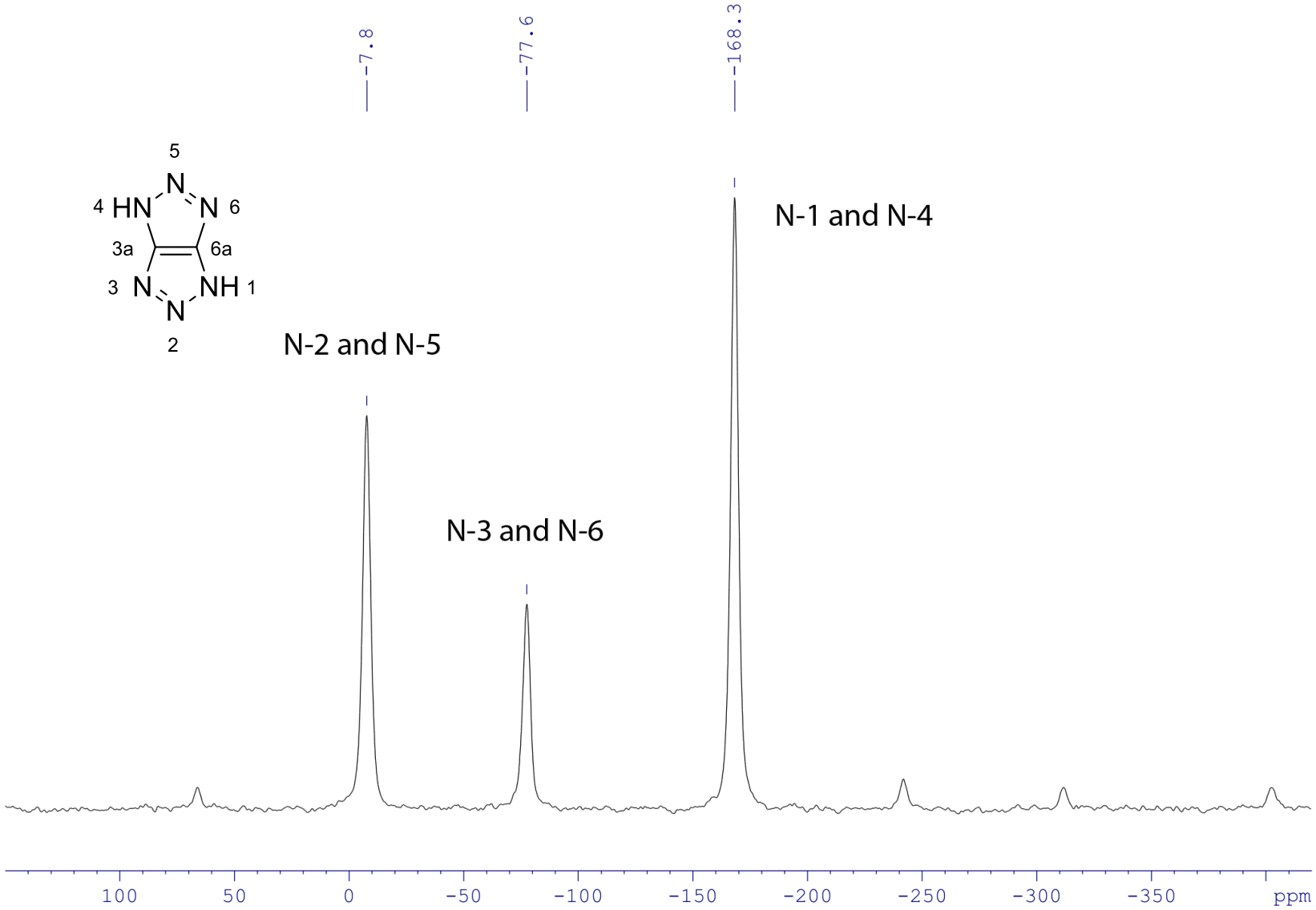

3.1.8. Solid-state {^{1}H–^{15}N} HMBS spectrum of TT 1 (1 msec CP)

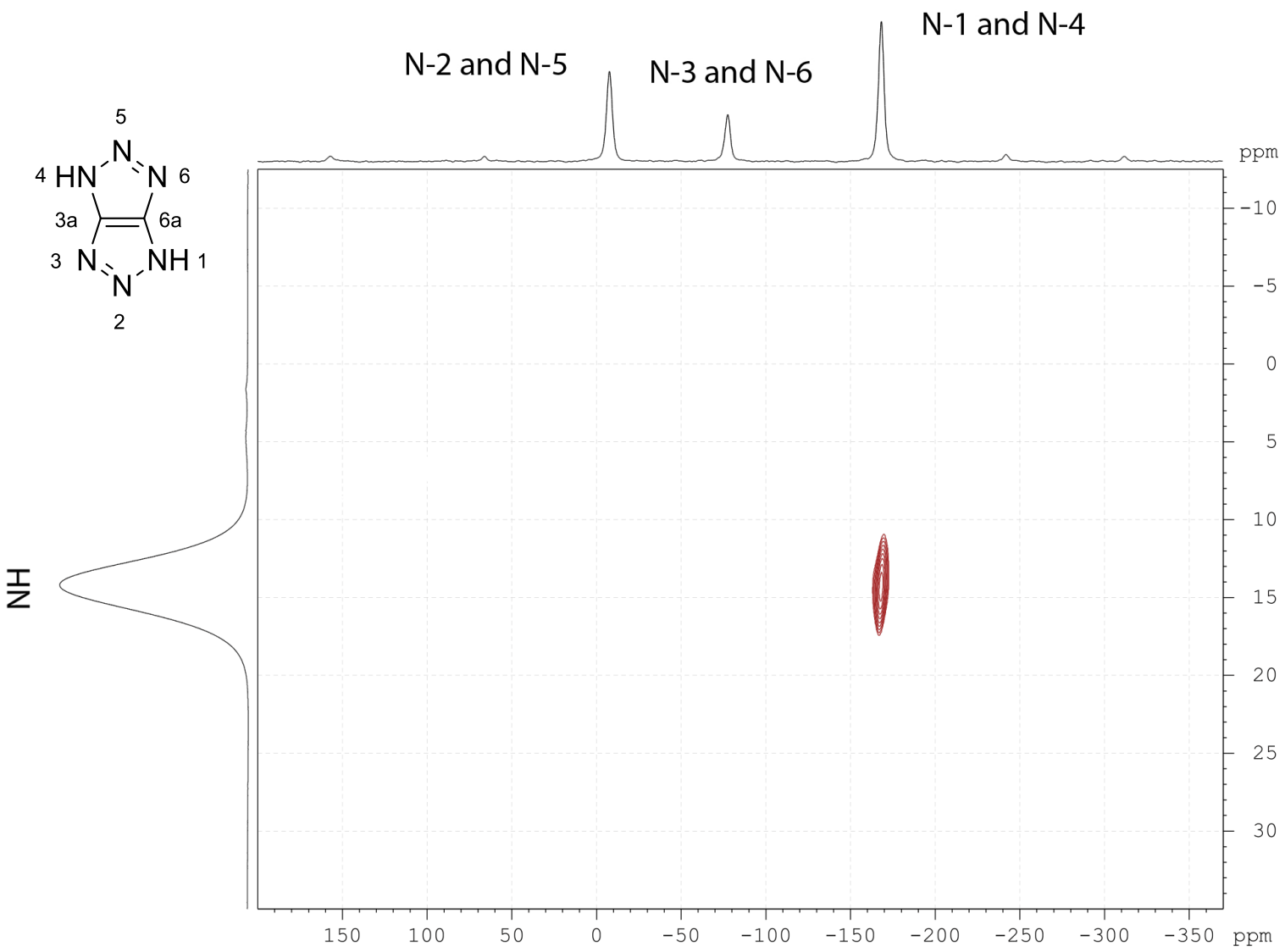

3.1.9. Solid-state {^{1}H–^{15}N} HMBS spectrum of TT 1 (6 msec CP)

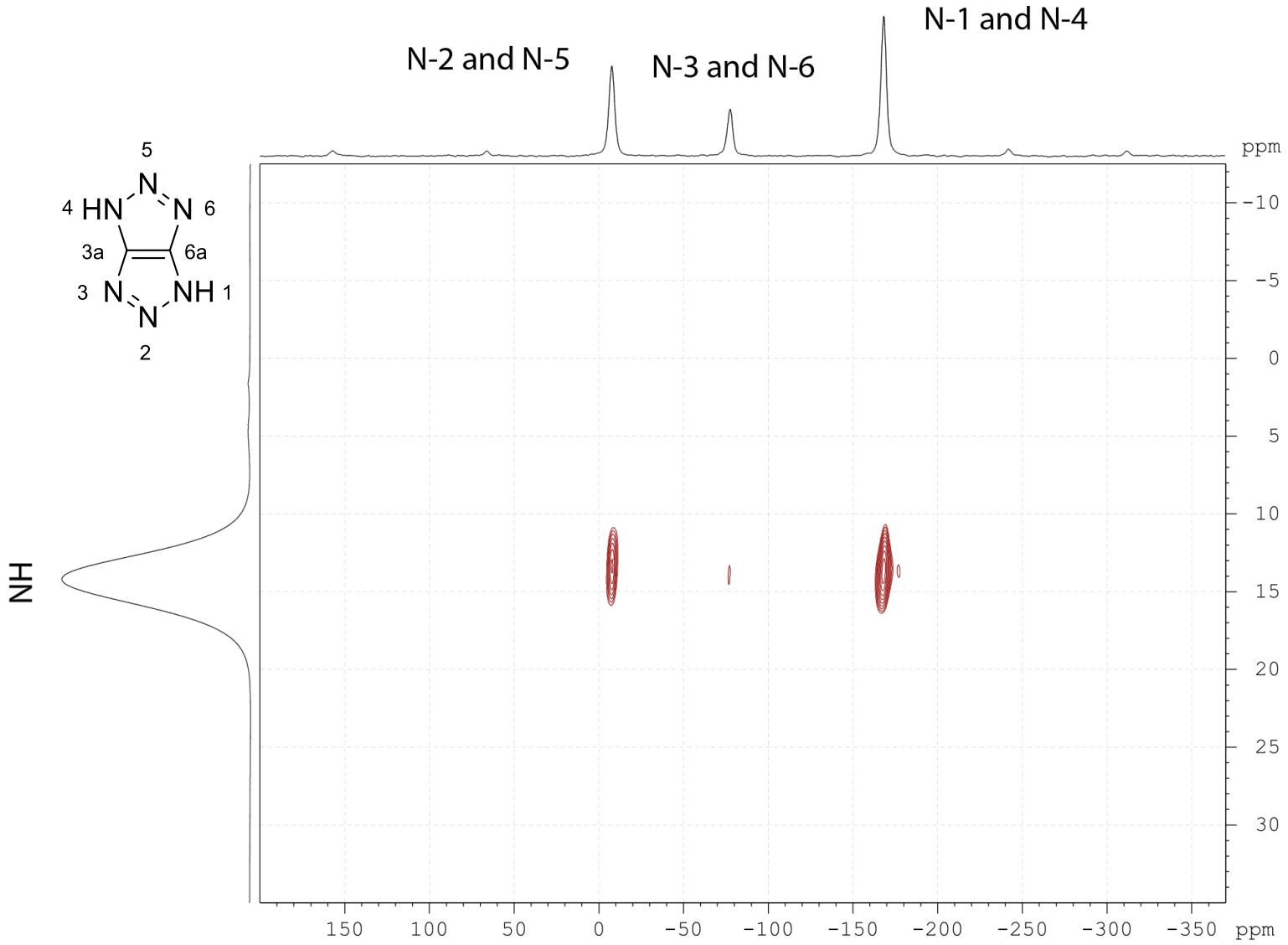

3.2.1. ^{1}H NMR spectrum of diazotriazole 3

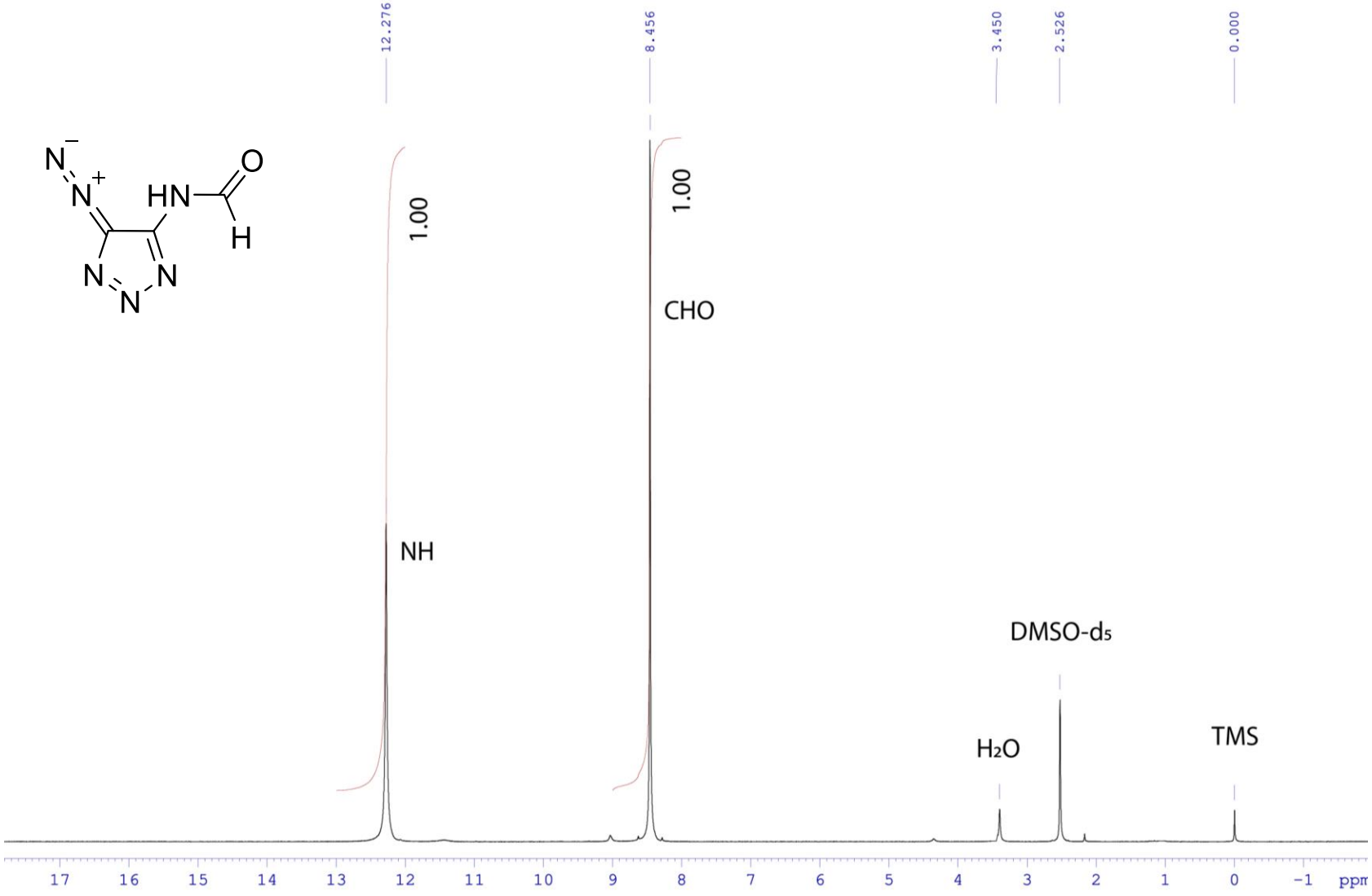

3.2.2. ^{13}C NMR spectrum of diazotriazole 3

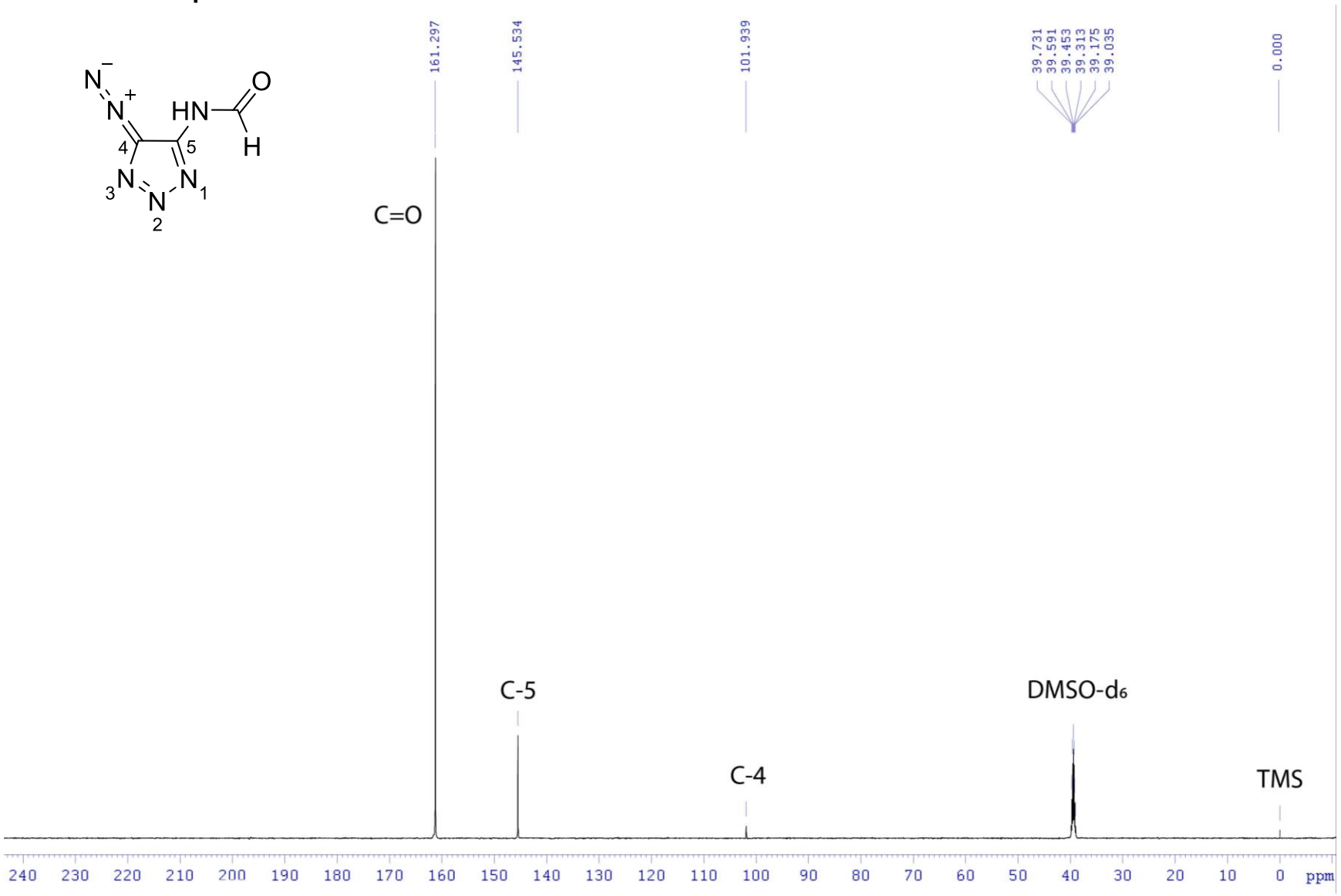

3.2.3. {^{1}H–^{13}C} HSQC spectrum of diazotriazole 3

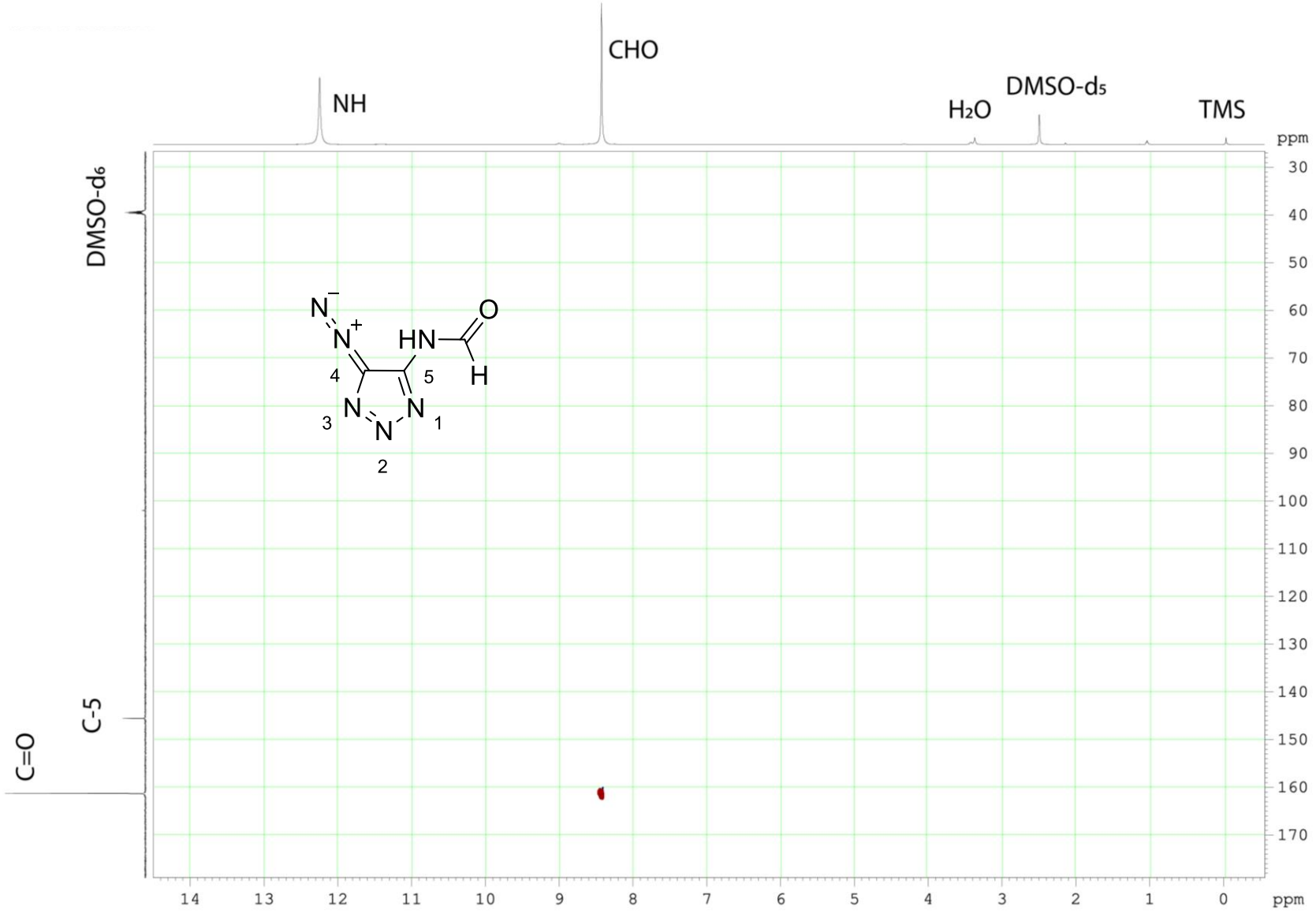

3.2.4. {^{1}H–^{13}C} HMBC spectrum of diazotriazole 3

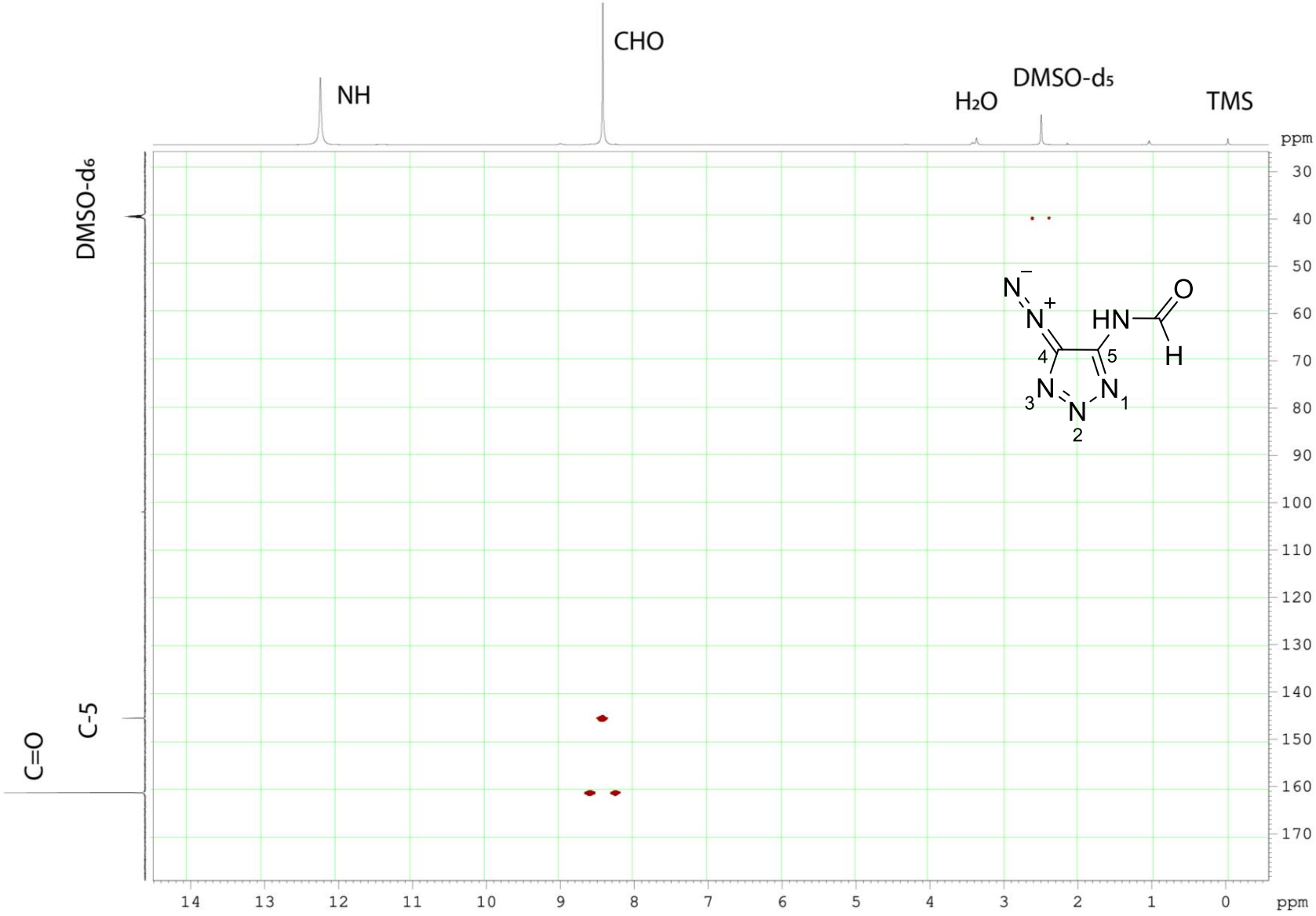

3.2.5. ^{14}N NMR spectrum of diazotriazole 3

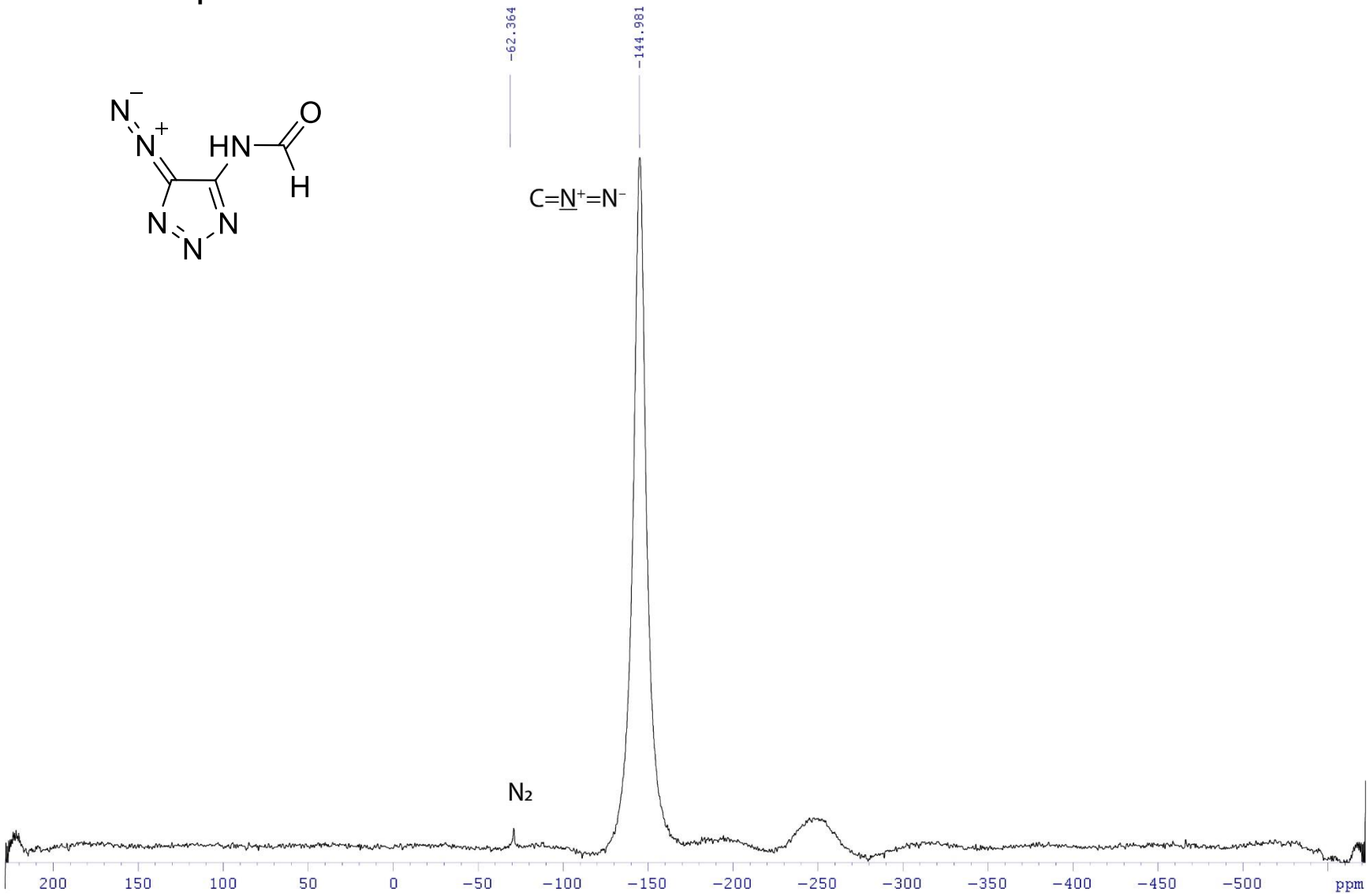

3.2.6. ^{15}N NMR [INVGATED] spectrum of diazotriazole 3

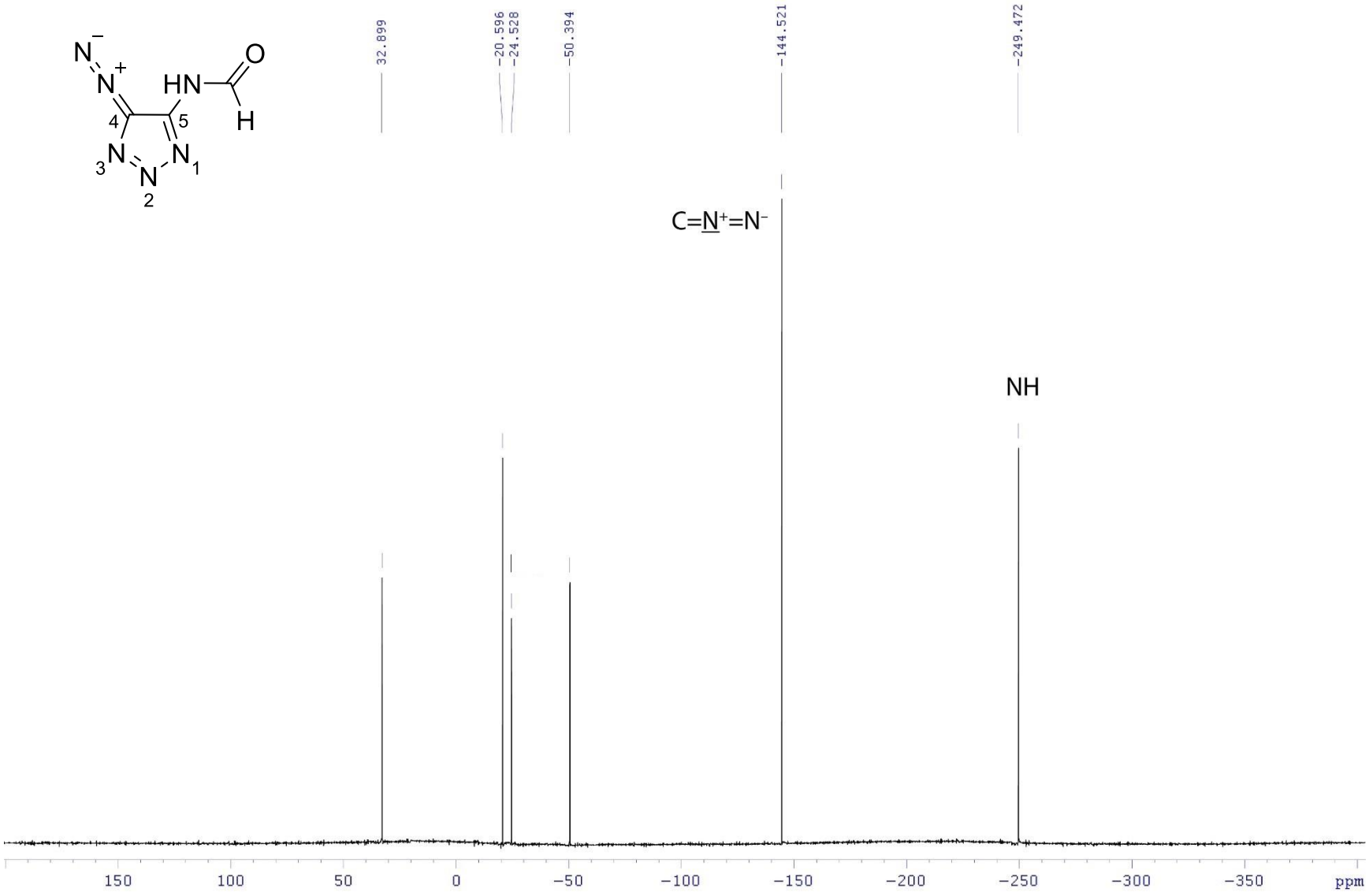

3.3.1. ^{1}H NMR spectrum of diazonium salt 4

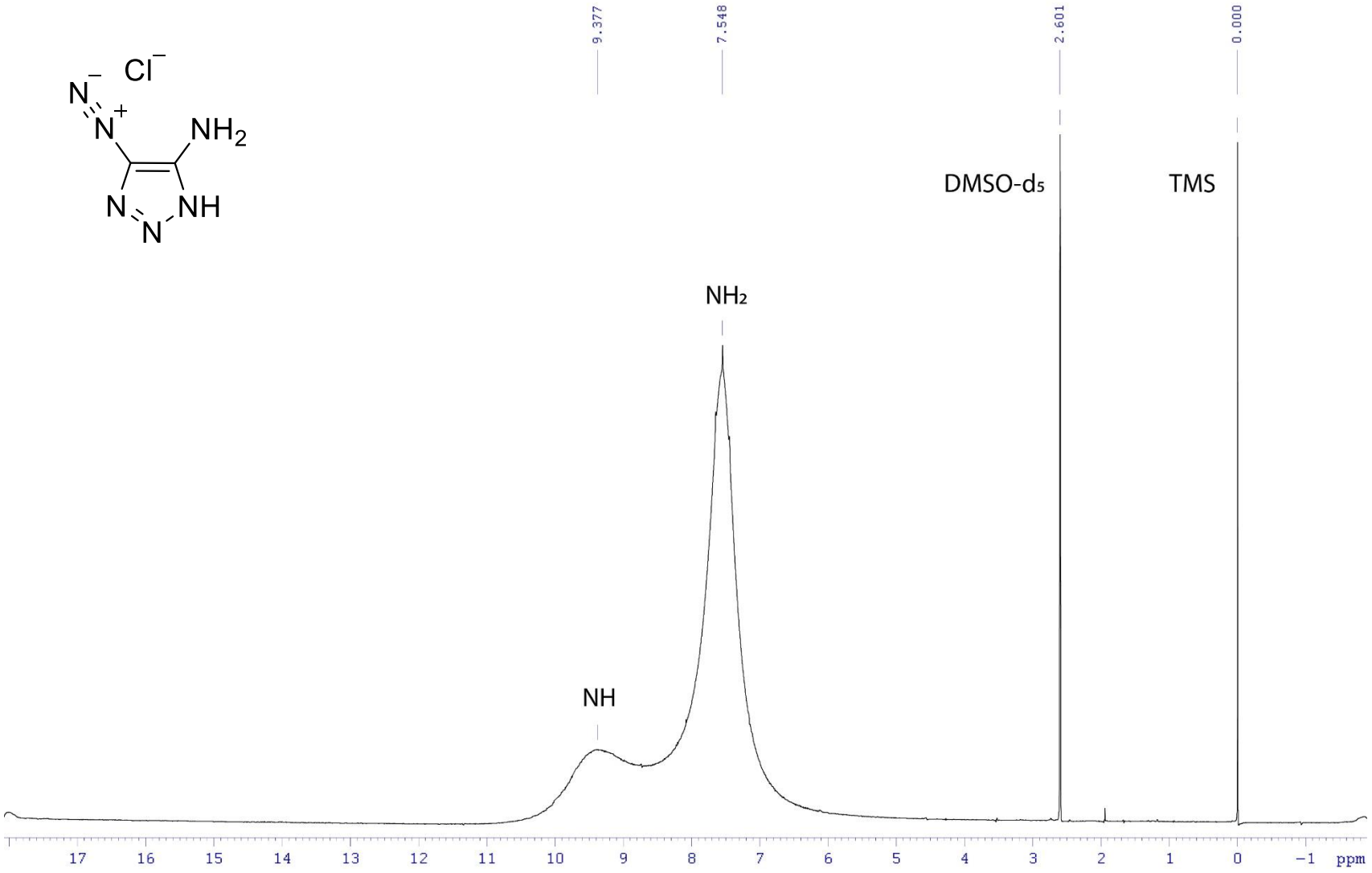

3.3.2. ^{13}C NMR spectrum of diazonium salt 4

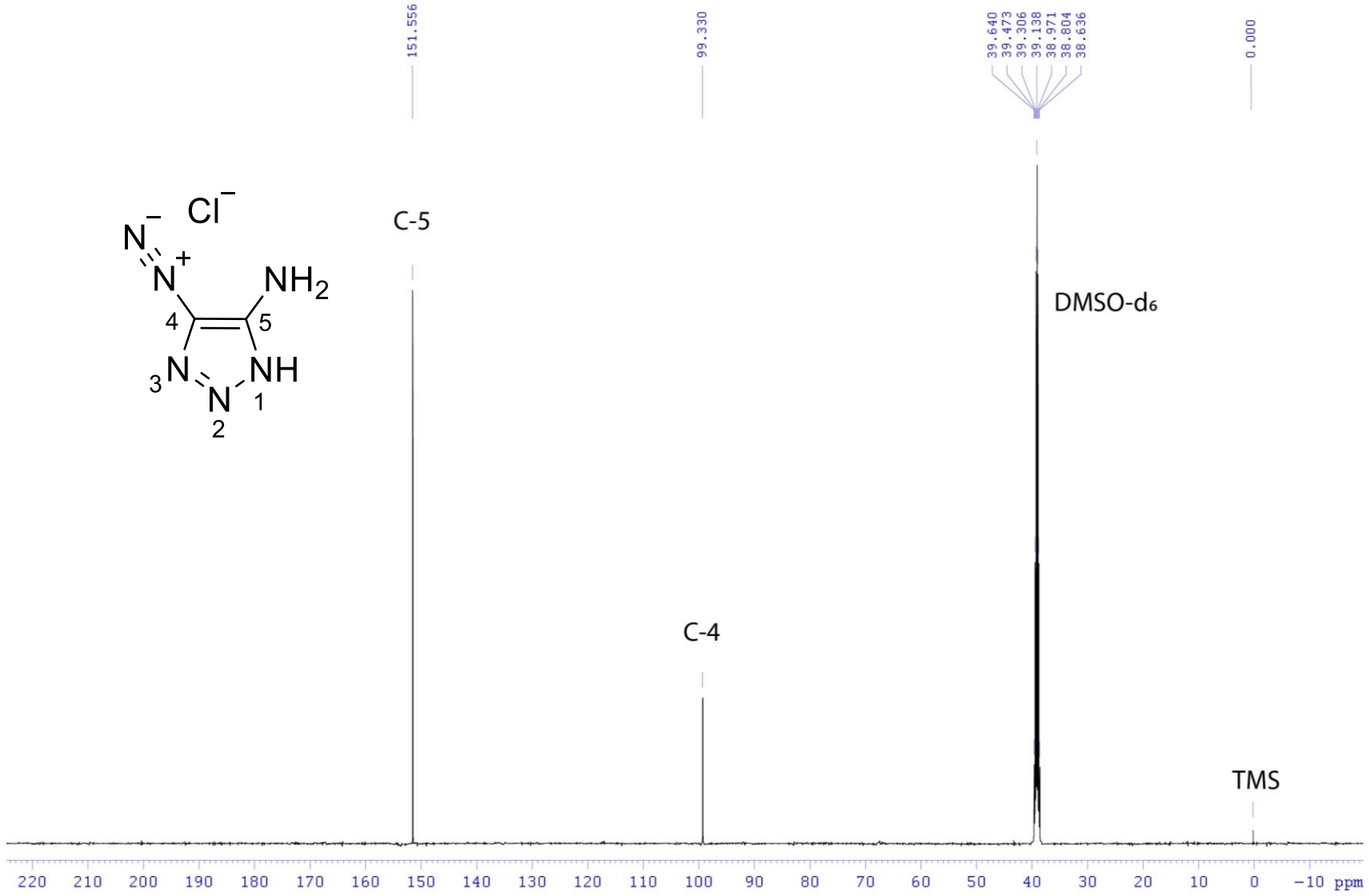

3.3.3. ^{14}N NMR spectrum of diazonium salt 4

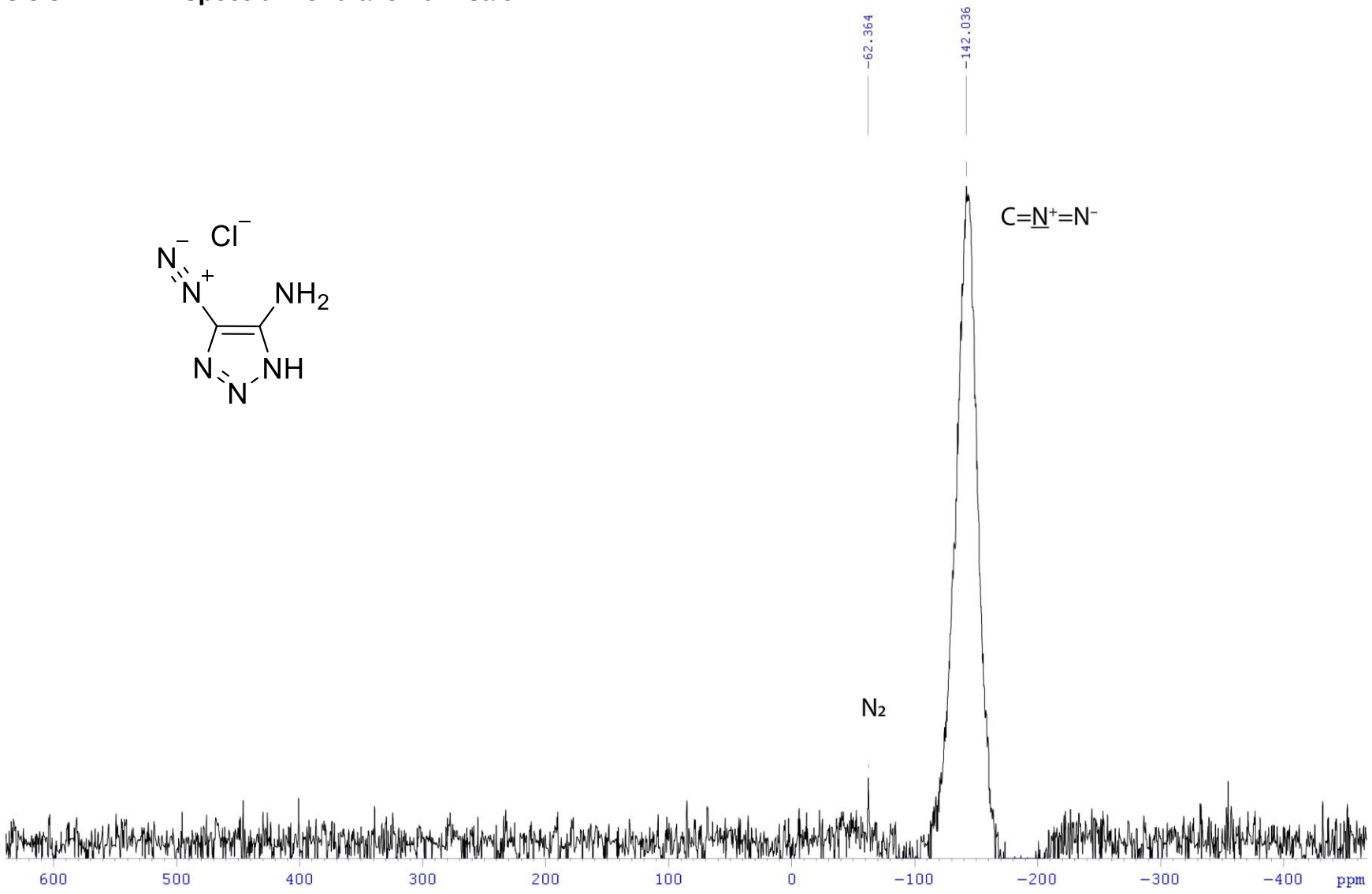

3.3.4. ^{15}N NMR [INVGATED] spectrum of diazonium salt 4

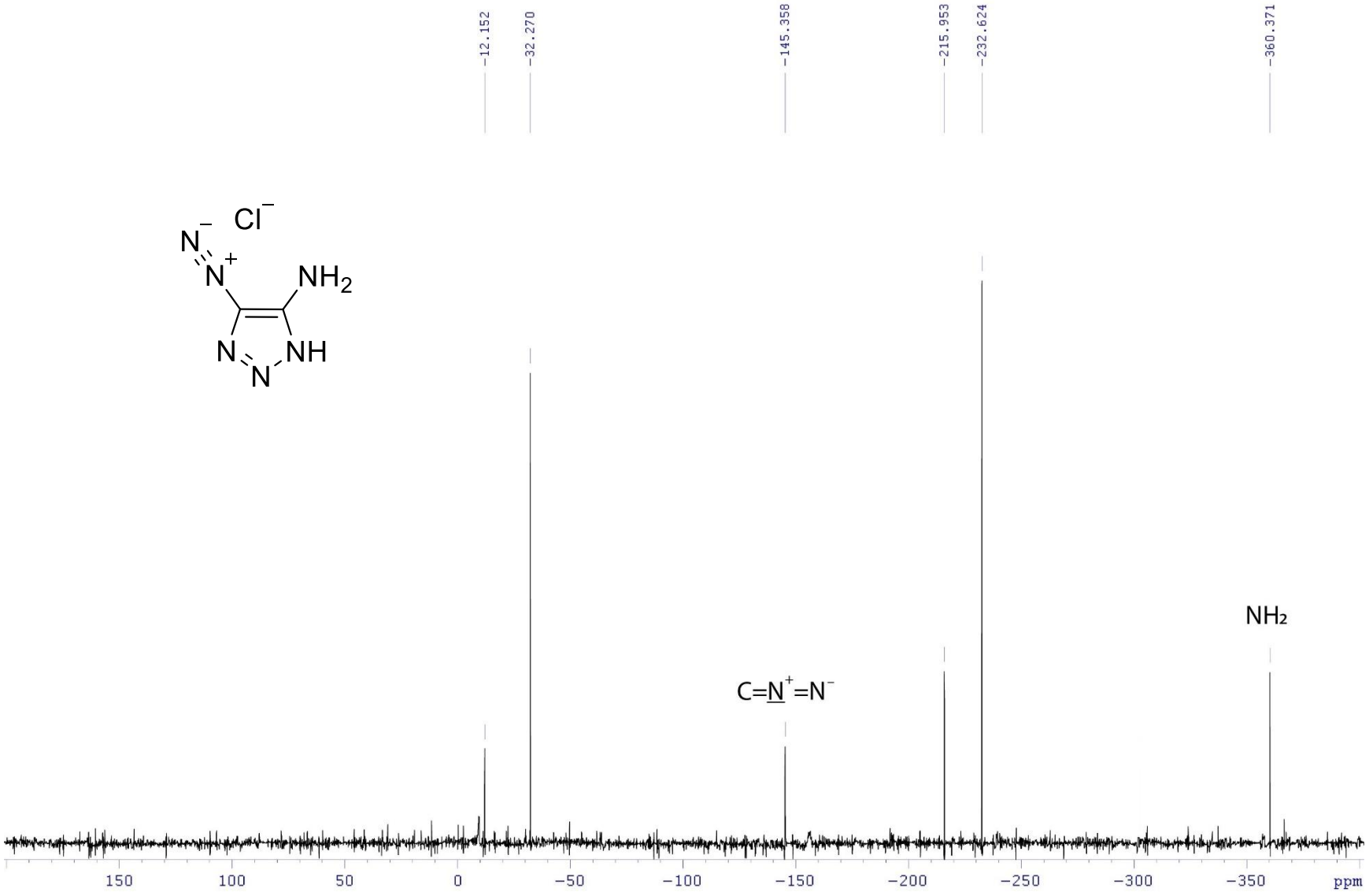

3.4.1. ^{13}C NMR spectrum of compound 5

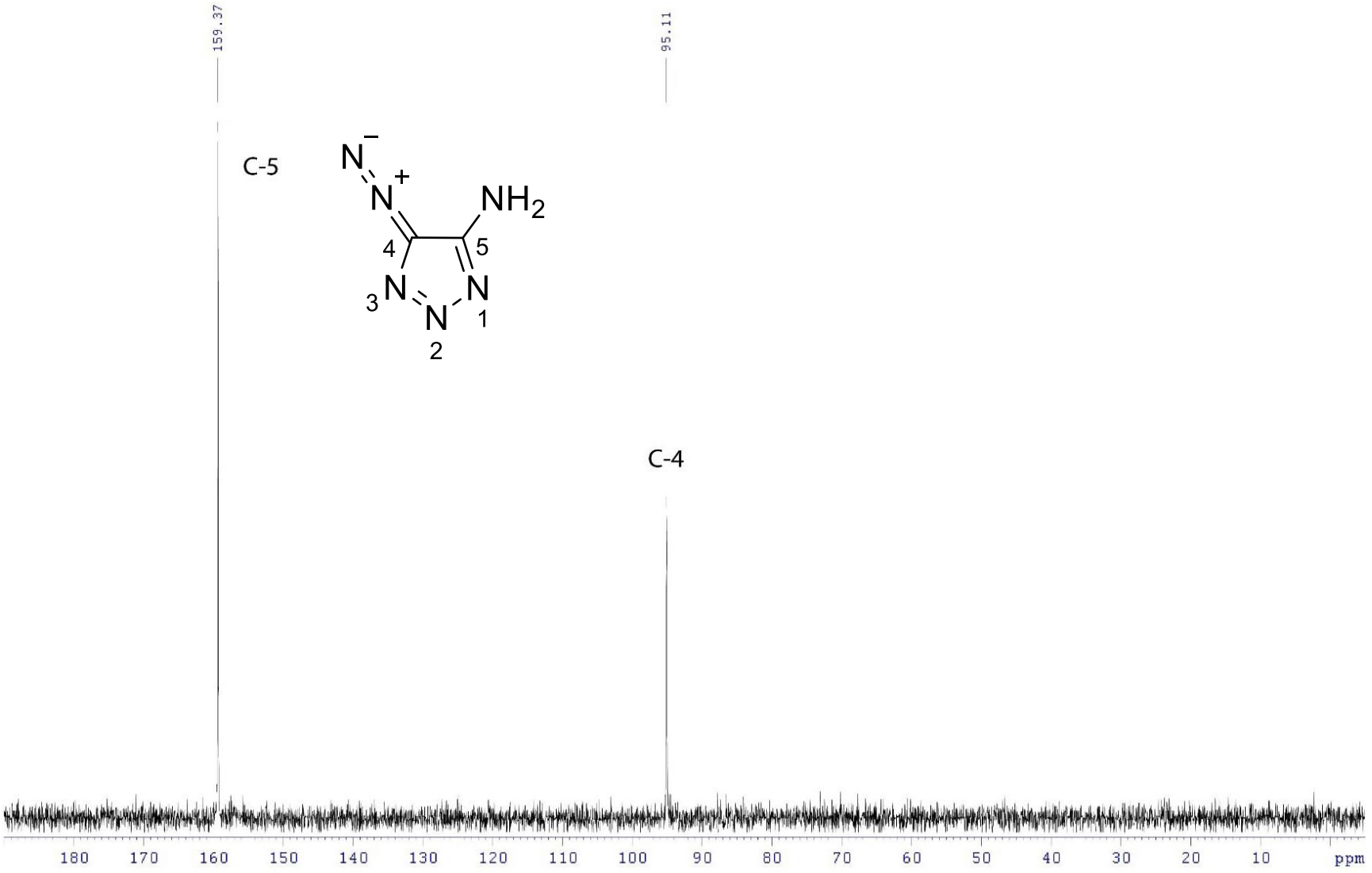

3.4.2. ^{14}N NMR spectrum of compound 5

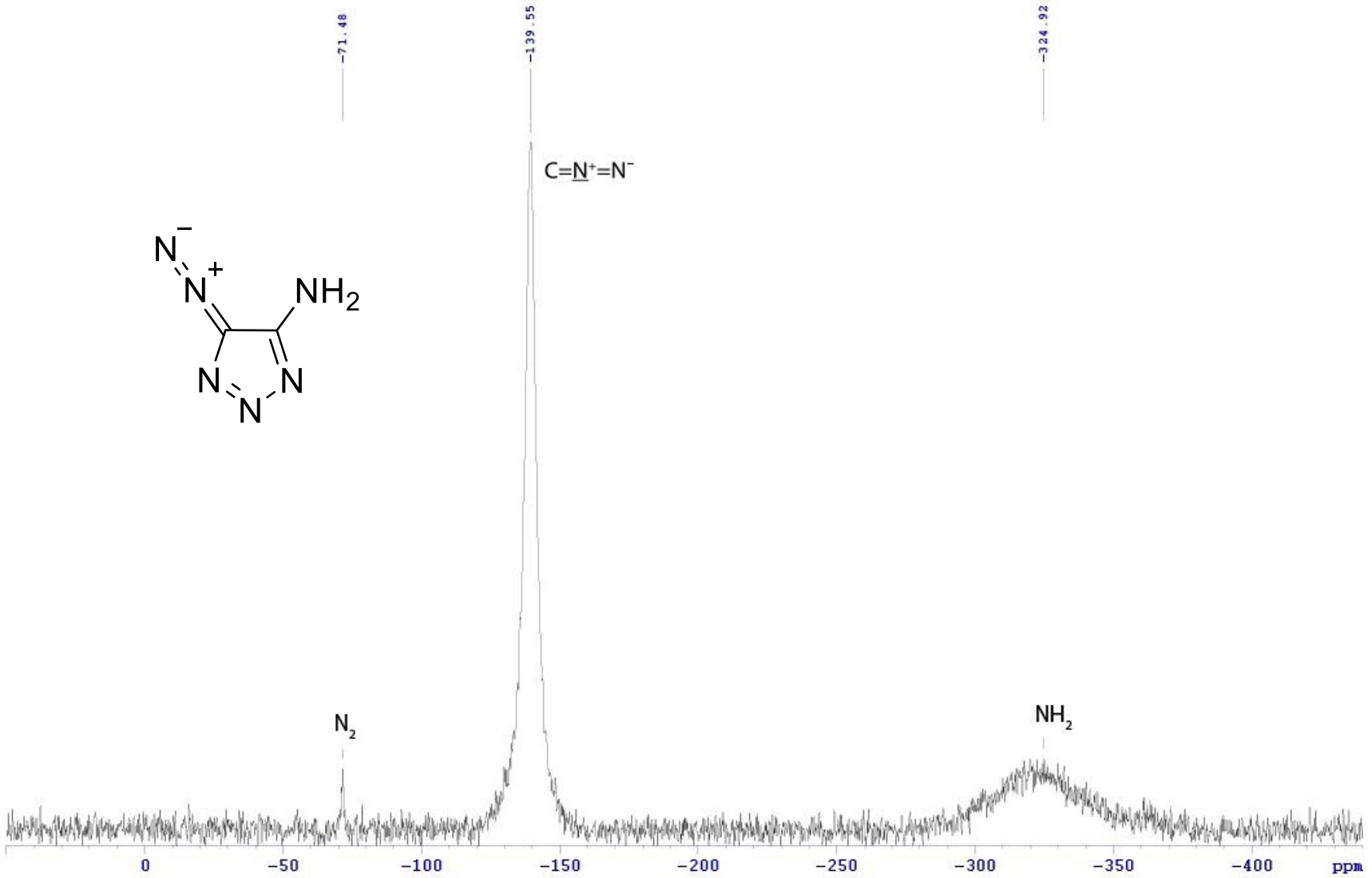

3.5.1. ^{13}C NMR spectrum of salt 6a

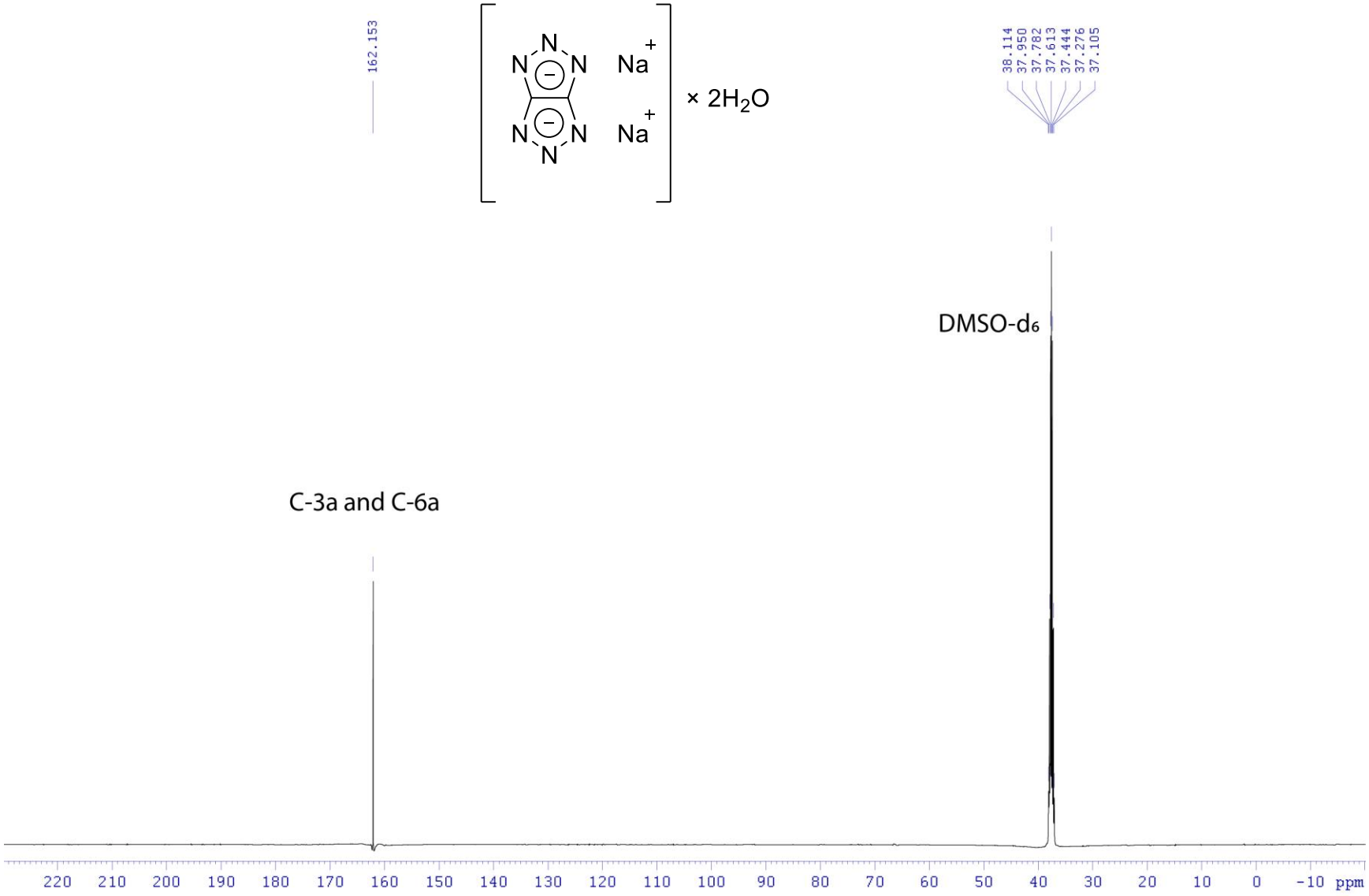

3.5.2. ^{15}N NMR [INVGATED] spectrum of salt 6a

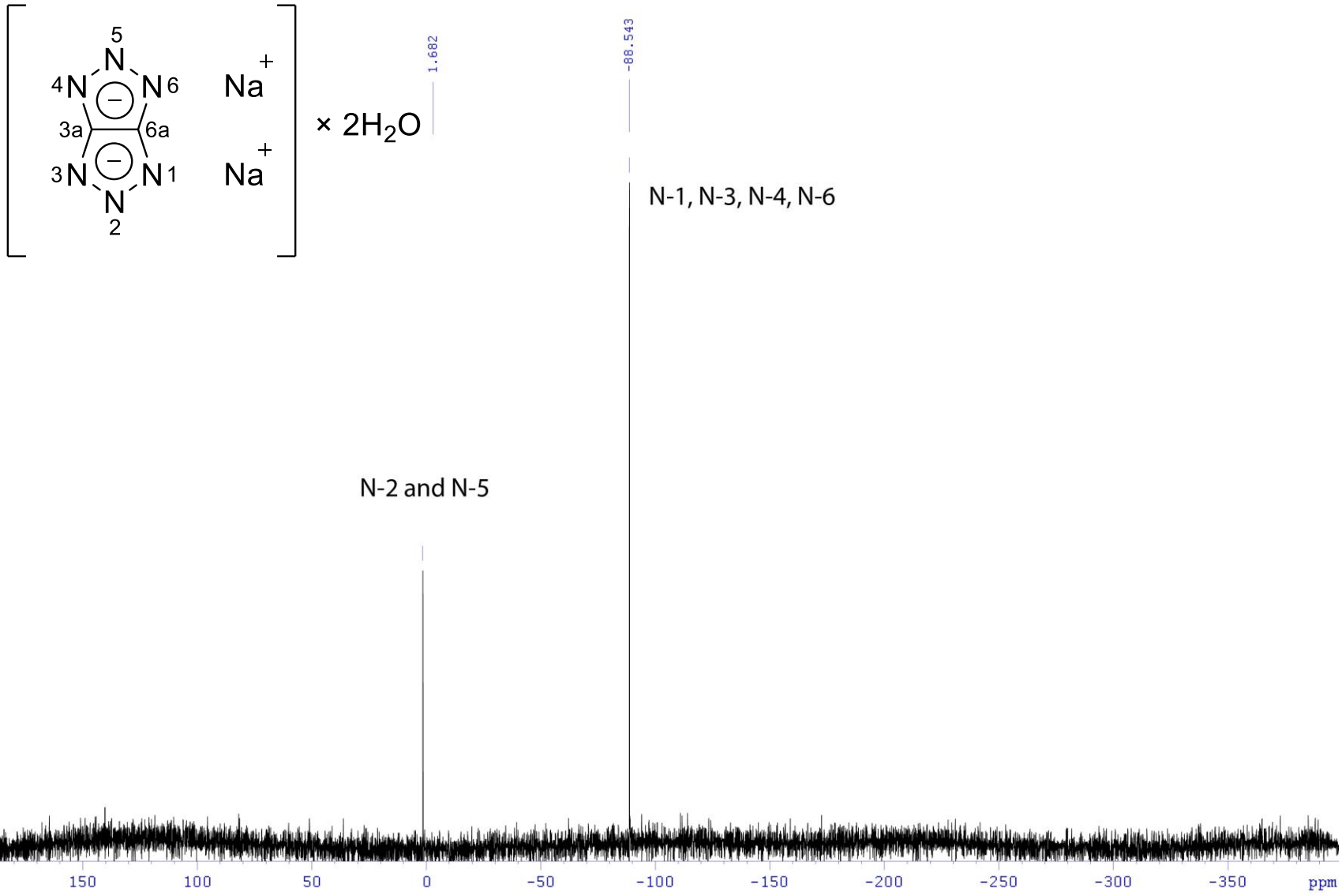

3.6.1. ^{13}C NMR spectrum of salt 6b

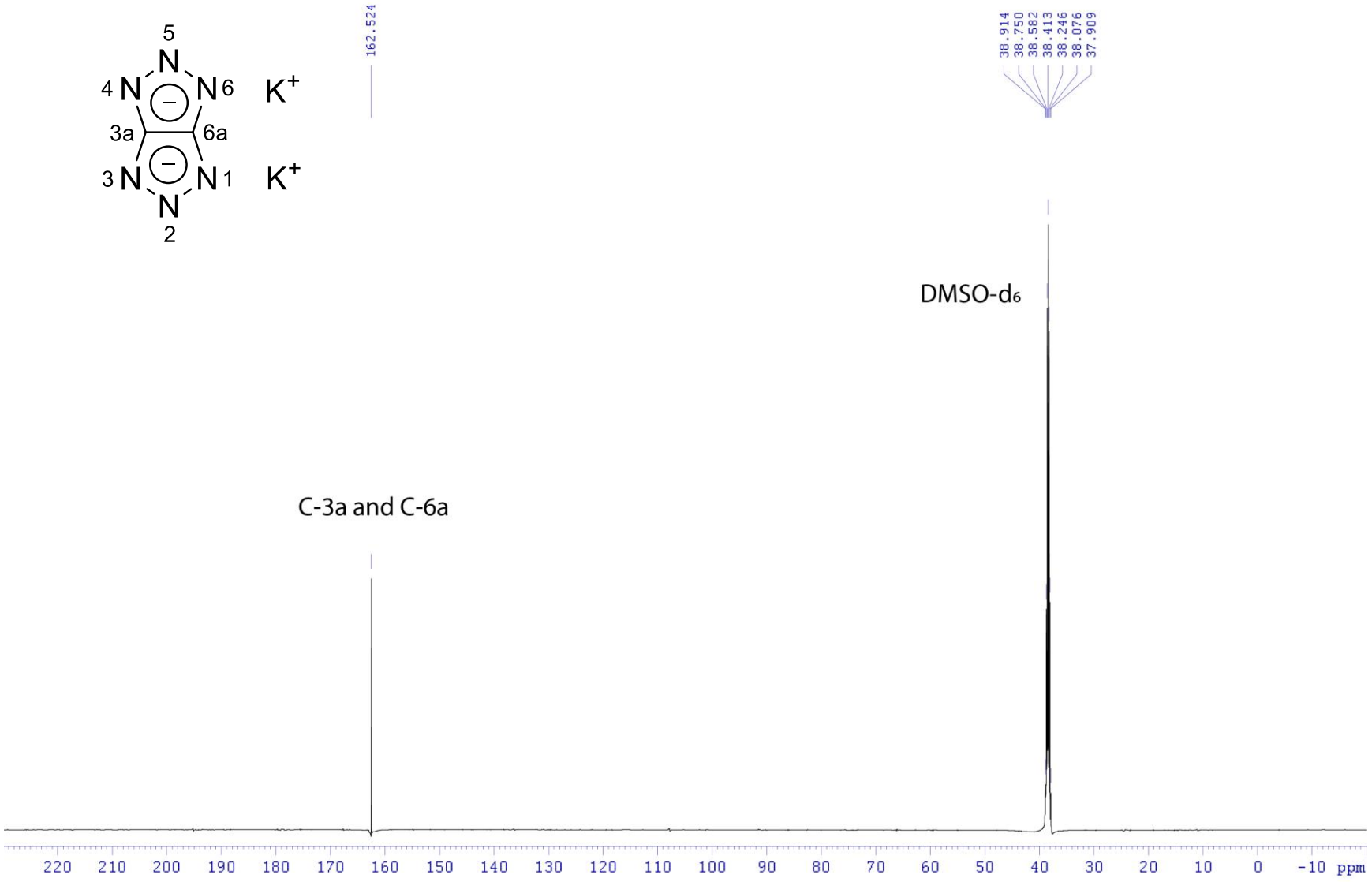

3.6.2. ^{15}N NMR [INVGATED] spectrum of salt 6b

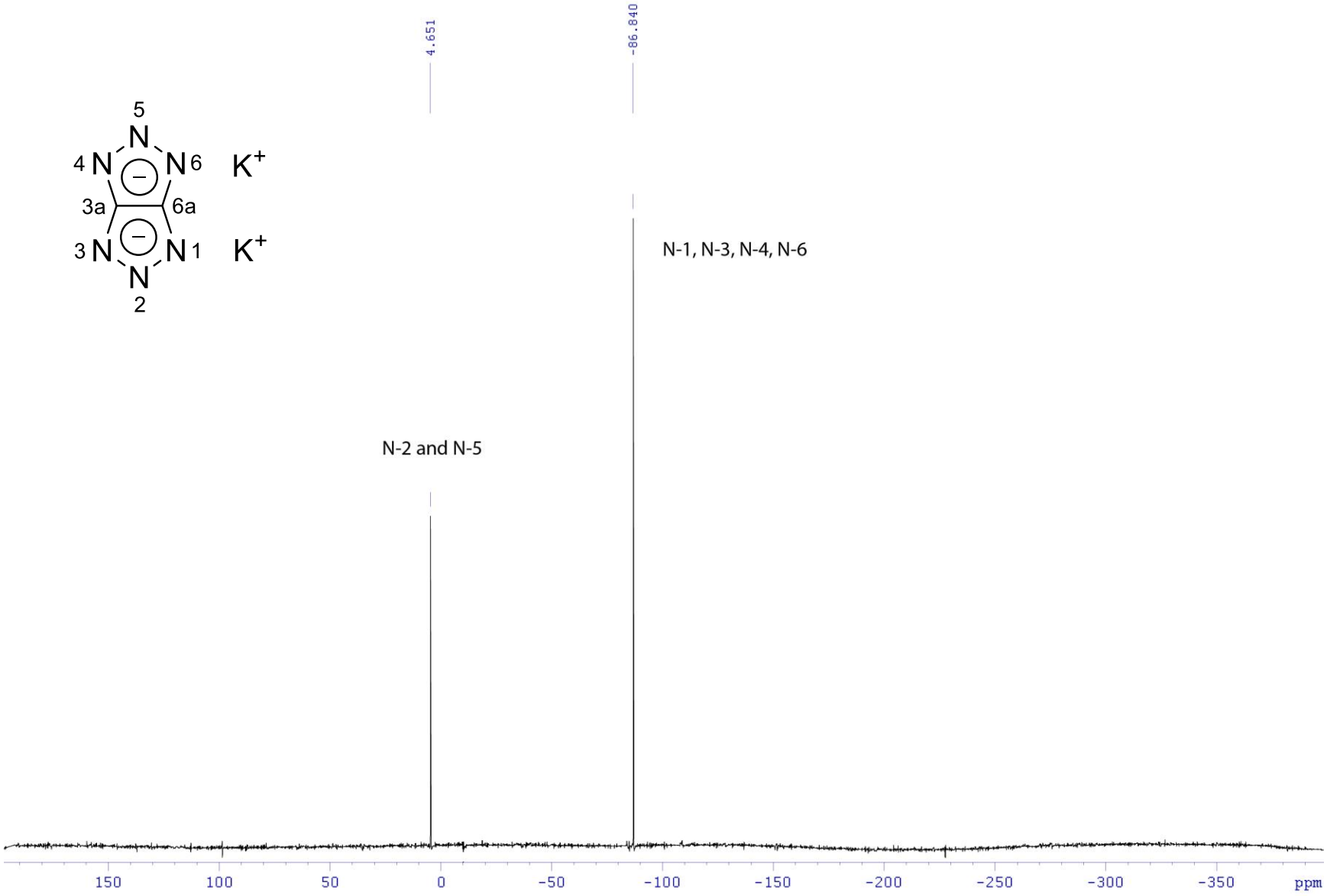

3.7.1. ^{1}H NMR spectrum of salt 6c·7H$_2$O

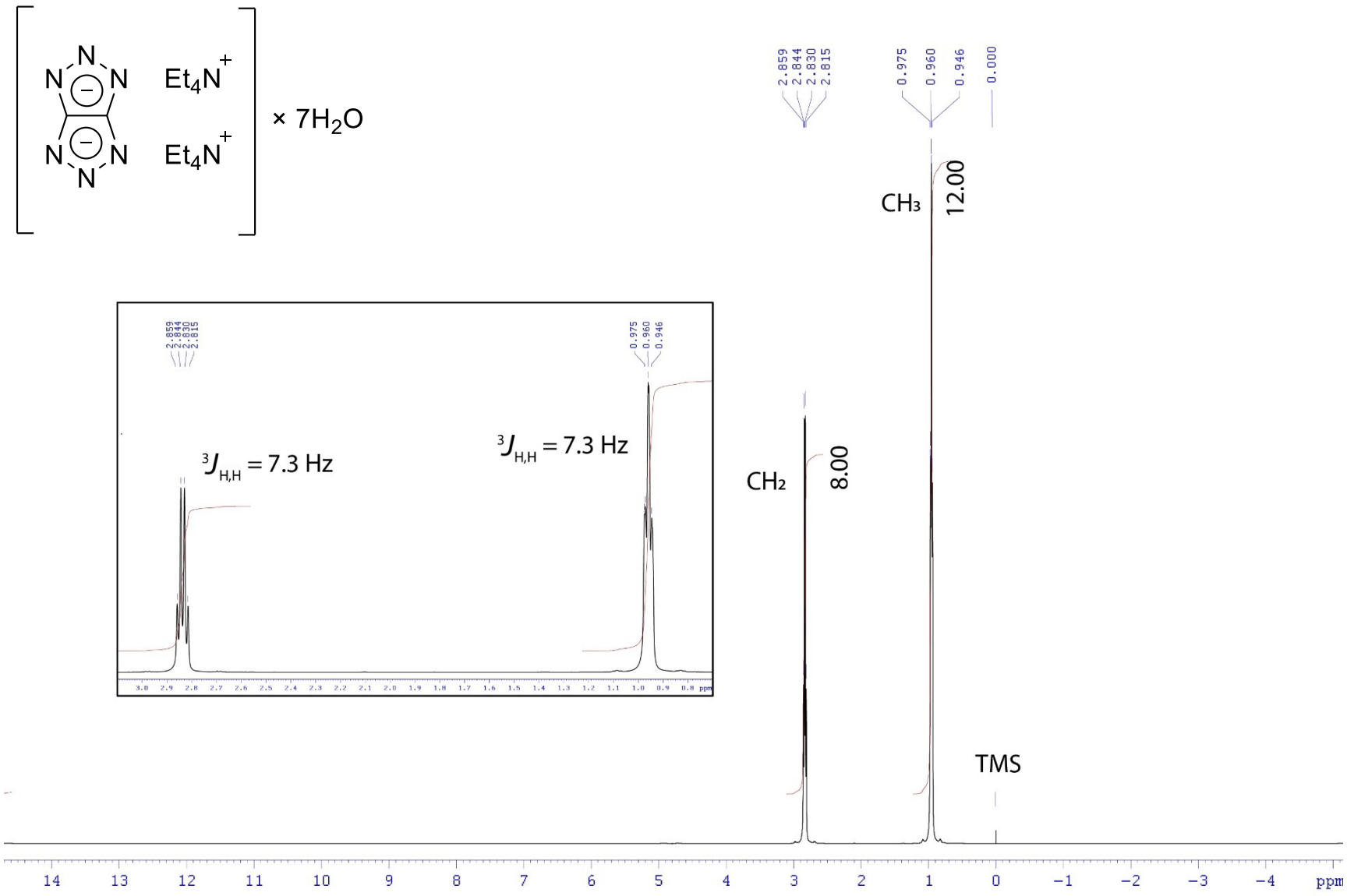

3.7.2. ^{13}C NMR spectrum of salt 6c·7H$_2$O

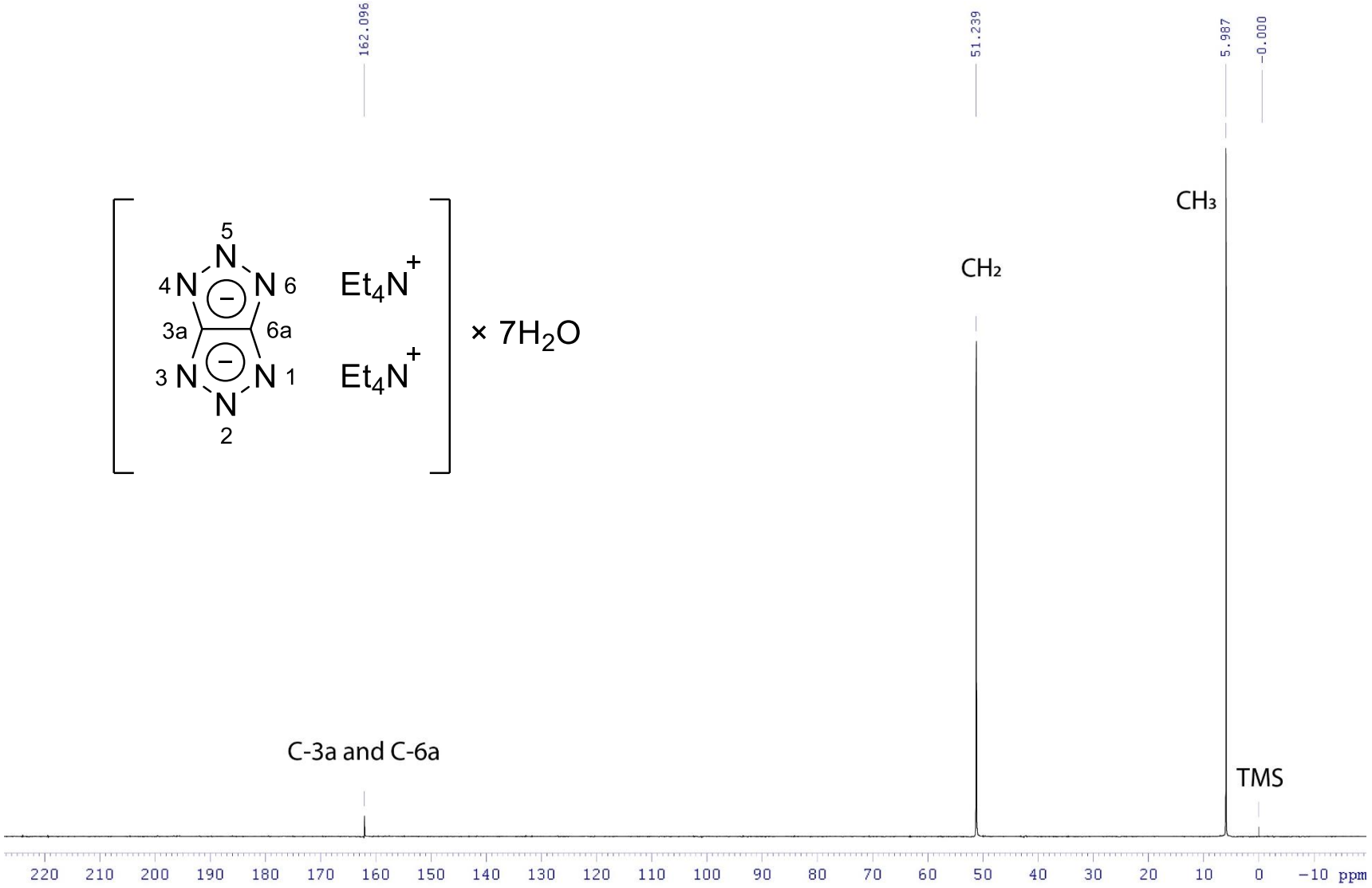

3.7.3. ^{14}N NMR spectrum of salt 6c·7H$_2$O

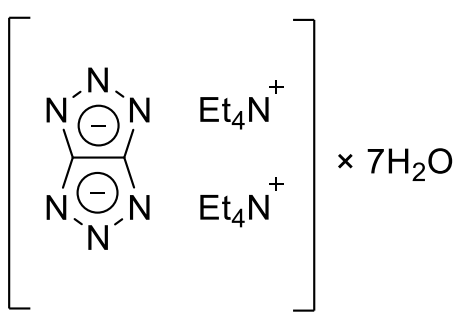

3.7.4. ^{15}N NMR [INVGATED] spectrum of compound 6c·7H$_2$O

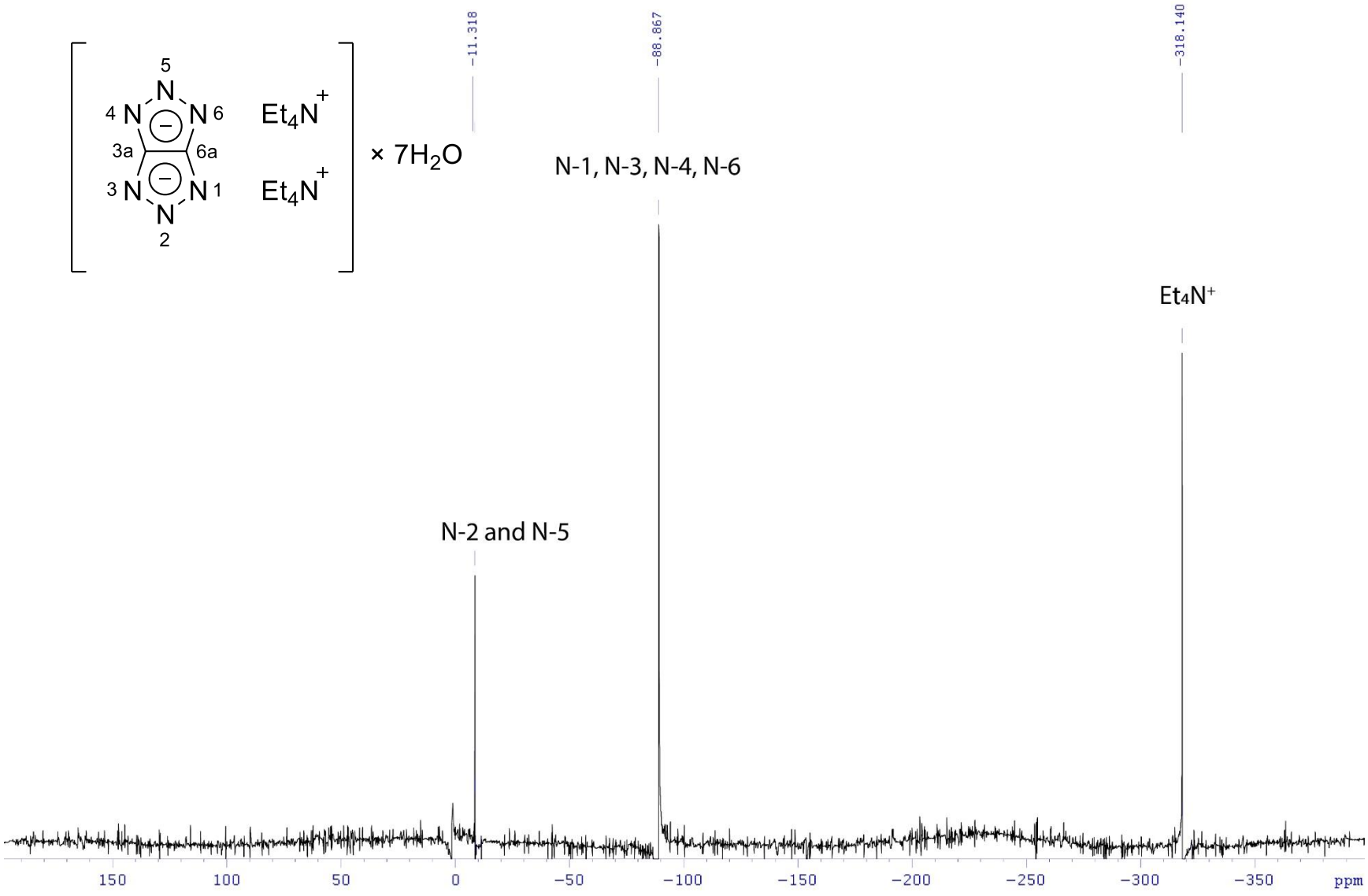

3.8.1. ^{1}H NMR spectrum of TT 7a

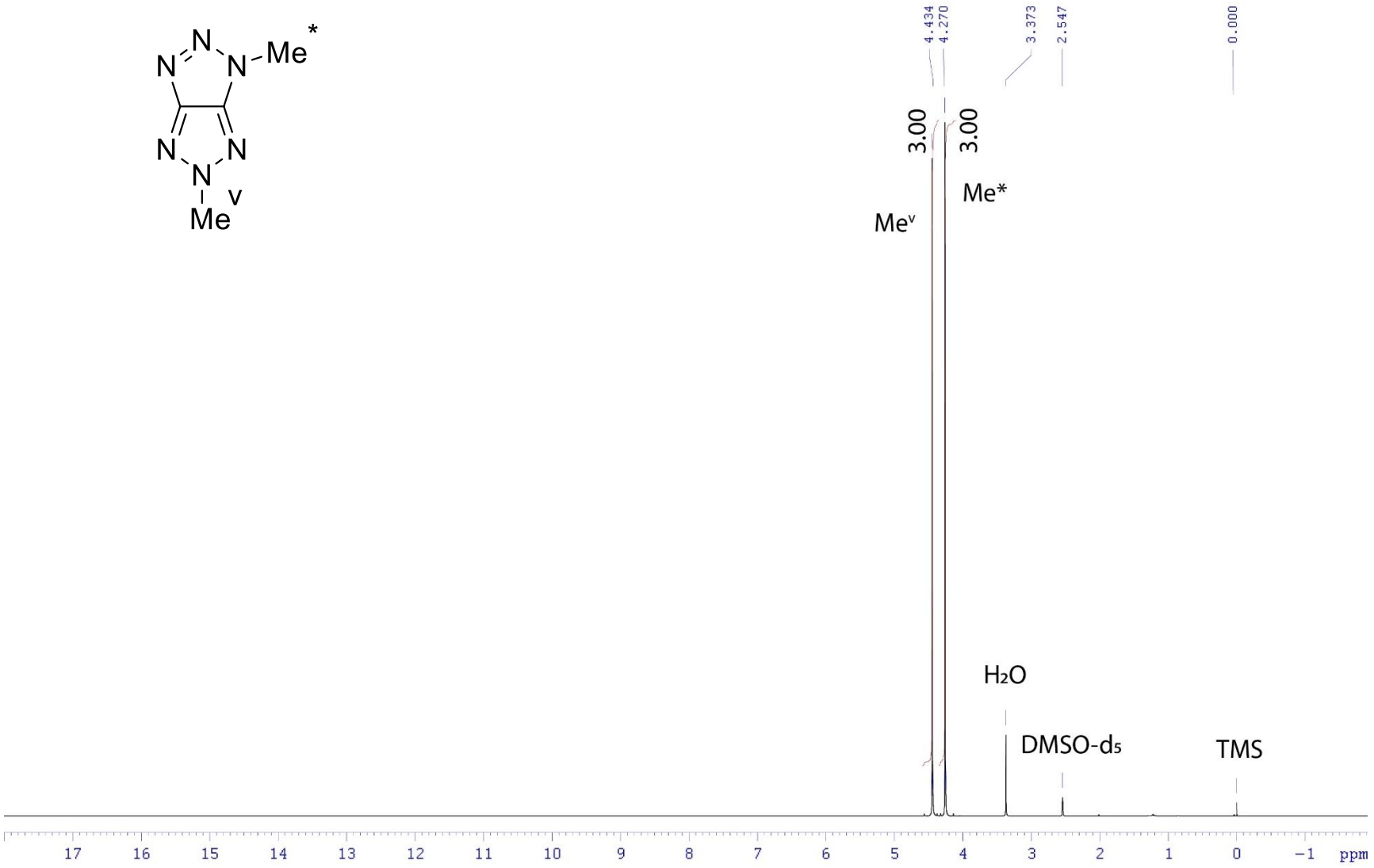

3.8.2. ^{13}C NMR spectrum of TT 7a

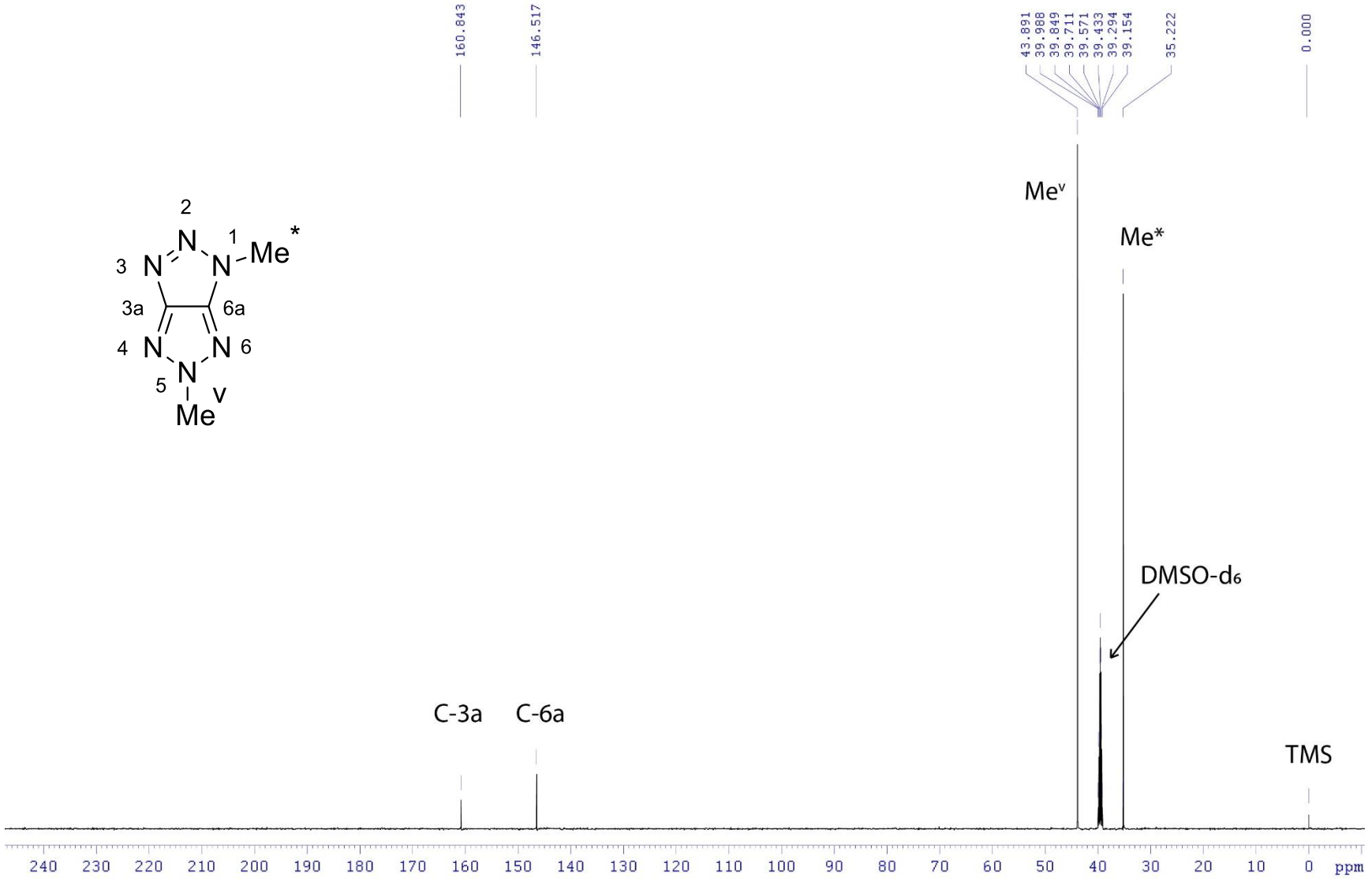

3.8.3. {^{1}H–^{13}C} HSQC spectrum of TT 7a

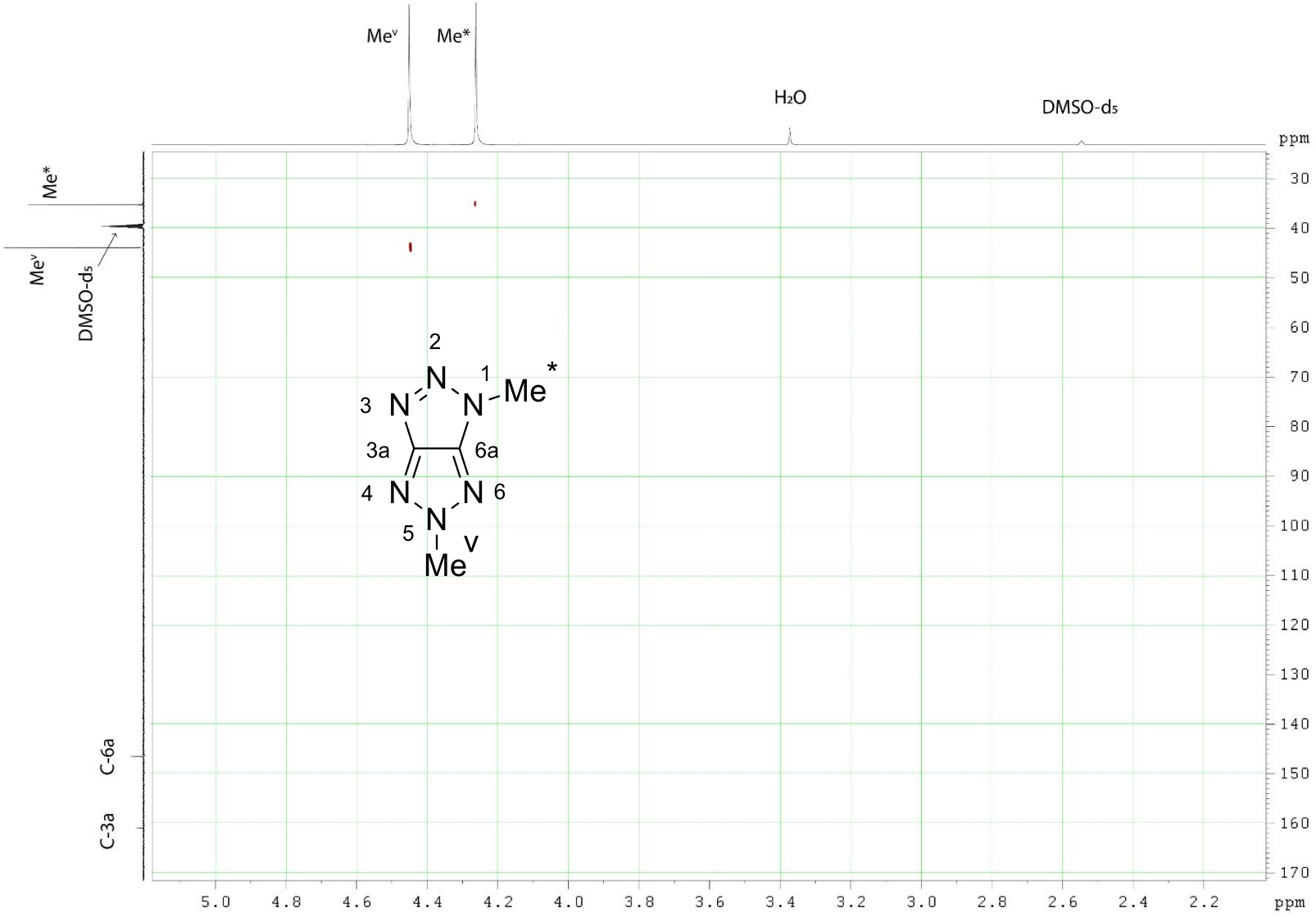

3.8.4. {^{1}H–^{13}C} HMBC spectrum of TT 7a

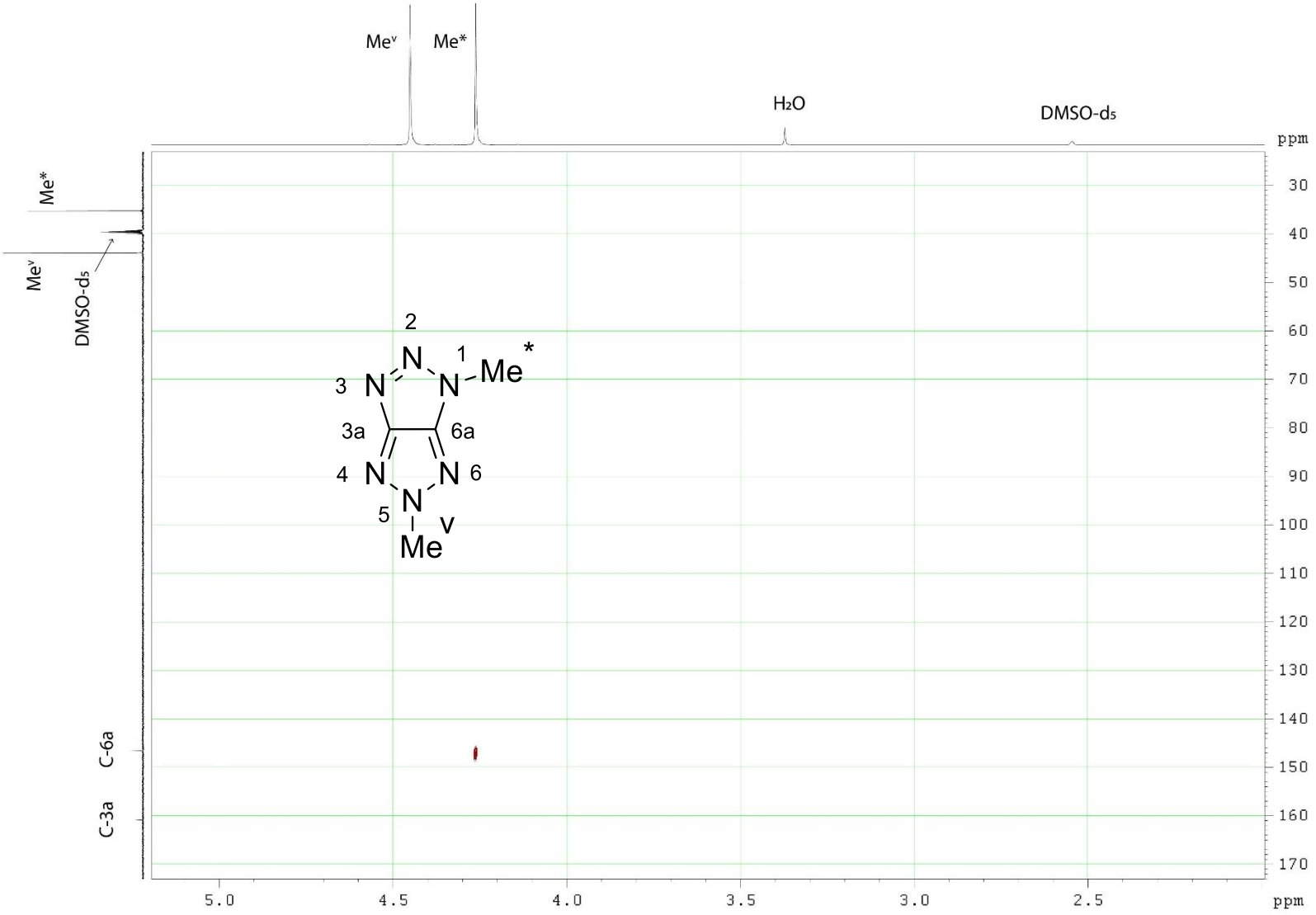

3.8.5. ^{14}N NMR spectrum of TT 7a

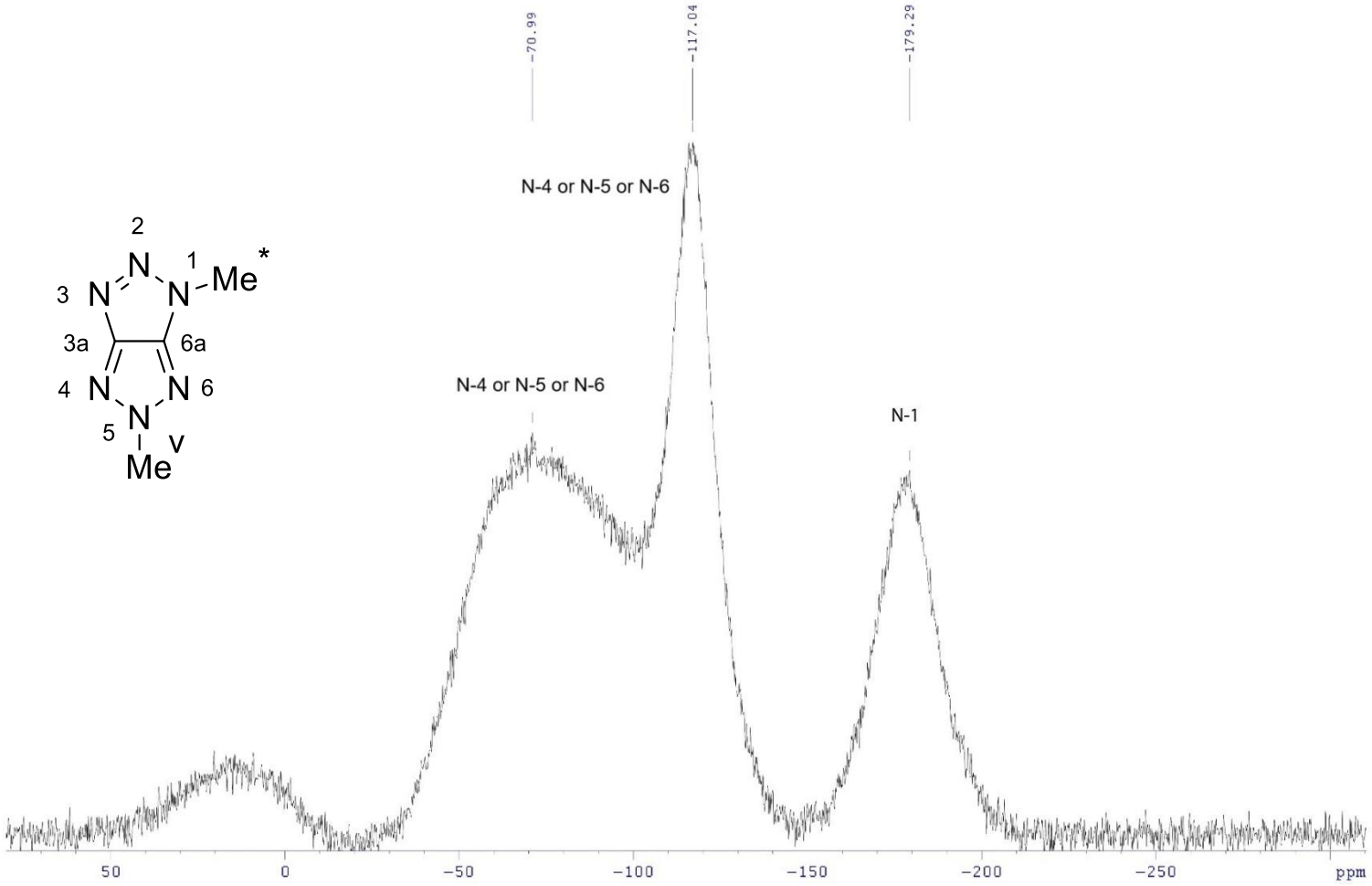

3.8.6. ^{15}N NMR [INVGATED] spectrum of TT 7a

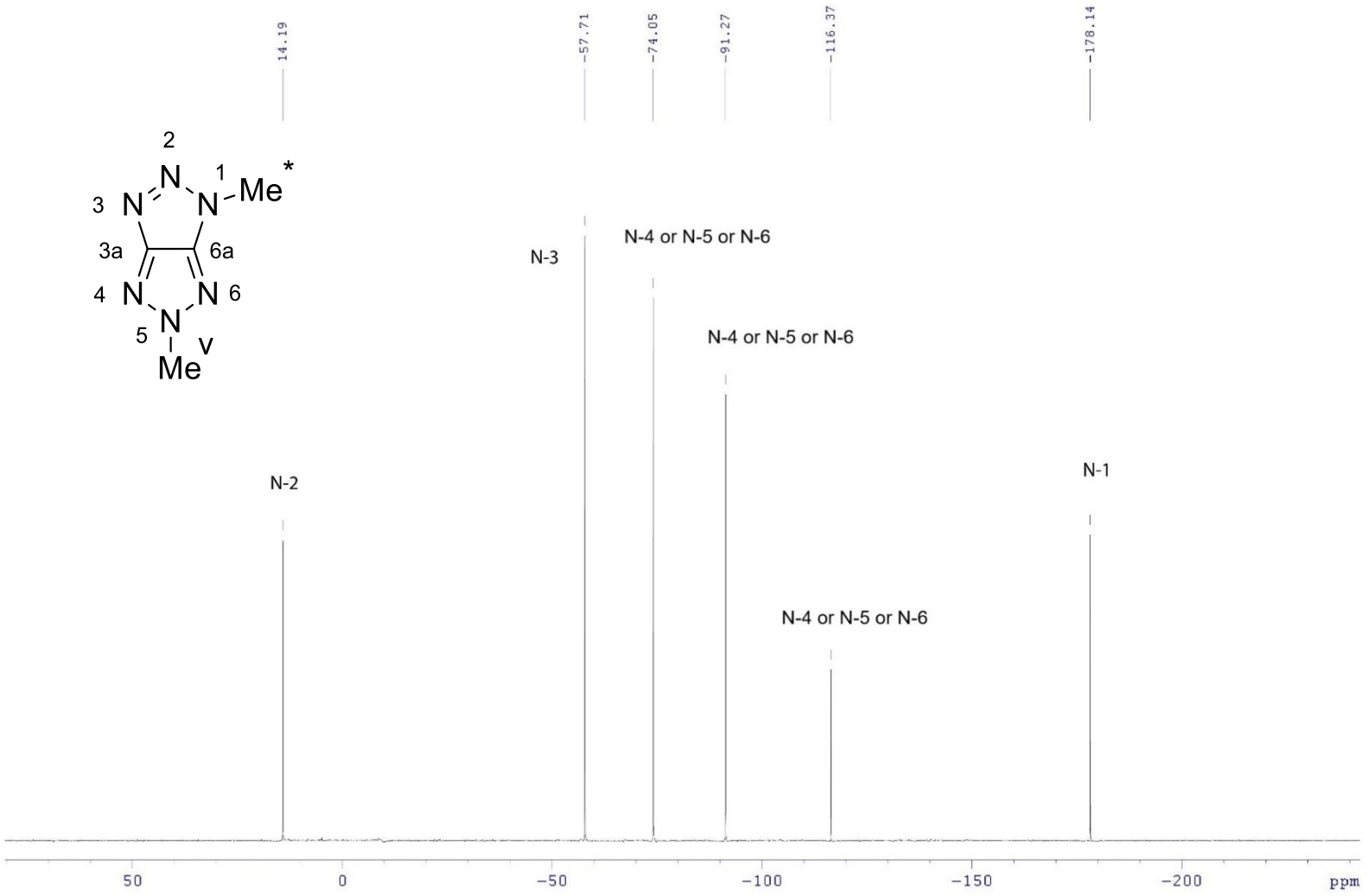

3.8.7. ^{15}N NMR [INEPT, with decoupling] spectrum of TT 7a

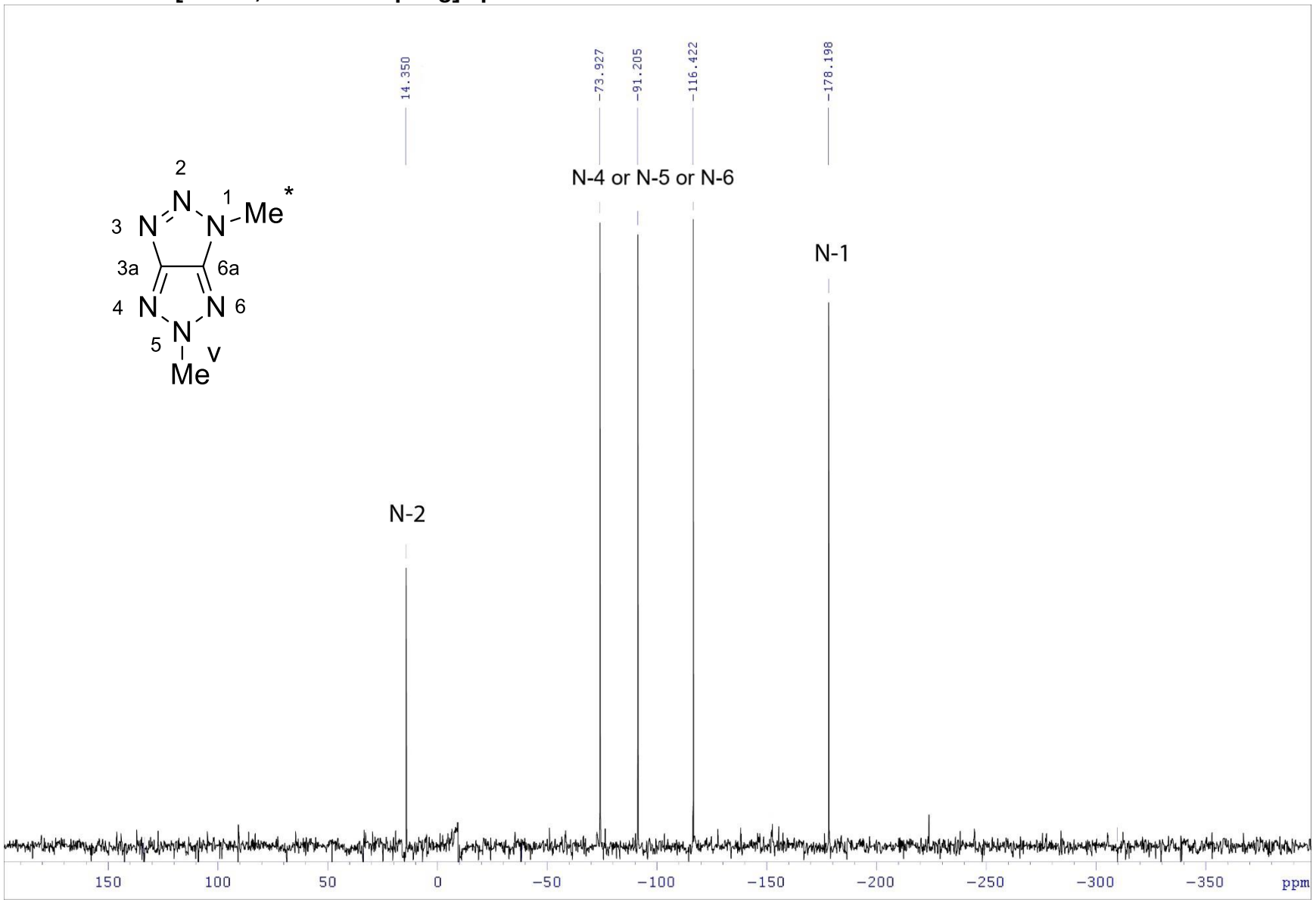

3.8.8. ^{15}N NMR [INEPT, without decoupling] spectrum of TT 7a

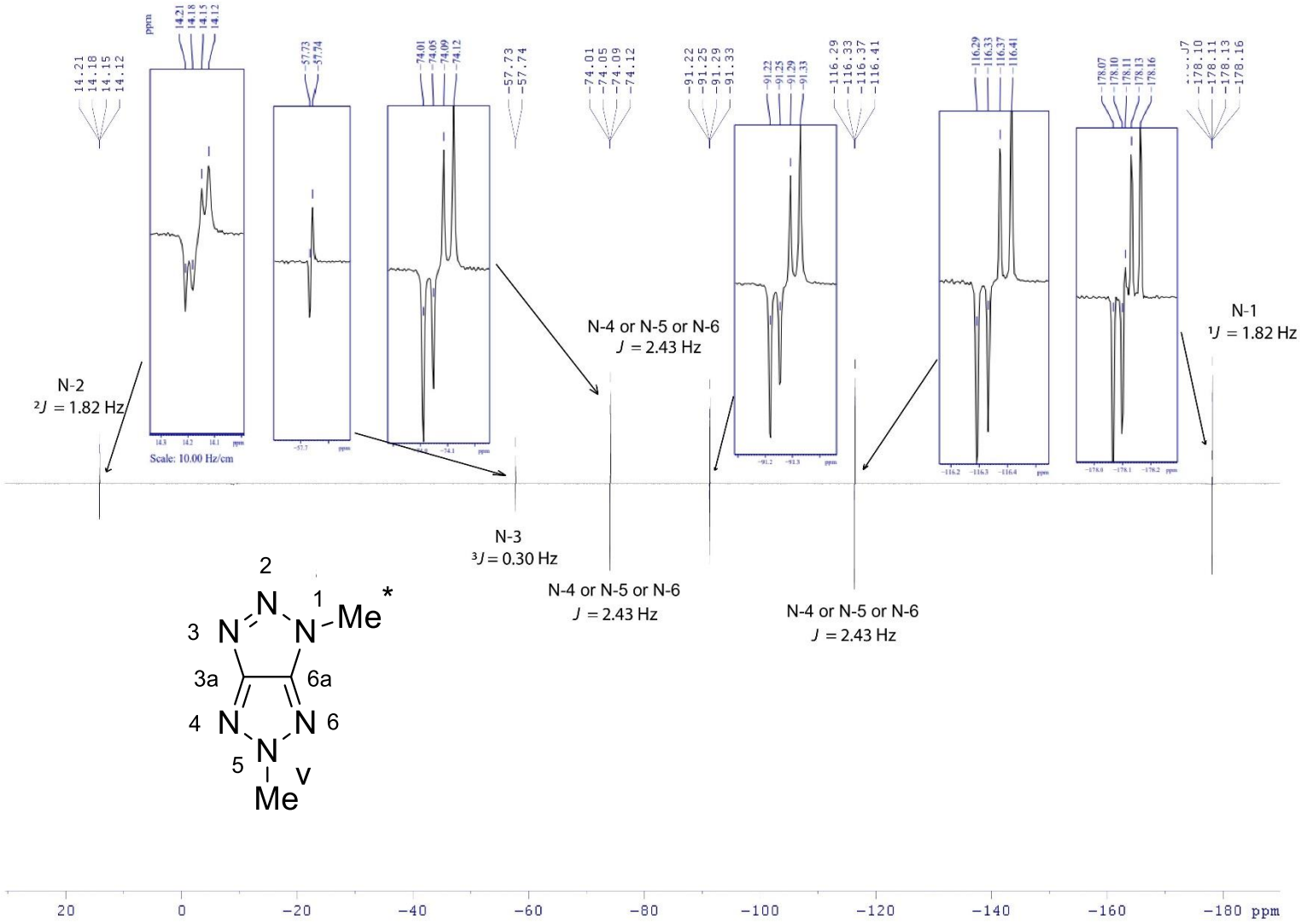

3.8.9. {^{1}H–^{15}N} HMBC spectrum of TT 7a

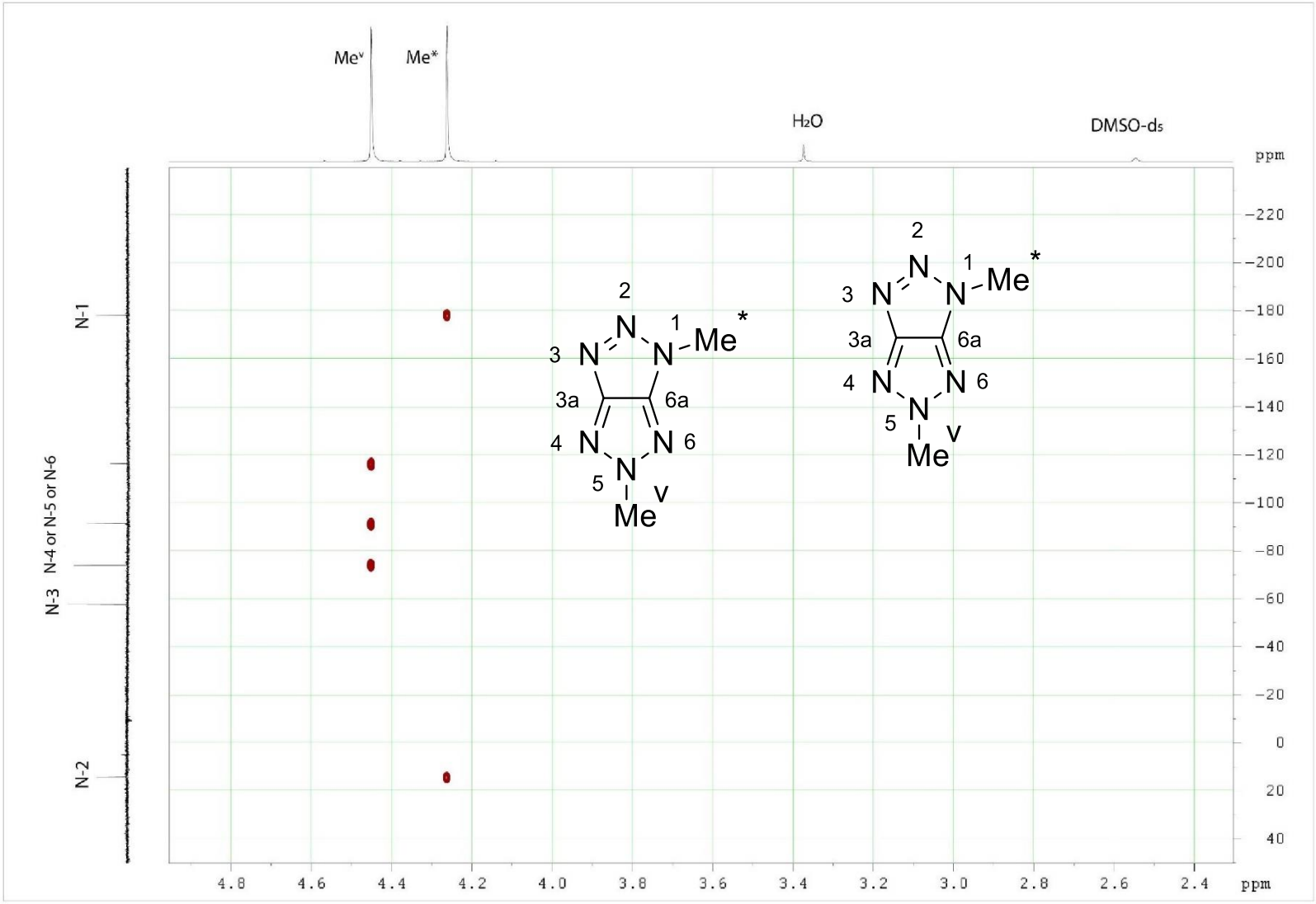

3.9.1. ^{1}H NMR spectrum of TT 7b

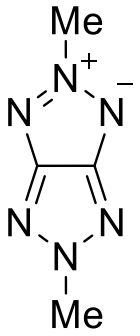

3.9.2. ^{13}C NMR spectrum of TT 7b

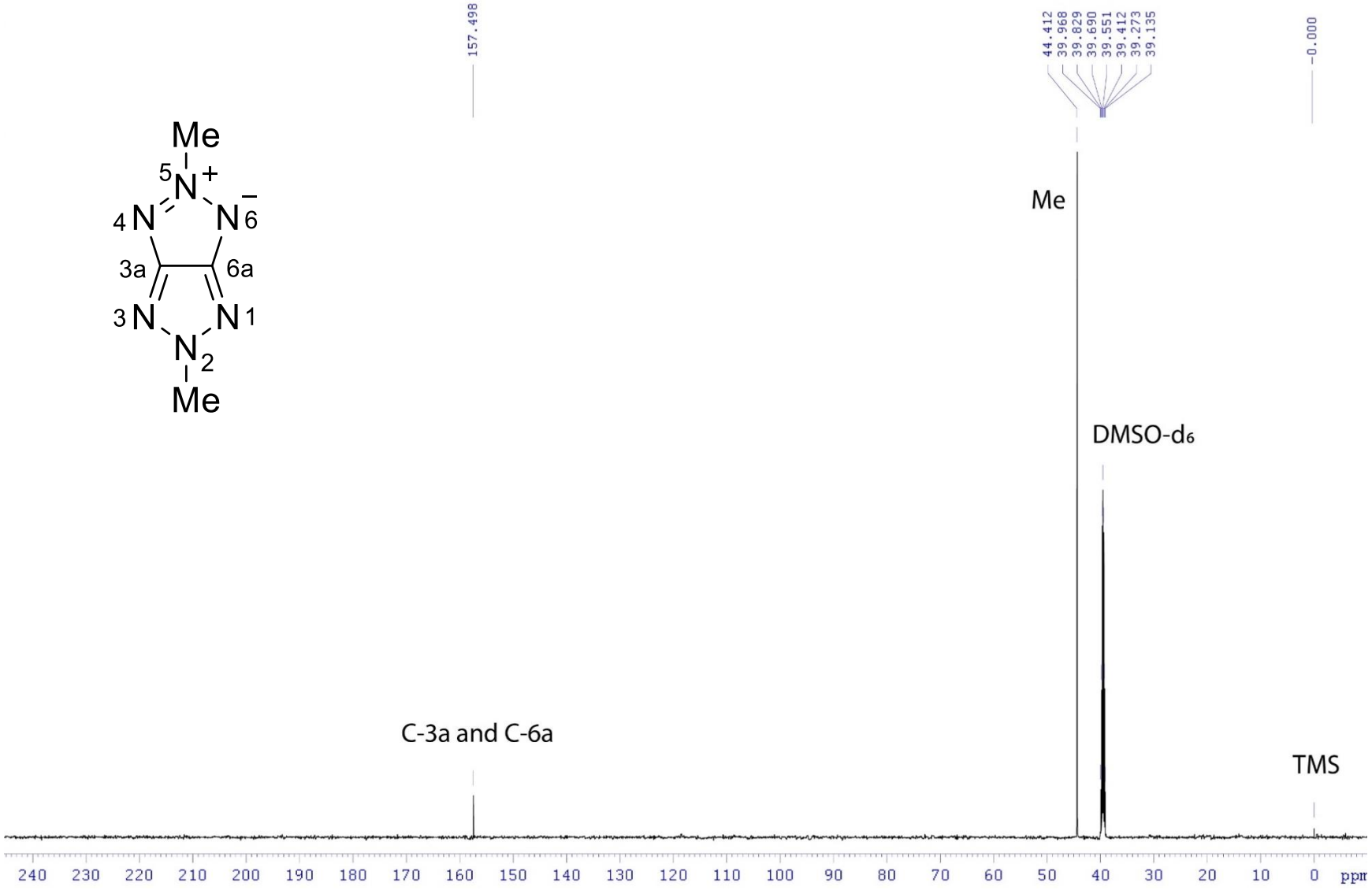

3.9.3. ^{14}N NMR spectrum of TT 7b

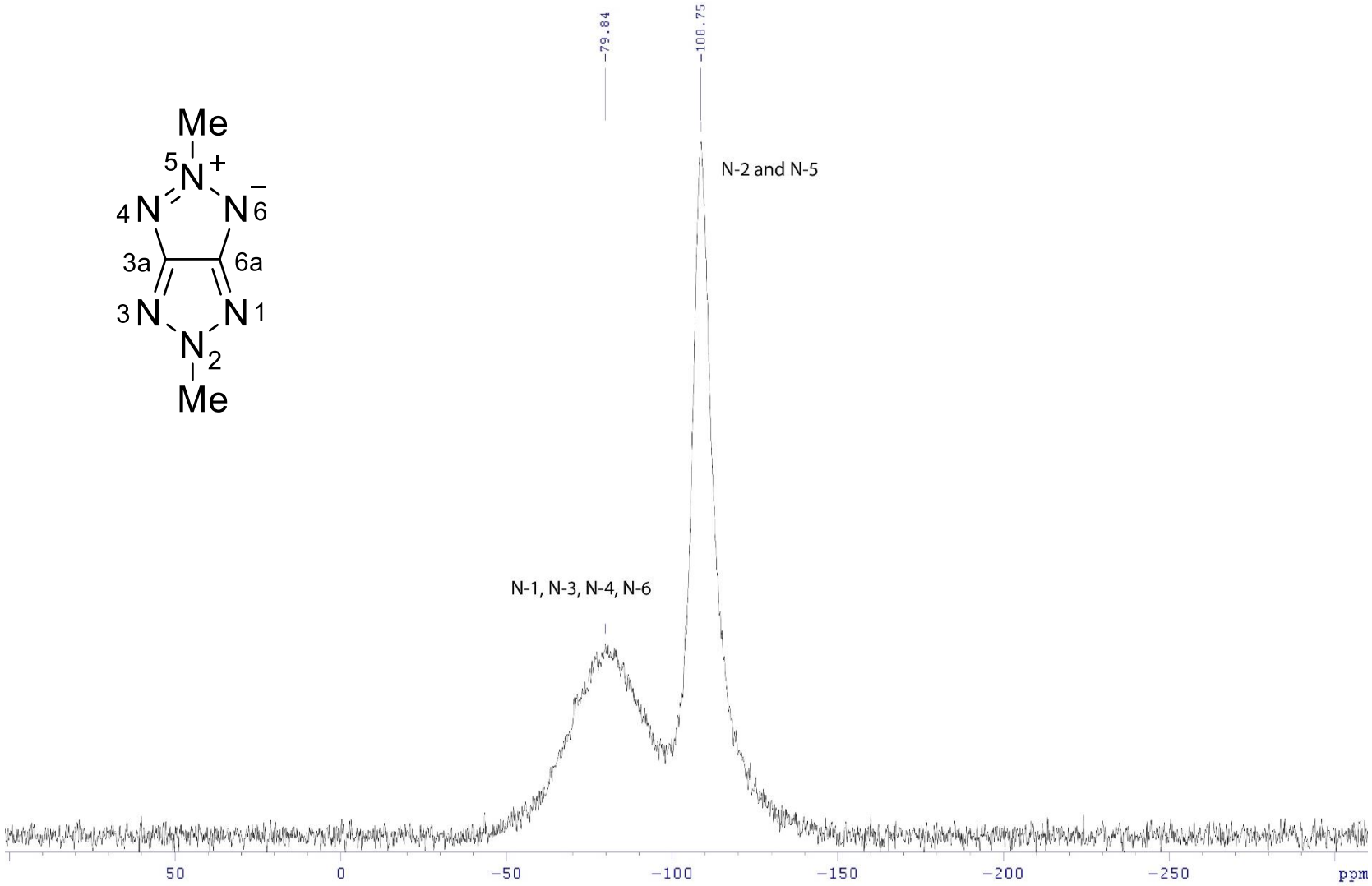

3.9.4. ^{15}N NMR [INVGATED] spectrum of TT 7b

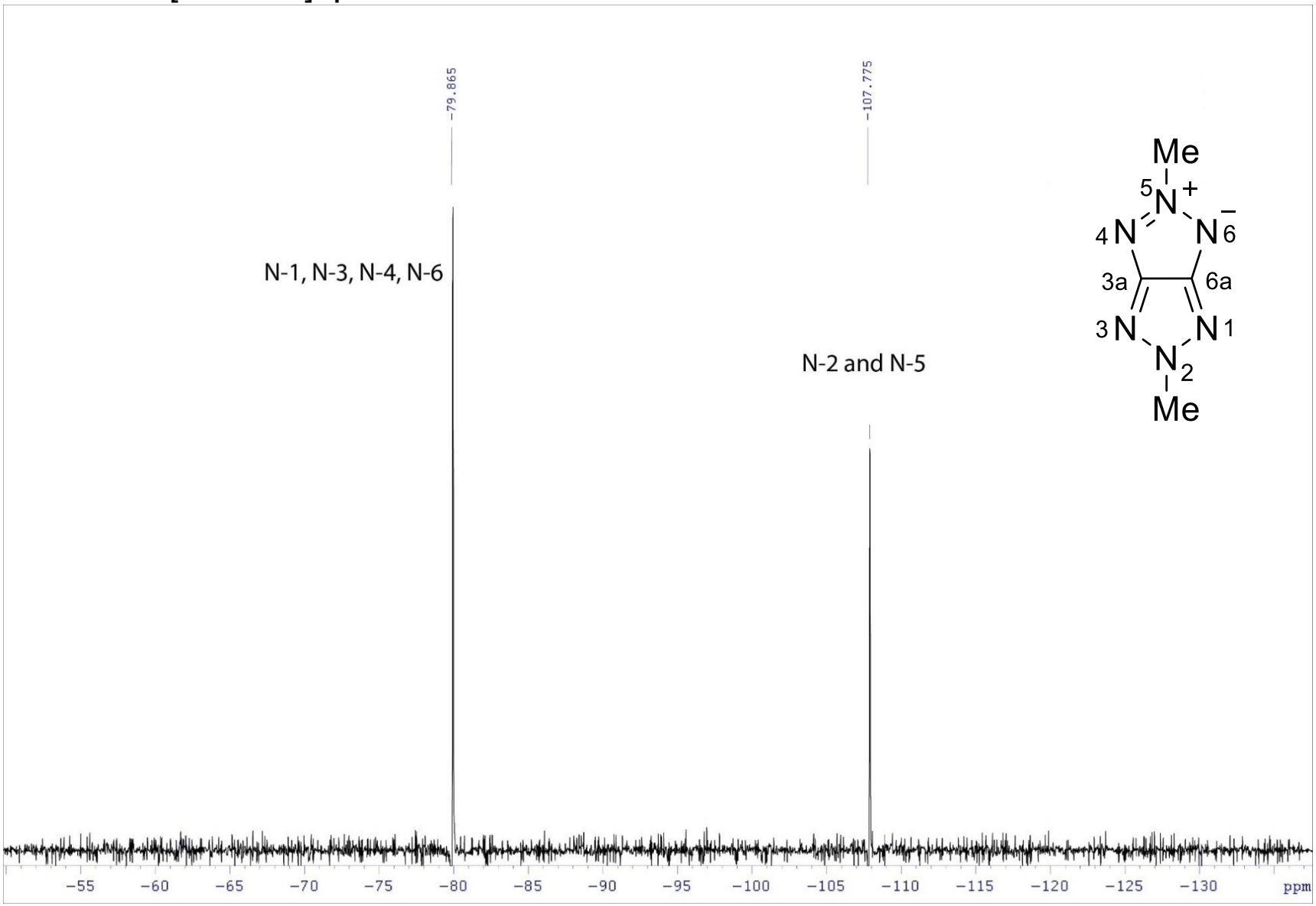

3.9.5. ^{15}N NMR [INEPT] spectrum of TT 7b

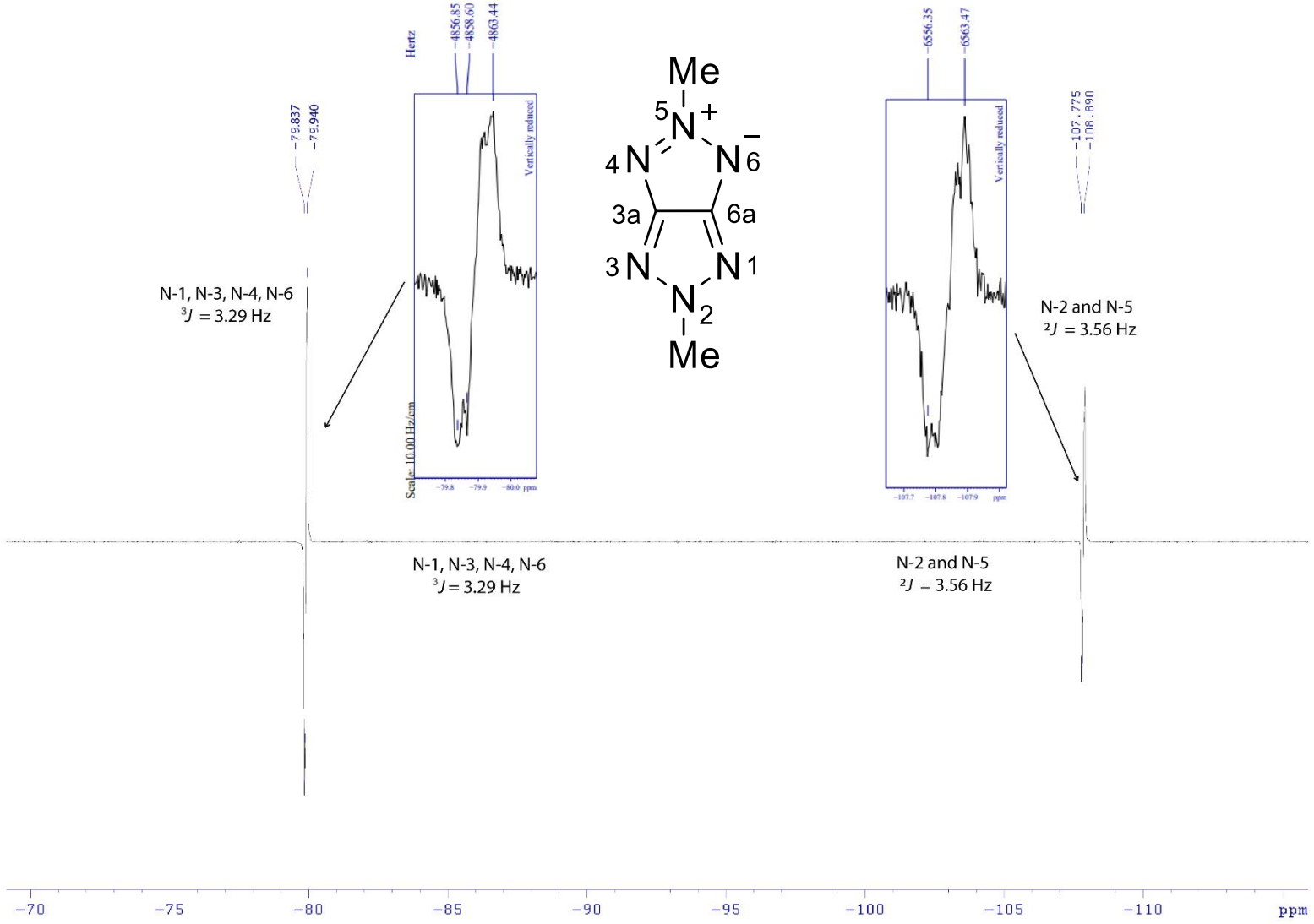

3.9.6. {^{1}H–^{15}N} HMBC spectrum of TT 7b

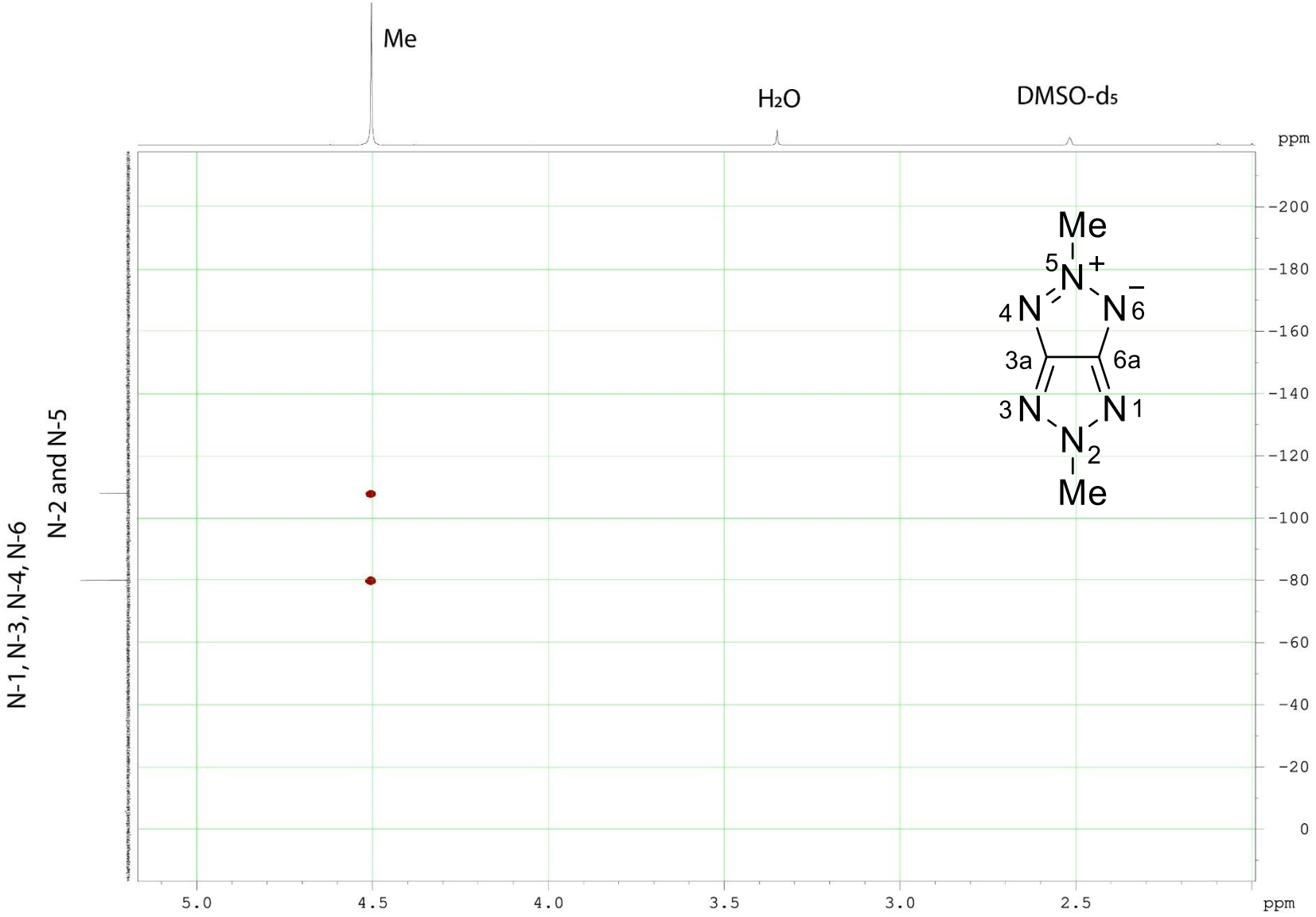

3.10.1. 1H NMR spectrum of TT 7c

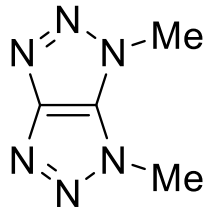

3.10.2. ^{13}C NMR spectrum of TT 7c

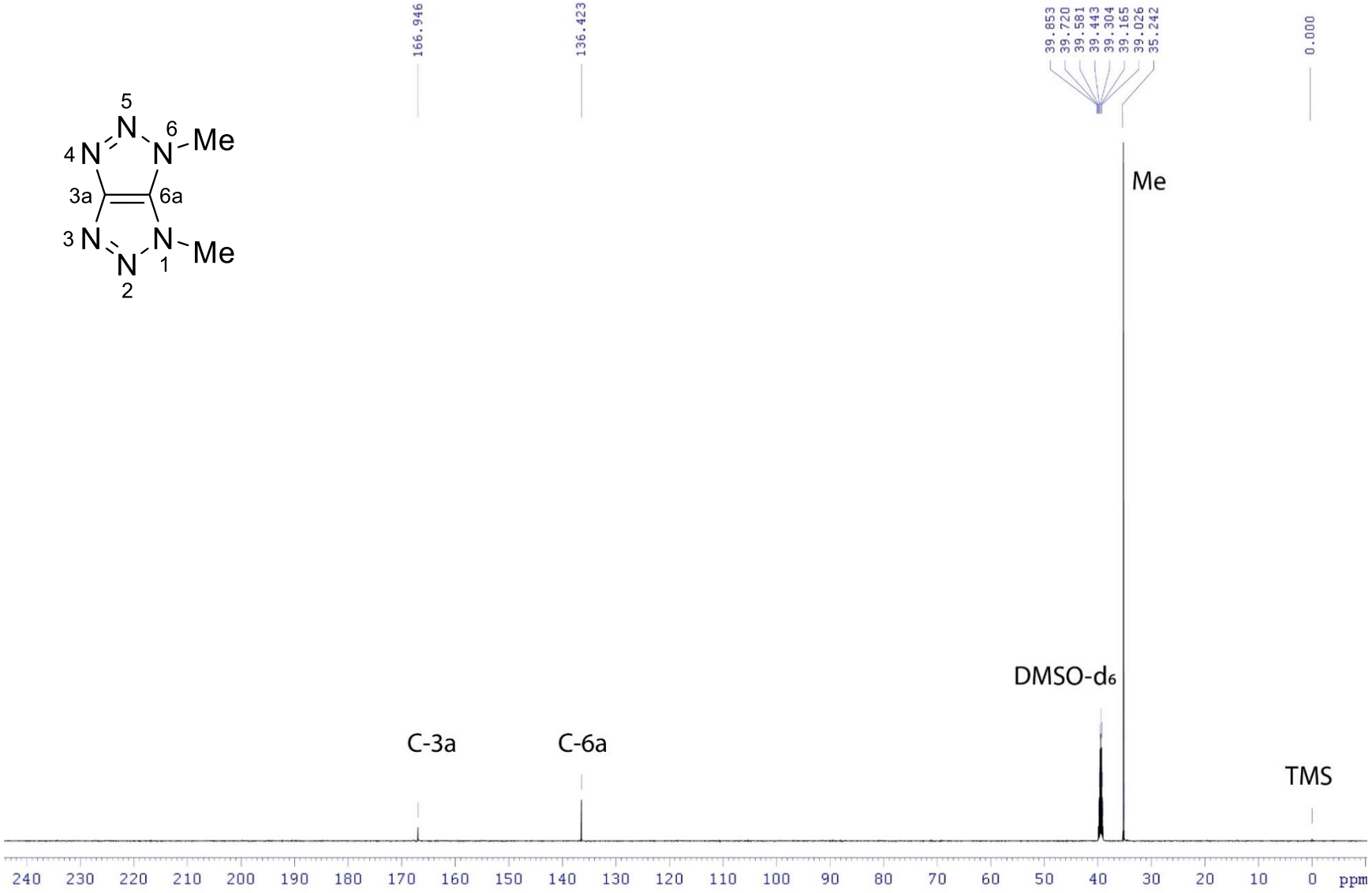

3.10.3. {^{1}H–^{13}C} HMBC spectrum of TT 7c

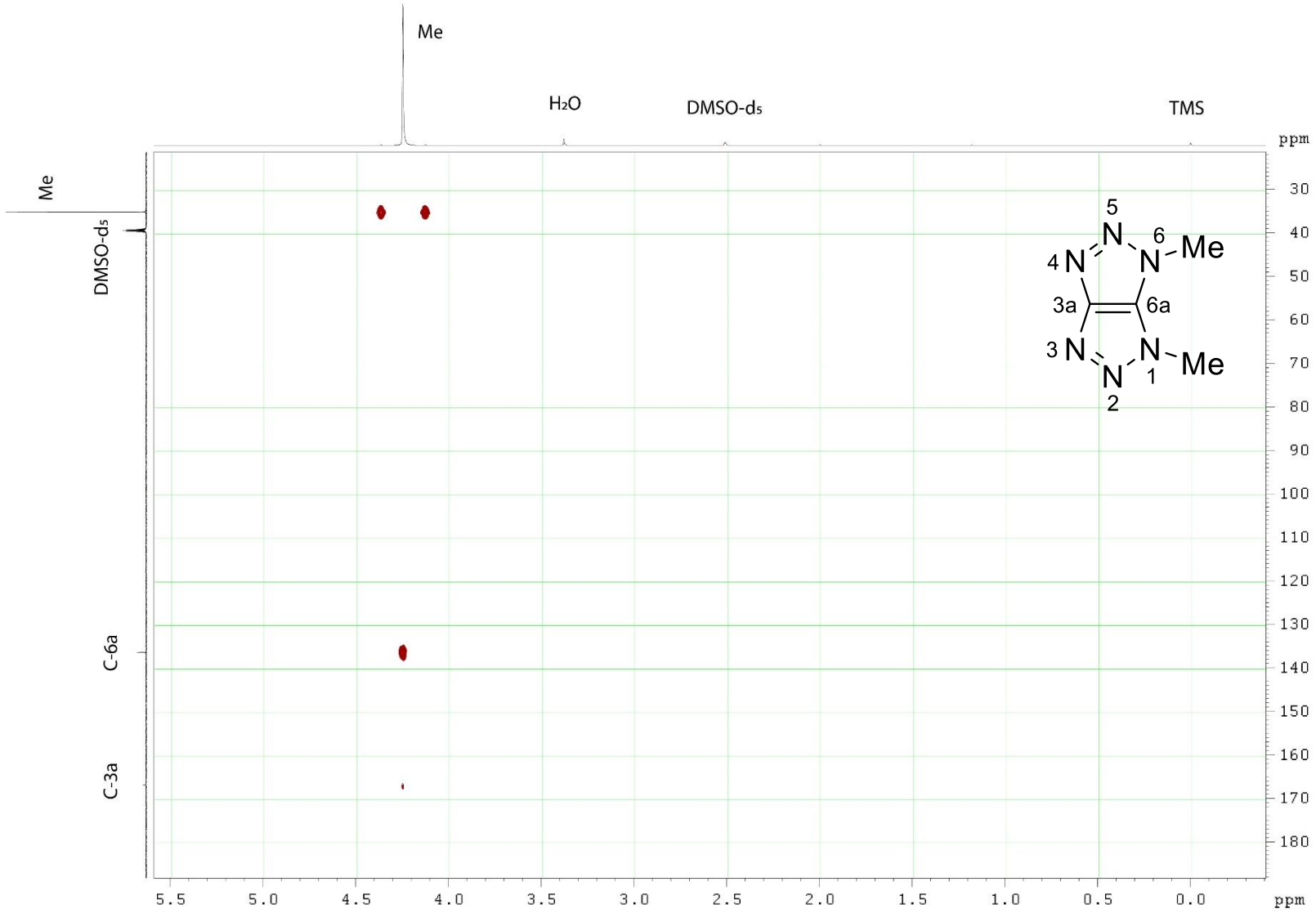

3.10.4. ^{14}N NMR spectrum of TT 7c

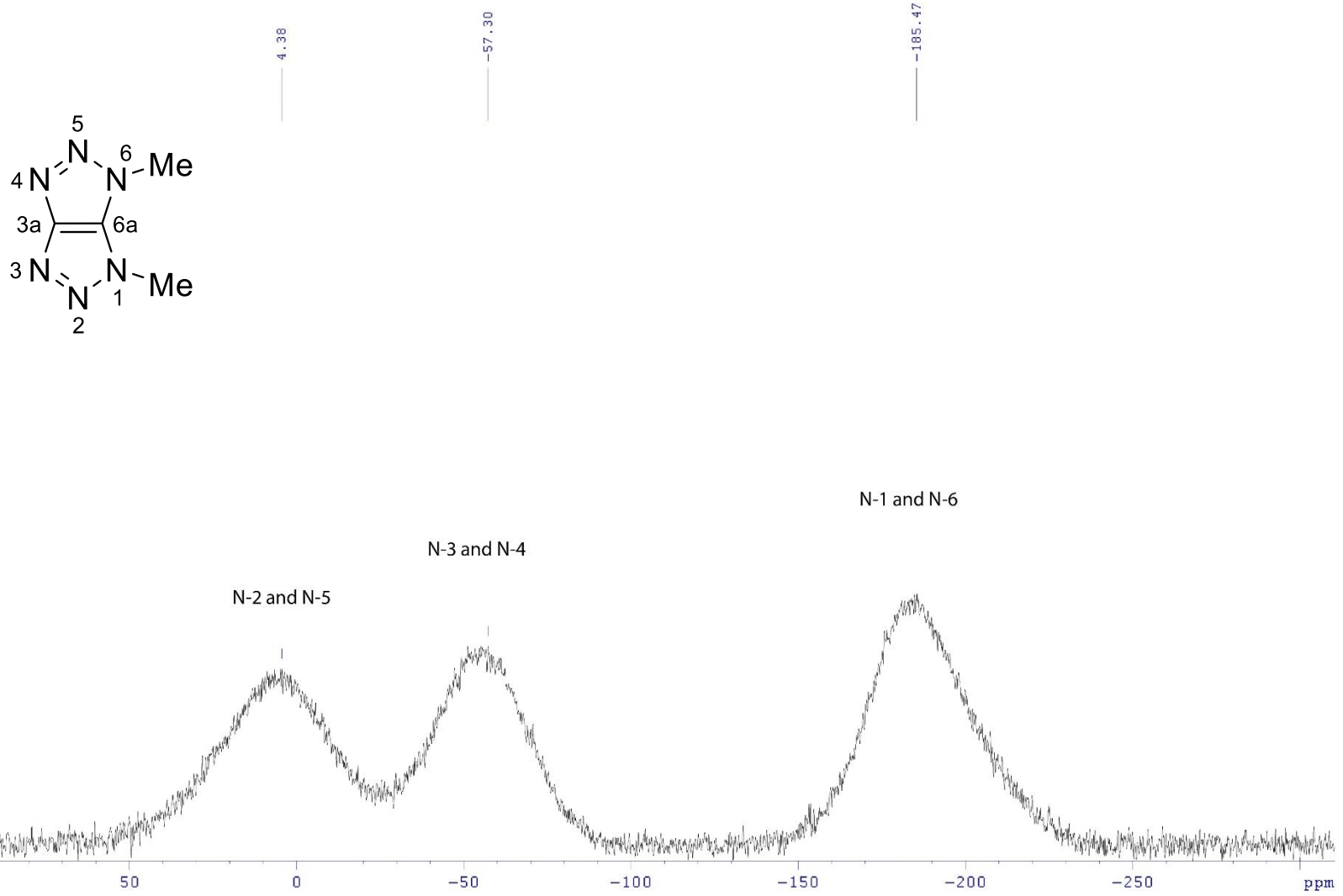

3.10.5. 15N NMR [INVGATED] spectrum of TT 7c

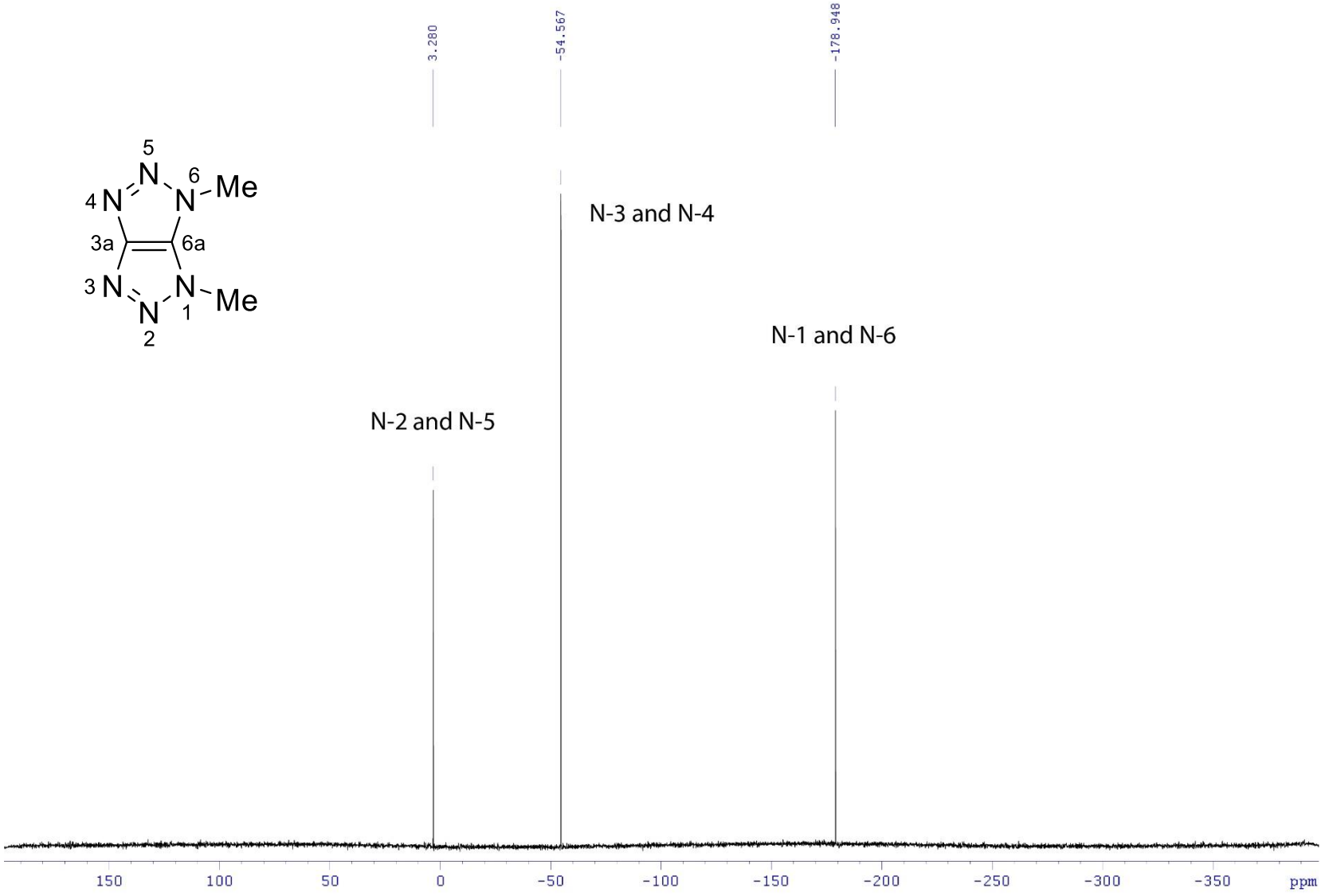

3.10.6. ^{15}N NMR [INEPT] spectrum of TT 7c

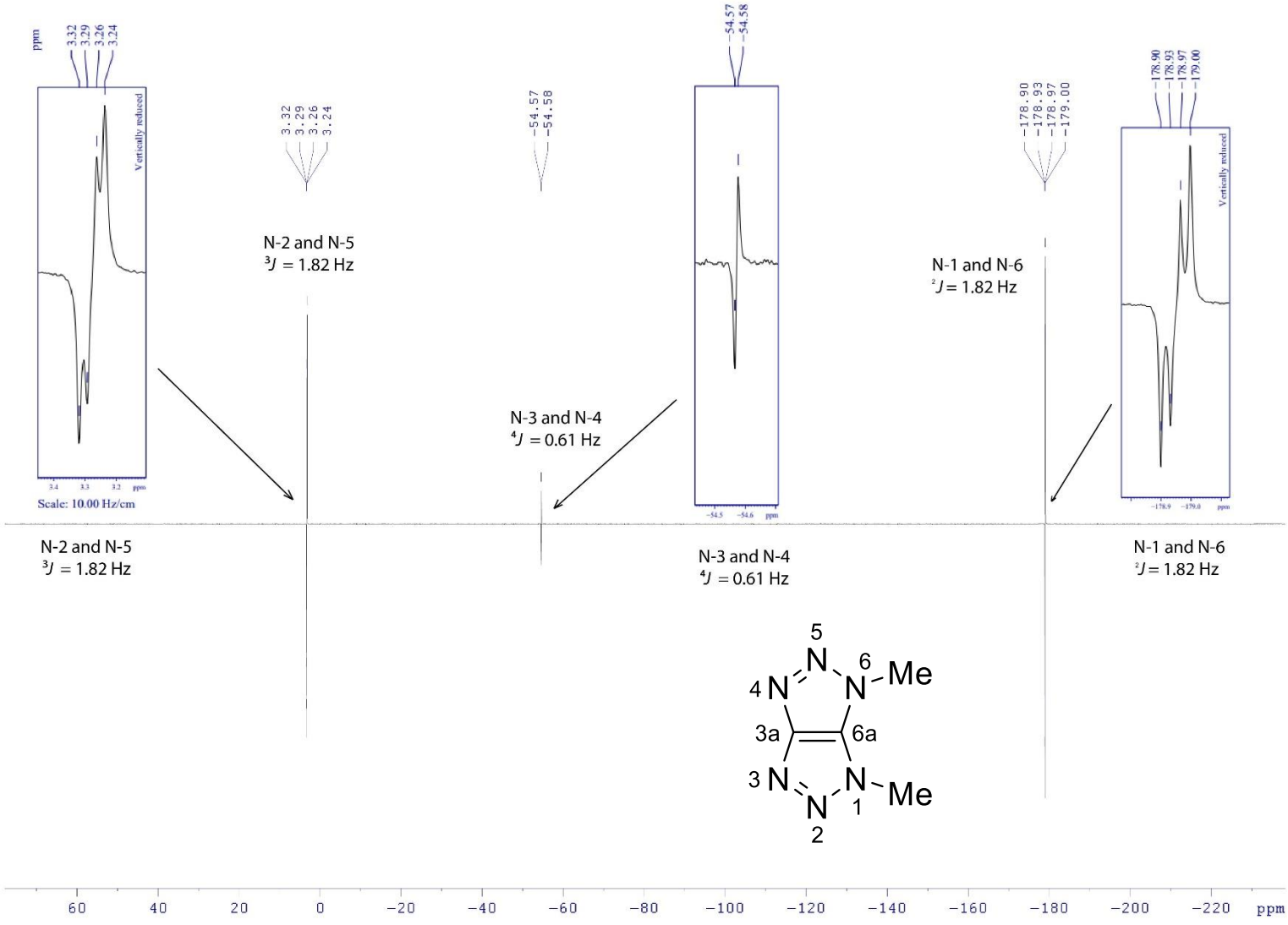

3.10.7. {^{1}H–^{15}N} HMBC spectrum of TT 7c

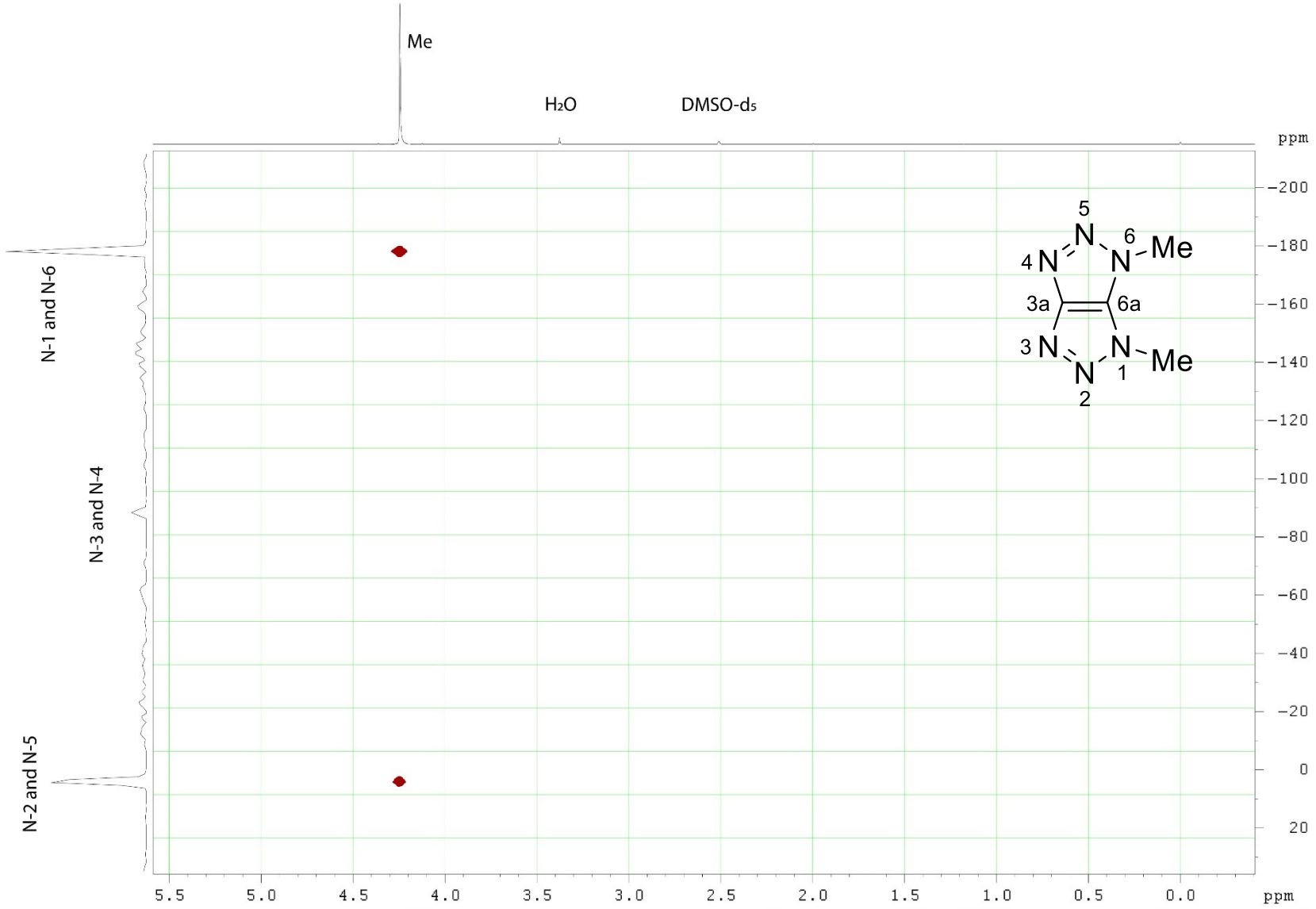

3.11.1. ^{1}H NMR spectrum of TT 7d

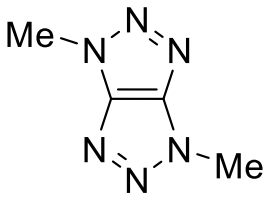

3.11.2. ^{13}C NMR spectrum of TT 7d

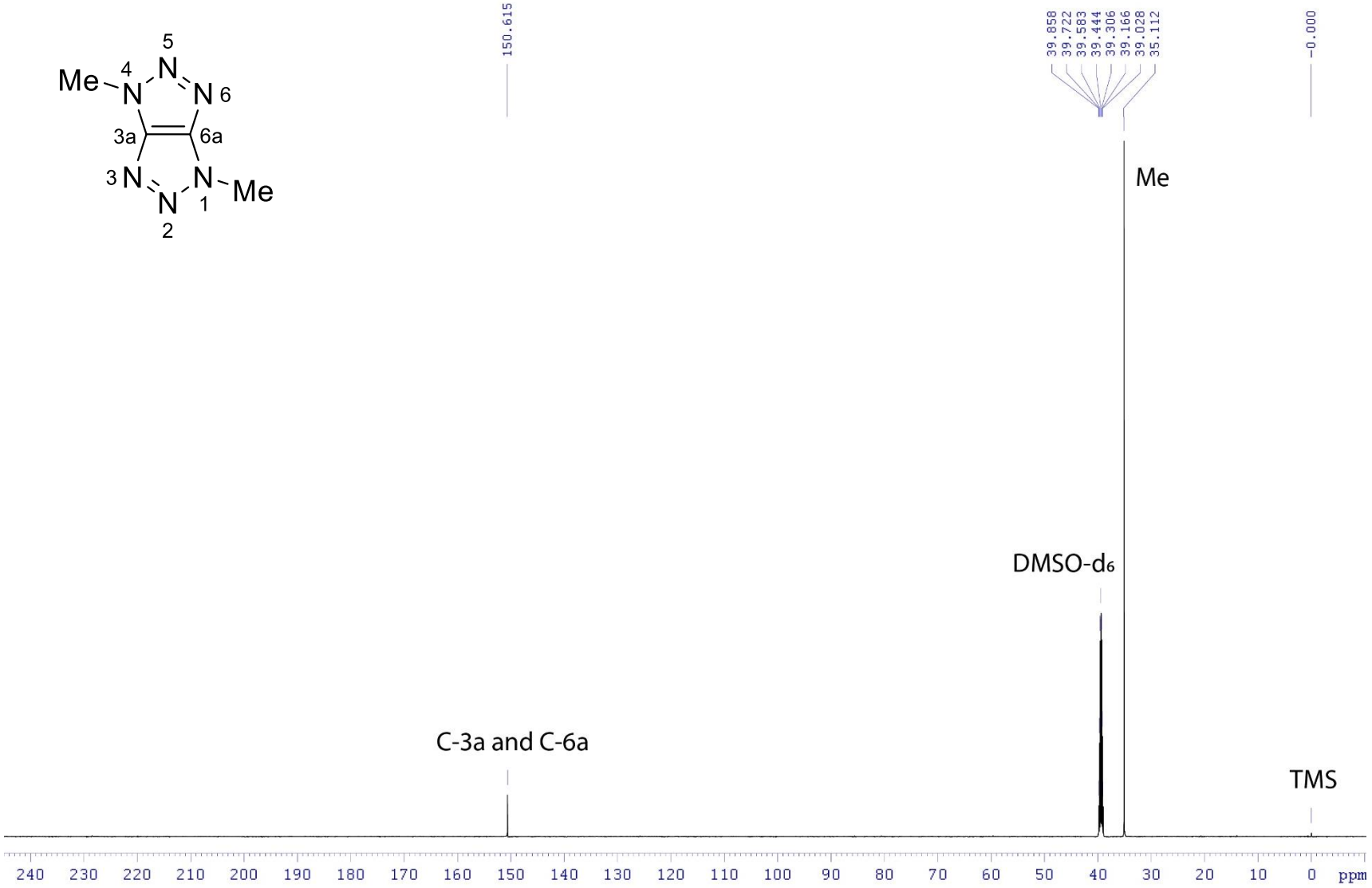

3.11.3. {^{1}H–^{13}C} HMBC spectrum of TT 7d

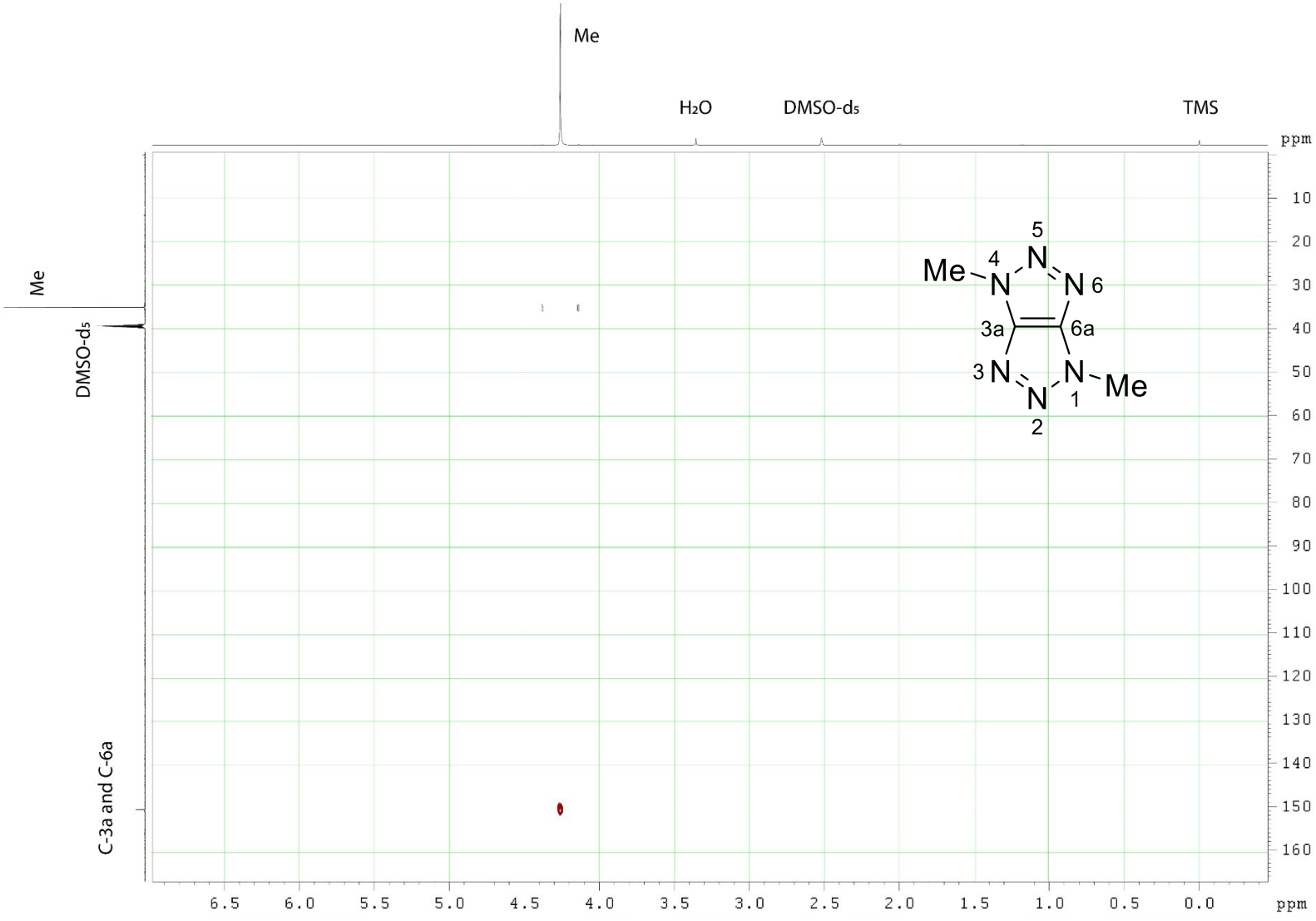

3.11.4. 14N NMR spectrum of TT 7d

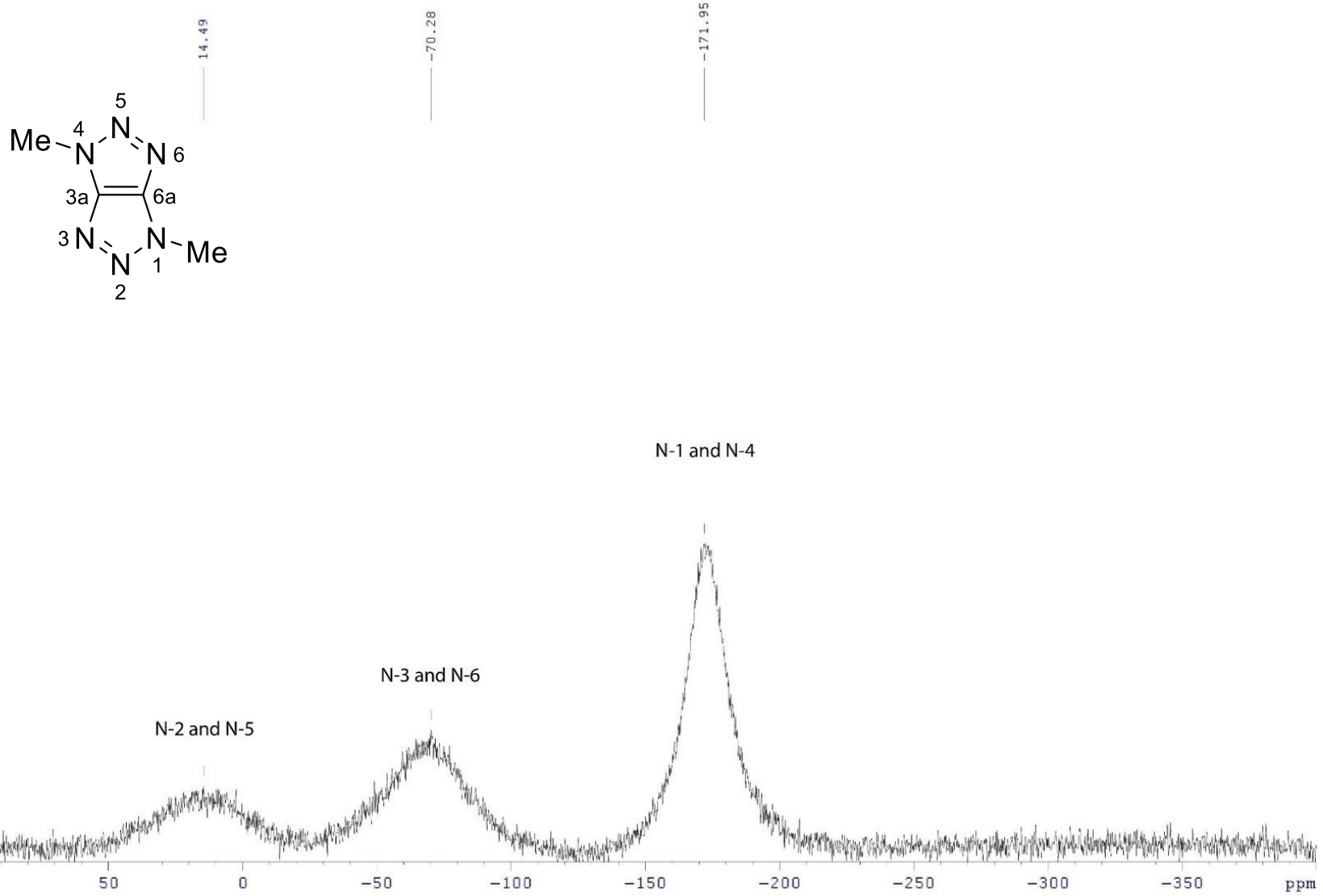

3.11.5. ^{15}N NMR [INVGATED] spectrum of TT 7d

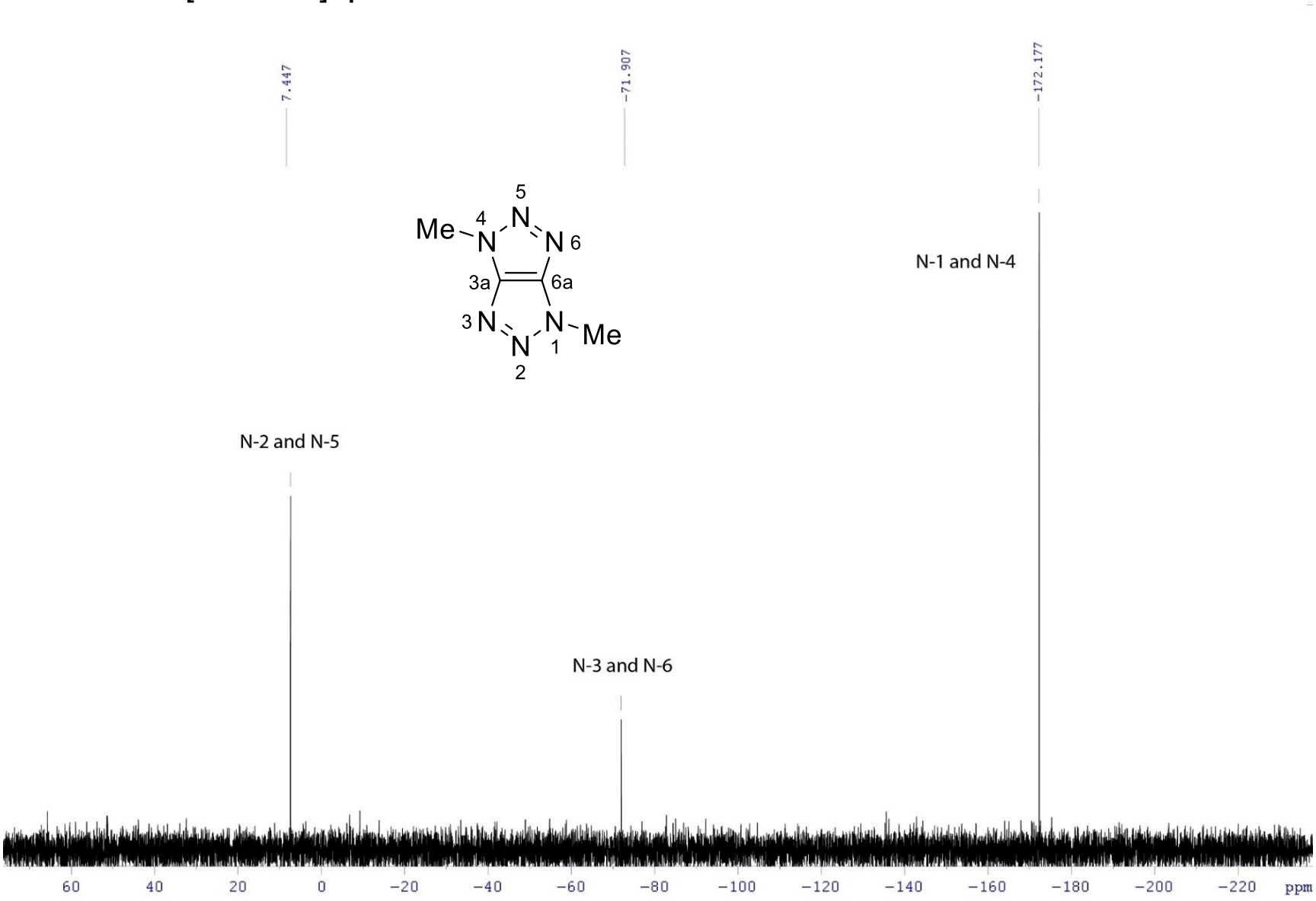

3.11.6. ^{15}N NMR [INEPT] spectrum of TT 7d

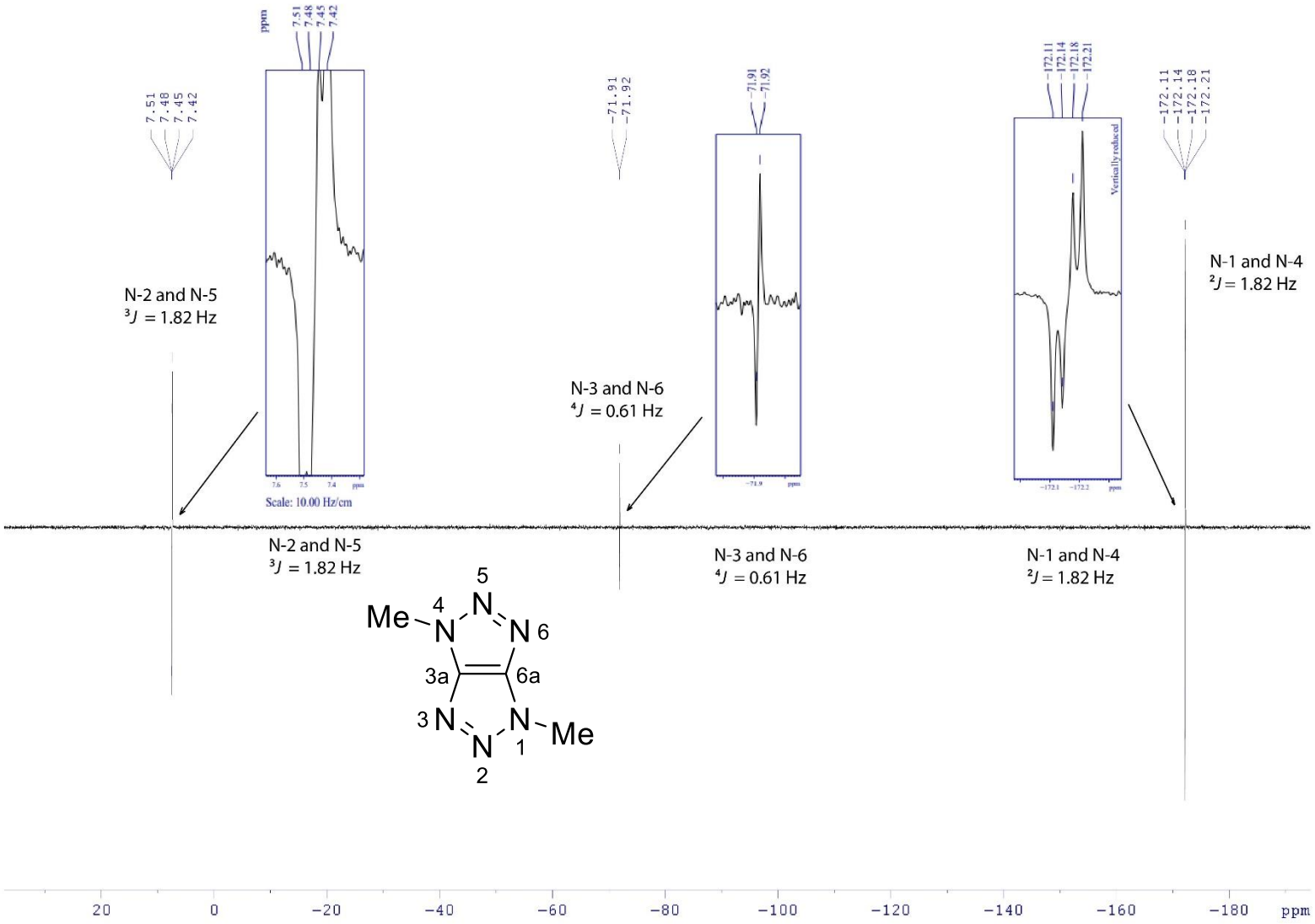

3.12.1. ^{1}H NMR spectrum of TT 8

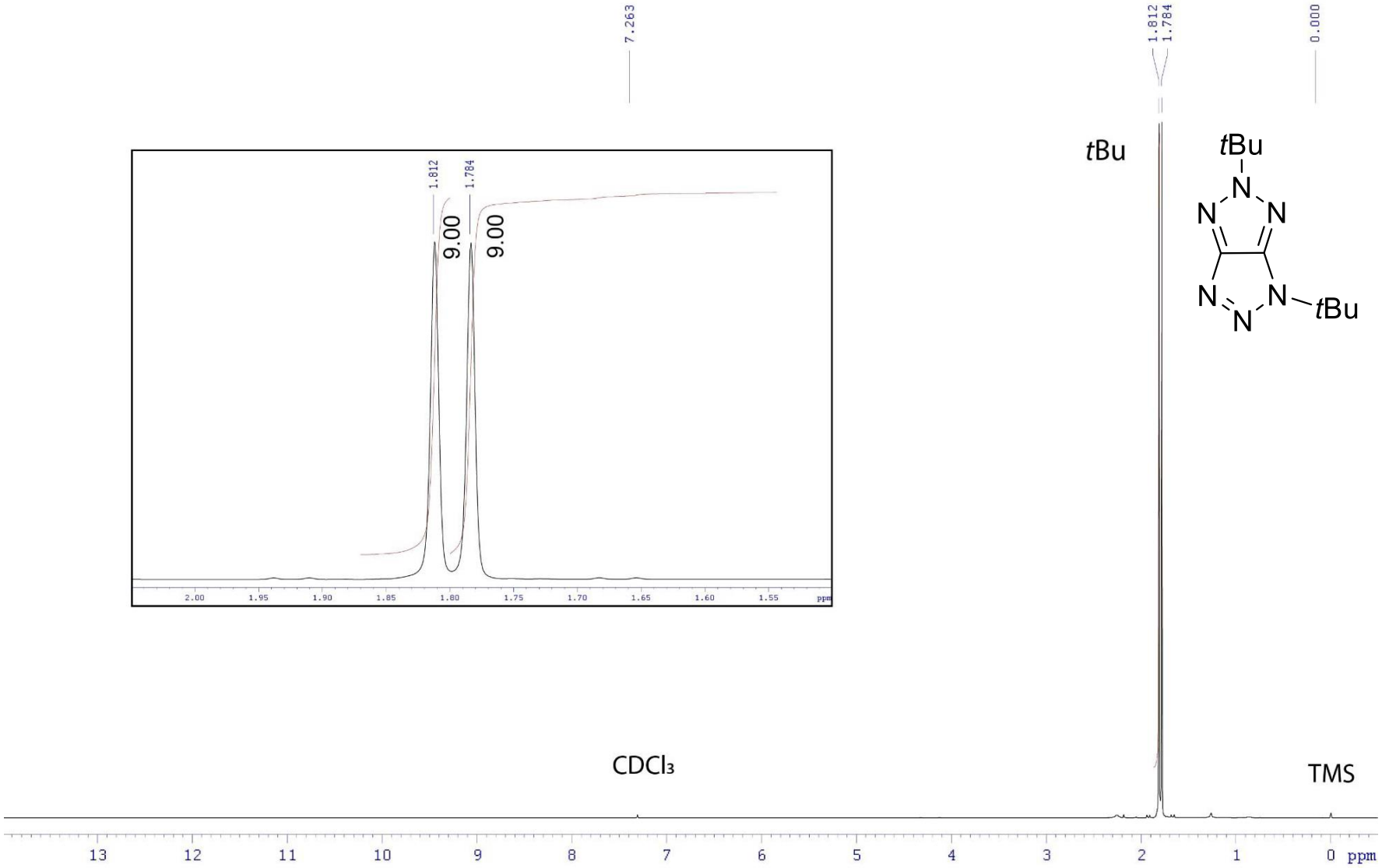

3.12.2. ^{13}C NMR spectrum of TT 8

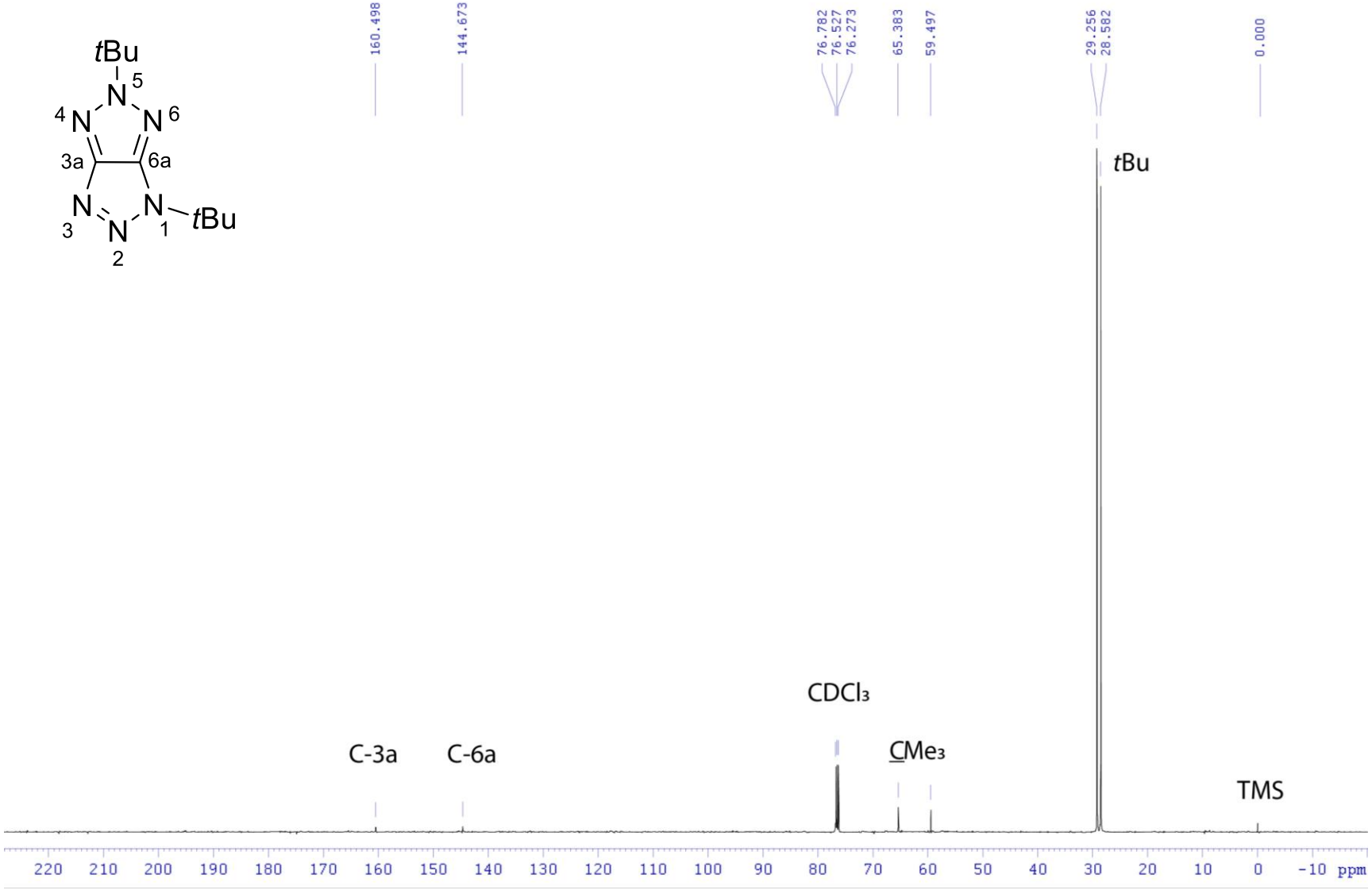

3.12.3 {^{1}H–^{13}C} HSQC spectrum of TT 8

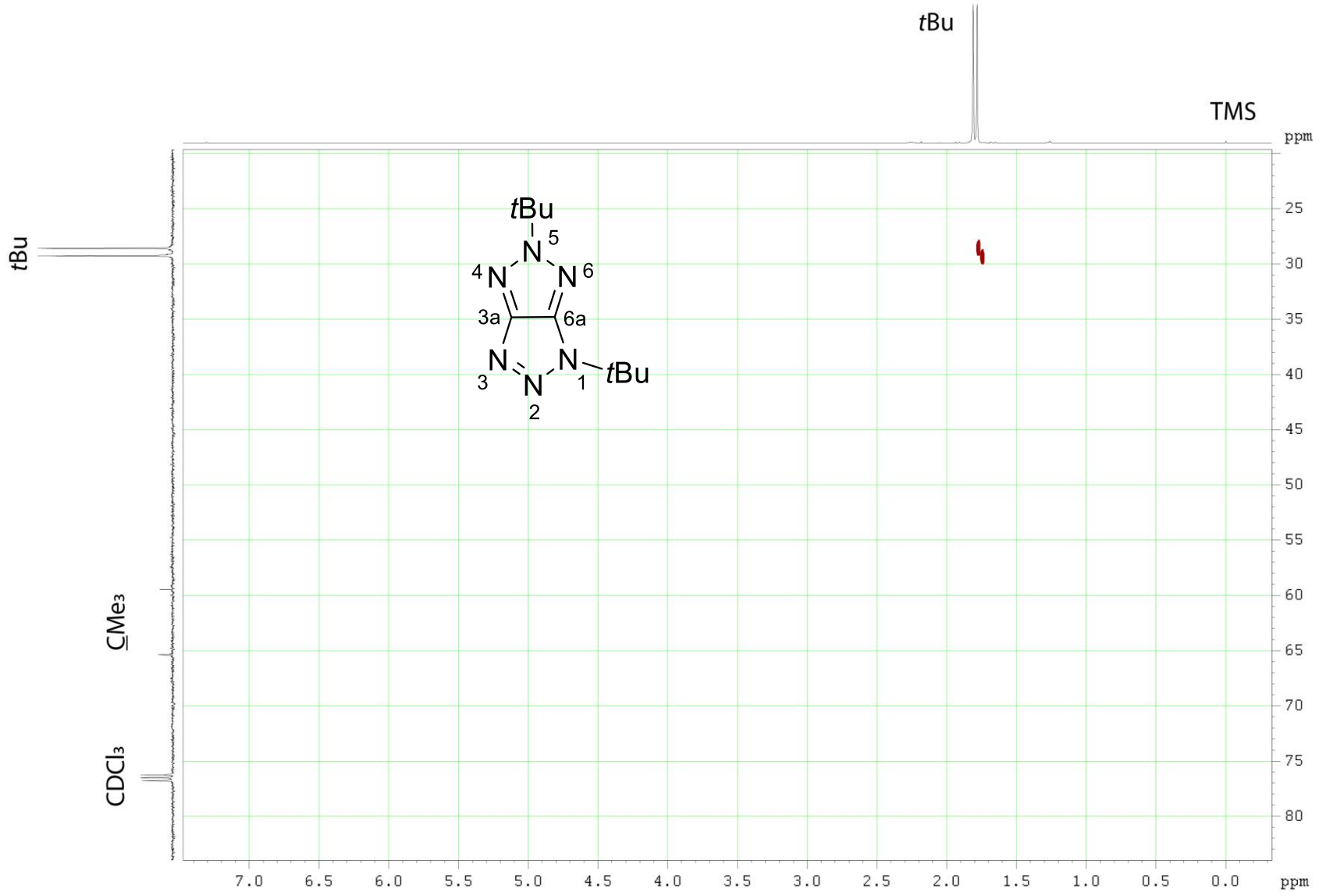

3.12.4. {^{1}H–^{13}C} HMBC spectrum of TT 8

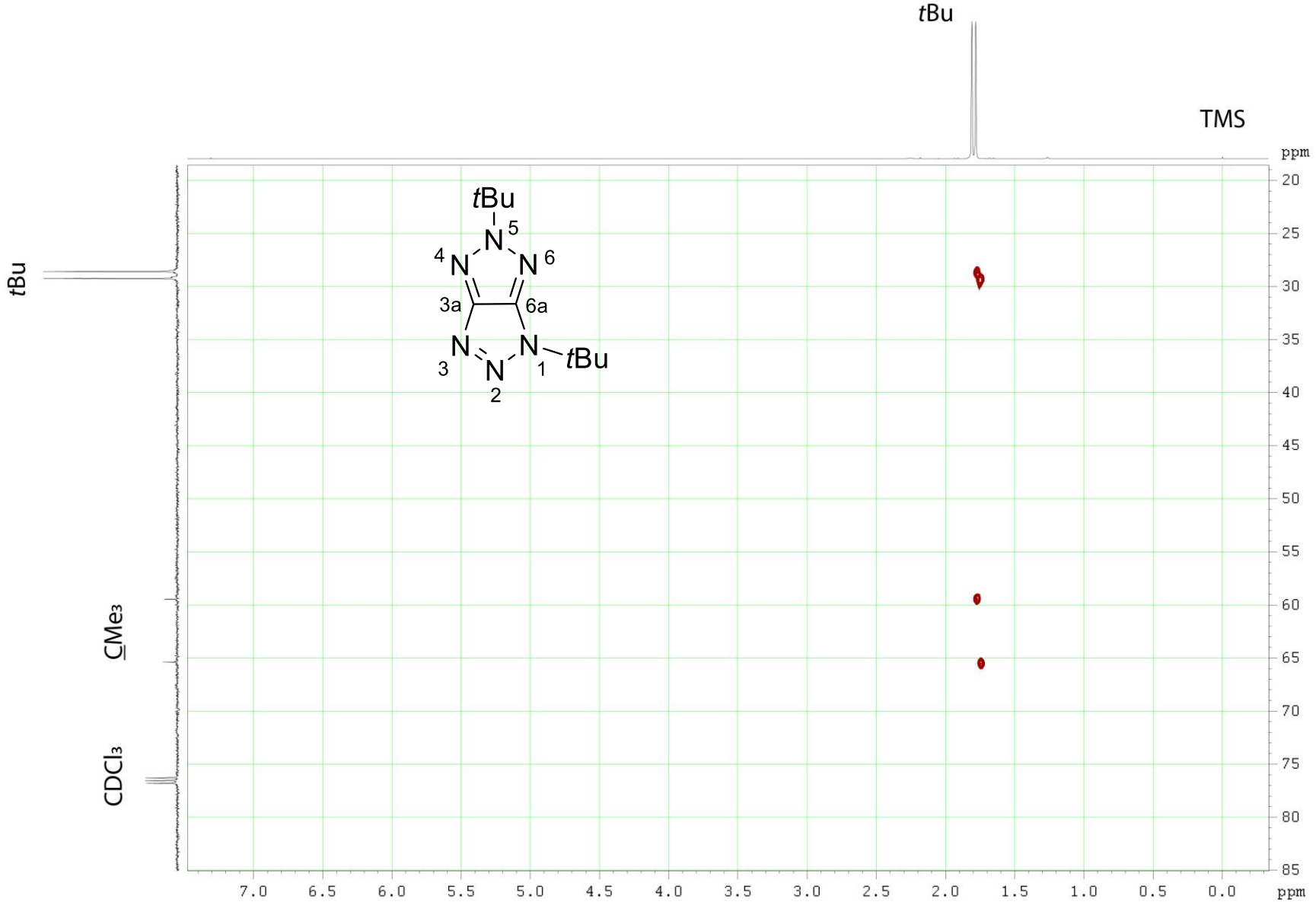

3.13.1. ^{1}H NMR spectrum of salt 9

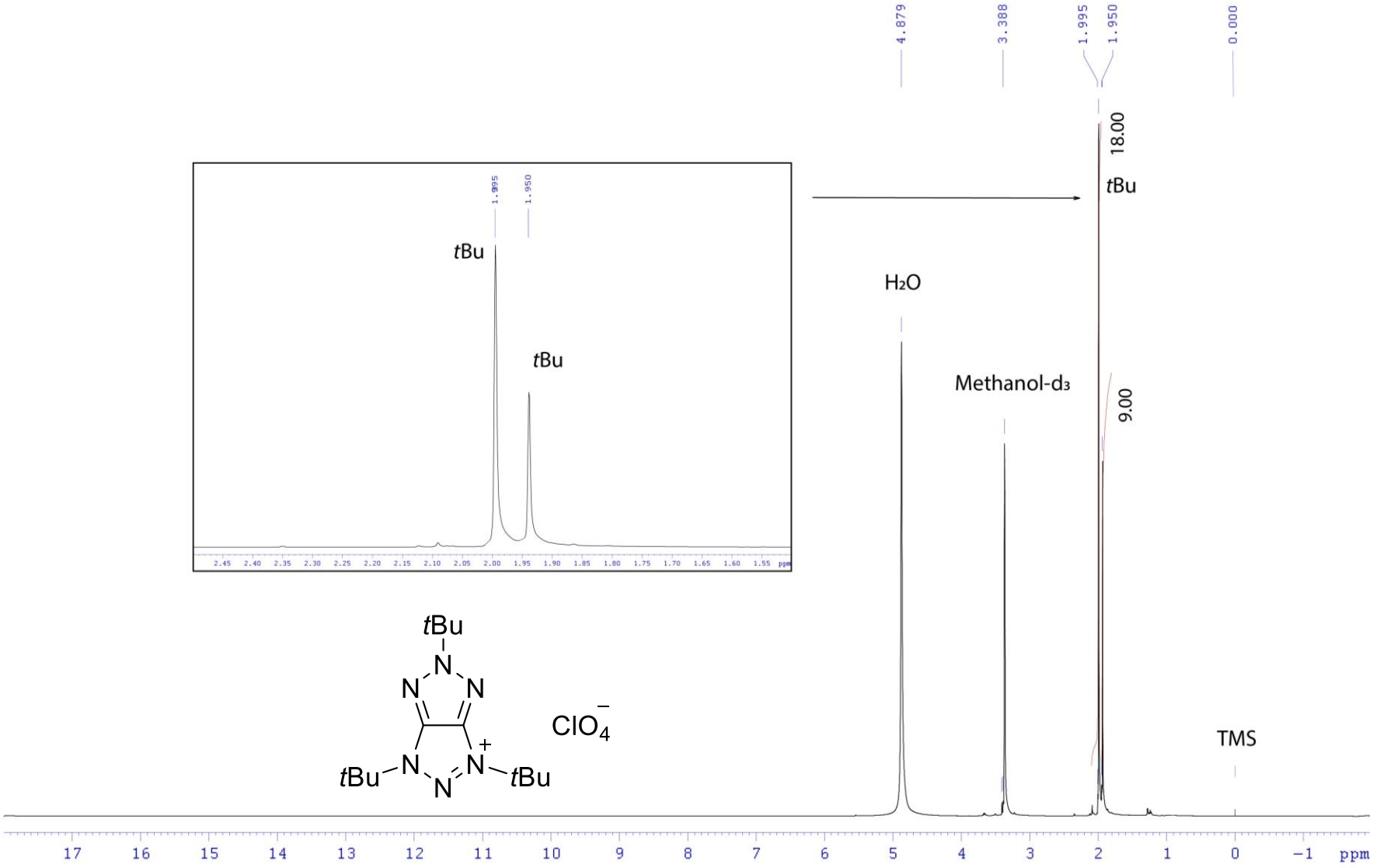

3.13.2. ^{13}C NMR spectrum of salt 9

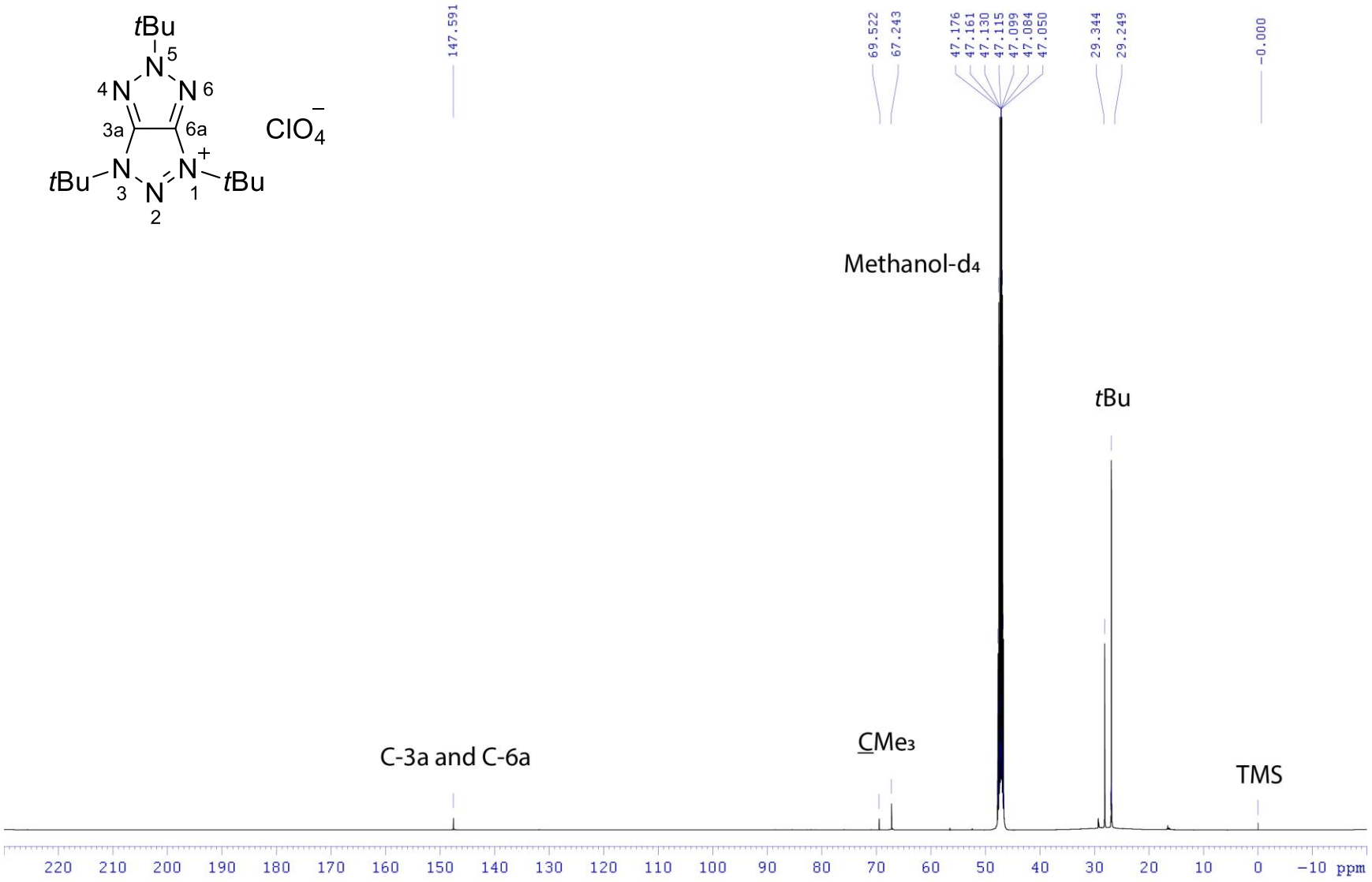

3.13.3. {^{1}H–^{15}N} HMBC spectrum of salt 9

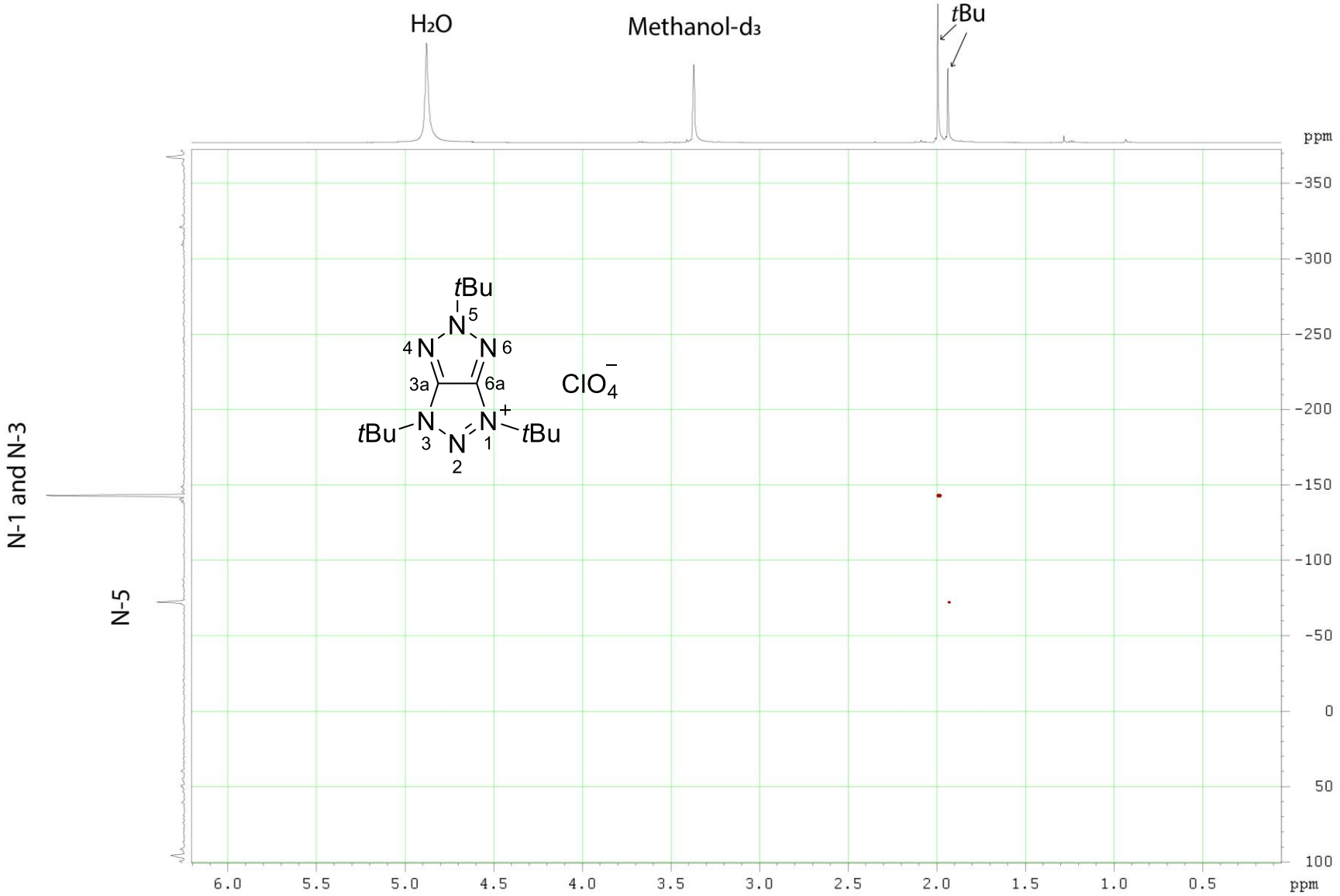

3.14.1. ^{1}H NMR spectrum of TT 10

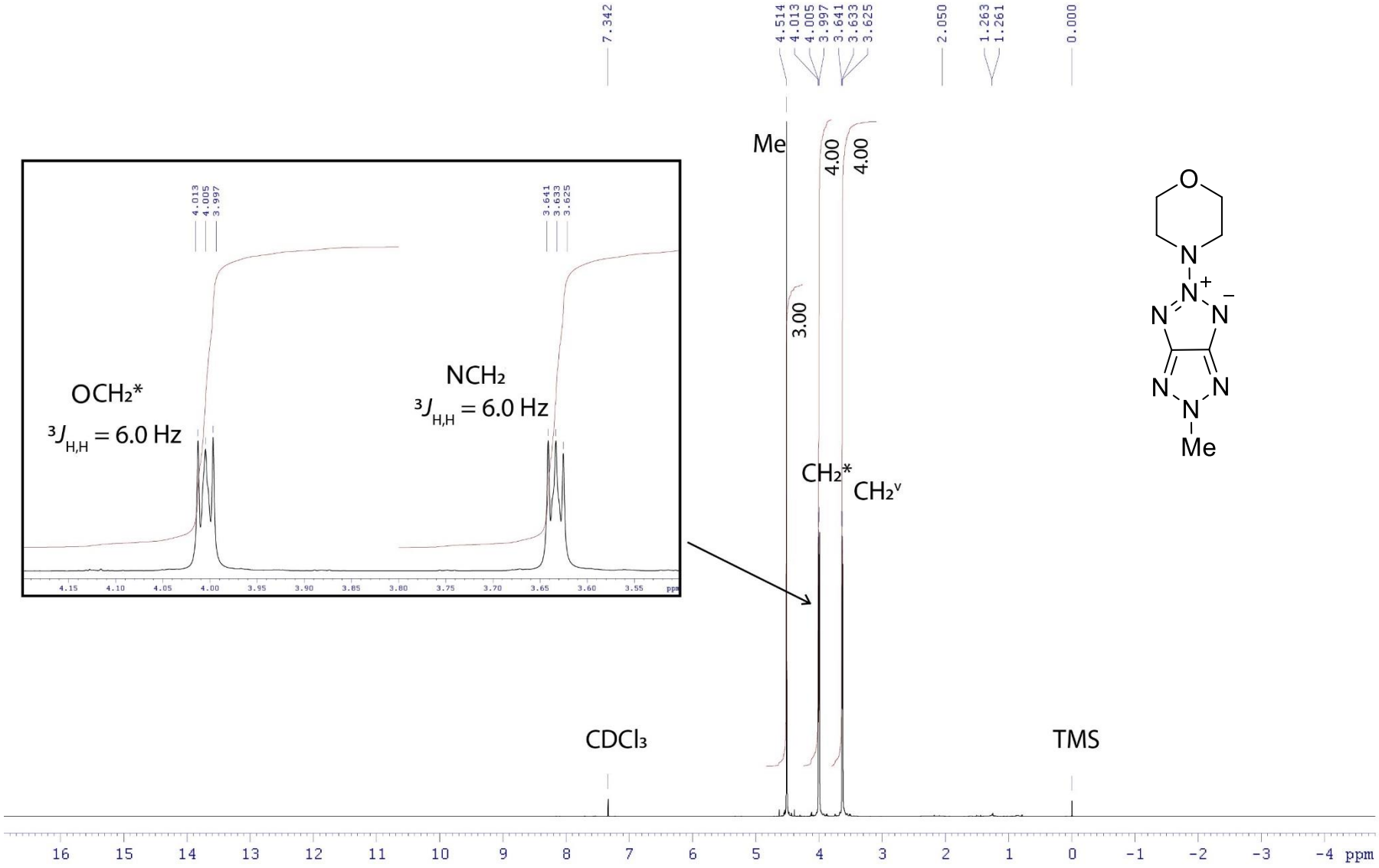

3.14.2. ^{13}C NMR spectrum of TT 10

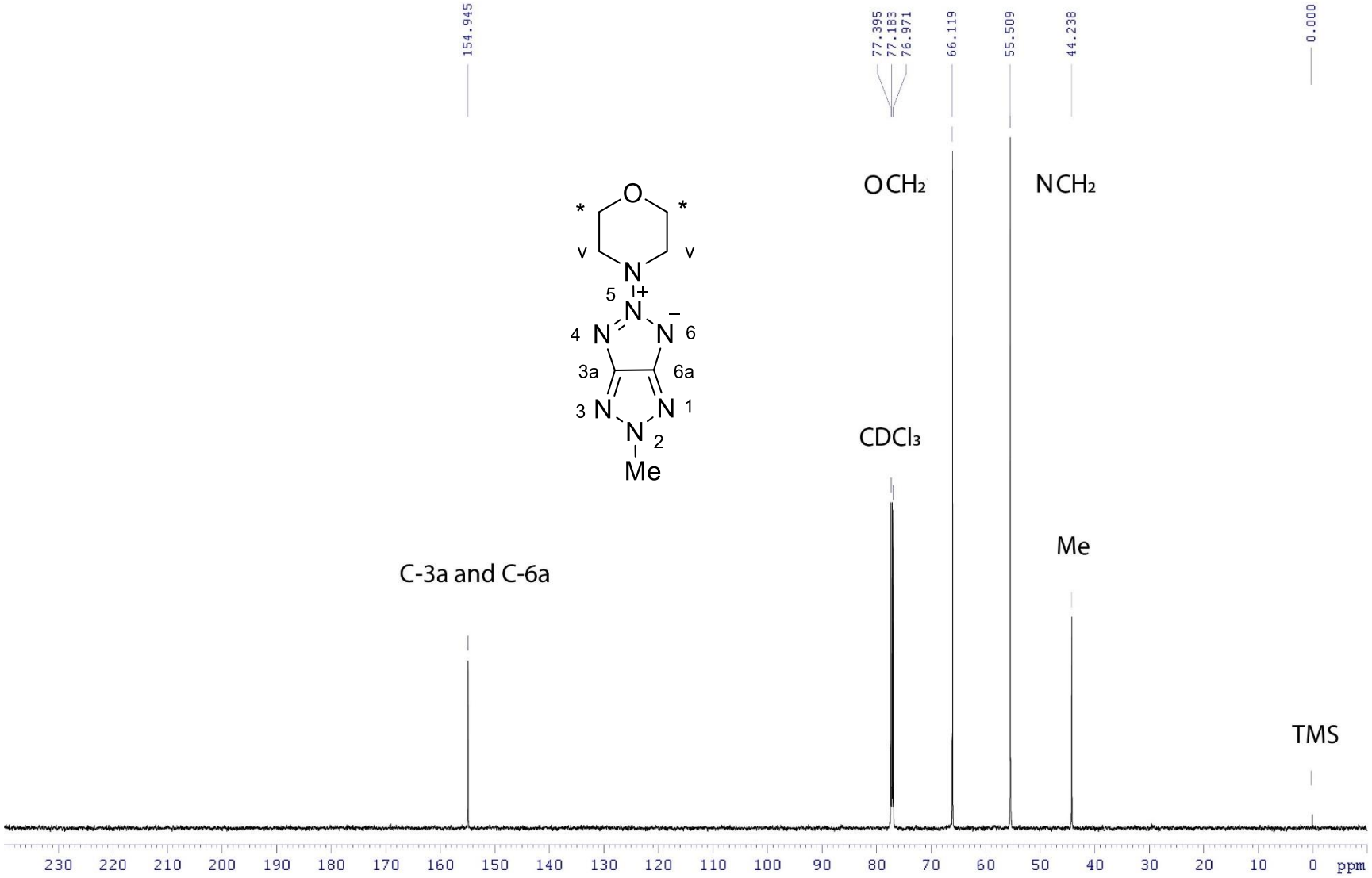

3.14.3. {^{1}H–^{13}C} HSQC spectrum of TT 10

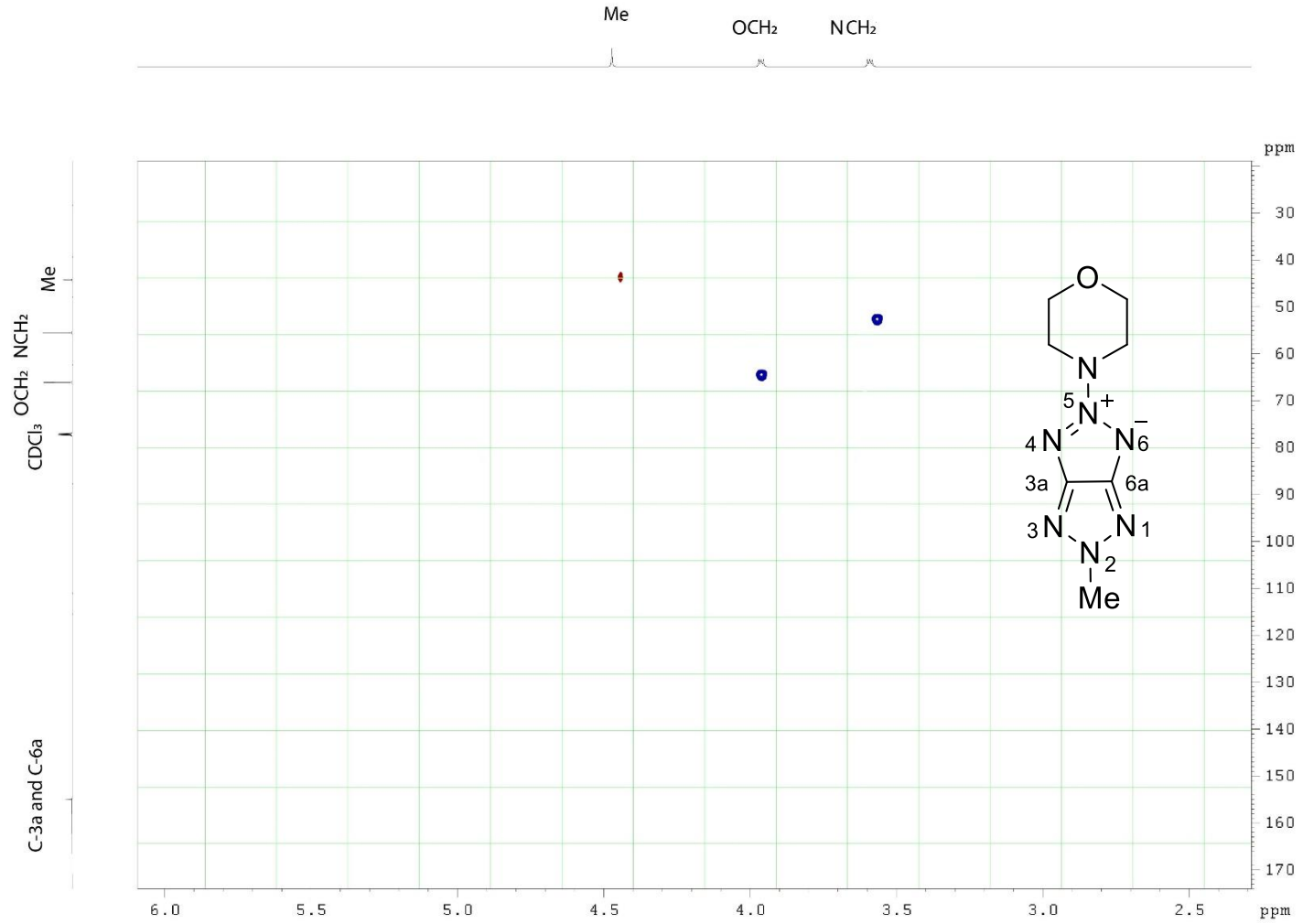

3.14.4. {^{1}H–^{13}C} HMBC spectrum of TT 10

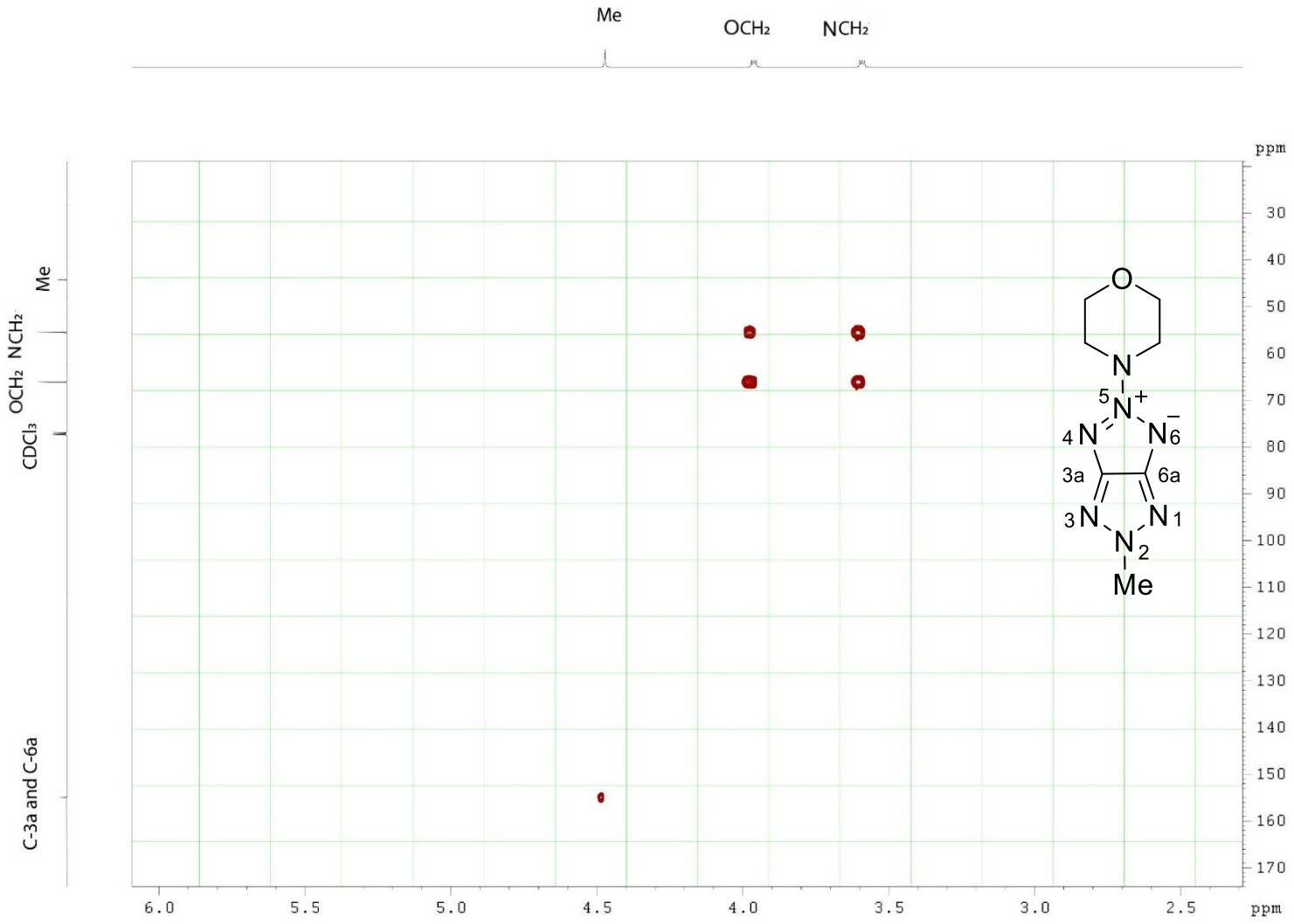

3.14.5. ^{15}N NMR spectrum of TT 10

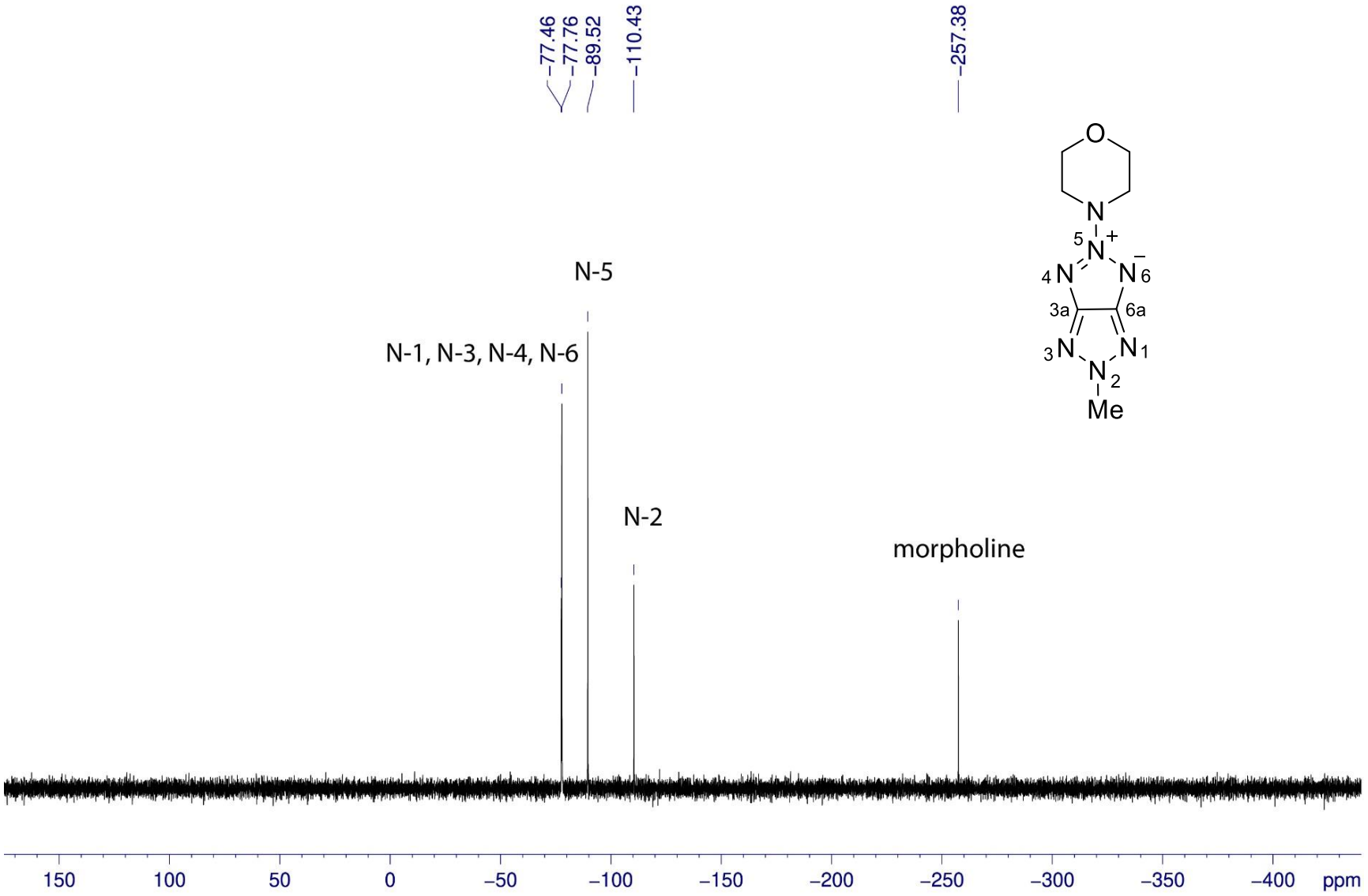

3.14.6. {^{1}H–^{15}N} HMBC spectrum of TT 10

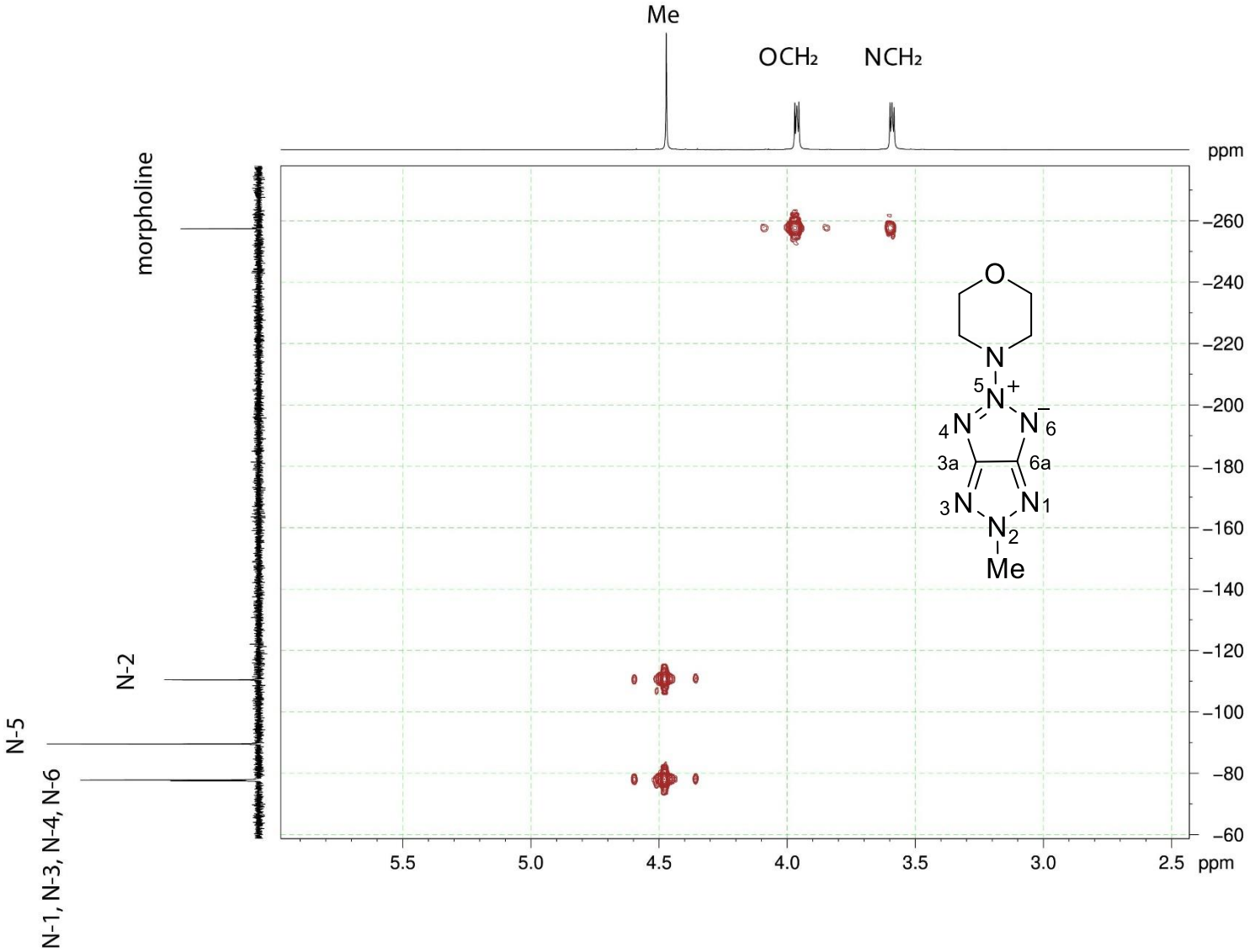

3.15.1. ^{1}H NMR spectrum of compound 11

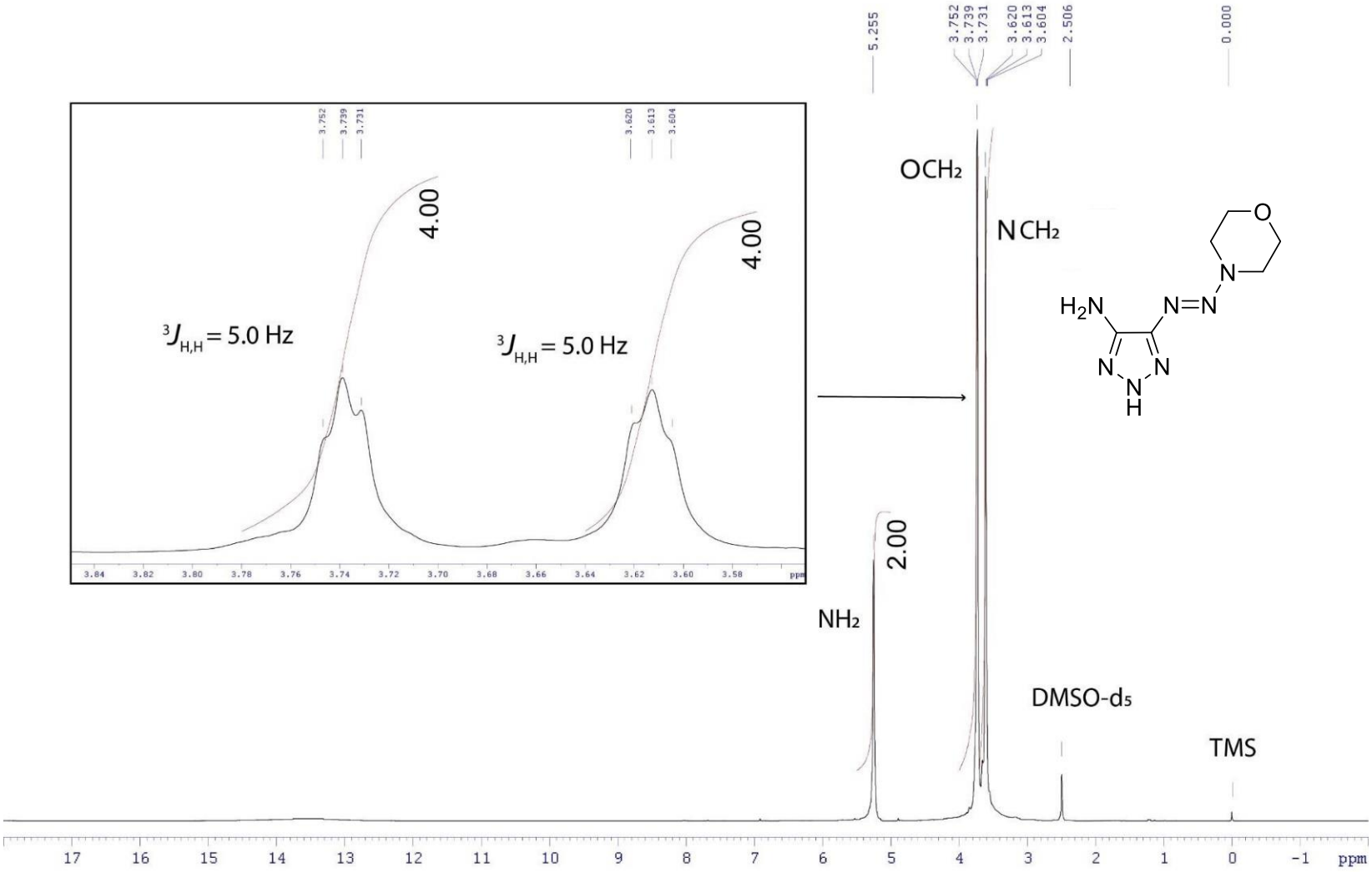

3.15.2. ^{13}C NMR spectrum of compound 11

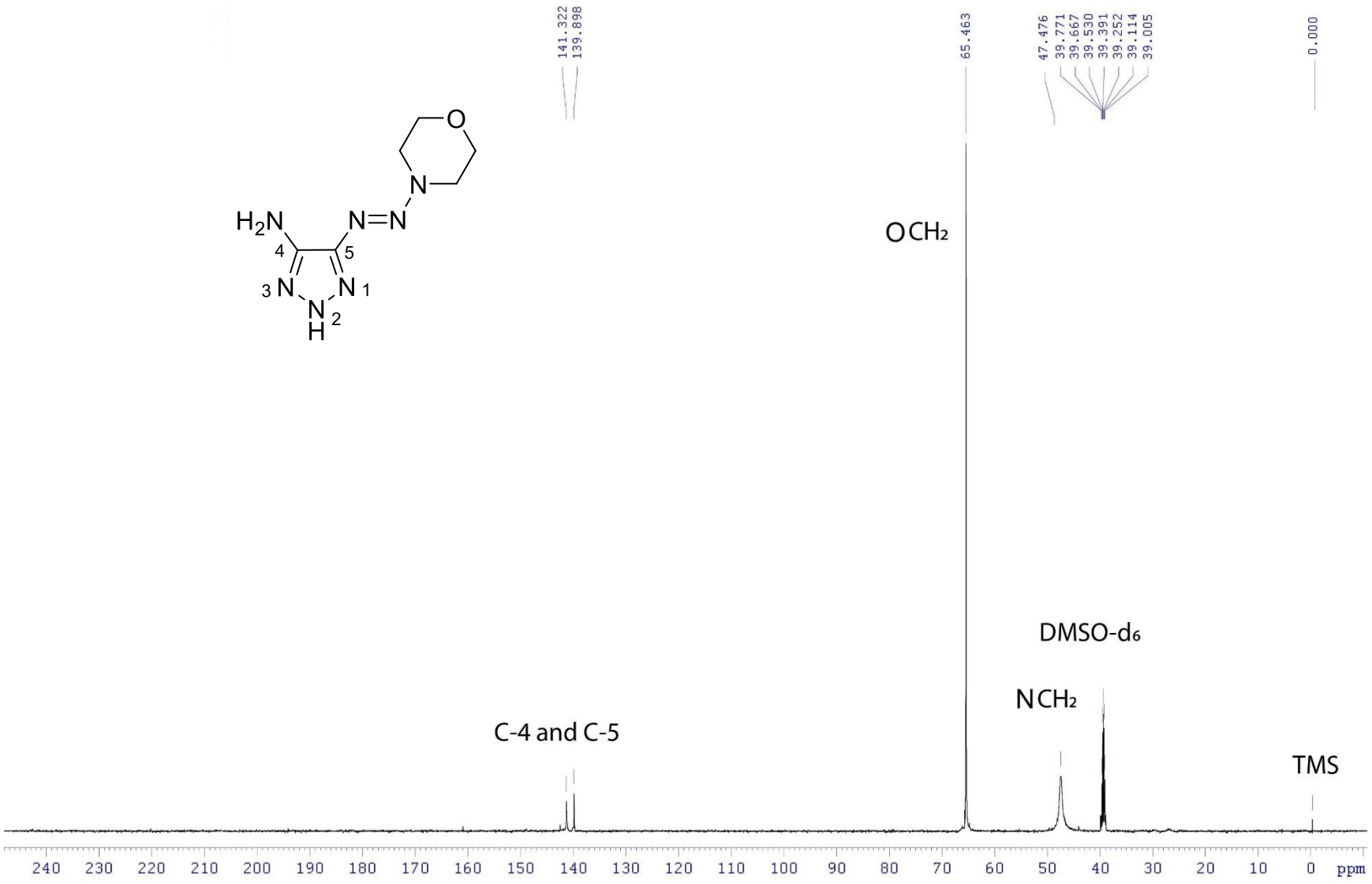

3.15.3. {^{1}H–^{13}C} HSQC spectrum of compound 11

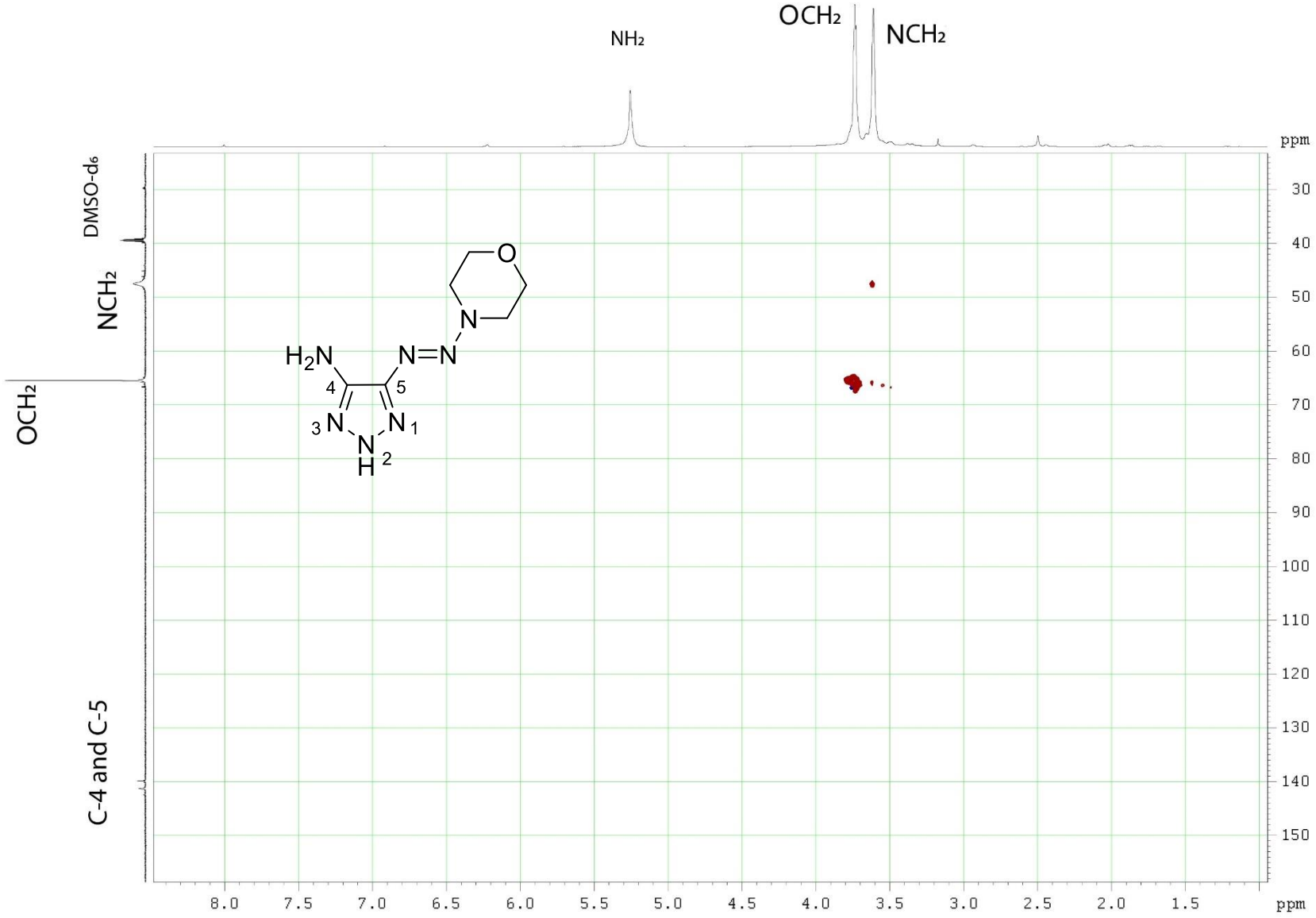

3.15.4. {^{1}H–^{13}C} HMBC spectrum of compound 11

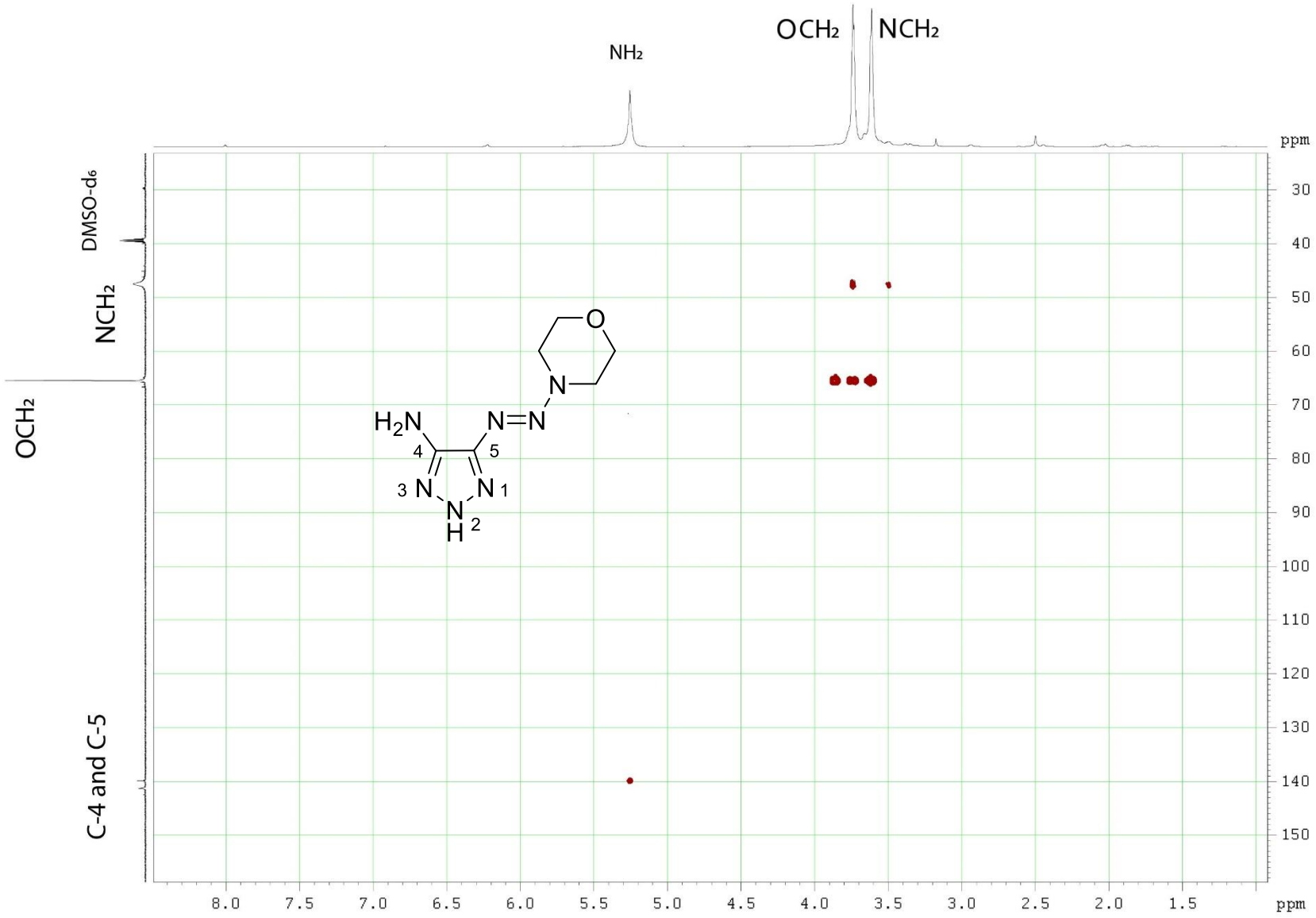

3.16.1. 1H NMR spectrum of compound 12

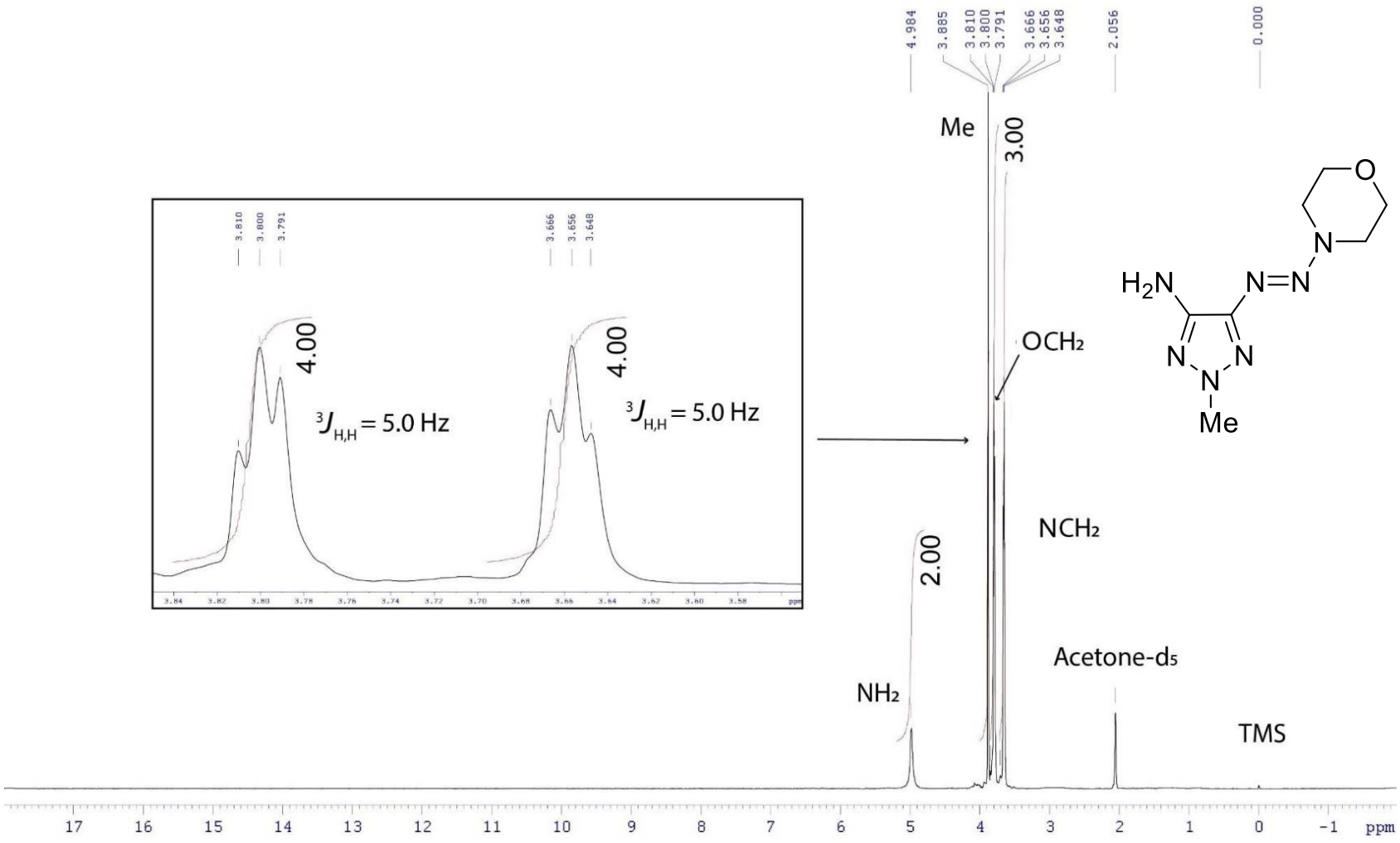

3.16.2. ^{13}C NMR spectrum of compound 12

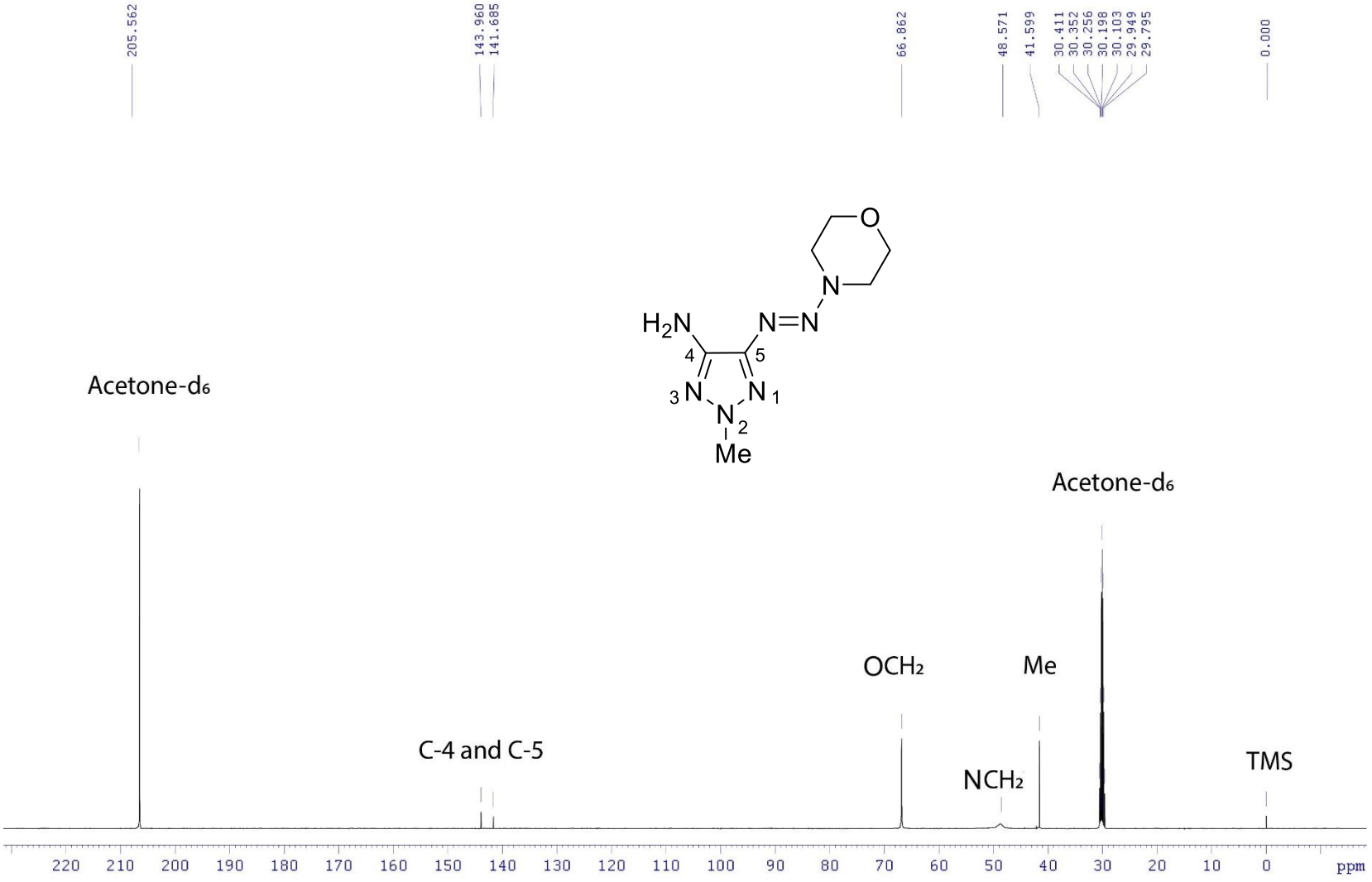

3.16.3. {^{1}H–^{13}C} HSQC spectrum of compound 12

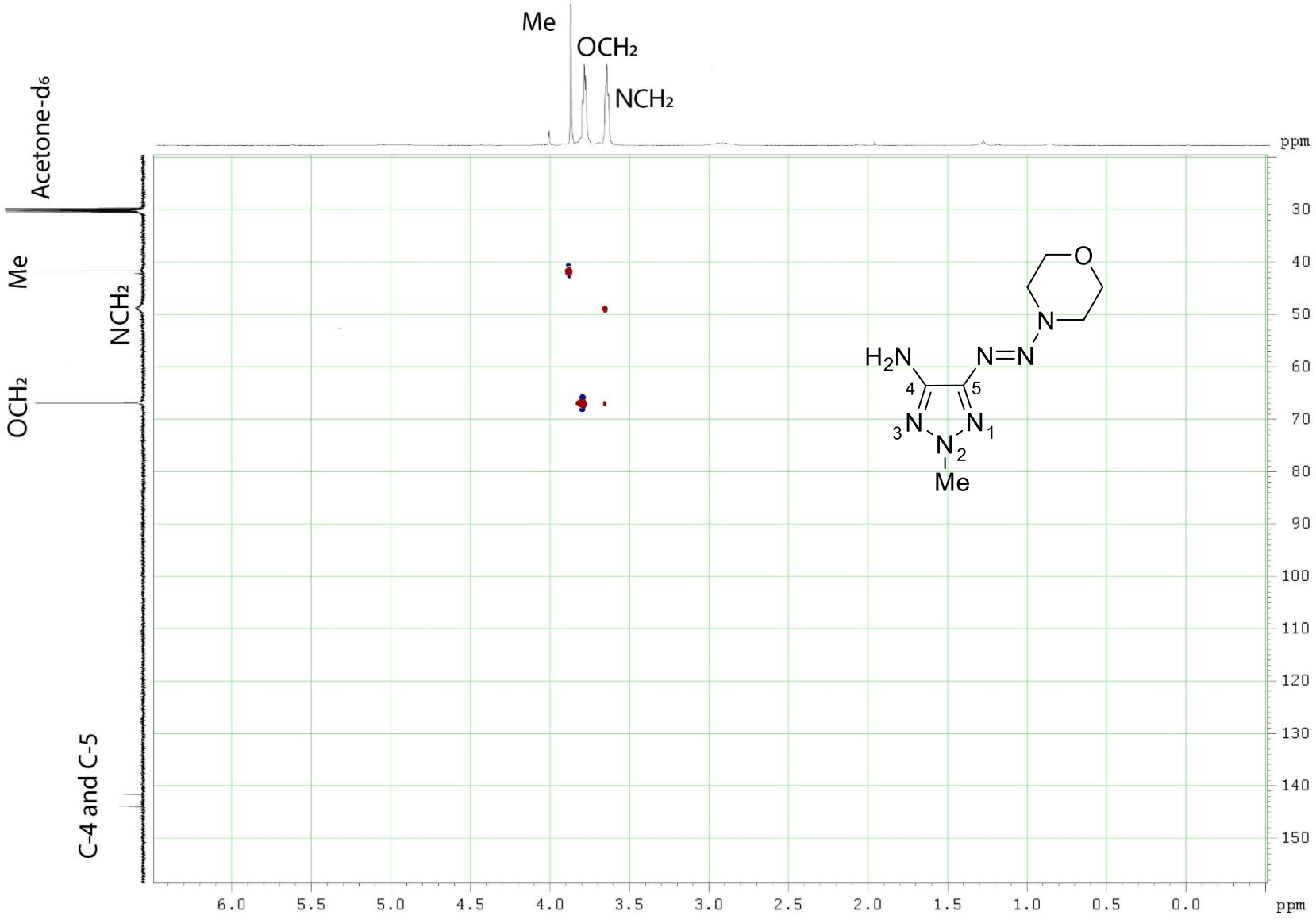

3.16.4. {^{1}H–^{13}C} HMBC spectrum of compound 12

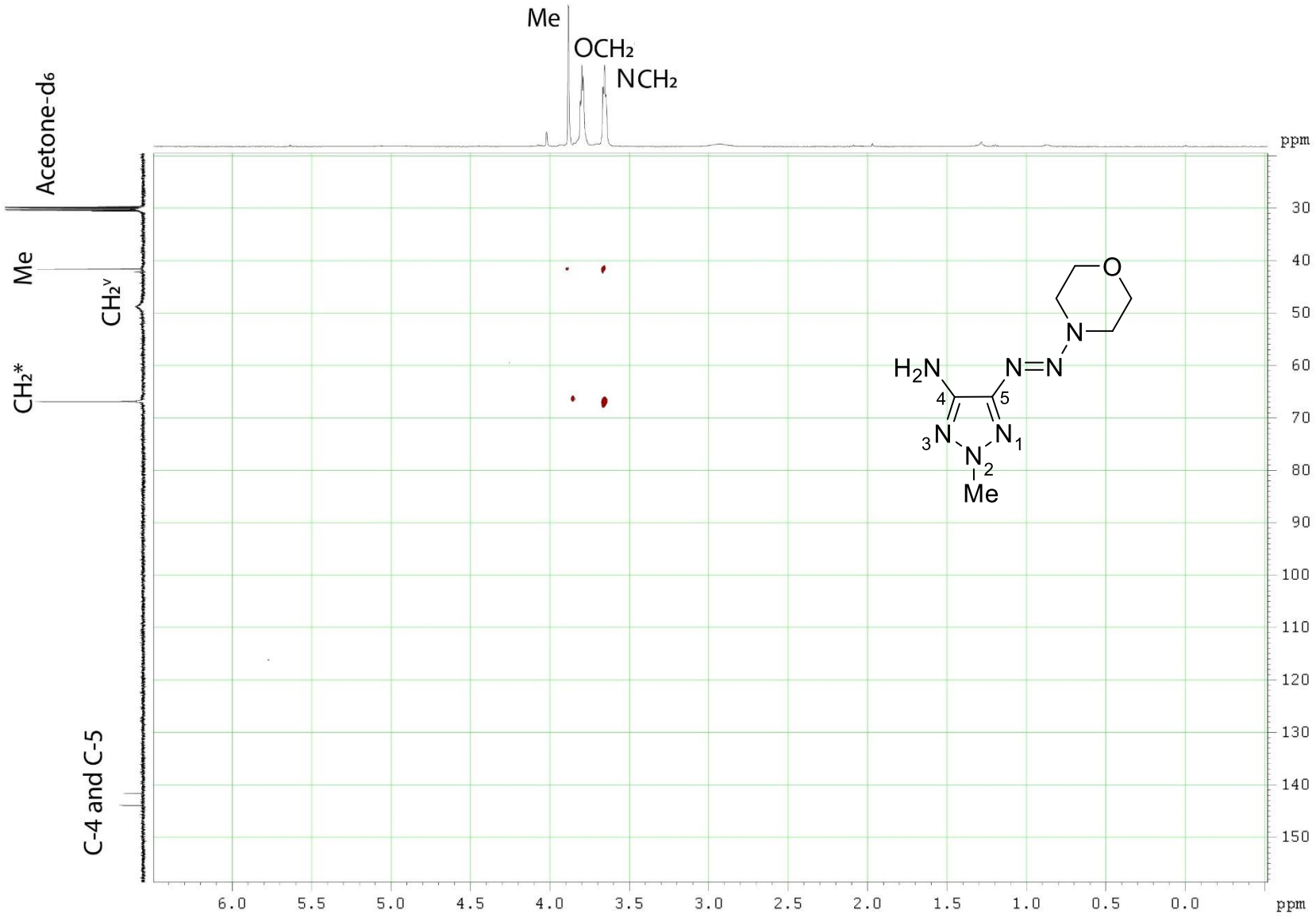

3.17.1. ^{1}H NMR spectrum of compound 13

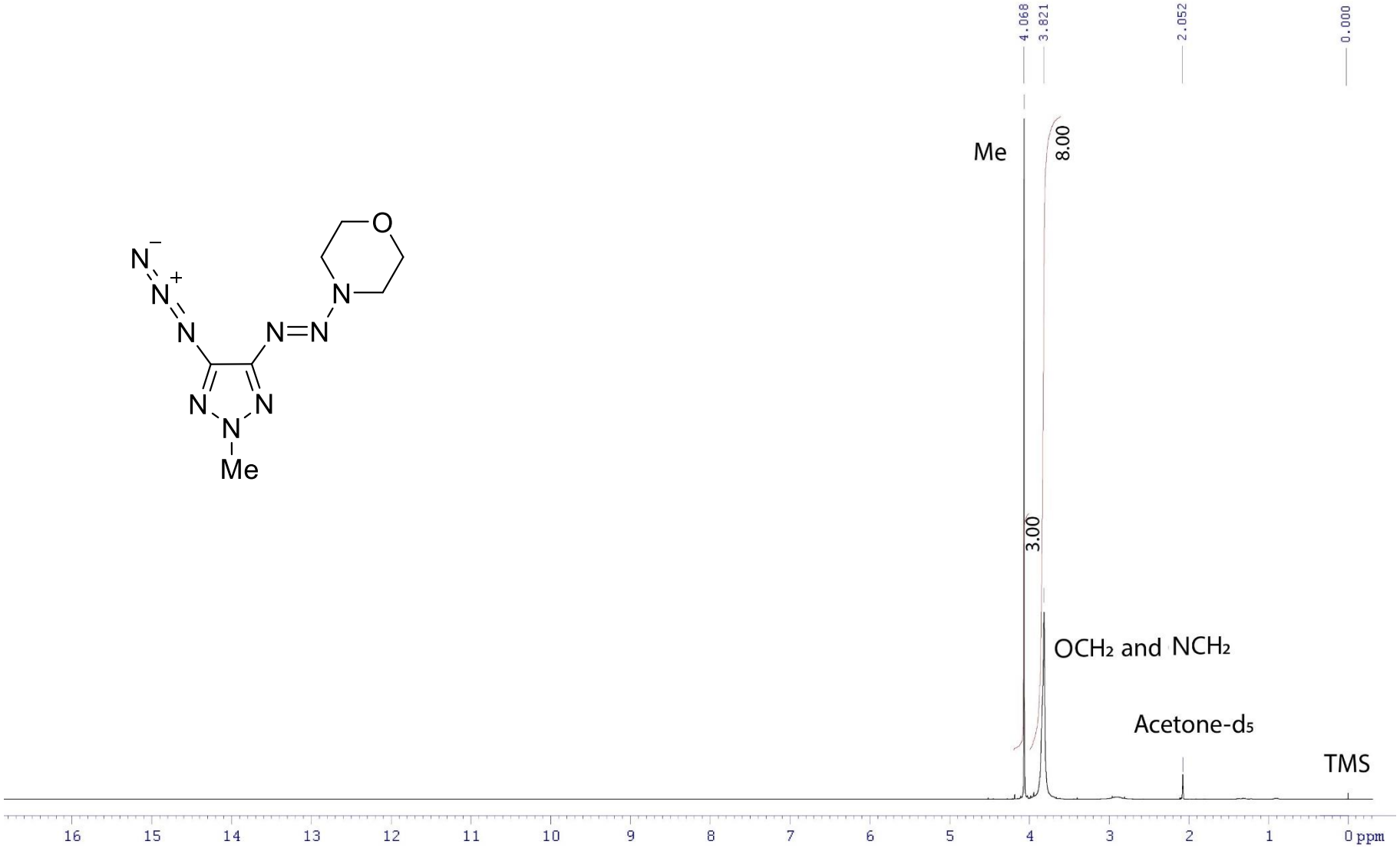

3.17.2. ^{13}C NMR spectrum of compound 13

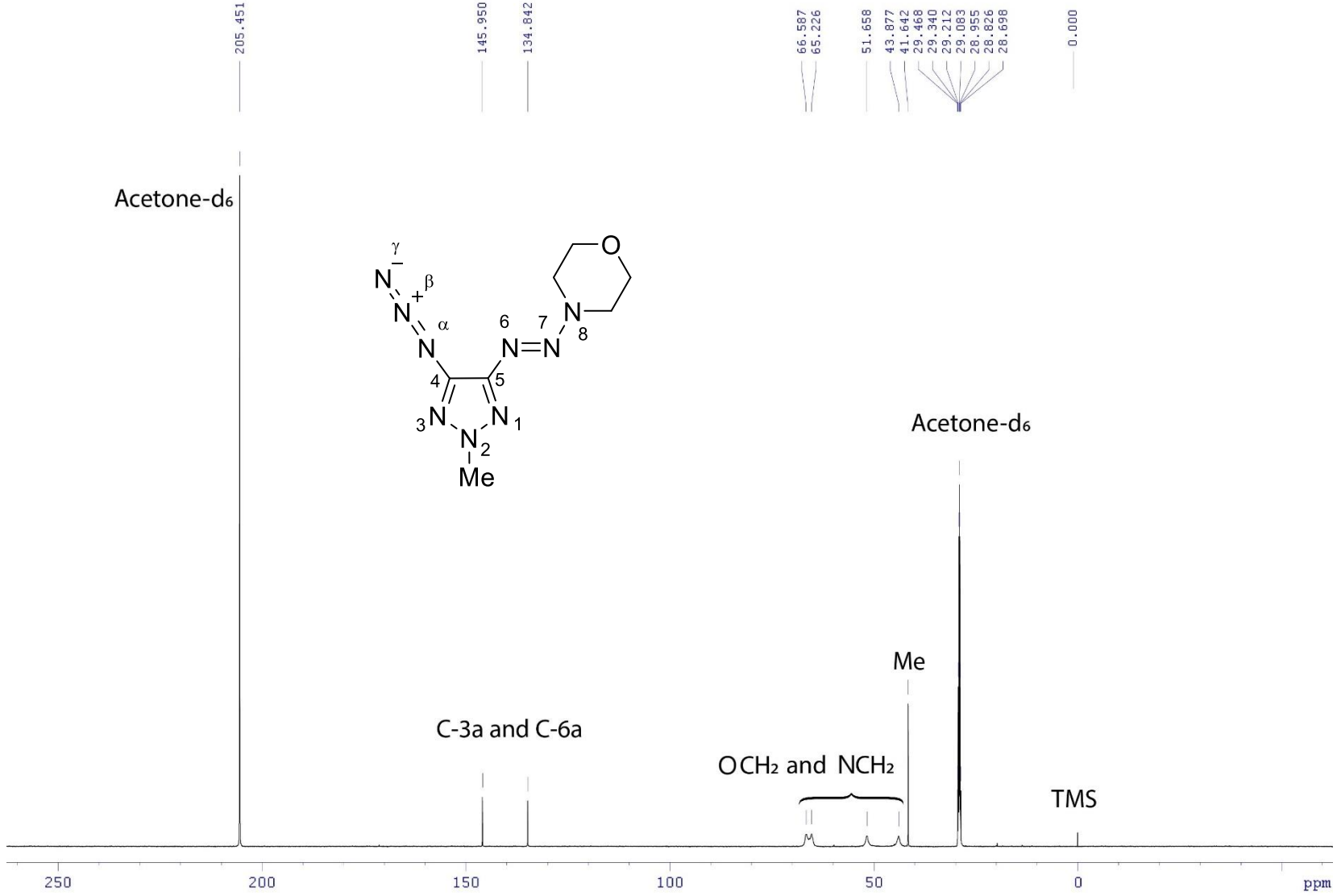

3.17.3. {^{1}H–^{13}C} HSQC spectrum of compound 13

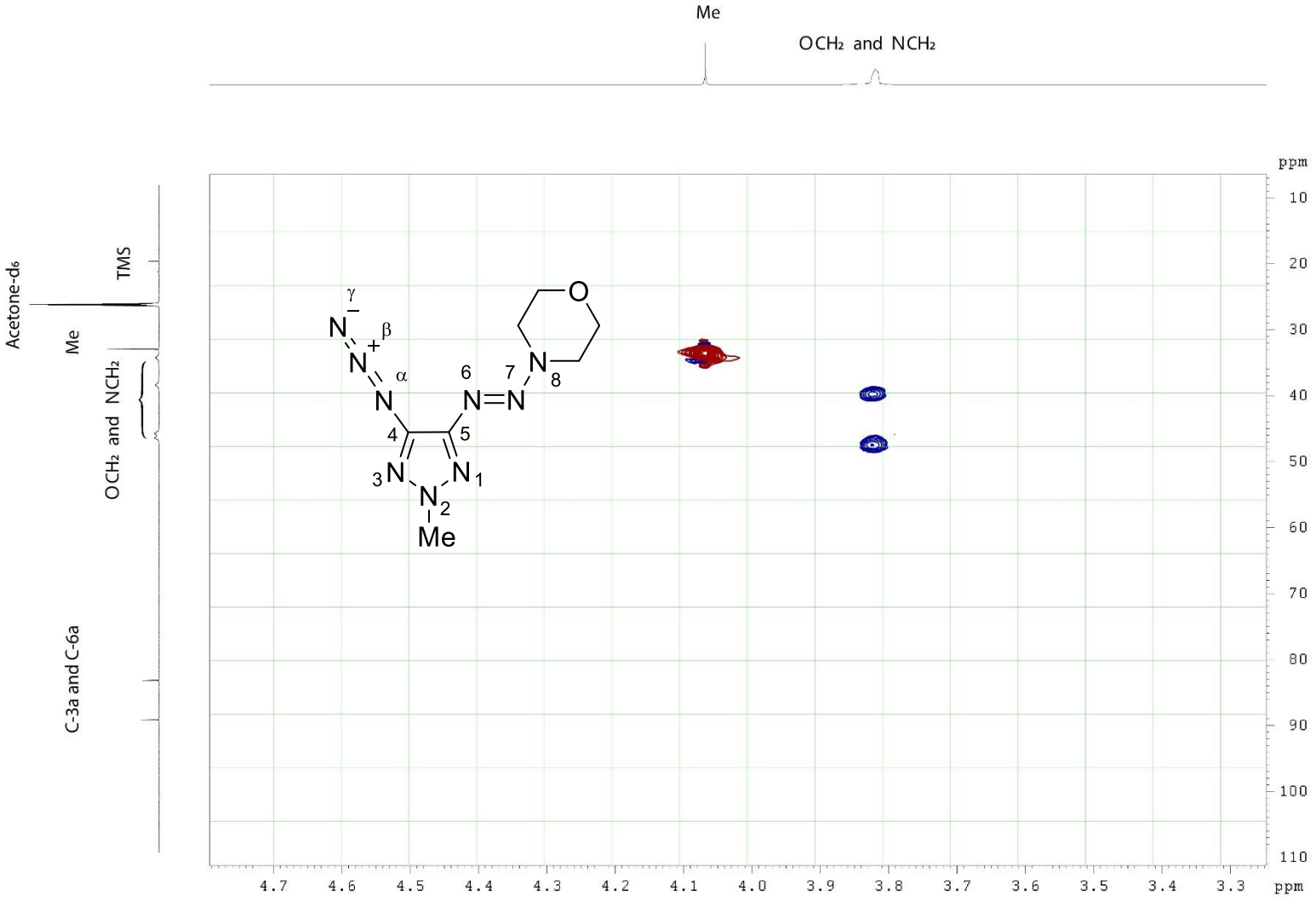

3.17.4. {1H–13C} HMBC spectrum of compound 13

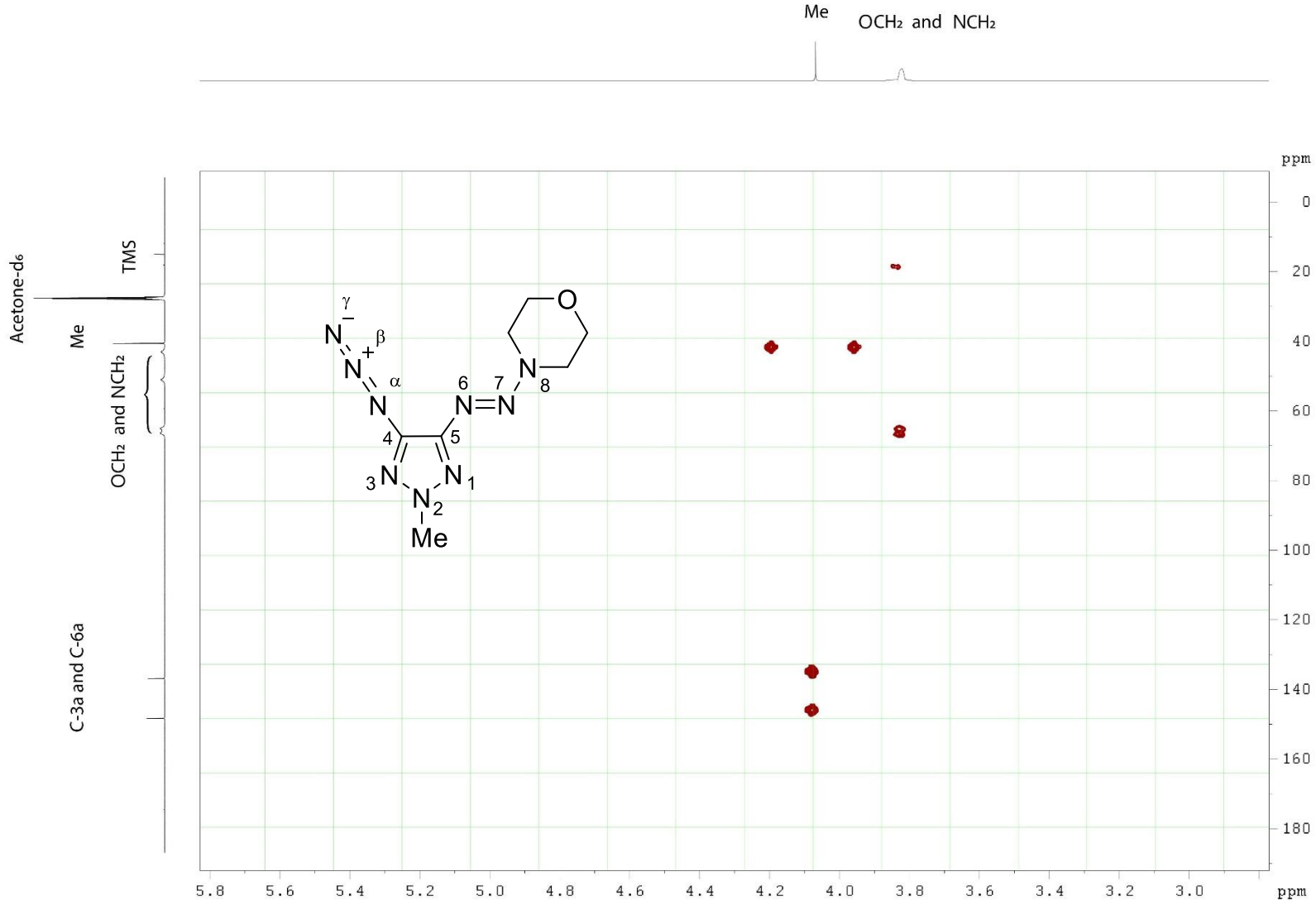

3.17.5. ^{14}N NMR spectrum of compound 13

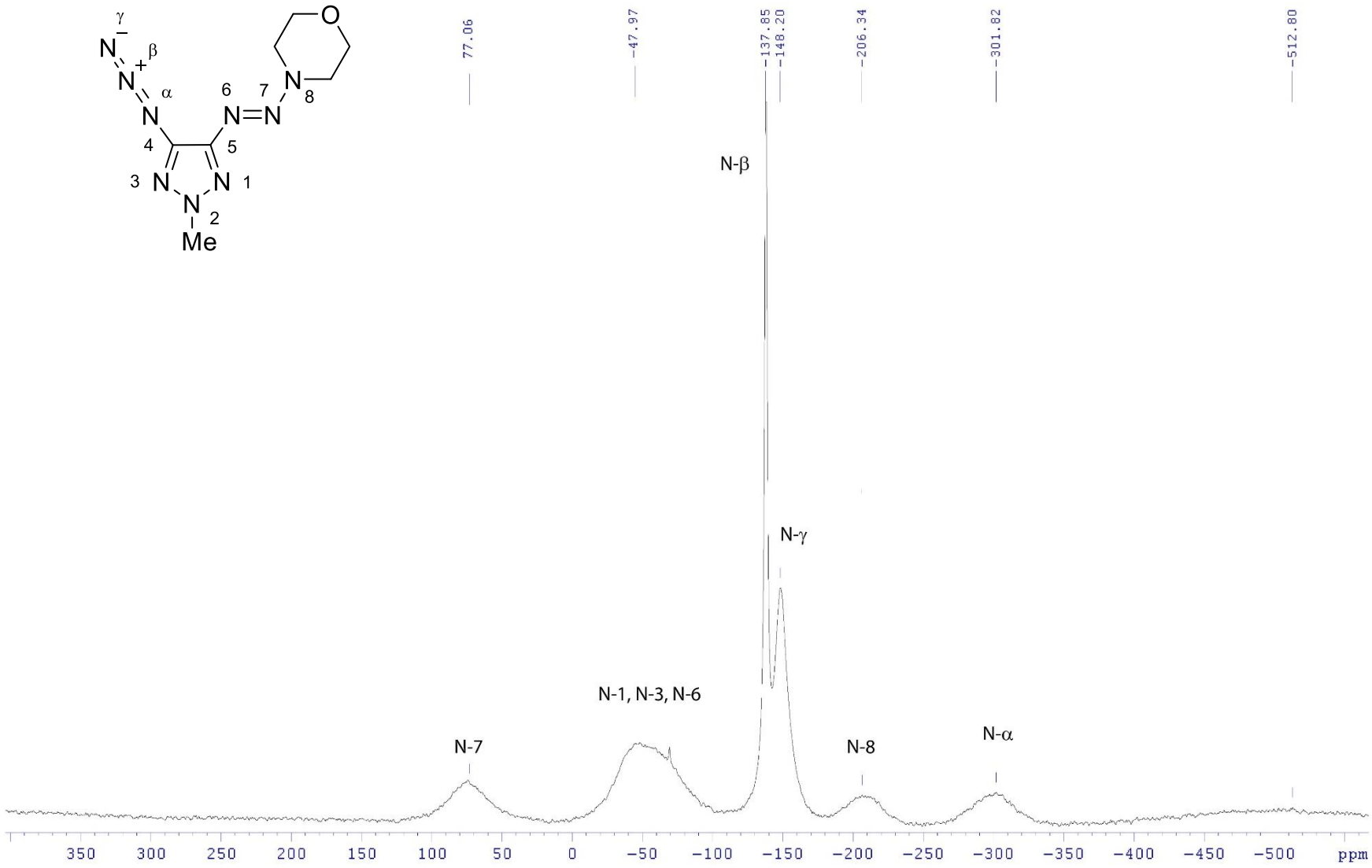

3.17.6. ^{15}N NMR spectrum of compound 13

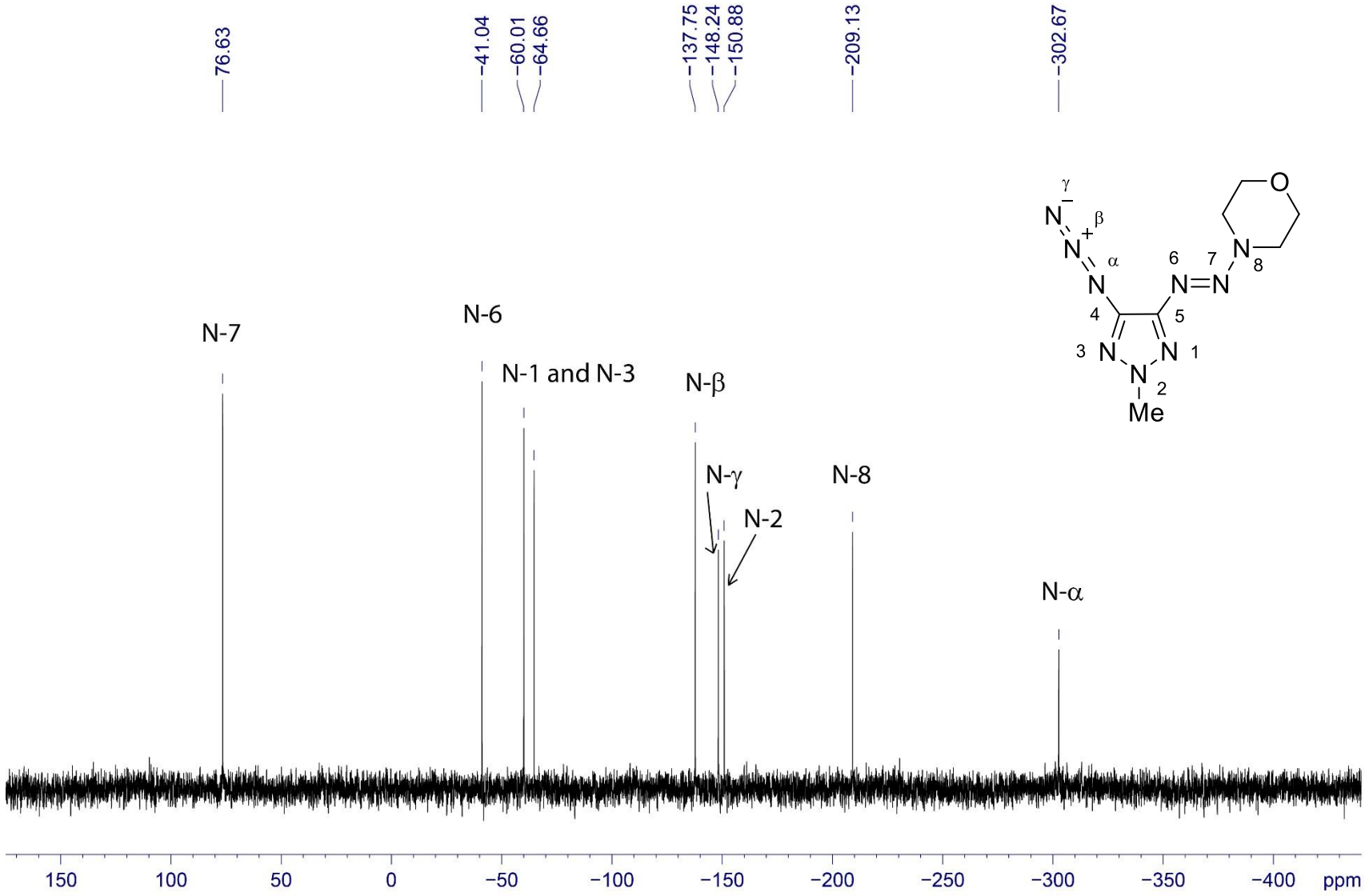

3.17.7. {^{1}H–^{15}N} HMBC spectrum of compound 13

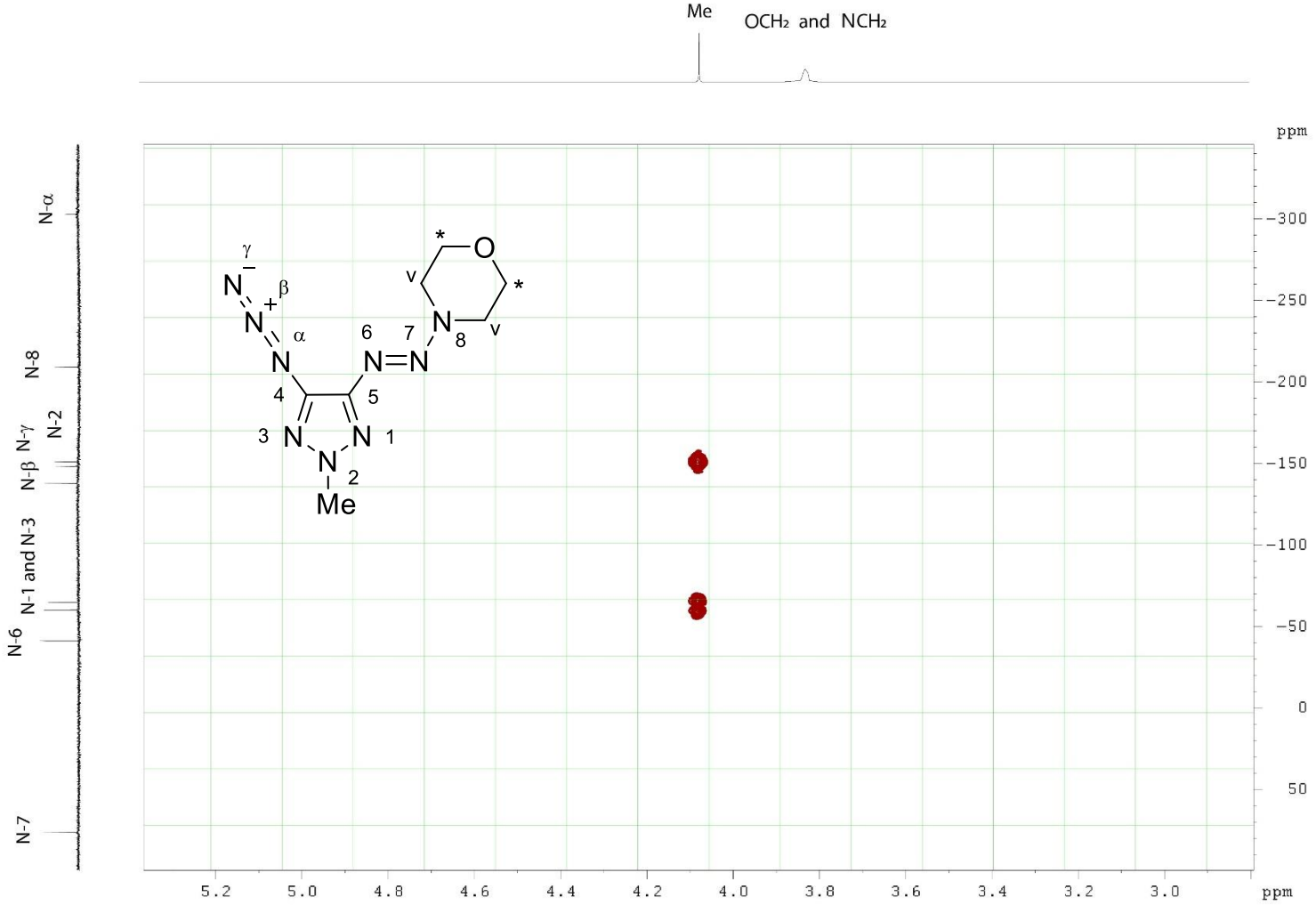

3.17.8 {^{1}H–^{15}N} HMBC spectrum of compound 13

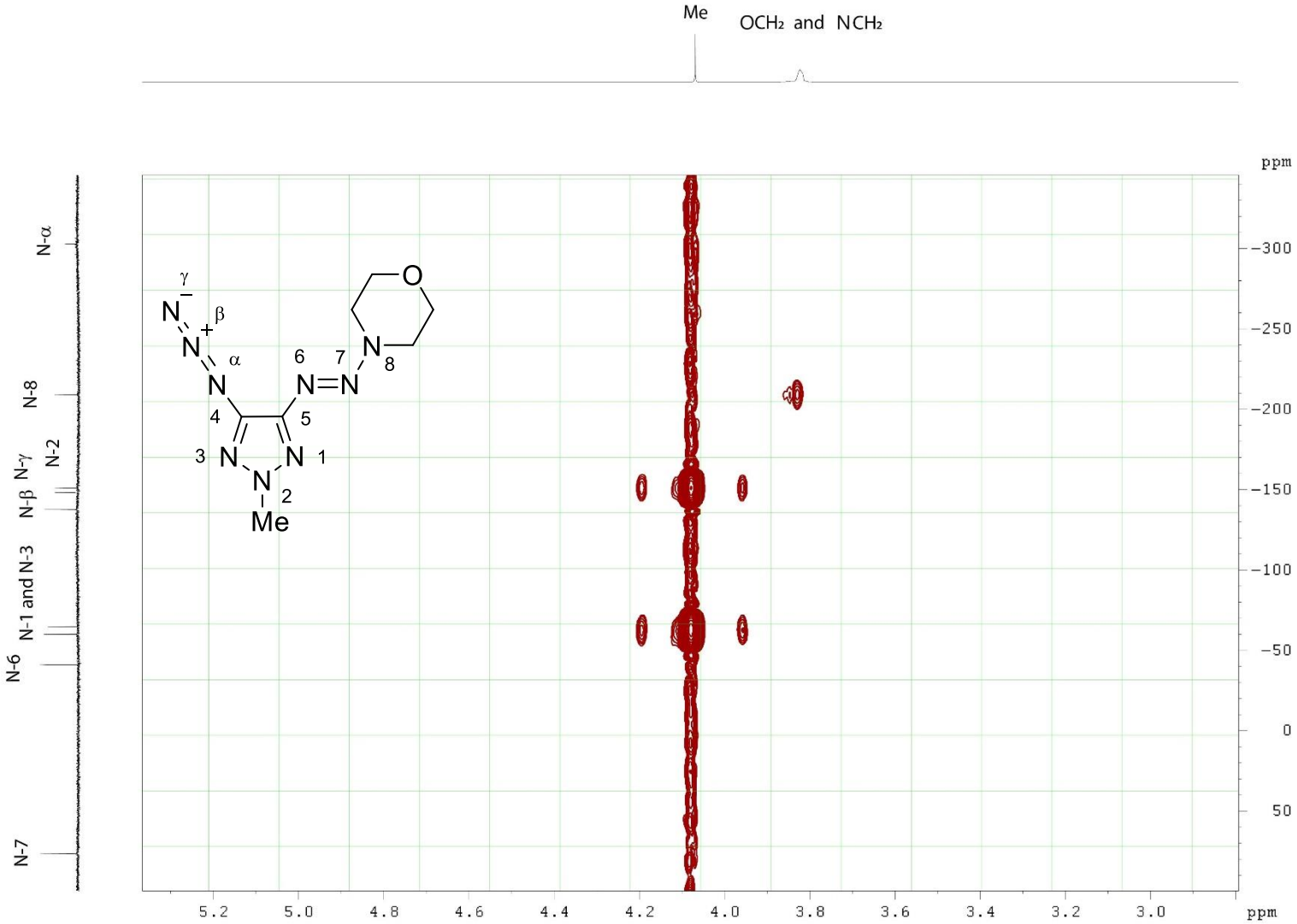

3.18. Solid-state NMR studies of $^{15}N/^{1}H$ CP polarization transfer

Further studies of $^{15}N/^{1}H$ CP polarization transfer in solid-state ^{15}N NMR spectra allow to examine the powder structure and the hydrogen bond network in more detail. Thus, ^{15}N CP/MAS spectra with different contact pulse times (from 2 msec to 18 msec) were recorded and its influence on the intensity of ^{15}N signals in the spectra was considered. And also, the same studies were performed using two-dimensional spectra ($^{15}N–^{1}H$ CP FSLG HETCOR) with a smooth change in the CP transfer duration. These experiments are based on the observation of the $^{15}N–^{1}H$ polarization transfer through dipole-dipole interactions between spins, which are transmitted through space, as well as through bonds. In this case, the strongest interactions are observed with direct chemical bonds between nuclei, which unambiguously allows identifying NH-groups (in the case under study), as well as observing hydrogen bonds with nitrogen atoms, the cross-peaks of which will be weaker than from direct NH-groups, but noticeably stronger than more distant N...H-contacts through space. Good calibration of the CP pulse durations (at the specific ramps and powers used on the instrument) allows one to quite reliably distinguish these interactions and estimate the distances between nuclei. As a result, N-1 atom is uniquely identified as NH-group (visible in 2D experiments at CP 0.5–1 msec), N-2 atom has a strong hydrogen bond with a neighboring molecule (visible at CP more than 2–3 msec), and N-3 atom does not have direct interaction with protons, although weak long-range interactions through space can be observed at CP greater than 7–8 msec (the spectra in Fig. S1 clearly demonstrate this). The data obtained from solid-state NMR spectroscopy studies are in excellent agreement with the powder X-ray diffraction data (see above).

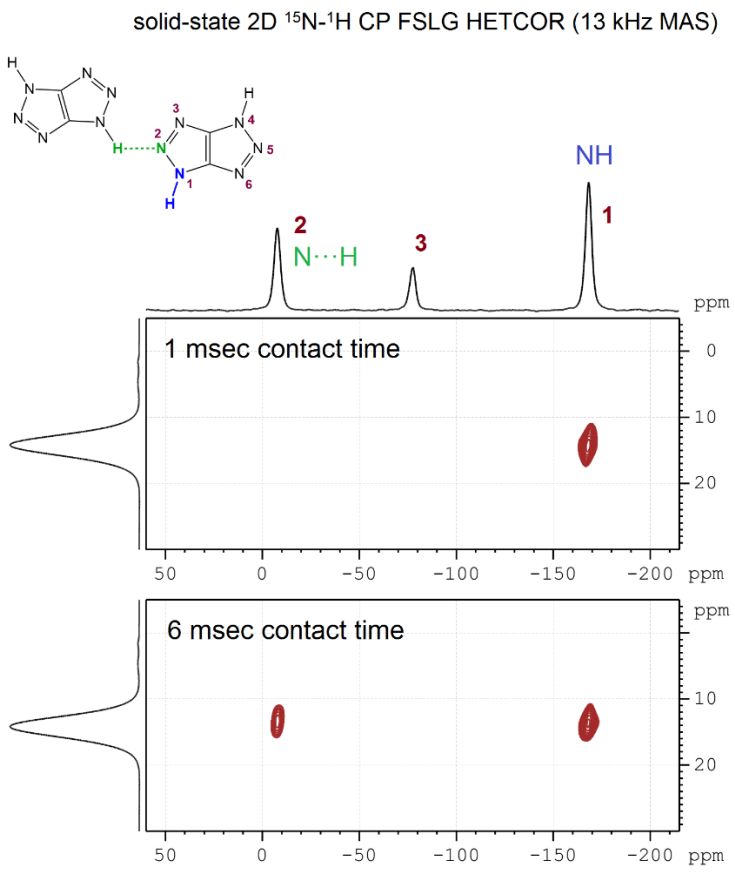

Fig. S1. Solid-state 2D ^{15}N–^{1}H correlation NMR spectra (CP FSLG HETCOR, 13 kHz MAS, with different contact times from 1 to 6 msec) for solid TT **1**; NH-group and N-atom with a hydrogen bond are clearly visible (1 and 6 msec, respectively), while N-3 have no notable correlations.

4. X-Ray Data

4.1. Single crystal X-ray data

X-ray diffraction data for structures **3**, **4** and **9** were collected on a Bruker Smart Apex II diffractometer (equipped with Photon 2 area-detector, using φ- and ω-scan technique and graphite-monochromated MoKα-radiation), for structures **6c** and **7b** on a Bruker Quest diffractometer (Photon 3 area-detector, φ- and ω-scans, graphite-monochromated MoKα-radiation), and for structures **7c** and **12** on a four-circle Rigaku Synergy S diffractometer (HyPix6000HE area-detector, kappa geometry, shutterless ω-scan technique, monochromated CoKα-radiation). A semi-empirical absorption correction was applied either with the SADABS program[6] or the CrysAlisPro program[7] using the intensity data of the equivalent reflections. Structures were solved with the dual-space technique with the SHELXT program[8] and refined by a full-matrix least-squares technique on F^2 with anisotropic displacement parameters for non-hydrogen atoms. The hydrogen atoms of the amino groups were found from difference Fourier synthesis and refined in an isotropic approximation. All other hydrogen atoms were placed in calculated positions and refined in a riding model with isotropic displacement parameters U_{iso}(H) equal to 1.5U_{eq}(C) for methyl and to 1.2U_{eq}(C) for other fragments. The refinement was performed using the SHELXL program.[9] Detailed crystallographic information is provided in Table TS2. Full crystallographic data have been deposited at the Cambridge Crystallographic Data Center, CCDC 2382722-2382729. Copies of the data can be obtained free of charge from https://www.ccdc.cam.ac.uk/structures/.

Table TS2. Crystallographic data for crystal structures discussed in the paper.

Compound	**1**[#]	**3**	**4**	**6c**	**7b**	**7c**	**7d**	**9**	**12**
CCDC	2382714	2382724	2382725	2382727	2382726	2382729	2382722	2382723	2382728
Formula	$C_2H_2N_6$	$C_3H_2N_6O$	$C_2H_3ClN_6$	$C_{18}H_{54}N_8O_7$	$C_4H_6N_6$	$C_4H_6N_6$	$C_4H_6N_6$	$C_{14}H_{27}ClN_6O_4$	$C_7H_{11}N_7O$
M, g cm^{-3}	110	138.11	146.55	494.69	138.15	138.15	138.15	378.86	211.24
T, K	298	120	100	100	100	100	100	140	100
Crystal system	monoclinic	orthorhom-bic	monoclinic	monoclinic	monoclinic	triclinic	triclinic	orthorhom-bic	monoclinic
Space group	$P2_1/n$	$P2_12_12_1$	$P2_1/n$	$C2/c$	$P2_1/n$	P-1	P-1	$P2_12_12_1$	$P2_1/c$
Z / Z'	2 / 0.5	4 / 1	4 / 1	4 / 0.5	2 / 0.5	4 / 2	1 / 0.5	4 / 1	4 / 1
a, Å	3.59786 (13)	3.6557(5)	6.5074(3)	12.0258(5)	3.8790(3)	7.3490(2)	4.1132(6)	10.1984(9)	10.72920 (10)
b, Å	11.9961(4)	10.3968 (14)	13.0530 (6)	9.4375(4)	6.2602(5)	7.9396(2)	6.0633(8)	13.0426 (11)	7.51940 (10)
c, Å	4.7679(2)	13.7717 (18)	7.7581(4)	25.3166 (12)	12.9022 (11)	10.7583(3)	6.1413(8)	14.4939 (12)	12.34630 (10)
α, °						95.085(2)	92.207(5)		
β, °	105.2851 (6)		114.532 (2)	103.7400 (10)	98.274(2)	92.657(2)	96.659(5)		96.7760 (10)
γ, °						96.029(2)	100.975(5)		
V, Å^3	198.505 (13)	523.43 (12)	599.49(5)	2791.0(2)	310.05(4)	620.82(3)	149.06(4)	1927.9(3)	989.107 (18)
d_{calc}, g cm^{-3}	1.842	1.753	1.624	1.177	1.480	1.478	1.539	1.305	1.419

Table TS2 (continued)

Compound	**1**[#]	**3**	**47**	**6c**	**7b**	**7c**	**7d**	**9**	**12**
Radiation type	CuKα	MoKα	MoKα	MoKα	MoKα	CuKα	MoKα	MoKα	CuKα
μ, cm^{-1}	12.25	1.42	5.47	0.9	1.08	9.03	1.12	2.29	8.71
$2\theta_{max}$, °	90	60	60	60	60	161	60	60	161
Collected reflns.		6619	9814	22344	4193	16271	2152	25453	13803
Independent reflns.		1541	1749	4106	905	2700	860	5619	2168
Reflns with. I>2s(I)		1345	1483	3135	868	2510	716	4521	2093
R_1		0.0312	0.0263	0.0450	0.0379	0.0416	0.0424	0.0407	0.0385
wR_2		0.0783	0.0734	0.1205	0.0984	0.1065	0.1117	0.1054	0.0975
GOF		0.999	1.151	1.015	1.070	1.038	1.015	1.081	1.090
Residual density, e Å^{-3}(d_{max}/d_{min})		0.254/ –0.204	0.412/ –0.315	0.294/ –0.217	0.524/ –0.232	0.318/ –0.289	0.402/ –0.331	0.343/ –0.371	0.355/ –0.221
R_{bragg}	0.0089								
R_{wp}	0.041								

The structure of TT **1** was solved and refined from powder diffraction data.

4.2. Powder X-ray diffraction

The powder X-ray diffraction study of TT **1** was performed on a Bruker AXS D8 Advance Vario diffractometer equipped with a primary monochromator (CuKα_1, λ = 1.54056 Å) and a LynxEye position sensitive detector. The sample was placed between two polyester (Mylar®) films and rotated at a speed of 60 deg·min^{-1}. Data collections was performed in the transmission mode at ambient temperature (ca. 298 K) with a step size of 0.01° for the 2θ range of 6.2–90.4°.

The diffraction pattern of the samples **1** was indexed using the SVD (singular value decomposition) indexing algorithm[10] as implemented in the Bruker TOPAS 5.0 software,[11] and the space group was determined using the analysis of systematic absences. The parallel tempering approach implemented in the FOX[12] package was used for the crystal structure solution in direct space. The restrained Rietveld refinement (in TOPAS 5.0) was performed using the methodology described elsewhere[13]. The position of the hydrogen atom in **1** cannot be located from the solution, and it was assigned based on the results of periodic DFT calculations. Note that the unconstrained refinement of **1** starting from the DFT-optimized atomic positions did not drastically change the structure. The agreement between DFT-optimized and refined structures can be considered as an additional indication of the validity of the refined model.[14] The final fit of the calculated and experimental PXRD patterns is shown in Fig. S2. The refined structure has been deposited at the Cambridge Crystallographic Data Center, CCDC 2382714, the copy of the data can be obtained free of charge from https://www.ccdc.cam.ac.uk/structures/.

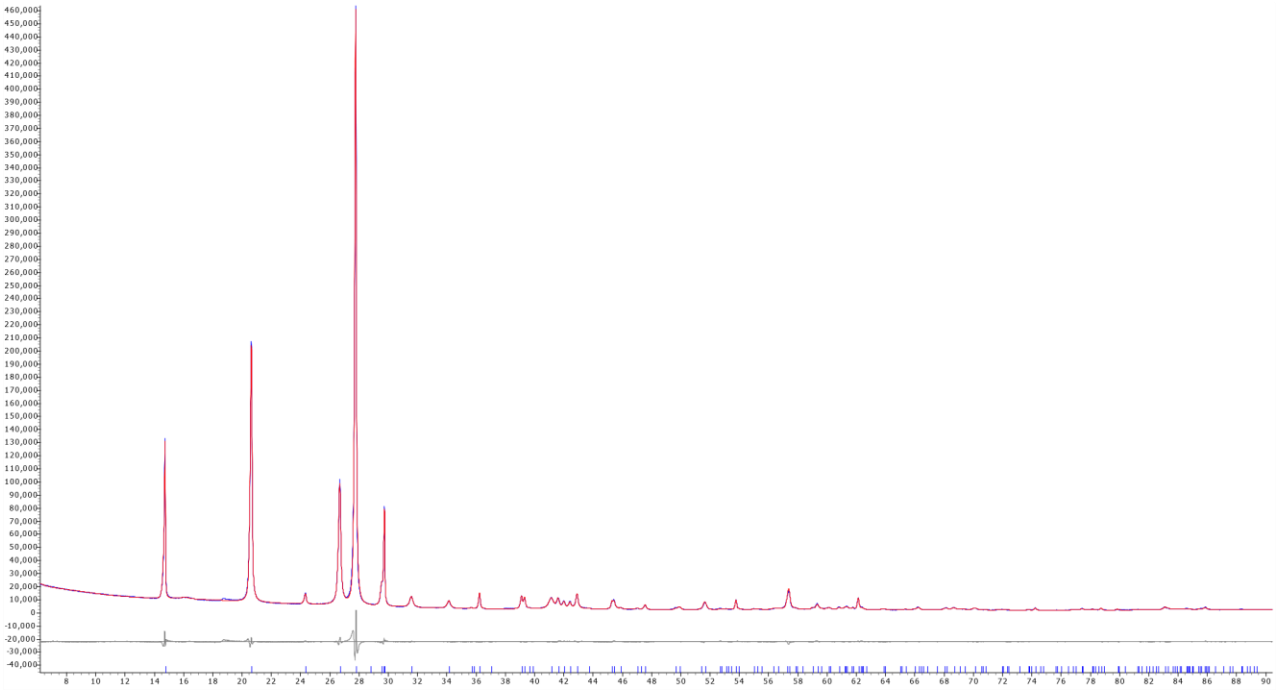

Fig. S2. The calculated (red line), experimental (blue line), and difference (gray line) powder diffraction patterns of the refined TT **1** structure.

4.3. Computation details

Periodic DFT calculations were performed with the CRYSTAL17[15] software package using the dispersion-corrected PBE0-D3[16] functional with Becke–Jonson damping[17] and the POB-TZVP[18] basis set optimized for calculation of periodic structures. The atomic coordinates of TT **1** were optimized using the experimental unit cell parameters, symmetry and initial coordinates from the crystal structure solution, with two different positions of the added H atoms corresponding to the 1,5- and 2,4-protonated isomers. The shrinking factor 4 4 4 was used for the Monkhorst-Pack grid, yielding a total of 30 k-points in the irreducible Brillouin zone. Harmonic frequencies in the γ-point for crystals were calculated using the numerical algorithm, with two atomic displacements in each Cartesian direction, the absence of imaginary frequencies proved the optimized models to be minima. To calculate the lattice and cohesive energies of the isomers of **1**, the wavefunction of optimized isolated molecules and molecules in crystal geometry were computed. The CRYSTAL17 implementation of the counterpoise approach was used to apply the basis set superposition error correction, employing additional basis functions

placed around atomic positions within a radius of 6 Å (MOLEBSSE keyword) for the isolated molecule calculation.

Atomic coordinates of the 1,5-diprotonated TT 1 crystal structure, optimized by the PBE0-D3/POB-TZVP method, in CIF format:

```
data_kanov5
_symmetry_cell_setting          monoclinic
_symmetry_space_group_name_H-M   'P 21/n'
loop_
_symmetry_equiv_pos_site_id
_symmetry_equiv_pos_as_xyz
1 x,y,z
2 1/2–x,1/2+y,1/2–z
3 –x, –y, –z
4 1/2+x,1/2-y,1/2+z
_cell_length_a                  3.60290
_cell_length_b                  12.01430
_cell_length_c                   4.77450
_cell_angle_alpha               90
_cell_angle_beta                105.2910
_cell_angle_gamma               90
_cell_volume                    199.354
loop_
_atom_site_label
_atom_site_type_symbol
_atom_site_fract_x
_atom_site_fract_y
_atom_site_fract_z
N1 N 0.63480 0.12234 0.65768
N2 N 0.40025 0.16639 0.41200
N3 N 0.23715 0.08559 0.23004
C3A C 0.62468 0.01054 0.63395
H1 H 0.78286 0.17613 0.81298
```

Atomic coordinates of the 1,5-diprotonated TT 1 isolated molecule, optimized by the PBE0-D3/POB-TZVP method, in XYZ format:

```
10
kanov5-h1-isol+c2h
N         1.28069      -1.05015       0.00000
N        -1.28069       1.05015       0.00000
H         1.72180      -1.94970       0.00000
H        -1.72180       1.94970       0.00000
N        -2.06940      -0.08050       0.00000
N         2.06940       0.08050       0.00000
N        -1.28616      -1.15015       0.00000
N         1.28616       1.15015       0.00000
C        -0.01840      -0.68474       0.00000
C         0.01840       0.68474       0.00000
```

Atomic coordinates of the 2,5-diprotonated TT 1 crystal structure, optimized by the PBE0-D3/POB-TZVP method, in CIF format:

```
data_kanov5-h2
_symmetry_cell_setting          monoclinic
_symmetry_space_group_name_H-M   'P 21/n'
loop_
_symmetry_equiv_pos_site_id
_symmetry_equiv_pos_as_xyz
1 x,y,z
2 1/2-x,1/2+y,1/2-z
3 -x,-y,-z
4 1/2+x,1/2-y,1/2+z
_cell_length_a                 3.60290
_cell_length_b                 12.01430
_cell_length_c                 4.77450
_cell_angle_alpha               90
_cell_angle_beta                105.2910
_cell_angle_gamma               90
_cell_volume                   199.354
loop_
_atom_site_label
_atom_site_type_symbol
_atom_site_fract_x
_atom_site_fract_y
_atom_site_fract_z
N1 N -0.36449 0.13021 -0.36175
N2 N -0.61061 0.15488 -0.61921
N3 N -0.77862 0.07155 -0.79133
C3A C -0.62598 -0.01771 -0.63099
H2 H -0.67355 0.23669 -0.68237
```

Atomic coordinates of the 2,5-diprotonated TT 1 isolated molecule, optimized by the PBE0-D3/POB-TZVP method, in XYZ format:

```
10
kanov5-h2-isol+d2h
N        -1.26221        1.16489        0.00000
N         1.26221       -1.16489        0.00000
N        -1.26221       -1.16489        0.00000
N         1.26221        1.16489        0.00000
N        -1.93509        0.00000        0.00000
N         1.93509        0.00000        0.00000
C         0.00000       -0.70270        0.00000
C         0.00000        0.70270        0.00000
H        -2.94032        0.00000        0.00000
H         2.94032        0.00000        0.00000
```

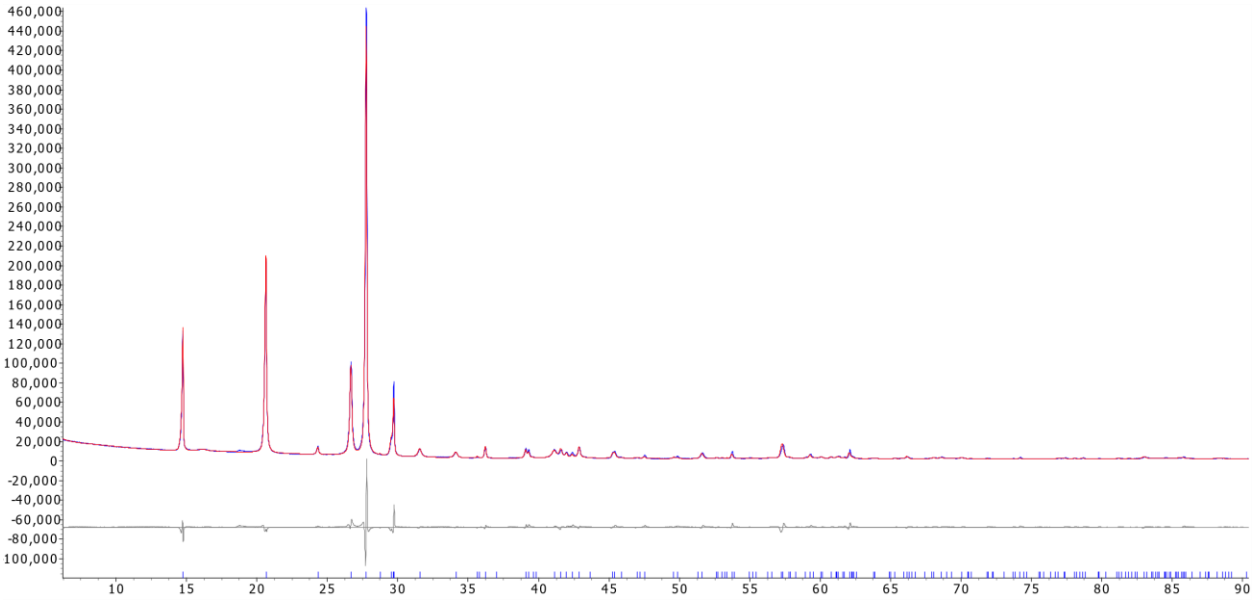

Fig. S3. The fit of the calculated powder diffraction pattern (red line), derived from the PBE0-D3/POB-TZVP optimized structure of the 1,4-diprotonated isomer of TT **1** to the experimental pattern (blue line), and their difference (grey line). The coordinates of the atoms and the unit cell parameters were kept fixed at the DFT-optimized values; the same isotropic displacement parameter was refined for all non-H atoms. R_{wp} = 0.088, R_{bragg} = 0.034.

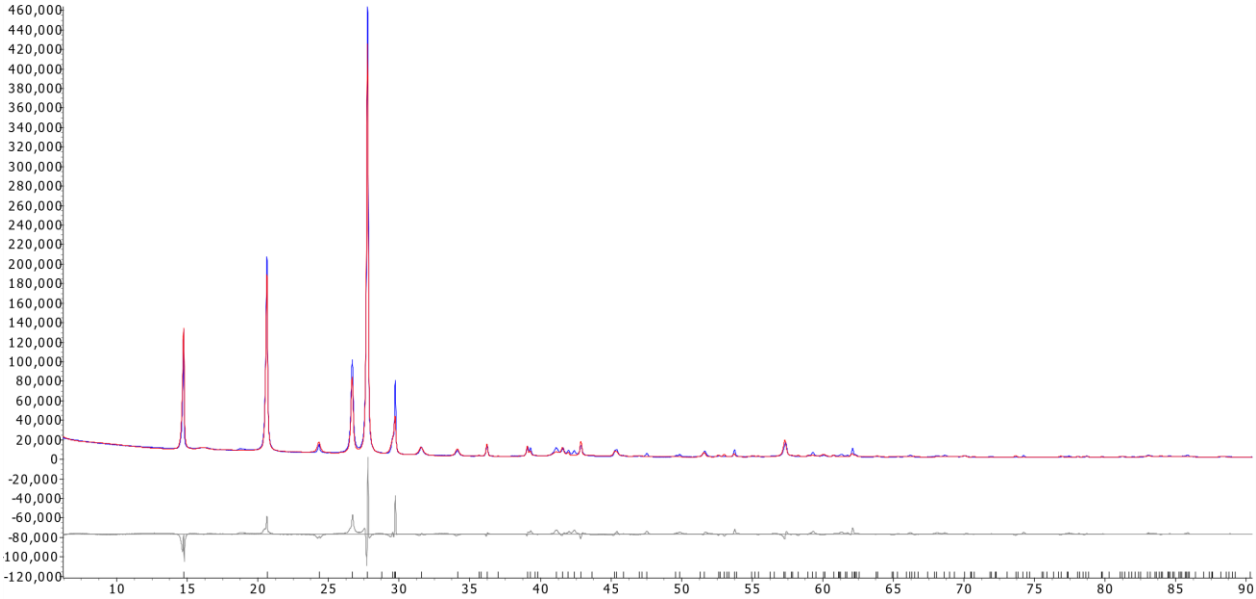

Fig. S4. The fit of the calculated powder diffraction pattern (red line), derived from the PBE0-D3/POB-TZVP optimized structure of the 1,5-diprotonated isomer of TT **1** to the experimental pattern (blue line), and their difference (grey line). The coordinates of the atoms and the unit cell parameters were kept fixed at the DFT-optimized values; the same isotropic displacement parameter was refined for all non-H atoms. R_{wp} = 0.137, R_{bragg} = 0.092.

4.4. Discussion of single crystal X-ray structures

General remarks on molecular geometries

The molecular geometry of all the structures discussed in this paper was subjected to the Mogul geometry check[19] to find a match between the geometric parameters of a given structure and the corresponding values for similar fragments listed in the Cambridge Structural Database (CSD)[20]. In general, most of the parameters were classified as “usual”. Most of the exceptions had relatively low values of z-score, a numerical measure of the (normalized) deviation of the observed value from the mean for hits found by the Mogul search. Thus, the z-score values were between the standard threshold of 2.0, and did not exceed 3.0. In addition, in many cases the definition of "similar structures" was too broad, and when the analogue fragments were selected manually, the values fell within the normal range. For instance, in the molecule **12** N–N=C angles in 1,2,3-triazole

is considered to be slightly higher than the average values, but if tetrazole analogues are excluded, the observed values of ca. 103.9° are very typical.

Diazotriazole 3 and diazonium salt 4

Both molecule **3** and the diazonium cation in salt **4** contain the N–N fragment attached to one of the carbon atoms of the triazole ring. A comparison of the bond lengths in these structures is provided in Table TS3. Interestingly, protonation of the nitrogen atom N1 in the salt structure leads to only minor changes in bond lengths, such as lengthening of the N1–N2 and N1–C5 bonds. More notable is the change in bond angles, with the increase of the angle N2–N1–C5 by ca. 5.2° and decrease of the adjacent angle N1–N2–N3 by ca. 4.2°, supporting a slight increase in the single character of the N1–N2 bond and the double character of the N2–N3 bond. At the same time, the N1 atom remains planar with the sum of the bond angles equal to 360.0°.

An interesting question arises about the nature and bond character of the N6–N7 bond exocyclic to the triazole ring. The N6–N7 bond itself is very short (1.1027(18) and 1.1056(14) A in **3** and **4**) with the length typical of a triple bond, shorter than the terminal bond in azides (ca. 1.13 Å, data from the International Tables for Crystallography (2006). Vol. C. ch. 9.5, pp. 790–811), and is comparable to the N–N bond in aromatic diazonium salts (1.099±0.017 Å, calculated for structures of 75 salts in CSD v. 5.45, November 2023). However, the adjacent C4–N6 bond (1.3580(19) and 1.3407(14) Å in **3** and **4**) is of the length intermediate between the single (1.37–1.43 Å) and double bond (ca. 1.30 Å) and notably shorter than in aromatic diazonium salts (1.406±0.032Å for the same set of 75 salts in the CSD). Considering the apparently effective conjugation in the triazole ring, the equalized bond distances in this ring, but with relatively long N3–C4 and C4–C5 bonds, the structure is better described as a diazo compound than as an internal diazonium salt with the anionic character of one of the N atoms in **3**.

Table TS3. Selected bond lengths (Å) and angles (°) in crystals **3** and **4**.

	3	**4**
bond lengths		
N1–N2	1.363(2)	1.3816(14)
N1–C5	1.336(2)	1.3473(14)
N2–N3	1.3111(18)	1.2865(14)
N3–C4	1.363(2)	1.3780(14)
C4–C5	1.402(2)	1.4110(15)
N6–C4	1.3580(19)	1.3407(14)
N6–N7	1.1027(18)	1.1056(14)
N8–C5	1.384(2)	1.3167(15)
bond angles		
N1–N2–N3	113.16(13)	108.99(9)
N2–N3–C4	104.48(13)	106.83(10)
N3–C4–C5	109.65(13)	111.03(10)
N1–C5–C4	106.17(14)	101.42(9)
N2–N1–C5	106.54(13)	111.71(9)
N3–C4–N6	118.48(14)	121.92(10)
C5–C4–N6	131.52(14)	127.04(10)
C4–N6–N7	175.95(17)	178.19(12)
N1–C5–N8	122.25(15)	126.88(10)
C4–C5–N8	131.58(15)	131.68(11)
N2–N1–H1		117.4(10)
C5–N1–H1		130.9(11)

The presence of the H atom available for H-bonding, lead to formation of H-bonded chains in crystal packing of compound **3** (Fig. S5), formed by relatively strong bonds with the central atom N2 of the triazole ring (N···N 2.8681(19), H···N 1.898 Å, N–H···N 159° with N–H set to 1.015 Å).

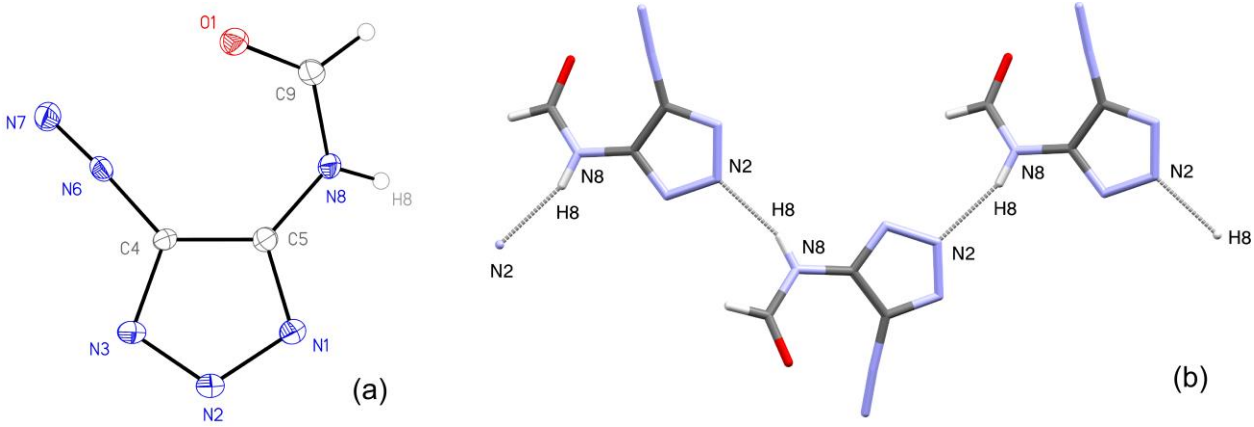

Fig. S5. General view of the compound **3** in crystal; non-hydrogen atoms are represented by probability ellipsoids of atomic displacements (p = 50 %) (a). The H-bonded chains in **3** formed by the 2-fold screw axis along the crystallographic *b* axis (b).

In the crystal of salt **4**, all three H atoms form H-bonds with the chlorine anion. The strongest bond is necessarily between the protonated atom N1 and the anion (N···Cl 3.0473(10), H···Cl 2.050 Å, N–H···Cl 167° with N–H 1.015 Å), while the bonds with the exocyclic amino-group are longer (N···Cl 3.1862(11) and 3.2257(11), H···Cl 2.179 and 2.211 Å, N–H···Cl 171 and 178°). In total, the H-bonds connects molecules into ribbons via the formation of $R^2_4(8)$ and $R^2_4(12)$ rings (Fig. S6)

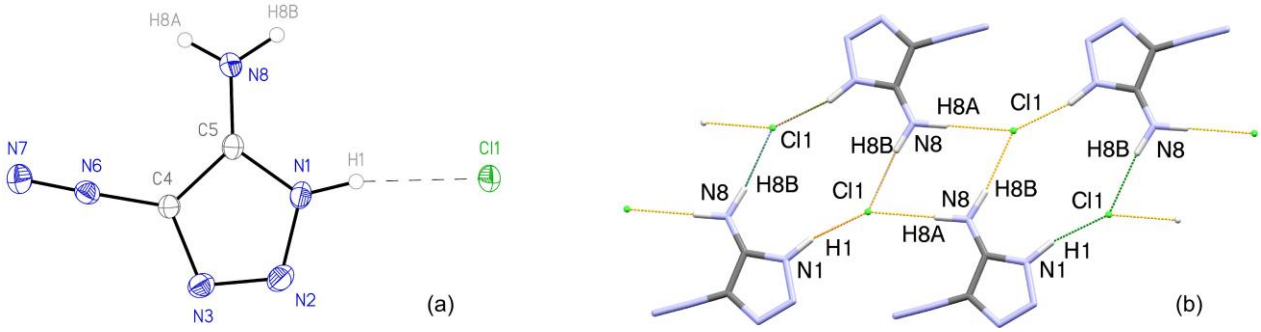

Fig. S6. General view of the anion and the cation of the salt **4** in crystal; non-hydrogen atoms are represented by probability ellipsoids of atomic displacements (p = 50 %) (**a**); H-bonded ribbons in crystal of salt **4** (**b**).

Isomeric dimethyl derivatives 7b and 7c (and comparison with 7d from the main text)

The inversion center is a very common symmetry element in crystal structures of molecular compounds. Interestingly, the 1,4- and 2,5-derivatives, **7d** and **7b** with the most symmetric achievable point groups C_{2h} and D_{2h}, indeed crystallize with a half of the molecule in the independent part of the unit cell and lie on the inversion center. On the other hand, the 1,6-isomer that is characterized by C_{2v} maximal possible symmetry occupies in the crystal a general position, moreover, it the crystal contains two crystallographically independent molecules per unit cell.

Bond lengths and angles of the non-disordered single-crystal structures containing the TT core are summarized in Table TS4. Analysis of these geometrical parameters reveals that molecules **7c** and **7d** and with a methyl substituent attached to a lateral N atom can be adequately described by a canonical structure. In these cases, the N–N bond with a substituent connected to the one of the N atoms exhibits a more single-bond character, while the other N–N bond is significantly shorter, indicative of a double-bond character.

In contrast, molecule **7b**, with the methyl group attached to the central N atom, has an approximate D_{2h} symmetry with equalized N–N bond lengths. This suggests a delocalized bonding arrangement within the triazole ring, possibly represented by a resonance structure involving partially charged nitrogen atoms. Note that despite the delocalized electron density, the nitrogen atoms in these molecules maintain a planar arrangement, as evidenced by the sum of bond angles virtually equal to 360° in all cases.

Table TS4. Selected bond lenghts (Å) and angles in crystals **7b**, **7c** (two independent molecules A and B), **7d** and **9**.

	7b	**7c (A)**	**7c (B)**	**7d**	**9**
bonds					
N1–N2	1.3414(11)	1.3792(15)	1.3825(15)	1.3608(15)	1.321(3)
N2–N3	1.3398(11)	1.3115(17)	1.3136(16)	1.3299(14)	1.330(3)
N5–N6	1.3398(11)	1.3836(15)	1.3799(15)	1.3299(14)	1.349(3)
N4–N5	1.3414(11)	1.3101(16)	1.3114(16)	1.3608(15)	1.335(3)
N1–C6A	1.3538(12)	1.3444(16)	1.3437(16)	1.3561(15)	1.371(3)
N3–C3A	1.3528(12)	1.3684(17)	1.3661(18)	1.3590(16)	1.365(3)
N6–C6A	1.3528(12)	1.3432(15)	1.3433(16)	1.3590(16)	1.340(3)
N4–C3A	1.3538(12)	1.3690(17)	1.3710(17)	1.3561(15)	1.348(3)
C3A–C6A	1.3870(17)	1.3673(17)	1.3720(17)	1.364(2)	1.369(3)
N–C (1)	1.4591(12)	1.4595(17)	1.4576(15)	1.4535(15)	1.499(3)
N–C (2)	1.4591(12)	1.4505(16)	1.4509(16)	1.4535(15)	1.495(3)
N–C (3)					1.507(3)
angles					
N1–N2–N3	119.12(8)	110.16(10)	110.23(10)	110.52(10)	108.37(17)
N2–N3–C3A	100.44(7)	106.39(10)	106.19(11)	104.98(10)	109.07(17)
C6A–N1–N2	100.48(8)	107.42(10)	107.48(10)	108.13(10)	109.38(17)
N1–C6A–C3A	109.87(10)	106.52(11)	106.26(11)	105.02(13)	106.3(2)
C6A–C3A–N3	110.09(10)	109.51(11)	109.85(12)	111.35(13)	106.85(19)
N6–C6A–N1	140.05(9)	146.88(12)	147.07(12)	143.63(11)	142.5(2)
N3–C3A–N4	140.05(9)	140.90(12)	140.73(12)	143.63(11)	143.0(2)
N5–N4–C3A	100.48(8)	106.36(10)	106.16(10)	108.13(10)	99.97(17)
C6A–N6–N5	100.44(7)	107.29(10)	107.21(10)	104.98(10)	99.36(17)
N4–N5–N6	119.12(8)	110.18(10)	110.56(10)	110.52(10)	119.34(17)
C6A–C3A–N4	109.87(10)	109.57(11)	109.41(11)	105.02(13)	110.1(2)
N6–C6A–C3A	110.09(10)	106.59(11)	106.66(11)	111.35(13)	111.2(2)
C6A–N1–C7	120.80(8)	131.75(11)	131.49(11)	131.37(11)	
N2–N1–C7	120.06(8)	120.83(11)	121.03(11)	120.50(10)	
C6A–N6–C8	120.80(8)	131.52(11)	131.85(11)	131.37(11)	
N5–N6–C8	120.06(8)	121.12(10)	120.93(10)	120.50(10)	

The molecule **7b** in the crystal is located at an inversion center so that the independent part of the unit cell contains one half of the molecule (space group $P2_1/n$, Z' = 0.5). The methyl groups are apparently disordered, the peaks of the H atoms of both

components can be found from the difference Fourier synthesis, and the refined ratio of the components is 0.64:0.36. Except for the H atoms, the molecular geometry has nearly exact D_{2h} symmetry with Continuous Symmetry Measure[21] (CSM) equal to 0.005, and RMS deviation from the idealized symmetry of 0.007 Å (calculated with PLATON MOLSYM routine).

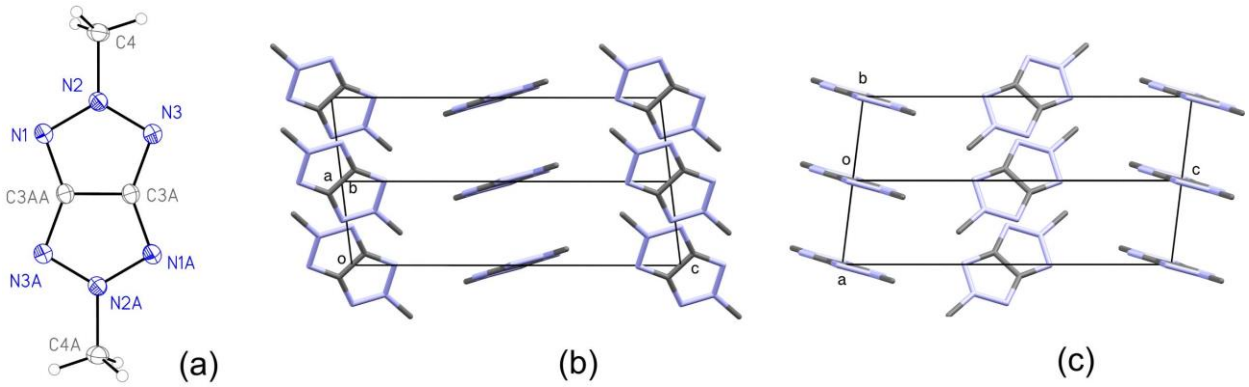

Fig. S7. General view of the compound **7b** in crystal, non-hydrogen atoms are represented by probability ellipsoids of atomic displacements (p = 50 %), the minor part of the disordered methyl group is omitted for clarity (a); fragments of crystal packing in the crystal **7b**, view along [1 1 0] and [0 –1 0] crystallographic directions ((b) and (c)), the hydrogen atoms are not shown.

Approximate molecular symmetry implies the equalization of the N1–N2 and N2–N3 bonds, so that their lengths are intermediate between the single and double bonds. In addition, the three bond angles around N2 atom are close to the perfect value of 120°.

The crystal packing of **7b** features chains of nearly coplanar molecules connected by C–H···N contacts in one direction, assembled into layers by π-stacking interactions in the perpendicular direction. In contrast to the 1,4-substituted analogues **1** and **7d**, the alternating layers are rotated relative to each other with the angle between the mean planes of the molecules equal to 57.7°.

As mentioned above, compound **7c** crystallizes with two crystallographically independent molecules in the unit cell in the space group P-1. The geometry of the independent molecules is essentially the same due to the rigid nature of the heterocyclic moiety.

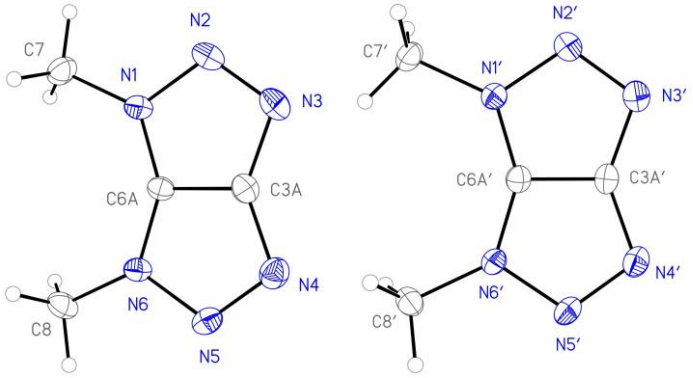

Fig. S8. General view of the crystallographically independent molecules of the compound **7c** in crystal; non-hydrogen atoms are represented by probability ellipsoids of atomic displacements (p = 50 %).

Both molecules in **7c** are characterized by an approximate C_{2v} symmetry, with CSM values of 0.0401 and 0.0089, and RMS deviation from the idealized geometry of 0.0200 and 0.0095 Å (as calculate by PLATON MOLSYM).

As in the case of two other isomers, the crystal packing of **7c** contain π-stacking between the molecules. However, in the case of 1,6-subsituted compound the layered adjustment of molecules seems not to be optimal, and only centrosymmetric dimeric associates are formed by each of due to π-stacking interaction by each of the crystallographic independent molecules, with the shortest distances N···C 3.271(2) and 3.330(2) Å.

Salts 6c and 9

The salt **6c** crystallizes as a polyhydrate in the centrosymmetric space group C2/c. The dianionic TT part is located on an inversion center, so the independent part of the unit cell contains one half of the anion, one cation, three water molecules in general position, and one water molecule on a 2-fold axis. Therefore, the salt is a 7-hydrate (anion : cation : water ratio is equal to 1 : 2 : 7).

While the cationic tetraethylammonium moiety is fully ordered, the anion is disordered by two positions with the refined relative occupancy of the components equal to 0.74:0.26 (Fig. S9). Due to the relatively large distance between the atomic coordinates of the disordered parts, the main component can be refined without restrictions (for the

minor component the SAME and ISOR instructions were used to set the geometry to be the same as for the man component and to restrain the anisotropic character of the thermal ellipsoids). Due to the disorder, it is not convenient to discuss the geometry of the anion in detail, but the refined model is very close to D_{2h} symmetry with equalized N–N and C–N distances.

Due to the presence of multiple H-bonds between the water molecules themselves and with the anion, the three water molecules in general positions are also disordered, following the disorder of the anion. In fact, all the nitrogen atoms of the anion are involved in H-bonds with N···O distances in the range of 2.8–3.0 Å, and the O···O distances corresponding to the bonds between the water molecules are in the range of 2.7–3.1 Å.

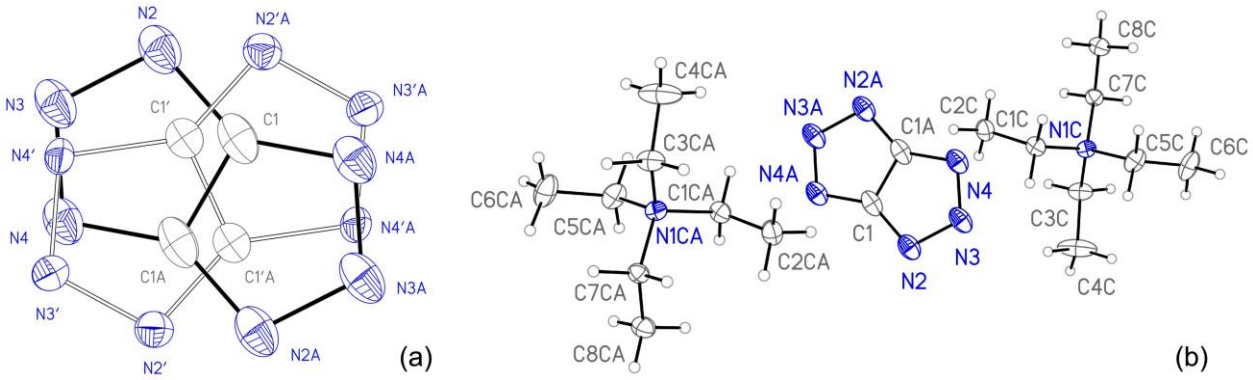

Fig. S9. Disorder of the dianion in salt **6c** (**a**); general view of the anion and cations in the crystal of the salt **6c** (**b**), non-hydrogen atoms are represented by probability ellipsoids of atomic displacements (p = 50 %), water molecules are omitted for clarity.

In salt **9**, the tris-*tert*-butyl substituted TT derivative is a cation and the anion is perchlorate (Fig. S10). The *tert*-butyl groups appear to be conformationally labile with relatively high anisotropic displacement parameters, while the TT core is more rigid. Apart from the *tert*-butyl groups, the heterocyclic moiety is relatively close to the maximum D_{2h} symmetry (CSM 0.1678, RMS 0.041 Å), although some geometric parameters are significantly different, so that the real symmetry is closer to C_{2v} point group.

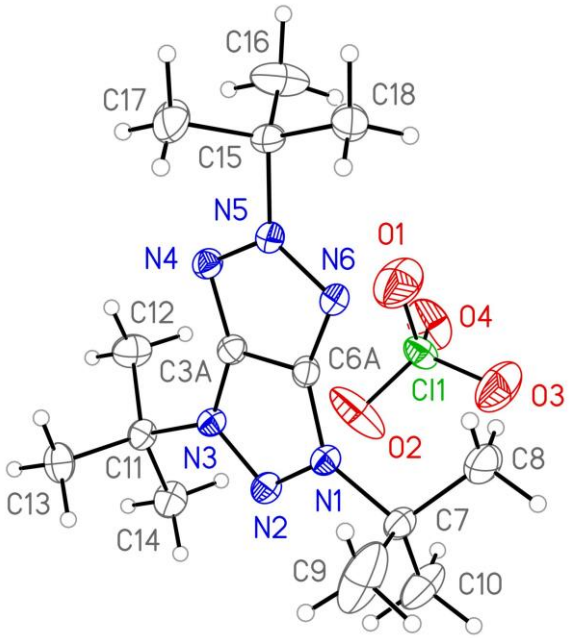

Fig. S10. General view of the anion and the cation of the salt **9** in crystal; non-hydrogen atoms are represented by probability ellipsoids of atomic displacements (p = 50 %).

In contrast to the non-charged analogues **7c** and **7d** the presence of the substituent on the lateral atoms N1 and N3 in the cation of salt **9** does not lead to a lengthening of the corresponding N1–N2 and N2–N3 bonds, so that they retain a double character. In addition, the presence of these *tert*-butyl groups has practically no effect on the geometry of the second triazole ring, which is very close to that observed in the 2,5-dimethyl derivative **7b**. The effective conjugation in both rings in the cation of salt **9** is supported by the equalized bond lengths and the planarity of all N atoms.

Due to the presence of the bulky *tert*-butyl substituents, the crystal packing of salt **9** does not involve direct interaction of the TT rings. Instead, the crystal packing is formed mainly by C–H···O contacts between the O atoms of the anion and the H atoms of the cation, and a number of shortened O···π contacts with the π-system of the cationic core (the shortest is 3.106(18) Å).

Crystal structure of compound **12**.

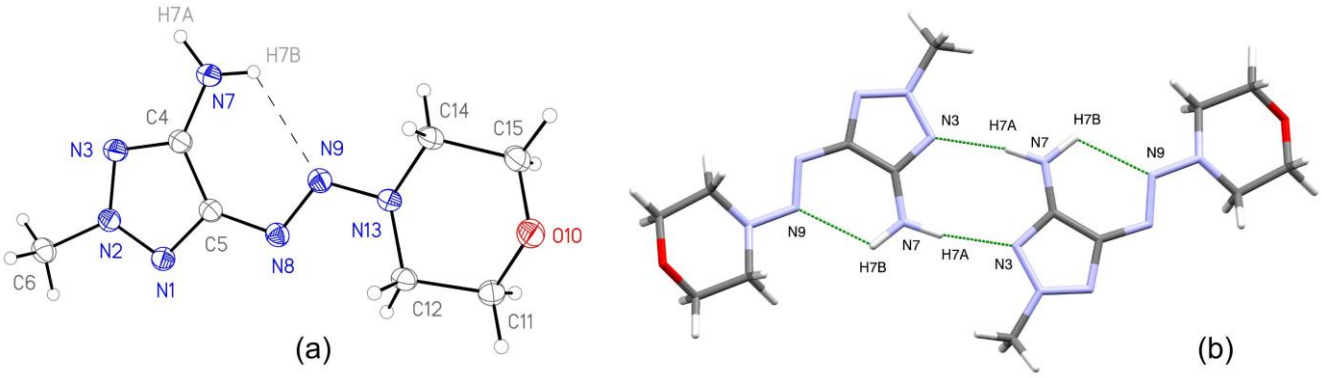

Fig. S11. General view of the molecule of the compound **12** in crystal; non-hydrogen atoms are represented by probability ellipsoids of atomic displacements (p = 50 %) (**a**), the centrosymmetric H-bonded dimer in crystal of **12** (**b**).

Molecule **12** crystallizes in the monoclinic space group $P2_1/c$. The molecular geometry is characterized by expected values of bond lengths and angles. The presence of the amino group leads to the formation of an intramolecular hydrogen bond N7–H7B···N9 of average strength (N···N 2.8859(15), H···N 2.289 Å, N–H···N 116° with N–H 1.015 Å). The second H atom of the amino group participates in an intermolecular H-bond with the atom N3 of the triazole ring (N···N 3.0664(15), H···N 2.062 Å, N–H···N 180°), which binds the molecules in centrosymmetric dimers typical of *ortho*-substituted aminotriazoles and related 5-membered nitrogen-containing compounds.

5. DSC Data

5.1. DSC of TT 1

Sample of TT **1** decomposes at 193 °C without melting (the extrapolated onset of exothermic peak).

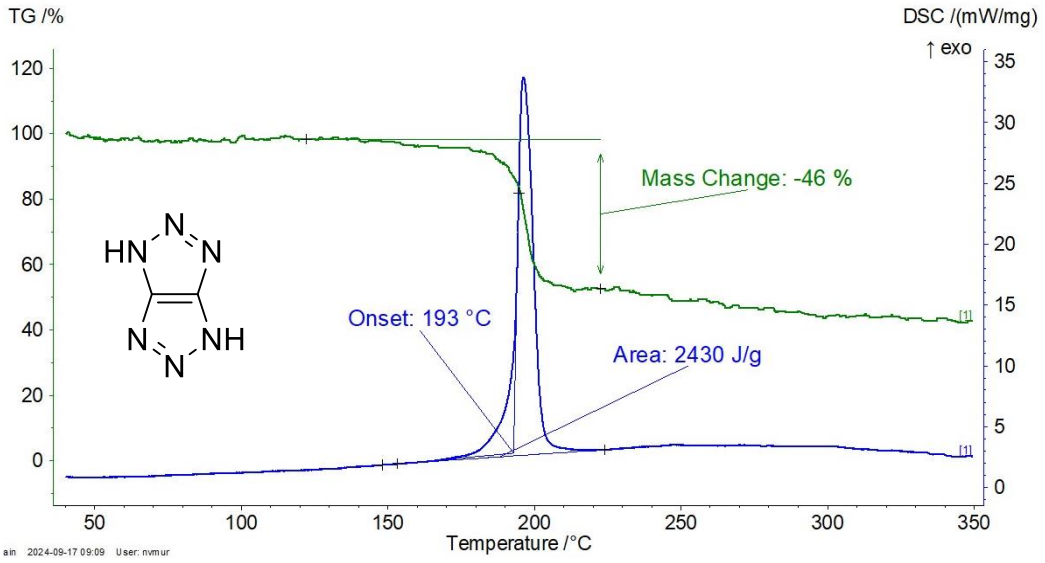

5.2. DSC of diazotriazole 3

Sample of diazotriazole **3** decomposes at 183 °C without melting (the extrapolated onset of exothermic peak).

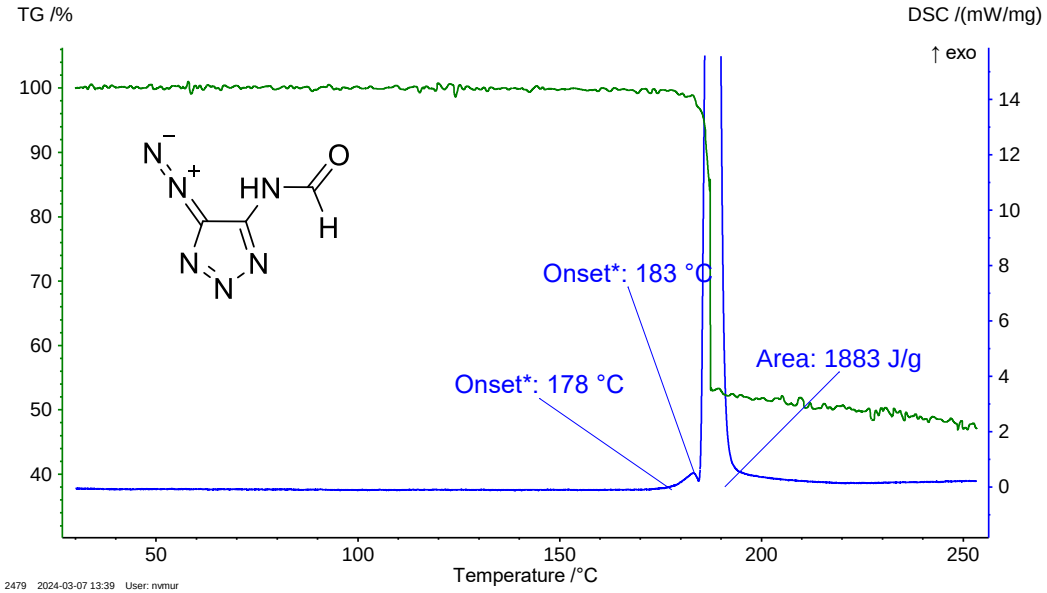

5.3. DSC of salt 4

Sample of salt **4** decomposes at 140 °C without melting (the extrapolated onset of exothermic peak).

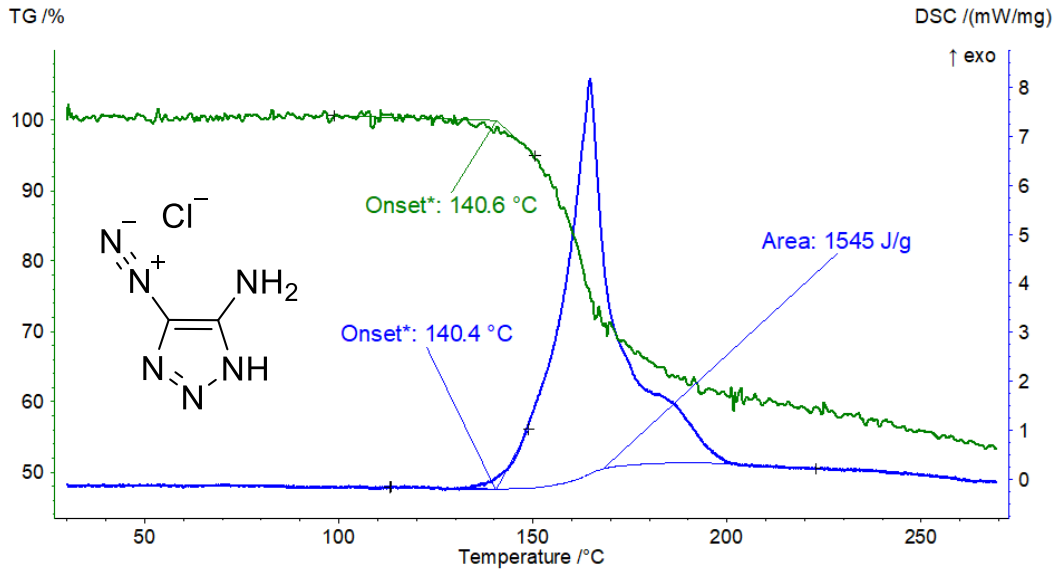

5.4. DSC of salt 6c·2H$_2$O

Sample of salt **6c**·2H$_2$O loses H$_2$O and then decomposes at 207 °C without melting (the extrapolated onset of exothermic peak).

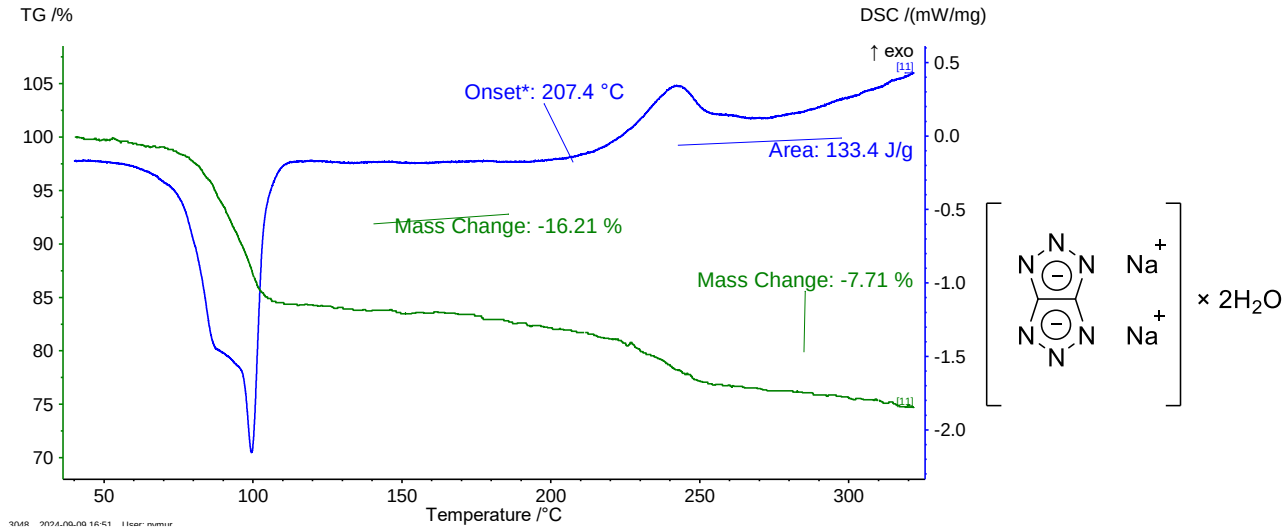

5.5. DSC of salt 6c·7H$_2$O

Sample of salt **6c**·7H$_2$O loses H$_2$O and then decomposes at 111 °C without melting (the extrapolated onset of exothermic peak).

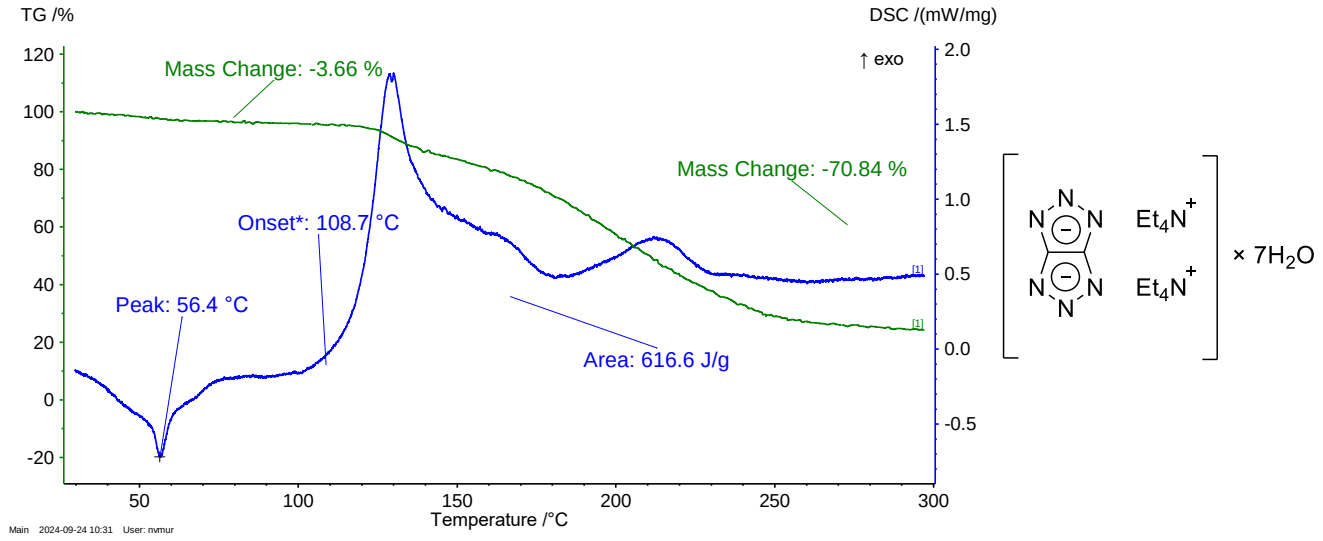

5.6. DSC of TT 7a

Once linearly heated under atmospheric pressure, sample reveals melting at 90 °C and evaporation phenomena. DSC curve of compound **7a** at atmospheric pressure:

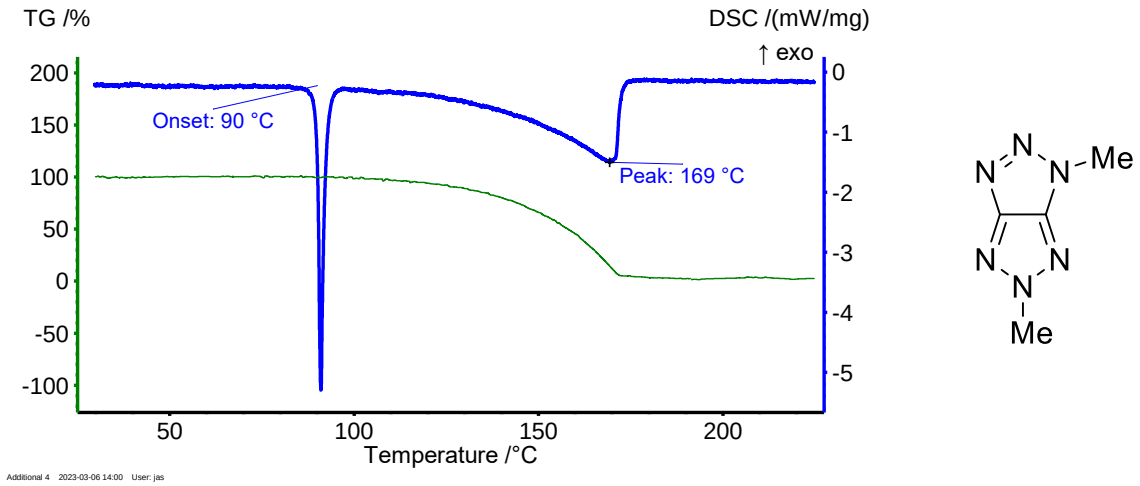

Application of the elevated pressure (2 MPa) suppresses the vaporization and allows observing melting of TT **7a** at 90 °C and its thermal decomposition with an extrapolated onset of 205 °C. DSC curve of compound **7a** at 2 MPa:

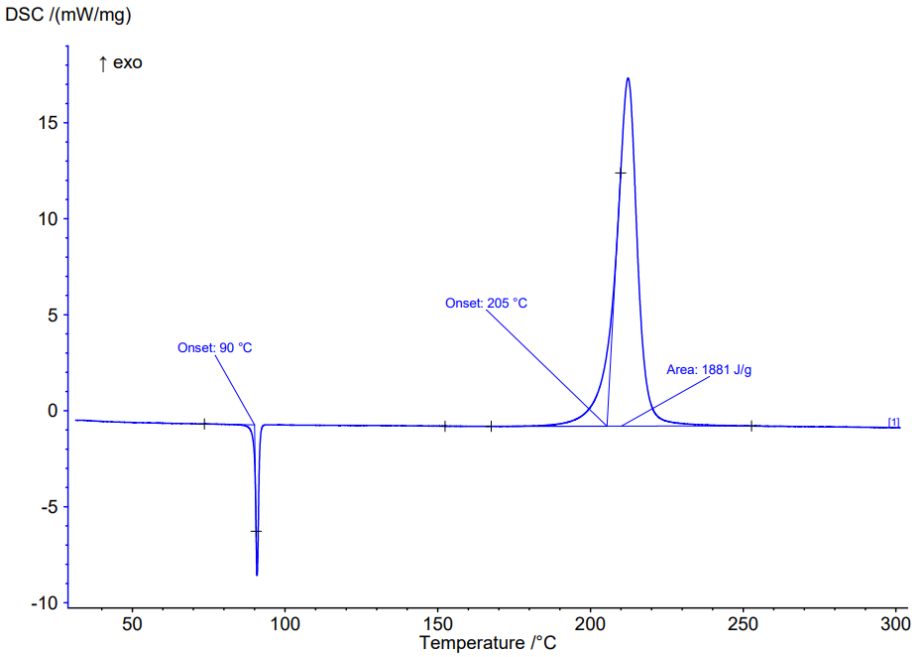

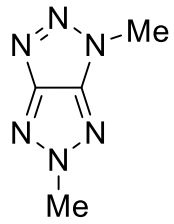

5.7. DSC of TT 7b

Sample of TT **7b** sublimes at heating at atmospheric pressure. DSC curve of compound **7b**:

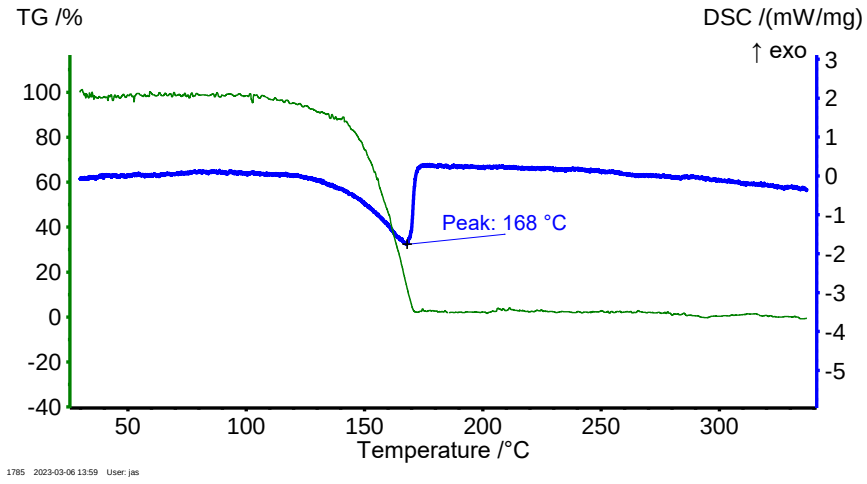

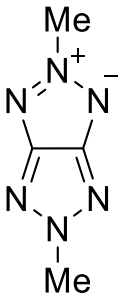

Application of the maximal accessible pressure within the DSC furnace (10 MPa) does not suppress the vaporization. We observe only evaporation of the sample of compound **7b**. DSC curve of compound **7b** at 10 MPa:

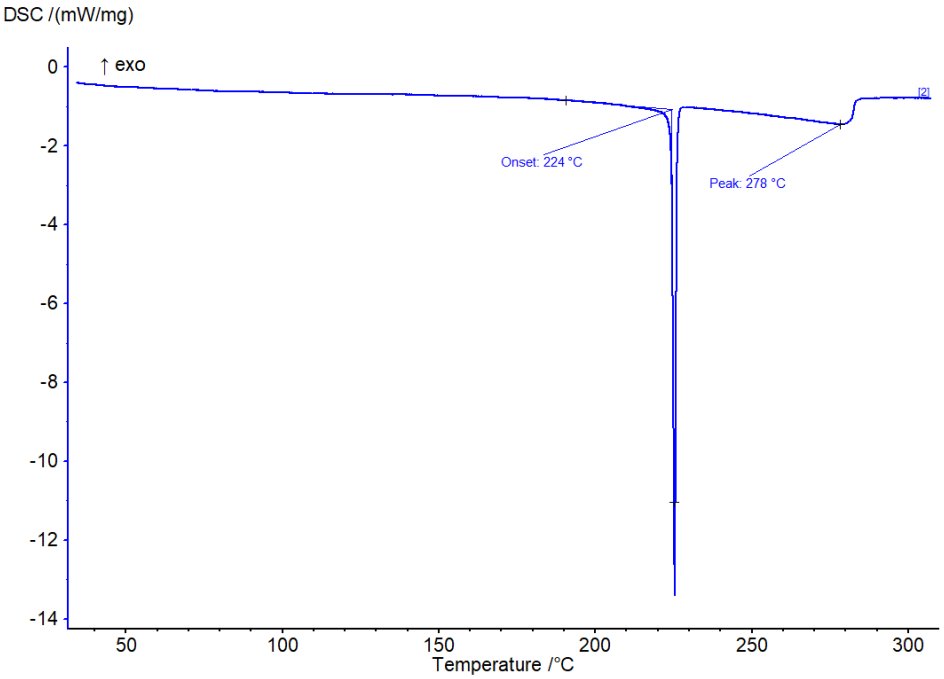

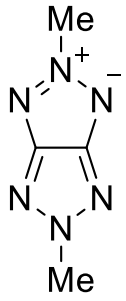

5.8. DSC of TT 7c

Sample of TT **7c** melts at 166 °C with subsequent decomposition at 166 °C (the extrapolated onset of exothermic peak). DSC curve of compound **7c**:

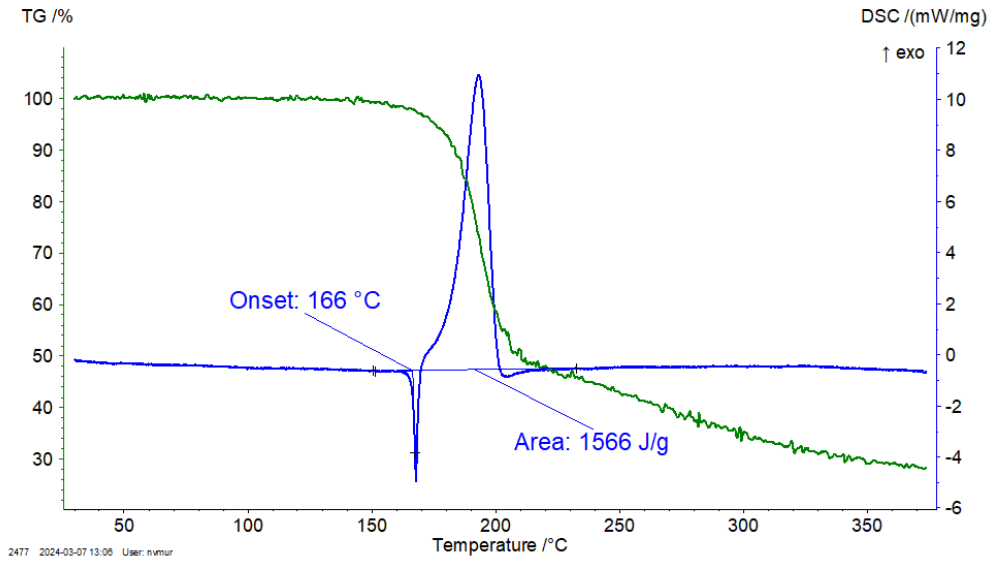

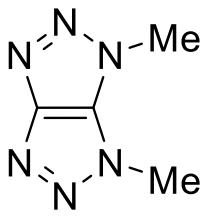

5.9. DSC of TT 7d

Sample of TT **7d** melts at 146 °C with subsequent decomposition at 180 °C (the extrapolated onset of exothermic peak). DSC curve of compound **7d**:

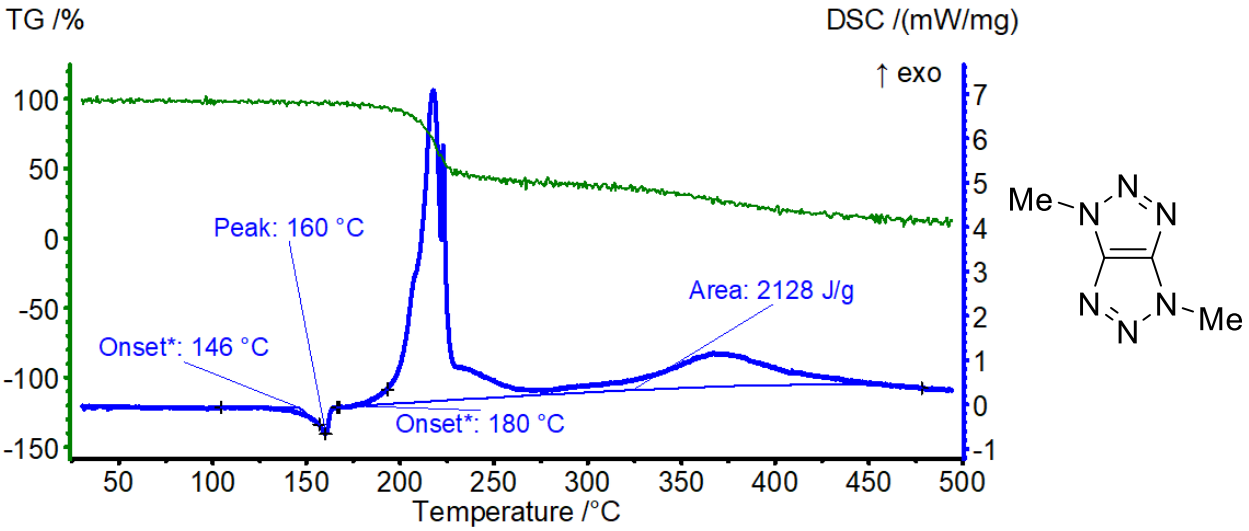

5.10. DSC of TT 8

Sample of TT **8** melts at 98 °C (the extrapolated onset of endothermic peak) with subsequent decomposition at 236 °C.

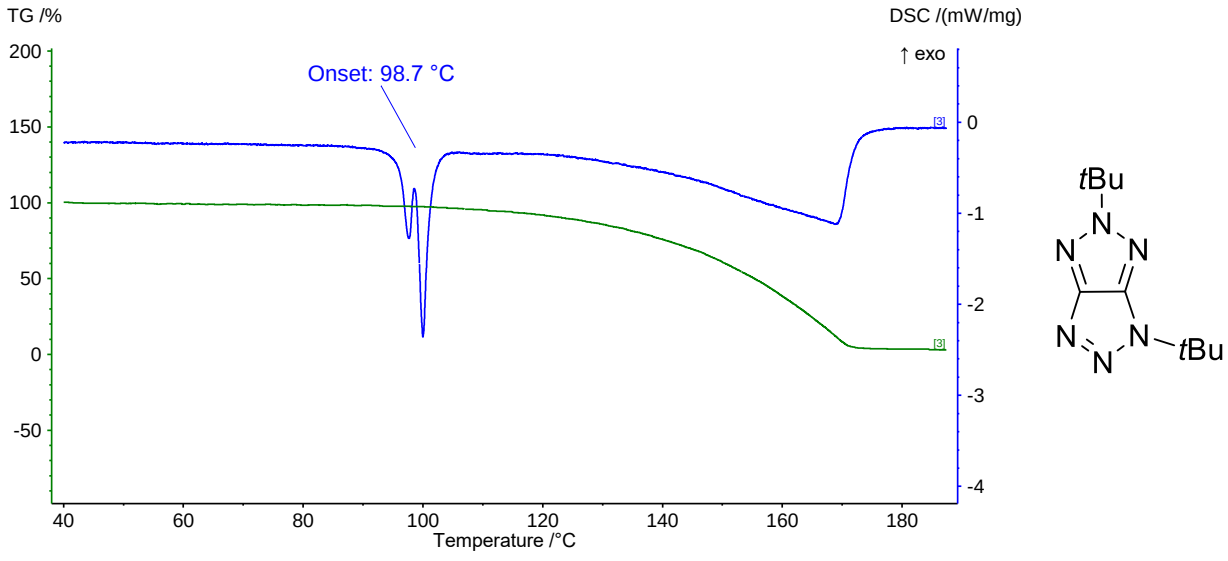

5.11. DSC of salt 9

Sample of salt **9** decomposes at 210 °C without melting (the extrapolated onset of exothermic peak).

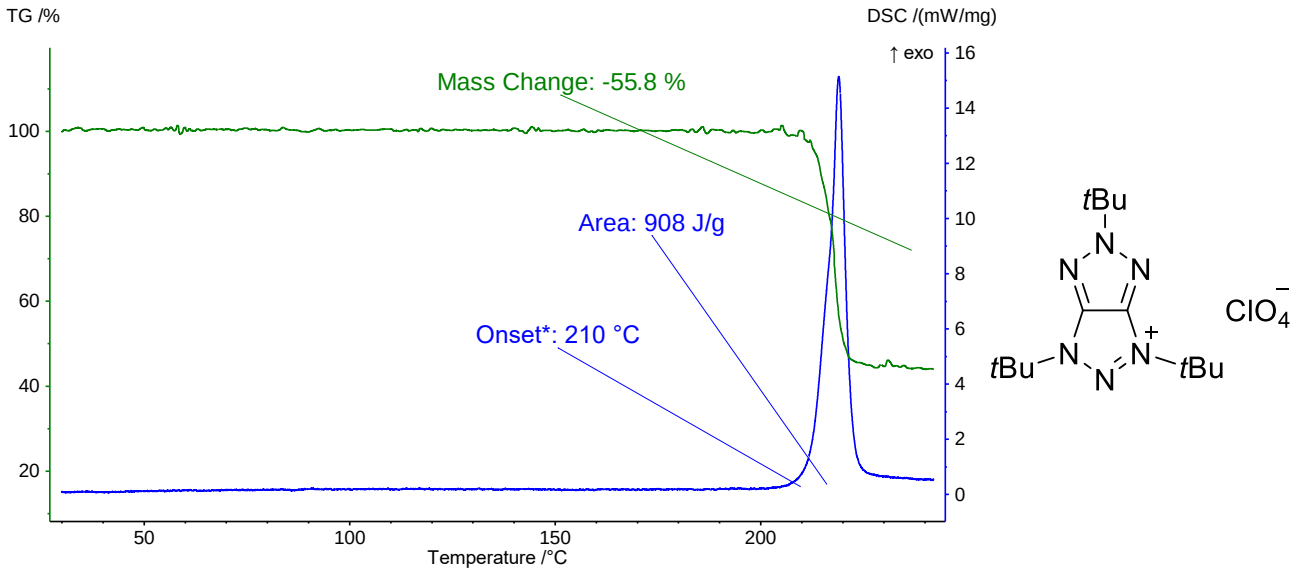

5.12. DSC of TT 10

Sample of TT **10** at heating under atmospheric pressure reveals melting at 163.6 °C with subsequent evaporation. DSC curve of compound **10** at atmospheric pressure:

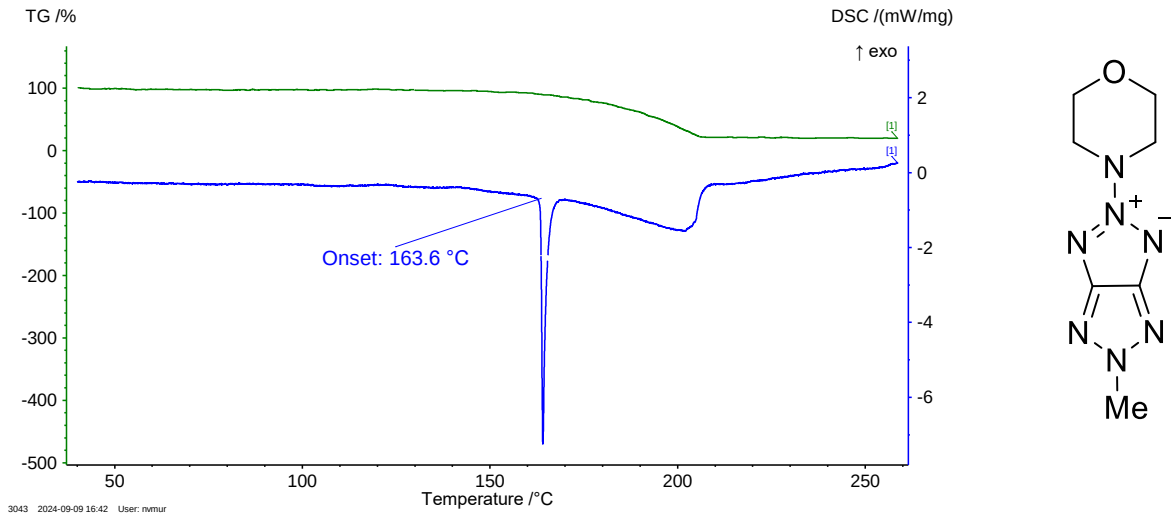

Additional testing at elevated pressure in DSC apparatus (2.0 MPa of nitrogen) shows that sample of TT **10** decomposes at 245 °C without melting (the extrapolated onset of exothermic peak). DSC curve of compound **10** at 2 MPa:

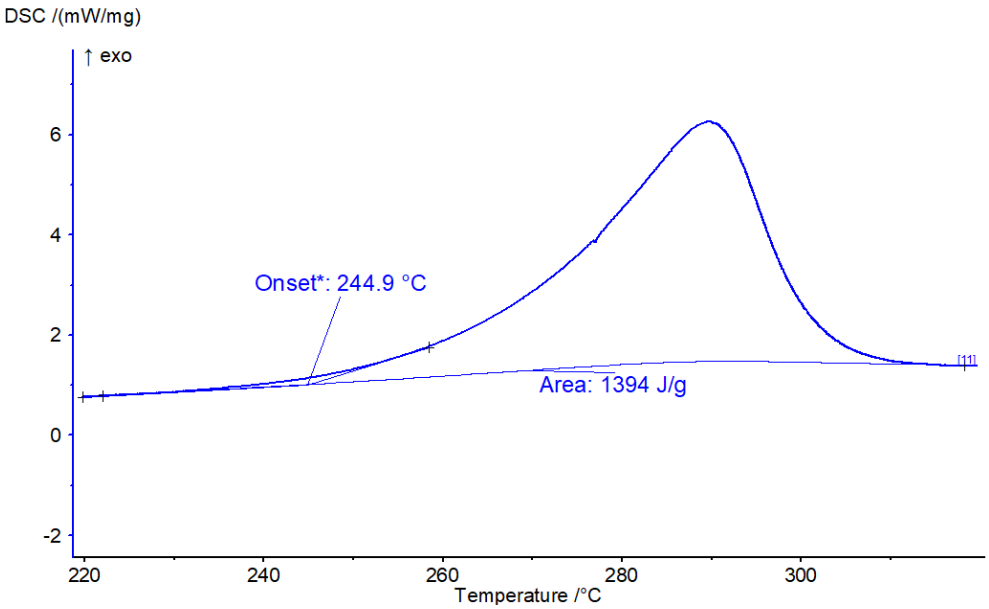

5.13. DSC of azidotriazole 13

Sample of compound **13** melts at 69 °C with subsequent decomposition at 110 °C (the extrapolated onset of exothermic peak).

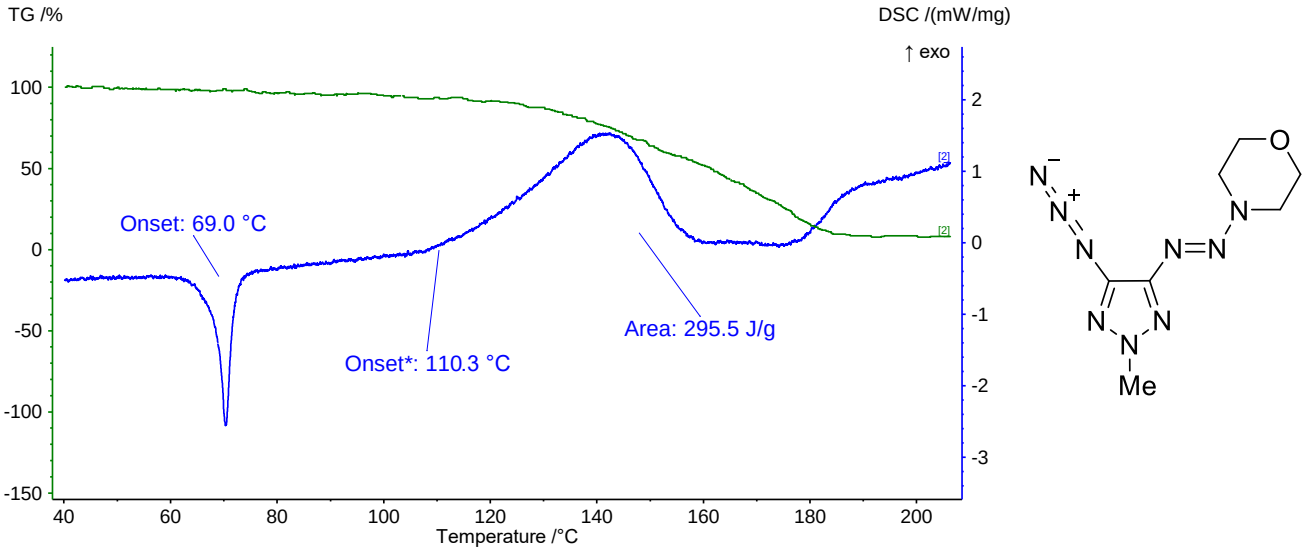

6. Thermal decomposition studies of TT 1

The thermal stability of solid TT **1** and its solution in 2,4,6-trinitrotoluene (w/w = 1 : 5) was initially investigated under non-isothermal conditions by differential scanning calorimetry (DSC) on a Xiang Yi instrument. The studies were conducted using aluminum pans with pierced lids at nitrogen flow rate 300 mL·min^{-1} (Fig. S12).

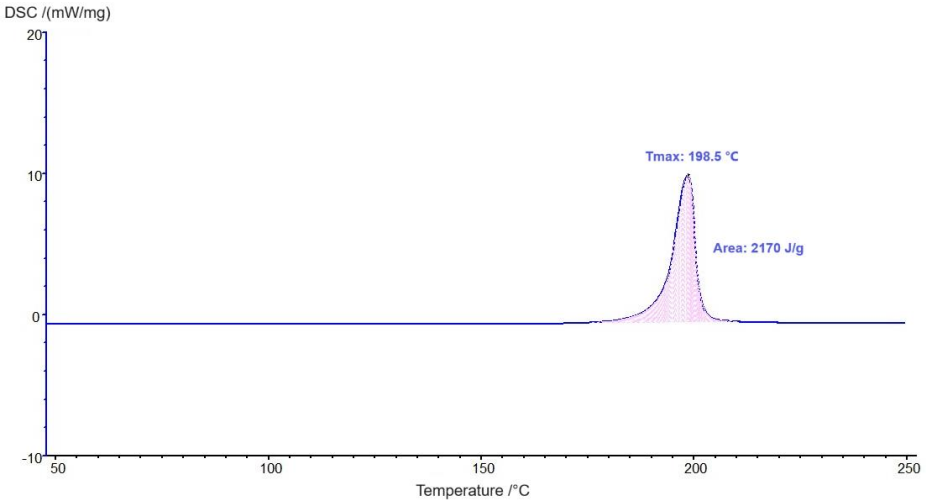

Fig. S12. DSC curve of TT **1** at a heating rate 5 °C·min^{-1}.

The Kissinger's equation[22] was used to calculate the kinetics of thermal decomposition by analyzing the maximum heat release temperatures on the DSC curves at different heating rates. The corresponding decomposition rate constants of TT **1** are presented in Table TS5.

Table TS5. DSC data for solid TT **1** and its solution in 2,4,6-trinitrotoluene.

Heating rate, °C·min^{-1}	Solid TT **1**		Solution of TT **1** in 2,4,6-trinitrotoluene	
	T_{max}, °C	$k_S \cdot 10^3$, s^{-1}	T_{max}, °C	$k_{liq} \cdot 10^3$, s^{-1}
5	198.5	11.31	157.8	7.60
10	203.4	22.15	164.2	14.76
15	206.0	32.86	170.2	21.55
20	211.0	42.92	172.0	28.50

T_{max} – the maximum heat release temperatures on the DSC curve; k_S – solid state rate constant; k_{liq} – liquid rate constant.

The decomposition of solid TT **1** was also investigated under isothermal conditions at 150 °C and 170 °C using thin-walled glass manometers of the compensation type, also known as glass Bourdon pressure gauge. A comprehensive account of the methodology can be found in the lit.[23] Experiments on the decomposition of TT **1** were carried out with a mass to volume ratio of about 10^{-3} g·cm^{-3}. At a temperature of 170 °C, the maximum gas release was 278 cm^3·g^{-1}, which is equivalent to 1.36 moles of gaseous products per mole of the starting material (Fig. S13).

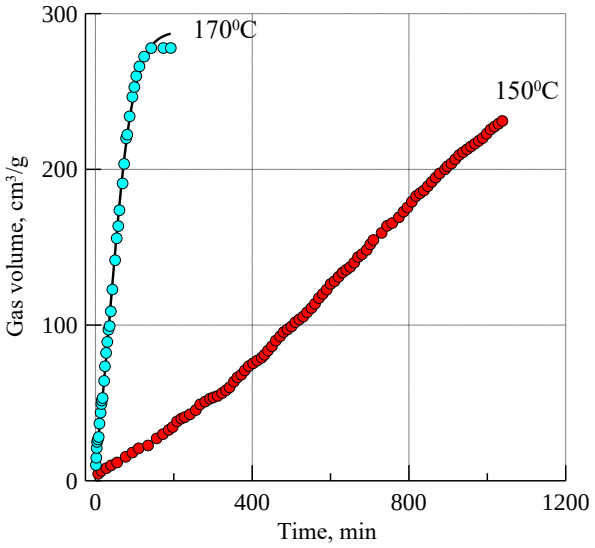

Fig. S13. Gas release curves for isothermal decomposition of TT **1** in solid state.

The decomposition of solid TT **1** and its solution in 2,4,6-trinitrotoluene proceeds with a weak acceleration and has therefore been described by a first-order equation with autocatalysis:[24]

$$V = V_{\infty} \cdot k_1 \cdot e^{((k1+k2)\cdot t)-1)} / (k_2 + k_1 \cdot e^{((k1+k2)\cdot t)}),$$

where V_{∞} is the maximum volume of evolved gases (in cm³) per gram of a sample, k_1 is a first-order rate constant of the non-catalytic stage, and k_2 is a pseudo first-order rate constant of the catalytic stage.

The constants obtained by the DSC method fall on the continuation of the kinetic straight line obtained in manometry when describing the acceleration stage (Fig. S14). The kinetic parameters are given in Table TS6.

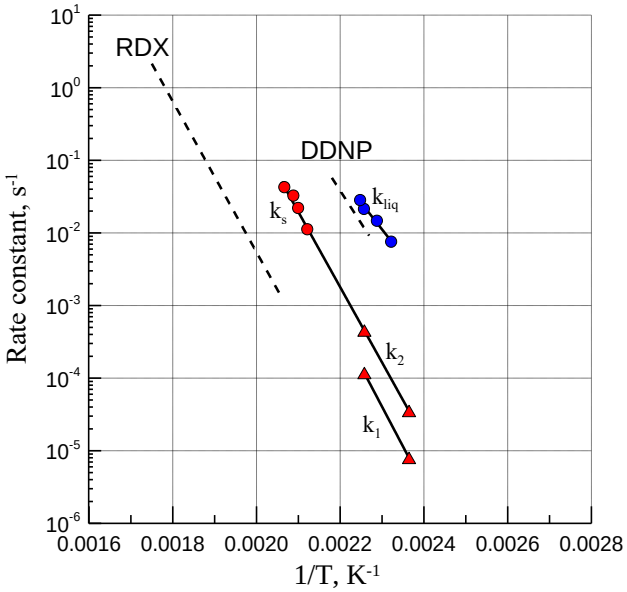

Fig. S14. The Arrhenius plot of the rate constants of TT **1** thermal decomposition in solid state (k_1, k_2 and k_s) and in solution (k_{liq}) obtained using isothermal manometry (triangles) and non-isothermal DSC (points) in comparison with decomposition data of RDX and 2-diazo-4,6-dinitrophenol (DDNP).

Table TS6. Kinetic data on the thermal decomposition of TT **1**.

Temperature interval, °C	Method	Log A	E_a, kJ·mol^{-1}	Coef. of determination
150–170	M(k_1)	20.79	209.6	1.00
150–170	M(k_2)	20.08	198.6	1.00
198–211	DSC	20.93	205.1	0.954
150–211	M(k_2)+DSC	20.38	201.1	0.999
158–172	DSC(k_{liq})	14.96	140.8	0.986

M – isothermal decomposition in manometers; DSC – non-isothermal decomposition; DSC(k_{liq}) – non-isothermal decomposition of TT **1** solution in 2,4,6-trinitrotoluene; A – pre-exponential factor in the Arrhenius equation; E_a – activation energy.

It is unlikely that the acceleration of decomposition of TT **1** is due to autocatalysis. The bulk decomposition residue also shows that melting is not the cause of the acceleration of decomposition. The slow acceleration of decomposition is probably due to the crystals cracking from thermal shock. This is also evidenced by the agreement between the kinetic data of the acceleration stage under isothermal conditions and the non-isothermal DSC data, which were obtained under a more pronounced thermal shock. The decomposition of TT **1** in the solid state can be described by the Arrhenius equation: $k_1 = 6.18 \cdot 10^{20} \cdot e^{(-25215/T)}$ characterizes the decomposition in a defect-free crystal lattice, while $k_2 = 1.20 \cdot 10^{20} \cdot e^{(-23890/T)}$ characterizes the decomposition at crystal defects. The activation energies E_a of these two processes are quite high (210 and 199 kJ·mol^{-1}, respectively) (see Table TS6). This is likely due to the occurrence of a preliminary ring-opening reaction, as observed in the decomposition of tetrazoles.[25]

In order to test this assumption, we conducted a study of the decomposition of TT **1** in a solution of 2,4,6-trinitrotoluene, the melting point of which is 80.9 °C, and whose thermal stability significantly exceeds that of TT **1**. The decomposition constants of TT **1** in solution were found to be more than two orders of magnitude higher than the initial decomposition rate of TT **1** in the solid state (see Fig. S14). They are described by the Arrhenius equation with values characteristic of ordinary thermal decomposition: $k_{liq} = 9.14 \cdot 10^{14} \cdot e^{(-16930/T)}$ (temperature range 158–172 °C, activation energy E_a = 141 kJ·mol^{-1}). Obviously, in contrast to the solid phase, the ring-opening reaction in solution proceeds without any particular difficulties. It is noteworthy that the kinetic data obtained for the decomposition of TT **1** in solution are similar to those observed for the decomposition of 2-diazo-4,6-dinitrophenol (DDNP)[26] (see Fig. S14).

7. Calorimetric measurements

The main method for determining the enthalpy of formation of energetic compounds is combustion calorimetry. The measurements were performed on a precision automatic combustion calorimeter with an isothermal shell (designed by the Laboratory of Thermodynamics of High-Energy Systems of the Federal Research Center of Chemical Physics named after N. N. Semenov of the Russian Academy of Sciences for the combustion of energetic compounds).[27]

Basic design features of the calorimeter used in this study: 1) small heat equivalent (~500 cal·degree^{-1}) with a large volume of bomb (200 cm^3); 2) simple installation bomb calorimeter – just remove the cap shell and the calorimetric vessel, drop the bomb and close the cover; 3) continuously thermostatic shell; 4) permanently fixed to the sheath liquid hermetic calorimeter vessel is in the form of a glass with double walls (calorimeter constant volume of fluid that delivers constant heat equivalent); 5) low measurement error. The calorimeter allows you to measure the thermal effect of the combustion reaction of substances with an extended uncertainty of 0.01–0.02%. Calibration of the calorimeter was carried out with the reference benzoic acid of the K-1 brand produced by the D. I. Mendeleev Institute of Metrology. The combustion energy of benzoic acid under standard conditions was 6322.6±1.2 cal·g^{-1}. The absence of a systematic error in calorimetric measurements was controlled by burning secondary reference substances-succinic and hippuric acids, whose combustion energies on this calorimeter were 3020.3±0.6 cal·g^{-1} (0.02%) and 5631.4±3.4 cal·g^{-1} (0.06%), respectively. Sample of the studied compound TT **1** was burned in a platinum crucible. Pressed tablets of TT **1** were weighed on Bunge microanalytic scales with an error of 2·10^{-6} g. The suspended sample of the substance was placed in a calorimetric bomb and filled with oxygen. The initial oxygen pressure during the combustion of all substances is about 30 atm (3 MPa). Before the experiment, 1 mL of distilled water was injected into the bomb to create a saturated vapor pressure and dissolve the nitrogen oxides formed during the combustion process.

The samples were ignited with a cotton thread, which in turn was ignited by incandescent platinum wire (diameter 0.3 mm) with a dosed pulse of current supplied from a special device. The combustion energy of cotton yarn was measured in a series of seven experiments and amounted to 3968.9 ±1.6 cal·g^{-1}. When determining the

combustion energy, corrections for the thermal effects of nitric acid formation, heat exchange of a calorimetric vessel with an isothermal shell, and the combustion energy of the auxiliary substance and cotton thread were taken into account. A detailed procedure for preparing samples and conducting an experiment was described earlier.[28]

Modern developments in certain areas of technology require the use of precision thermochemical characteristics of components, without which it is impossible to correctly solve applied problems.

Table TS7 shows the experimental values of the combustion energy ($-\Delta U'_B$, cal·g^{-1}) of the studied compounds under the conditions of a calorimetric bomb.

Table TS7. Experimental values of the combustion energy ($-\Delta U'_B$, cal·g^{-1}) of the TT **1** under the conditions of a calorimetric bomb.

N	m	ΔT	Q	q_a	q_i	q_N	q_{cot}	$-\Delta U'_B$
1	0.073357	2.06145	1108.54	843.68	7.19	2.40	9.51	3350.2
2	0.074082	2.13409	1147.61	879.15	7.18	2.42	10.53	3352.1
3	0.070158	2.15277	1157.65	904.21	7.22	2.31	8.79	3351.3
4	0.071317	2.25663	1213.50	957.09	7.24	1.78	8.52	3349.4
5	0.070023	2.22241	1195.10	942.96	7.21	1.75	8.41	3352.8
								$-\Delta U'_B$ = 3351.2 ±1.6 cal·g^{-1}

N – the ordinal number of the experiment; m – weight of the sample of the compound in vacuum, g; ΔT – corrected temperature rise in the calorimeter, degrees; Q – the amount of heat measured in the experiment, cal; q_a – heat of the combustion of the auxiliary substance benzoic acid, cal; q_i – ignition energy, cal; q_N − correction for the formation of nitric acid, cal; q_{cot} − heat generation from combustion of the cotton thread, cal; $\Delta U'_B$ − combustion energy of a substance in the bomb, cal·g^{-1}.

Experimental thermochemical characteristics of TT **1** are presented in Table TS8.

The combustion reaction of TT **1** proceeds in accordance with the stoichiometry of equation (1):

$$C_2H_2N_{6(cr)} + 2.5O_{2(g)} = 2CO_{2(g)} + H_2O_{(l)} + 3N_{2(g)} \quad (1),$$

where the subscripts cr, g, and l correspond to the crystalline, gaseous, and liquid states, respectively.

The standard enthalpy of formation of TT **1** is calculated based on the enthalpy of combustion in accordance with equation (2):

$$\Delta H^\circ_f [C_2H_2N_6]_{(cr)} = 2\Delta H^\circ_f [CO_2]_{(g)} + \Delta H^\circ_f [H_2O]_{(l)} - \Delta H^\circ_c \quad (2),$$

where ΔH°_c – the standard enthalpy of combustion of the corresponding compound, kcal·mol^{-1}, and ΔH°_f – the standard enthalpy of its formation, kcal·mol^{-1}.

When calculating the standard enthalpies of formation of the studied compounds, we used the reference values of the enthalpies of formation of combustion products:[29]

$\Delta H^\circ_f[CO_2]_{(g)} = -94.051 \pm 0.031$ kcal·mol^{-1} and

$\Delta H^\circ_f[H_2O]_{(l)} = -68.315 \pm 0.009$ kcal·mol^{-1}.

Table TS8. Experimental thermochemical characteristics of TT **1**.

$-\Delta U'_B$, cal·g^{-1}	ΔH°_c, kcal·mol^{-1}	ΔH°_f, kcal·mol^{-1}	ΔH°_f, kcal·kg^{-1}
3351.2 ±1.6	–367.0 ± 0.2	110.6 ± 0.2	1004.6 ± 1.8

$-\Delta U'_B$ – energy of combustion of under bomb conditions;

ΔH°_c – standard enthalpy of combustion;

ΔH°_f – standard enthalpy of formation.

7. References

1. Standardization Agreement 4489 (STANAG 4489), Explosives, Impact Sensitivity Tests, NATO, Brussels, 1999.

2. Standardization Agreement 4487 (STANAG 4487), Explosives, Impact Sensitivity Tests, NATO, Brussels, 2002.

3. N. V. Muravyev, D. D. Meerov, K.A. Monogarov, I. N. Melnikov, E. K. Kosareva, L. L. Fershtat, A. B. Sheremetev, I. L. Dalinger, I. V. Fomenkov, A. N. Pivkina, *Chem Eng J.*, 2021, **421**, 129804.

4. V. G. Andrianov, V. G. Semenikhina, A. V. Eremeev, *Chem. Heterocycl. Compd.*, 1992, **28**, 803–807.

5. E. V. Shulishov, I. P. Klimenko, Y. V. Tomilov, Synth. Org. Compd. Part 3. Russ, *MAX PRESS*, Moscow, 2008, 266–269.

6. L. Krause, R. Herbst-Irmer, G. M. Sheldrick, D. Stalke, *J. Appl. Crystallogr.*, 2015, **48**, 3–10.

7. CrysAlisPro. Version 1.171.41.106a. Rigaku Oxford Diffraction, 2021.

8. G. M. Sheldrick, *Acta Cryst.* 2015, **A71**, 3–8.

9. a) G. M. Sheldrick, *Acta Cryst.* 2015, **C71**, 3–8; b) O. V. Dolomanov, L. J. Bourhis, R. J. Gildea, J. A. K. Howard, H. Puschmann, *J. Appl. Cryst.* 2009, **42**, 229–341.

10. A. A. Coelho, *J. Appl. Crystallogr.*, 2003, **36**, 86–95.

11. A. A. Coelho, *J. Appl. Crystallogr.*, 2018, **51**, 210–218.

12. V. Favre-Nicolin, R. Černý, *J. Appl. Crystallogr.*, 2002, **35**, 734–743.

13. A. O. Dmitrienko, I. S. Bushmarinov, *J. Appl. Crystallogr.*, 2015, **48**, 1777–1784.

14. J. van de Streek, M. A. Neumann, *Acta Crystallogr. B Struct. Sci. Cryst. Eng. Mater.*, 2014, **70**, 1020–1032.

15. R. Dovesi, A. Erba, R. Orlando, C. M. Zicovich-Wilson, B. Civalleri, L. Maschio, M. Rérat, S. Casassa, J. Baima and S. Salustro, et al., *Wiley Interdiscip. Rev.: Comput. Mol. Sci.*, 2018, **8**, e1360.

16. C. Adamo, V. Barone, *J. Chem. Phys.*, 1999, **110**, 6158–6170.

17. S. Grimme, S. Ehrlich, L. Goerigk, *J. Comput. Chem.*, 2011, **32**, 1456–1465.

18. M. F. Peintinger, D. V. Oliveira, T. Bredow, *J. Comput. Chem.*, 2013, **34**, 451–459.

19. I. J. Bruno, J. C. Cole, M. Kessler, J. Luo, W. D. S. Motherwell, L. H. Purkis, B. R. Smith, R. Taylor, R. I. Cooper, S. E. Harris, A. G. Orpen, *J. Chem. Inf. Comput. Sci.*, 2004, **44**, 2133–2144.
20. C. R. Groom, Bruno I. J., Lightfoot M.P., S. C. Ward, *Acta Crystallogr. B.*, 2016, **72**, 171–179.
21. H. Zabrodsky, S. Peleg, D. Avnir, *J. Am. Chem. Soc.*, 1992, **114**, 7843–7851.
22. H. E. Kissinger, *Anal. Chem.* 1957, **29**, 1702–1706.
23. V. V. Serushkin, V. P. Sinditskii, T. H. Hoang, S. A. Filatov, A. S. Shipulina, I. L. Dalinger, A. K. Shakhnes, A. B. Sheremetev, *J. Therm. Anal. Calorim.* 2018, **132**, 127–142.
24. N. M. Emanuel, D.G. Knorre. Course of chemical kinetics: textbook. 4th ed. *Moscow: Higher School*, Moscow, 1984.
25. V. P. Sinditskii, A. D. Smirnova, V. V. Serushkin, N. V. Yudin, I. A. Vatsadze, I. L. Dalinger, V. G. Kiselev, A. B. Sheremetev, *Thermochim. Acta.*, 2021, **698**, 178876.
26. Z. W. Yang, Y. C. Liu, D. C. Liu, L. W. Yan, J. Chen, *J. Hazard. Mater.*, 2010, **177**, 938–943.
27. Ya. O. Inozemtsev, A. B. Vorob'ev, A. V. Inozemtsev, Yu. N. Matyushin, *Combustion and Explosion*, 2014, **7**, 260–270.
28. T. S. Kon'kova, Yu. N. Matyushin, E. A. Miroshnichenko, A. B. Vorob'ev, *Russ. Chem. Bull.*, 2009, **58**, 1–8.
29. J. D. Cox, D. D. Wagman, V. A. Medvedev. CODATA key values for thermodynamics. Final Report of the CODATA Task Group on Key Values for Thermodynamics, New York, Washington, Philadelphia, London, 1989.